

EFFICIENT AIR-WATER HEAT PUMPS FOR HIGH TEMPERATURE LIFT RESIDENTIAL HEATING, INCLUDING OIL MIGRATION ASPECTS

THÈSE N° 2998 (2004)

PRÉSENTÉE À LA FACULTÉ SCIENCES ET TECHNIQUES DE L'INGÉNIEUR

Institut des sciences de l'énergie

SECTION DE GÉNIE MÉCANIQUE

ÉCOLE POLYTECHNIQUE FÉDÉRALE DE LAUSANNE

POUR L'OBTENTION DU GRADE DE DOCTEUR ÈS SCIENCES

PAR

Michele ZEHNDER

ingénieur mécanicien diplômé EPF
de nationalité suisse et originaire d'Aadorf (TG)

acceptée sur proposition du jury:

Prof. D. Favrat, directeur de thèse
Prof. T. Kopp, rapporteur
Prof. J. Lebrun, rapporteur
Prof. J. Thome, rapporteur

Lausanne, EPFL
2004

Abstract

This thesis presents a system approach with the aim to develop improved concepts for small capacity, high temperature lift air-water heat pumps. These are intended to replace fuel fired heating systems in the residential sector, which leads to a major reduction of the local greenhouse gas emissions. Unfavorable temperature conditions set by the existing heat distribution systems and by the use of atmospheric air, as the only accessible heat source, have to be overcome. The proposed concepts are intended to cover the total application range and to provide the full heat demand without any additional (electric) heat supply.

A systematic approach, using a multi objective optimization tool, has been applied to evaluate possible alternate refrigerants, which perform best, regarding to the system COP and the specific heat output. All the optimal refrigerant blends are composed by flammable refrigerants and a potential increase of the COP of 8% (compared to the commercial blend R-407C) has been determined. These potential improvements highly depend on the acceptance to use flammable refrigerants, as can be shown by this evaluation.

The standard concepts of small capacity heat pumps suffer from a restricted application range and show highly decreasing performances (COP and provided heat) at extreme operating conditions. From the examination of the thermodynamic cycle, different improved concepts are proposed and are assembled in a generalized super-configuration. The most promising concepts have been built as prototype units and have been tested in laboratory. These concepts are: a) the two-stage compression cycles with economizer heat exchanger or b) with economizer flash tank at the intermediate pressure level, c) the booster-compressor setup, d) the one-stage compression cycle including a new developed hermetic compressor, which enables intermediate injection of saturated vapor flow and e) a small capacity auxiliary cycle for liquid subcooling. In all these concepts the application range could be extended, by achieving reduced discharge temperatures and the heat rate provided at extreme operating conditions could be substantially increased (20%-35%, +100% for the booster setup), using the same compressor and evaporator size. System COP has been improved (~5%) over a large application range, and specifically in high temperature lift operating conditions.

The experimental evaluation reveals the major problem of unbalanced oil migration in two-stage compression cycles (except for the booster concept). An extensive evaluation has been applied, to analyze the oil migration in two-stage compression heat pumps. A new developed measurement technique, using a Fourier Transform Infrared Spectrometry combined with a high pressure supporting ATR cell, has been calibrated (with a lower detection limit at 0.2% - 0.4%, and a sensitivity of 0.1%) with the used refrigerant-oil mixtures (R-134a/POE oil and R-407C/POE oil). It has been applied to perform on-line oil concentration measurements during two-stage and one-stage steady stage and during transitory operating modes.

A generalized steady state simulation model has been developed including namely the new developed compressor model with an intermediate injection port, considering the geometrical flow path of the tested prototype compressors. A flow map based extensive heat transfer model is integrated into a finned tube evaporator model and taking into account oil effects on the heat transfer. General models of plate heat exchangers and for capillary tube expansion devices complete this modular simulation model, on which the concepts of the super-configuration can be calculated and some parametric analysis has been performed. An in house developed fluid interface module includes the fluid properties calculation program Refprop and allows to define new mixtures or to use the large number of predefined refrigerants.

Zusammenfassung

Diese Dissertation basiert auf einem ganzheitlichen system-orientierten Ansatz, mittels welchem neue Konzepte für Hochtemperatur-Anwendungen mit Luft-Wasser Kleinwärmepumpen (WP) erarbeitet werden. Diese sollen bestehende Öl- oder Gasheizungen ersetzen, womit ein wesentlicher Beitrag zu Verminderung der lokalen CO₂ Emissionen geleistet werden kann. Die erarbeiteten Konzepte müssen auf einem hohen Temperaturhub und ganzjährig, ohne Zusatzheizung, betrieben werden können. Die Arbeitsbedingungen sind durch das bestehende Heizungsnetz und durch die Wahl der Umgebungsluft als Wärmequelle bestimmt.

Neue Kältemittelgemische, welche die bestmögliche Kombination von COP und spezifischer Heizleistung aufweisen, wurden mittels einer multikriteriellen Optimierung berechnet. Alle optimalen Gemische bestehen aus brennbaren Kältemitteln und ein Verbesserungspotenzial von 8% im COP (bezüglich R-407C) wurde ermittelt. Diese potenzielle Verbesserung hängt von der Akzeptanz brennbarer Stoffe in der Wärmepumpenanwendung ab.

Standard WP-Kreisprozesse sind stark in ihrem Anwendungsbereich eingeschränkt und fallen mit ihren Leistungsmerkmalen bei höherem Temperaturhub stark ab. Durch die Untersuchung des thermodynamischen Prozesses konnten mehrere verbesserte Konzepte erarbeitet werden, welche in einer Grafik zusammengefasst wurden. Verschiedene Lösungen konnten im Labor aufgebaut und getestet werden, diese sind: a) Zwei-stufige WP mit 'Economizer' Wärmeübertrager oder mit b) Zwischendruckbehälter oder mit c) 'Booster' Kompressor als Zusatzverdichter, d) ein-stufige WP mit neu entwickeltem Kompressor mit angepasstem Zwischeneinspritzungs-Einlass für Dampfeinspritzung während der Kompression und Economizer Wärmeübertrager und e) ein-stufige WP mit Hilfskreislauf zur Kondensatunterkühlung. Bei all diesen Konzepten konnte eine wesentliche Erweiterung des Anwendungsgebietes durch Reduktion der Verdichter-Austrittstemperaturen erreicht werden. Bei gleicher Verdichtergrösse und gleichem Verdampfer, konnte die Basis-Heizleistung wesentlich erhöht werden (20%-35%, +100% bei 'Booster') und gleichzeitig konnte der COP etwas erhöht werden (~5%).

Messungen an WP mit zwei seriellen Kompressions-Stufen (ausser beim 'Booster'-Betrieb) haben gezeigt, dass sich das von den Verdichtern zur Schmierung benötigte Öl durch Migration in den unteren Verdichter verschiebt und dadurch bei kontinuierlichem Betrieb die Schmierung im oberen Verdichter nicht mehr gewährleistet ist. Diese Ölmigration wurde näher untersucht und eine neu entwickelte kontinuierliche Öl-Konzentrations Messung, basierend auf einem Fourier Transformations Infrarot Spektrometers und einer ATR-Zelle, konnte mit den Kältemittel-Öl Gemischen (R-134a/POE Öl und R-407C/POE Öl) kalibriert werden (untere Messgrenze: 0.2% - 0.4%, Sensibilität: 0.1%). Diese Mess-Methode wurde im zwei- und ein-stufigen bei stationärem, sowie im dynamischen Betrieb eingesetzt.

Ein für den stationären Betrieb entwickeltes Wärmepumpen-Simulationsmodell beinhaltet namentlich ein neu entwickeltes Kompressionsmodell, welches die geometrischen Grundlagen der Zwischeneinspritzung der getesteten hermetischen Prototyp-Verdichter berücksichtigt. Ein auf physikalischen Mechanismen basierendes Verdampfungsmodell wurde in ein eigens programmiertes Lamellen-Verdampfer Berechnungsmodell eingegliedert. Einwirkungen von Ölanteilen im Kältemittel wurden im Wärmeübergang berücksichtigt. Die Modelle von den Plattenwärmeübertragern und des Kapillar-Rohres ergänzen das Simulationsprogramm und alle berücksichtigten Kreisprozesse können berechnet werden. Eine eigene Schnittstelle für die Berechnung von thermodynamischen und physikalischen Stoffwerten, wurde ebenfalls entwickelt und beinhaltet das Berechnungsprogramm Refprop.

Résumé

Ce travail de thèse est basé sur une approche système ayant pour but de développer des pompes à chaleur (PAC) air-eau de haute performance pourvues de fonctionner dans des applications à des hauts rapports de températures externes. Ces unités remplacent des systèmes de chauffage résidentiel, qui sont souvent à base d'énergie fossile. Par leur remplacement une contribution majeure de réduction d'émissions locales de gaz à effet de serre pourrait être obtenue. Des niveaux de températures élevées dans ces systèmes de chauffage actuels et l'utilisation de l'air externe comme source principale de chaleur, posent des conditions de fonctionnement particulièrement difficiles et des systèmes améliorés seront choisis en fonction de cette utilisation.

Une approche systématique, basée sur un outil d'optimisation multi-objectif, est proposée pour évaluer de nouveaux mélanges de réfrigérants qui montrent les meilleures performances de COP et de puissance de chauffage spécifique. Tout les mélanges identifiés sont composés de réfrigérants inflammables et un potentiel d'amélioration maximal de 8% au niveau du COP (comparé au mélange R-407C) à été identifié.

Les concepts standards des PAC de petite taille fonctionnent dans un domaine d'application fortement réduit et leurs performances chutent considérablement aux conditions extrêmes. Par une analyse thermodynamique, plusieurs solutions de cycles à performance améliorée ont été identifiées et sont représentées dans une superstructure. Les concepts les plus prometteurs ont été testés en laboratoire. Ces concepts sont : a) PAC bi-étagée avec échangeur économiseur ou b) avec réservoir intermédiaire à séparation de phase c) ou concept de compresseur 'Booster', d) PAC mono-étagée avec un nouveau type de compresseur avec port d'injection intermédiaire qui est adapté pour l'injection de vapeur saturée, e) PAC à cycle auxiliaire de sous-refroidissement. Le domaine d'utilisation de ces approches est considérablement étendu, grâce à une réduction importante des températures de fin de compression. La puissance de chauffage de base est augmentée de (20%-35%, +100% concept 'Booster') tout en conservant la même taille de compresseur et d'évaporateur. Le COP a pu être amélioré sur un large plage de fonctionnement ($\sim 5\%$).

Les expériences ont relevé le problème majeur de mauvaise répartition d'huile de lubrification dans les concepts à compression bi-étagée (à l'exception du concept 'Booster'). Une analyse détaillée a été poursuivie, afin de mesurer et analyser plus précisément ce phénomène dans les cycles bi-étagés et de pouvoir identifier des solutions stables de fonctionnement. Une nouvelle approche de mesures en ligne de la concentration massique d'huile dissoute dans des mélanges de réfrigérants est appliquée. Par un spectromètre infrarouge à transformée de Fourier et une cellule de mesure à réflexion totale, des tests de calibrage avec les couples R-134a/huile polyolester et R-407C/huile polyolester ont été effectués (avec une limite inférieure de détection d'huile de 0.2% - 0.4% et une sensibilité de 0.1%). La méthode a été appliquée pour mesurer la concentration d'huile migrante dans une pompe à chaleur en fonctionnement bi- et mono-étagé, en régime permanent et en régimes transitoires.

Un modèle de simulation généralisé a été développé incluant notamment un nouveau modèle de compresseur avec port d'injection intermédiaire, incluant une description physique de la géométrie d'injection correspondante aux compresseurs prototypes testées en laboratoire. Un modèle de transfert de chaleur, basé sur des cartes d'écoulement et incluant l'impact de l'huile a été considéré pour la modélisation des évaporateurs à ailettes. Des modèles généralisés d'échangeurs à plaques et de capillaires complètent ce programme de simulation modulaire, qui permet de calculer les cycles améliorés considérés. Une interface de calcul de propriétés de fluides a été développée est permet d'intégrer les modules du programme Refprop, qui permet d'utiliser et de définir un grand nombre de mélanges de réfrigérants ou d'utiliser les fluides prédéfinis.

Acknowledgment

By these lines I want to address all my thanks to the persons, who enabled and contributed to this work and the great time I could spend at the LENI in Lausanne. To be able to formulate my thanks in a appropriate way I want to do so in the corresponding languages:

J'aimerais tout d'abord remercier Prof. Daniel Favrat pour m'avoir engagé en tant que responsable des projets pompe à chaleur au Laboratoire d'Énergétique Industrielle (LENI) et de m'avoir encouragé de commencer ce travail de thèse. J'aimerais surtout lui remercier pour ces appréciations tout au long de mon activité au sein du LENI, mais aussi pour ses sensibilités au niveau social.

J'aimerais remercier les Professeurs Jean Lebrun, Thomas Kopp et John Thome pour avoir accepté la tâche d'être co-rapporteur de cette thèse et donc du temps de m'avoir simplement consacré.

Pendant mes années comme assistant et doctorant j'ai vu passer beaucoup d'amis, mais très peu entre eux sont toujours restés : Merci Brigitte, Marc et Roger pour vos heures consacré à Migroil et PAC-HT derrière les factures ou avec le chalumeau en main, mais aussi pour tout le bon temps passé ensemble. D'autres personnes ont beaucoup contribué au bien-être au LENI et je tiens à remercier Diego, Xavier et Jürg pour leurs contributions diverses, Geoff et Adam pour leur savoir-faire dans FLINT, mais aussi de m'avoir dépassé en jonglage, Fredo et Stéphane pour avoir partagé la passion des pompes à chaleur et Hongtao de m'avoir accompagné à Beijing. Merci à vous tous !

Ohne das Interesse und die Unterstützung von Martin Zogg und Thomas Kopp vom Bundesamt für Energie wäre diese Arbeit nicht so komplett und so weit fortgeschritten. Ich möchte mich bei beiden herzlich bedanken. Aber auch die Unterstützung von der Hersteller-Seite hat mich sehr gefreut und ich danke allen für die sehr angenehme und interessante Zusammenarbeit: Georges Courtin und Vinicio Curti - Termogamma SA, Carlo Brugnoli - Cryotherm AG, Günther Reiner - Axima Refrigeration, Hansueli Bruderer und Hans Hohl - Satag Thermotechnik AG und Daniel Trüssel - KWT AG.

Meinen herzlichsten Dank möchte ich meiner Familie aussprechen, die mich während dieser langen und schliesslich sehr intensiven Zeit eine grosse Stütze waren und es stets bleiben werden. Linus und Annika und Laura-Maria - bei euch sehe ich, wie schnell die Zeit doch vergeht. Ich habe grosse Freude an euch, wachst weiter so! Silvia - herzlichen Dank für deine grosse Unterstützung. Ich möchte dir diese Arbeit widmen und freue mich auf eine spannende gemeinsame Zukunft - Viel Spass beim Lesen!

Lausanne, avril 2004

Contents

Abstract	i
Zusammenfassung	ii
Résumé	iii
1 Introduction	1
1.1 About this work	1
1.2 Theory of heat pump processes	3
1.3 Refrigerant selection - screening of new blends	9
1.3.1 Simulation conditions	11
1.3.2 Fluid properties and performance	11
1.3.3 Refrigerants in commercial products	15
1.3.4 Research of new substitution blends for high temperature air-water heat pumps	16
1.4 Market trends	22
1.5 Conclusions to the refrigerant selection	24
Bibliography	25
2 Improved heat pump design concepts	27
2.1 Improving efficiency - ways to go	27
2.1.1 Acting on the heating system	27
2.1.2 Improving the thermodynamic cycle	28
2.1.3 Facing the market	31
2.2 Superstructure	33
2.3 Selected configurations of high performance heat pump	38
2.3.1 Cycle with intermediate injection and heat exchanger	38
2.3.2 Heat pump with auxiliary cycle for liquid subcooling	46
2.3.3 The two-stage heat pump	50
2.4 Conclusions	63
Bibliography	67
3 Simulation model	69
3.1 Compressors	71
3.1.1 Scroll compressor model	75
3.1.2 Scroll compressor with intermediate injection port	83
3.2 Heat exchangers	93
3.2.1 Single-phase convective heat transfer	93
3.2.2 The modified Kattan-Thome-Favrat flow pattern map	94
3.2.3 Evaporating heat transfer model	98

3.2.4	Condensation heat transfer model	102
3.2.5	Finned tube evaporator	105
3.2.6	Plate heat exchangers	108
3.2.7	Coaxial tubular suction line heat exchanger	113
3.2.8	Influence of oil in heat transfer	114
3.2.8.1	Pure oil properties	115
3.2.8.2	Refrigerant-oil mixing models	119
3.2.8.3	Saturation temperature or solubility of refrigerant-oil mixtures	121
3.2.8.4	Enthalpy of vaporization	123
3.2.8.5	Modified heat transfer coefficient	123
3.3	Expansion devices	125
3.3.1	Basic equations	125
3.3.2	The flow regions	126
3.3.2.1	Entrance region	127
3.3.2.2	Liquid phase region	127
3.3.3	Friction factor	130
3.3.4	Resolution model	130
3.3.5	Validation of the capillary tube model	131
3.4	Conclusions to the simulation model	132
	Bibliography	135
4	Heat pump cycle simulation results	141
4.1	External conditions	141
4.1.1	Climatic conditions	141
4.1.2	Heat load and heat curve	142
4.1.3	Frosting/Defrosting	145
4.1.4	Hot Water Preparation and Integration	146
4.1.5	Auxiliary power	146
4.2	Cycle performances and system parameters	146
4.2.1	The enhanced heat pump cycle simulation program.	147
4.2.1.1	One-stage compression cycle	149
4.2.1.2	Two-stage compression cycles	158
4.2.1.3	Auxiliary cycle for liquid subcooling	166
4.2.2	Conclusions of the simulation results.	169
	Bibliography	171
5	Oil migration in heat pumps	173
5.1	Oil concentration measurement	173
5.1.1	Literature review of oil-concentration measurement techniques	173
5.1.2	Fourier Transform Infrared Spectrometry	176
5.1.3	Coriolis densimeter (Bopp&Reuther DIMF 2.0 TRV)	179
5.1.4	Mass sampling	179
5.2	Calibration tests	180
5.2.1	Calibration setup for oil-refrigerant concentration measurements	180
5.2.2	Pure fluid calibration	182
5.2.2.1	Vibrational-rotational infrared absorption spectra	182
5.2.2.2	Density measurements of pure refrigerants	185

5.2.3	Refrigerant-oil mixtures	185
5.2.3.1	Oil concentration calibration tests with the FT-IR method	185
5.2.3.2	Oil concentration measurements using Coriolis type densimeter	192
5.3	Oil migration in heat pump cycle	194
5.3.1	Oil traps and size of the piping	194
5.3.2	Liquid level measurement in the compressors	197
5.3.3	Oil mass concentration in single-stage and two-stage heat pump	198
5.3.3.1	Applied methods	198
5.3.3.2	Injection of a known quantity of oil into the circuit	199
5.3.3.3	Oil migration in steady state operating conditions	204
5.3.3.4	Transitory effects on oil migration during steady state heating	207
5.4	Propositions for balanced operating conditions in two-stage compression cycles	209
5.5	Conclusions	211
	Bibliography	213
	6 General Conclusions and Outlook	215
	Symbols	219
	Appendix A	225
A.1	Exergy analysis applied to an air-water heat pump unit.	225
A.2	Precisions of measured data	228
A.3	The enhanced heat pump model - Toolbox	230
A.4	Simulation input data of available components	230
A.4.1	Compressors	230
A.4.2	Finned tube evaporator	233
A.4.3	Plate heat exchangers	234
A.5	Experimental setup and listings of elements.	235
A.5.1	Brine-water heat pump, economizer cycle with intermediate liquid injection port compressor	235
A.5.2	Air-water heat pump, economizer cycle with new intermediate vapor injection port compressor	237
A.5.3	Brine-water heat pump with high pressure ratio main compressor and auxiliary subcooling cycle	239
A.5.4	Two-stage compression air-water heat pump, including oil migration measurements	241
	Curriculum Vitae	245

1. Introduction

1.1 About this work

The Kyoto protocol in 1997 is the most significant recent act concluded by the international community aiming a protection of the global environment. Regulation mechanisms for the **reduction of greenhouse gas emissions** are proposed. This reduction could only be achieved by reinforcing the use of modern technologies allowing a more rational use of non renewable energy sources and by an increased reliance on emission free energy conversion technologies. When it comes to providing heat services, heat pumps are an essential technology in the transformation chain for heat supply and substantial reductions of the primary energy consumption and the emissions of greenhouse gases can be obtained, as shown in Figure 1.1. The **heat pump is identified as being the key element for high efficiency** solutions, reducing the waste energy in the transformation chain of medium temperature heat production.

As the First Law efficiency of heat pumps is highest for low temperature difference between the external thermal sources, primary application targets have been low temperature heating applications, where they gradually become competitive to traditional oil and gas boilers. However, a major application area is the substitution or retrofit of house heating devices at medium to high temperature or the further distribution of heating heat pumps in colder climates.

The object of this thesis is a **contribution to key aspects of the engineering** of such relatively **high temperature lift vapor compression heat pumps** for the residential heating. This work addresses the following key aspects:

- A systematic approach to the selection of appropriate refrigerants, including new blends, by means of a modern optimization tool.
- The collection of experimental results contributing to a better knowledge of advanced heat pump cycles, including
 - Economizer cycles with compressors allowing intermediate injection of vapor.
 - Two-stage compression cycles and *booster* compressor concepts.
 - Separated compression cycles for liquid subcooling and parallel heating or to provide heat to a secondary, higher temperature level.

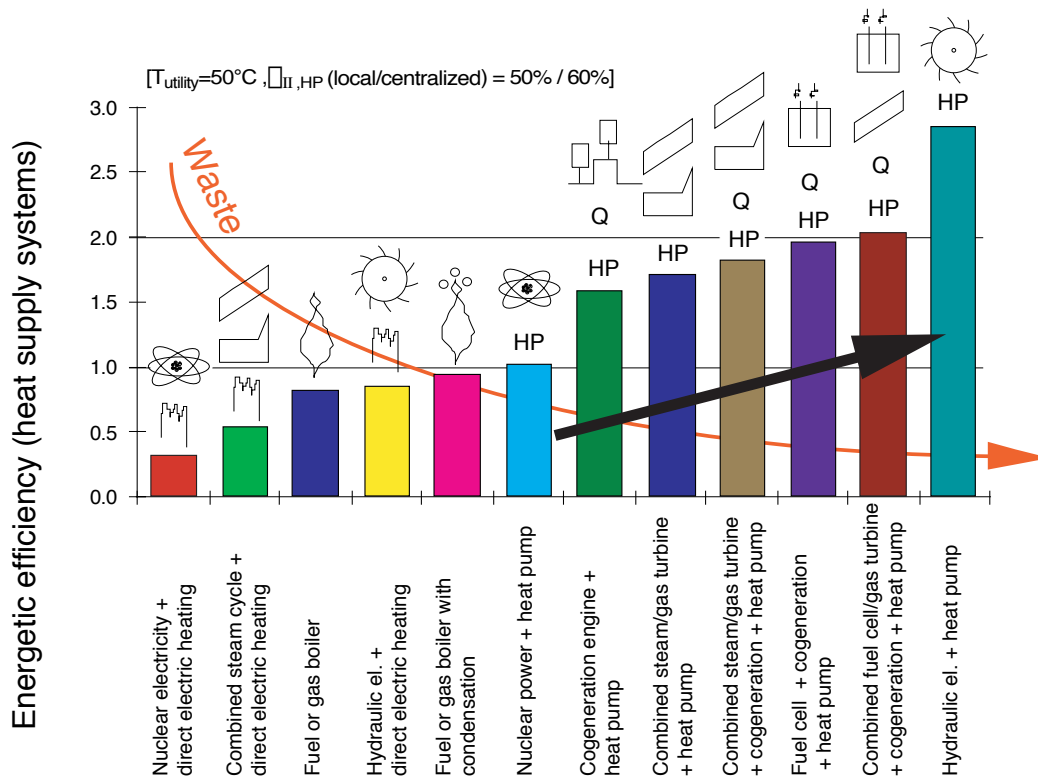


Figure 1.1: Energetic efficiency of alternative technologies for heating at 50°C: centralized heat distribution (network thermal losses 5%, heat pump exergy eff. 60%, network temperature 65°C), local heat production (heat pump exergy eff. 50% $T_{atm}=0^{\circ}\text{C}$.), $T_{atm}=0^{\circ}\text{C}$, updated from [Favrat and Tastavi, 1995].

- The development of a generalized simulation model including all the investigated enhanced solutions.
- Detailed experimental investigation of the migration of oil through the heat pump cycle, specifically in two-stage compression cycles, where it consists of a major problem in reliability and safety, for continuous operating mode.

The first chapter shows an overview of the content of this work and provides the theoretical background, considering the heat pump applications. The aspect of the refrigerant selection is discussed by means of an original **screening method of new possible refrigerant (mixtures)**, which is based on a **multi-objective optimization approach**.

In chapter 2, different design concepts related to the thermodynamic cycle (with a proposed **superstructure**), are presented, which enable highly extended application ranges and have improved efficiency at a larger external temperature lift. **Test results** of the selected and realized solutions are presented and discussed.

To allow an extended interpretation of the test results (often limited to one or two refrigerants), a **steady state simulation model** has been developed (chapter 3), including a new simulation approach for a **scroll compressor with intermediate vapor injection port** and a **flow map based evaporation heat transfer model**, using namely the results obtained by [Kattan, 1996; Zürcher, 2000]. The model is completed by a general model of the plate heat exchangers and the capillary tube (used in the intermediate injection stage). These component descriptions allow to calculate the proposed heat pump cycles and to perform parametric optimization on the system design. A specific heating curve has been selected to compare the simulation results of the different setup. All these theoretical results are presented in chapter 4.

Two-stage compression cycles are identified as the most effective solution and allow modulated heat output. A major challenge in the design of the two-stage compression approach in small to medium capacity heat pumps, is the **migrating oil** which is transported by the refrigerant through the cycle. A new proposed measurement approach using the powerful Fourier Transform Infrared Spectroscopy, enables accurate **on-line oil concentration measurement**, even for zeotropic refrigerant mixtures with oil. This method also allows the control of the composition of the used refrigerant blends. Calibration tests and on-line oil-migration measurements in a single-stage and two-stage compression heat pump cycle are presented in chapter 5.

1.2 Theory of heat pump processes

The **thermodynamic cycle** for a freezer, a refrigerator, an air conditioning unit or a heat pump is identical. The characterization of each of these units is given by the temperature level of the utility. With a refrigerator, the purpose is to maintain a room at specific cooling conditions (stable temperature at 4°C), while heat is rejected at ambient temperature. A heat pump in general transforms energy from a lower temperature level to a higher, requiring an exergy input, which can be either:

- Mechanical energy in so called bi-thermal vapor compression systems.
- Thermal energy in so called tri-thermal systems like the absorption systems.
- Electrical energy in thermo-electric and magnetic heat pumping systems.

The ideal case of a heat pump process operated between two thermal sources at constant temperature, is represented by the **Carnot cycle**, delimited by *two isentropic and two isothermal transformations*, see rectangle in the Figure 1.2. All the transformations are reversible and the process can be operated indifferently as a heat pump (counter-clockwise) or as a work generating cycle (clockwise). The isentropic transformation can be interpreted as an adiabatic and friction-free compression or expansion with exchange of work, while the two isothermal transformations are transformations with exchange of heat, supposing an infinite heat exchange surface.

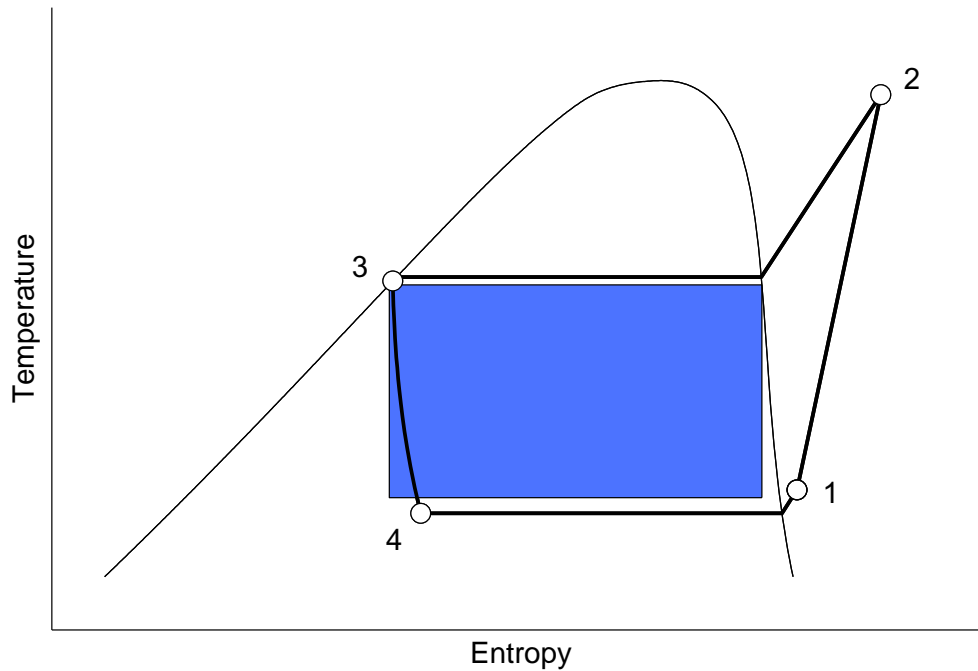


Figure 1.2: Comparison of the theoretical heat pump cycle (Carnot cycle) with the reversed Rankine cycle on a T - s diagram.

As the Carnot process represents the theoretical cycle, engineers and chemists had to imagine how to realize the cycle in practice. Heat exchange with no temperature change can be achieved by phase change of fluids. To meet the different saturation temperature levels, the fluid must change in pressure, which is done by compression of vapor, or by a change of the chemical composition, see the *absorption heat pumps*. The cycle of a vapor compression heat pump is termed as the **reversed Rankine cycle** (1-2-3-4-1 in Figure 1.2), referring to the Rankine cycle for steam power plants.

Considering the effective temperature glide of the external flows, traversing the heat exchangers, the Carnot cycle does not represent the most efficient cycle anymore and a *Lorenz* cycle with adapted temperature glides in both heat exchangers, minimizes temperature difference and thus entropy creation during the heat transfer (Fig. 1.3).

Performance indicators:

For the example of an air-water heat pump, some performance indicators are calculated, in order to show the quality of the cycle. The energy balance is applied to the external system frontier, which includes the heat pump unit and its external flows. On the air side, the fan and the air channels from outside aspiration until the rejection to the atmosphere are considered. On the hydronic heating system, the pump and the piping from and to the supposed water buffer tank are included.

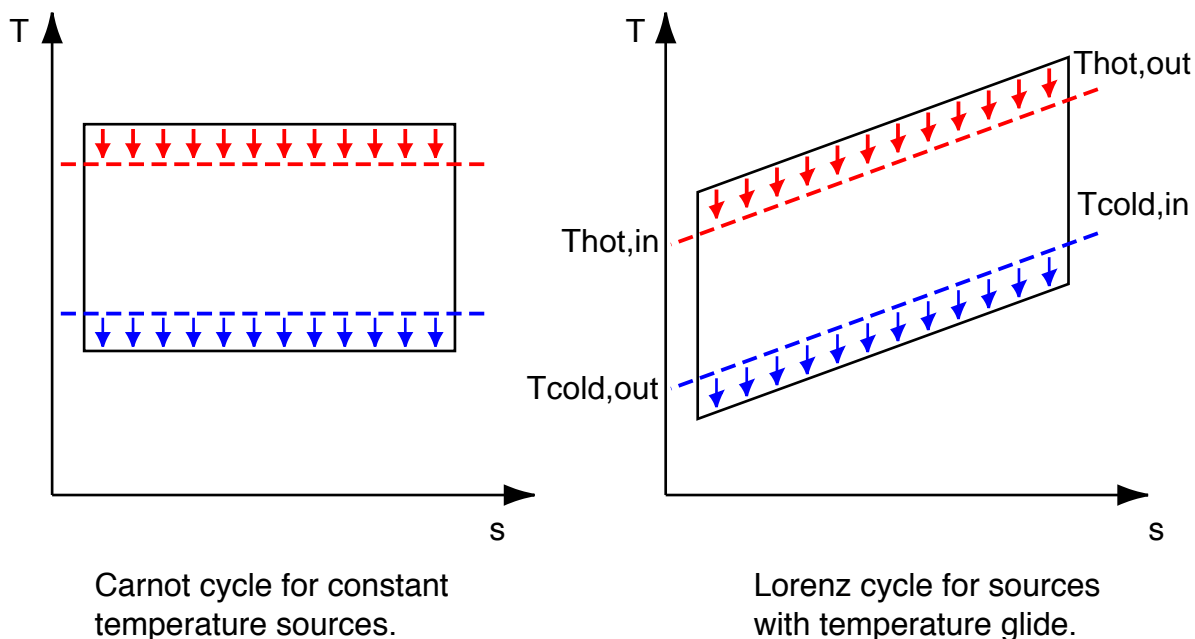


Figure 1.3: Comparison of Carnot and Lorenz cycles, respective to their adapted application cases.

In steady state conditions the energy balance is composed of the three contributions^{1,2}:

$$\sum \dot{E}_{work}^+ + \dot{Y}_{cold}^+ - \dot{Y}_{hot}^- = 0 \quad (1.1)$$

with the energy transformation rates:

$$\text{cold source: } \dot{Y}_{cold}^+ = \dot{M}_{cold} (h_{cold,in} - h_{cold,out})$$

$$\text{hot sink: } \dot{Y}_{hot}^- = \dot{M}_{hot} (h_{hot,out} - h_{hot,in})$$

and with the work inputs: $\sum \dot{E}_{work}^+$ all high level exergy inputs (here in electric form)

The **energy efficiency** η_I (also referred as the 1st law efficiency) of heat pump cycles is calculated, using the expression

$$\eta_I = COP = \frac{\dot{Y}_{hot}^-}{\sum \dot{E}_{work}^+} \underset{HP}{\text{air-water}} \frac{\dot{Q}_{hot} + \dot{E}_{pump}}{\sum \dot{E}_{cp} + \dot{E}_{fan} + \dot{E}_{pump}} \underset{\dot{Q}_{hot} \gg \dot{E}_{pump}}{\approx} \frac{\dot{Q}_{hot}}{\sum \dot{E}_{cp} + \dot{E}_{fan} + \dot{E}_{pump}} \quad (1.2)$$

This number, which is greater than unity, is also referred as the **Coefficient of Performance (COP)** for heat pump systems. The missing energy input in the denominator, is the freely accessible energy from the environment, and has therefore not to be accounted on the efficiency definition.

¹The variations of kinetic and potential energy represent in this context a negligible contribution to the energy balance, and the two terms are not considered.

²Concepts and theoretical approach correspond to the textbook [Borel, 1991] (4th edition, in preparation), where the concept of *energy transformation* is here expressed by Y in order to prevent the confusion with *work*, that the initial designation of W was inducing. Exponents $+/-$ act to the flow direction.

This entirely renewable energy can be extracted by heat exchange, from the atmospheric air, the soil or from surface water sources (lakes and rivers). While the coefficient of performance is mostly applied to quasi instantaneous operating conditions (ratio of heat output to consumed (electric) energy over a representative working cycle), it is also calculated for the time space of a heating season (seasonal COP or **SCOP**) and enables appropriate system comparison.

Measured seasonal performances and their evolution over several years of more than 120 installed heat pumps of different types, are presented in [Erb et al., 2001], showing a high stability of the efficiency during several years heating of the installed units.

A much more expressive indicator in energy conversion systems is the **exergetic efficiency** η_{II} (or 2nd law efficiency). Energy terms are replaced by the corresponding exergy in- and outputs¹. For a given atmospheric temperature T_{atm} the exergetic terms are calculated according to:

$$\sum \dot{E}_w^+ - \dot{E}_{y,hot}^- + \dot{E}_{y,cold}^+ = \dot{L}_{system} \quad (1.3)$$

with the exergy transformation rates, in general: (1.4)

$$\dot{E}_y^+ = \dot{M}(k_{in} - k_{out}), \text{ using the co-enthalpy, with } k = h - T_{atm}s$$

and the exergy work rate: $\sum \dot{E}_w^+$

As in the definition of the COP, the exergetic contribution $\dot{E}_{y,cold}$, has not to be added to the definition of the 2nd law efficiency for heating heat pumps.

$$\eta_{II} = \frac{\dot{E}_{y,hot}^*}{\sum \dot{E}_w} = \frac{\int_{hot} \left(1 - \frac{T_{atm}}{T_{hot}}\right)^{**} \delta \dot{Q}_{hot}}{\sum \dot{E}_w} \quad (1.5)$$

$$*) \dot{E}_{y,hot} = \dot{M}_w \Delta k = \dot{M}_w \Delta h - \dot{M}_w T_{atm} \Delta s \stackrel{\dot{Q}_{hot} \gg \dot{E}_{pump}}{=} \dot{Q}_{hot} - \int \frac{T_{atm}}{T_{hot}} \delta \dot{Q}_{hot}$$

$$**) \left(1 - \frac{T_{atm}}{T_{hot}}\right) \text{ is commonly known as the } \textit{Carnot factor}. \quad (1.6)$$

A theoretical (reversible) heat pump cycle is characterized with an isentropic compression and expansion and with ideal heat exchange (no temperature difference between the external flow and the refrigerant circulating inside the closed heat pump cycle). With given temperature glides, the exchanged heat rates are calculated with the integral of the function $T dS$ and result in

¹An explicit numerical example comparing the exergetic losses (irreversibilities) in two types of heat pump cycles, is given in the Annex A.1.

$$\dot{Q}_{hot} = \left(T_{hot,in} + \frac{\Delta T_{hot}}{2} \right) \Delta S \quad (1.7)$$

$$\dot{Q}_{cold} = \left(T_{cold,out} + \frac{\Delta T_{cold}}{2} \right) \Delta S \quad (1.8)$$

with $S =$ total entropy

The first law efficiency for the reversible *Lorenz cycle* is

$$\eta_{I,Lorenz} = COP_{Lorenz} = \frac{\dot{Q}_{hot}}{\dot{Q}_{hot} - \dot{Q}_{cold}} = \left(1 - \frac{\dot{Q}_{cold}}{\dot{Q}_{hot}} \right)^{-1} = \left(1 - \frac{T_{cold,in} + T_{cold,out}}{T_{hot,in} + T_{hot,out}} \right)^{-1} \quad (1.9)$$

Note: With constant source temperatures the equation of the *Lorenz cycle* COP is providing the *Carnot cycle* coefficient of performance. In applications with symmetric temperature glides on the external flow ($\Delta T_{hot} = \Delta T_{cold}$), the COP values of the Carnot cycle and the Lorenz cycle differ only marginally¹.

The evolution of the theoretical coefficient of performance is shown in Figure 1.4, using the simplified expression of the Carnot cycle COP, which is given with:

$$\eta_{I,Carnot} = COP_{Carnot} = \left(1 - \frac{T_{cold}}{T_{hot}} \right) \quad (1.10)$$

The comparison of measured cycle performance with the corresponding theoretical value leads to a simplified expression of the exergetic efficiency, where the theoretical cycle COP is the Lorenz cycle COP².

$$\eta_{II,Lorenz} = \frac{COP_{real}}{COP_{Lorenz}} = \left(1 - \frac{T_{cold,in} + T_{cold,out}}{T_{hot,in} + T_{hot,out}} \right) COP_{real} \text{ for } T_{cold} = T_{atm} \quad (1.11)$$

Tested³ brine/water (B0/W35) and water/water (W10/W35) domestic heat pumps show maximum exergetic efficiency (according to eq. 1.11) of 57%. Extending the system frontiers to the air of the heated room (at 20°C) and not only to the hydronic heat distribution system the best exergetic efficiency drops to 24%. Improved efficiency can be achieved in reducing as much as possible the system temperature difference. A second issue will be to find an environmentally benign

¹As an example shows: $T_{cold,in} = 0^\circ\text{C}$, $T_{hot,out} = 50^\circ\text{C}$, glide=10 K, the relative difference between COP_{Lorenz} and COP_{Carnot} is 1.5%.

²The Carnot cycle COP can be used conveniently, if no information about the external temperature glides is available.

³Collected test data (1993-2003) at the Swiss Heat Pump Test Center in Töss according to normalized conditions, EN-255, [WPZ, 1993-2003].

refrigerant, which allows direct contact with the external thermal sources (direct evaporation and condensation systems).

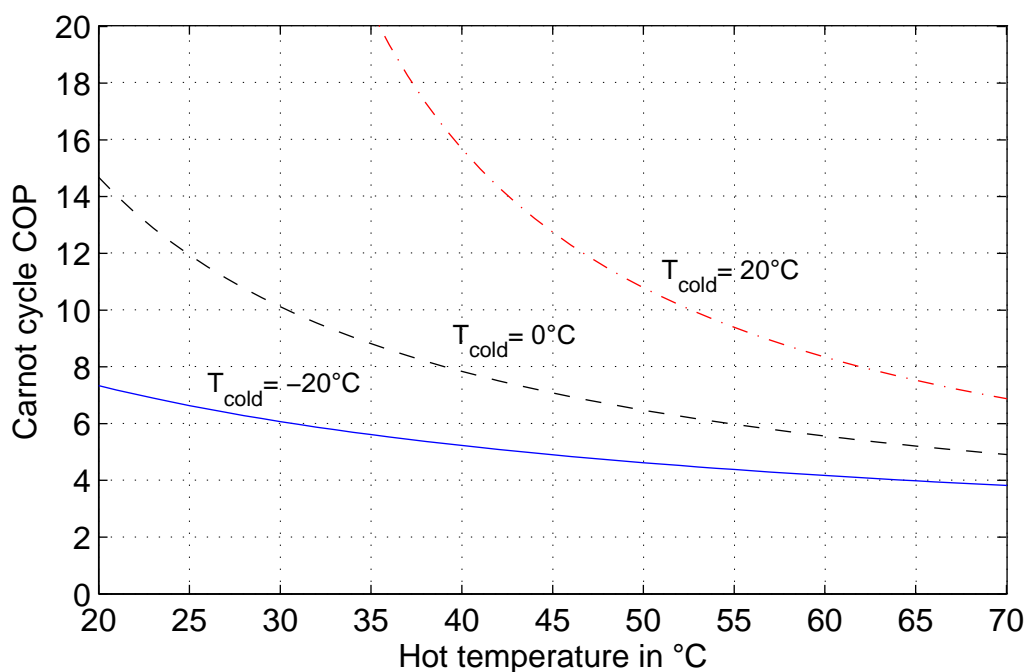


Figure 1.4: Heating COP for theoretical cycle (Carnot cycle), with variable ambient (cold) and heating (hot) temperatures.

In the case of the **retrofit of fuel boilers, in residential heating systems**, the external source temperatures are imposed by the house heating network and unless major building envelope retrofits are made, these can only marginally be modified. Nevertheless the imposed working conditions are much less adapted to a heat pump application than in the case of a newly designed heating system. **Hydronic heating distribution with temperatures up to 65°C or more** are very common, which correspond to the particular range of heat pump considered in this report. The selection criteria of the adapted heat pump type, which can replace the existing heating system, are:

- Water/brine source heat pumps
 - ++ Higher average efficiency.
 - + Less demanding in peak electricity consumption.
 - + Quiet, no ventilator.
 - + Compact system, reduced problems for accessibility in the house.
 - Expensive.
 - In some areas restrictions to use the ground, because of ground water protection.

- Air source heat pumps
 - ++ Economic.
 - Noise induced by the fan.
 - Low heat output at extreme operating conditions.
 - Need for defrosting.
 - Lower COP, except for domestic hot water in summer.

In cities and in retrofit conditions, air-water heat pumps are more realistic, but actual systems do not meet the requirements of the large majority of heating systems. **Solutions are presented in this work, in order to improve simultaneously the heat output characteristic, system efficiency and to extend the application range of air-water heat pumps.**

1.3 Refrigerant selection - screening of new blends

Many efforts in chemical engineering have been undertaken to find appropriate fluids for the refrigerating systems, considering safety and stability issues. Since the introduction of the fluorinated refrigerants in 1930 [Midgley and Henne, 1930], many different non-toxic and non-flammable refrigerants appeared on the market (for the different temperature ranges). In the late 1980's due to the accepted elimination of chlorinated refrigerants, several HFC refrigerants and (some selected mixtures) were identified as drop-in replacement of the most fluids used at that time, like: HFC-134a for CFC-12, HFC-404A for R-502 and HFC-407C (and R-410A) for HCFC-22. A large number of publications related to the refrigerant selection and to the screening of new refrigerants replacing the CFC and HCFC refrigerants can be found in the literature, e.g. [Calm, 1998; Didion, 1999; Vorster and Meyer, 2000]. Other studies are focusing on natural refrigerants, especially the hydrocarbons [Ghodbane, 1999; Granryd, 2001]. Only a few of the publications to our knowledge focus on higher temperature lift [Kazachki and Gage, 1997] and [Engler et al., 1999]. In the latter, a comparison of 82 pure candidates has been done over a wide range of evaporation and condensation pressures, comparing their performance, pressure ratio and discharge temperature in a theoretical heat pump cycle. **The results of the article show, that the best performing refrigerants are unfortunately all flammable (several hydrocarbons, ammonia and HFC-32).**

In order to complement the above mentioned results, a systematic approach is made here to evaluate best candidates of pure refrigerants or arbitrarily composed mixtures (up to 4 components), using an adaptive fluid interface code, called FLINT, internally developed at the LENI¹, which allows to run the REFPROP code (with version 7, [Lemmon et al., 2002]) within the developed

¹LENI=Laboratoire d'Energétique Industrielle (Laboratory of Industrial Energy Systems) at the Swiss Federal Polytechnical University in Lausanne, Switzerland.

Matlab models. **An evolutionary multi objective optimization tool**, MOO, developed by [Leyland, 2002; Molyneaux et al., 2001] is used to perform the systematic evaluation of new high performance refrigerant mixtures.

The evaluation of such fluids has to consider different aspects, which are listed here below:

- **Thermodynamic properties**

Normal boiling temperature $< -20^{\circ}\text{C}$

Critical temperature $> 70^{\circ}\text{C}^1$

Maximum system temperatures: Is limited by the thermal stability of the lubricant. Limiting the maximum system temperatures will generally have a positive impact for the lifetime of the compressor. However, no limit has been set for the present evaluation process.

Maximum pressure level: Has a direct impact on the fabrication costs of the heat pump. High pressure levels (> 30 bar) require non standard elements (and represent therefore a price premium) for developments in the near future. In the optimization process, no limit has been imposed.

- **Compatibility with materials**

For short term developments it is recommended to ensure compatibility with common materials of the refrigeration sector (mainly copper, steel and Teflon). Compatible materials are already available for most of the refrigerants considered in this work. One main exception is ammonia, which is not compatible with copper, and in combination with its high toxicity is not a major candidate for low cost systems. Ammonia is therefore excluded from the evaluation, but is kept for comparison in some of the figures.

- **Safety properties**

Flammability and toxicity for the fluid is a major concern in the design of heat pump units and will influence production costs. The resulting solutions will be post analyzed regarding these criteria.

- **Availability and price**

The availability of new types of refrigerants and mixtures is the most restrictive aspect for the selection of the fluid and the homologation process for new candidates can strongly delay their market introduction. Due to the worldwide low market share of heat pumps and mainly in the retrofit sector, it might take a while for propositions of new mixtures, adapted for this application, to be considered in large scale in the near future. Actual replacement candidates are limited to HFC blends, excluding flammable and highly toxic mixtures.

¹Trans-critical cycles (using e.g. CO₂ (R-744), Methane (HC-170)) are not considered in this work due to the important exergetic losses on the heating side, when temperature glide in the heat distribution system is small. Trans-critical cycles are more intensively considered in air-conditioning units for the automotive sector, where very compact systems are needed, or for hot water boilers, where a high temperature glide exists on the water side.

1.3.1 Simulation conditions

A semi theoretical approach has been chosen for the comparison of arbitrarily composed refrigerant blends. A heat pump cycle with suction line heat exchanger and pinch based heat exchanger models, has been simulated, using the following input parameters:

1. Adaptive air flow on the evaporator with fixed inlet and outlet temperatures of $0^{\circ}\text{C}/-4^{\circ}\text{C}$.
2. Heating water on the condenser with fixed temperature glide (in/out) of $45^{\circ}\text{C}/50^{\circ}\text{C}$.
3. Suction overheat (referred to the dew point saturation temperature) at compressor inlet of 6 K. In order to take the advantages of an eventual temperature glide of zeotropic mixtures, all the superheat is assumed to be taken by an internal suction line heat exchanger.
4. The pressure levels of the heat pump are calculated to meet the minimal temperature difference (pinch) in the heat exchangers, ΔT_{\min} : evaporator 4 K, condenser 2 K.
5. The compression efficiency is fixed to the value of 60% (isentropic efficiency). The volumetric efficiency is set to an ideal value of 100%.

In the considered case of a high temperature lift heat pump, the extreme operating condition is set to 65°C heating output temperature at the external air temperature of -12°C . This point corresponds therefore to the most demanding point in terms of heat rate, while cumulating the energy demand during a heating season, the most important heat requirements in function of the atmospheric temperature, are seen at moderate operating conditions. For the example of Zurich (see Fig. 4.2), the energy requirements are the most important at 0°C , at which this screening is applied to.

1.3.2 Fluid properties and performance

Refrigerant candidates with thermodynamical properties, which fit to the aimed application, are listed in Table 1.1 and their respective calculated performance is plotted in Figure 1.5.

The refrigerants in Figures 1.5-1.7 are visually separated into 3 classes: bullets (red): **HC + ammonia**, diamonds (black): **(H)CFC** and squares (blue): **(H)FC**. The (H)CFC's have been maintained in this comparison for academic reasons, although they are already suppressed from most markets for new systems, due to their ozone depletion potential - ODP. For this reason their physical and safety properties have not been included in the table. HFC's are considered in industry as the *long term* replacement refrigerants, but several European countries are about to heavily reduce the use of these refrigerants having a high global warming potential (GWP, see Table 1.1).

The non colored points on the Figure 1.5, represent the fluids which are only considered for the use in blends as their normal boiling point temperature is too high ($>-20^{\circ}\text{C}$) for the air-water heat pump application. Fluids presenting a lower critical temperature than 70°C and therefore leading to trans-critical cycles have not been included in the optimization procedure.

In addition to the calculated performances, the pressure level and the discharge line temperature are plotted. These are representative indicators for eventual increased system cost and for reliability. In actual components, pressure levels of max. 30 bar and temperatures $< 120^{\circ}\text{C}$ are common and should not be exceeded. Lower pressure ranges allow to design the heat exchangers with thinner walls, leading to improved heat transfer performance. The maximum discharge temperature criterion is less critical, since the improved concepts of air-water heat pumps facilitate a drastic reduction of these values at the extreme operating conditions. Figures 1.6 and 1.7 however show that ammonia (R-717) and methylene fluoride (HFC-32) are completely out of range for at least one of these criteria and would be highly penalized by increased cost.

Table 1.1: Physical properties, flammability and global warming potential of selected pure refrigerants, from [Calm, 1998]

Refrigerant Name	Molar Mass g/mol	NBP $^{\circ}\text{C}$	T crit $^{\circ}\text{C}$	TLV-TWA PPM	LFL %-vol.	HOC MJ/kg	GWP 100 years
HFC-32	52.02	-51.7	78.1	1000	14.4	9.4	550
HFC-125	120.02	-48.1	66.0	1000	none	-1.5	3400
R-1270	42.08	-47.7	92.4	600	2.0	-	~20
HFC-143a	84.04	-47.2	72.7	1000	7.0	10.3	4300
HC-290	44.1	-42.1	96.7	2500	2.1	50.3	~20
FC-218	188.02	-36.8	72.0	1000	none	-	8600
HC-C270	42.08	-33.5	125.2	-	2.4	49.4	-
R-717	17.03	-33.3	132.3	25	15.0	22.5	<1
HFC-134a	102.03	-26.1	101.1	1000	none	4.2	1300
HFC-152a	66.05	-24.0	113.3	1000	4.8	17.4	120
HFC-227ea	170.03	-16.4	101.7	1000	none	3.3	3500
R-600a	58.12	-11.7	134.7	800	1.7	49.4	~20
FC-C318	200.03	-6.0	115.2	1000	none	-	10000
HFC-236fa	152.04	-1.4	124.9	1000	none	-	9400
R-600	58.12	-0.6	152.0	800	1.5	49.5	~20
HFC-236ea	152.04	6.2	139.3	-	none	3.3	1200

NBP=normal boiling point; T crit=critical temperature; GWP=global warming potential;
 TLV-TWA=ACGIH Threshold Limit Value - Time Weighted Average;
 HOC=heat of combustion; LFL=lower flammability limit

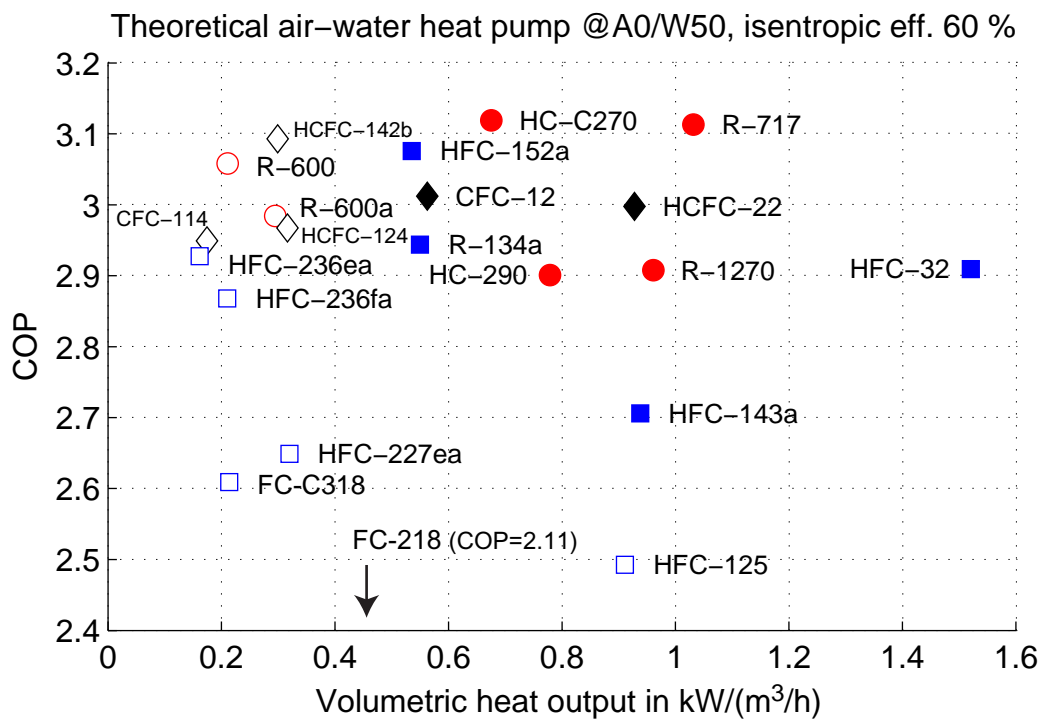


Figure 1.5: Performance chart COP vs Heat output / displacement volume (theoretical heat pump at air=0°C/water=50°C), pure refrigerants.

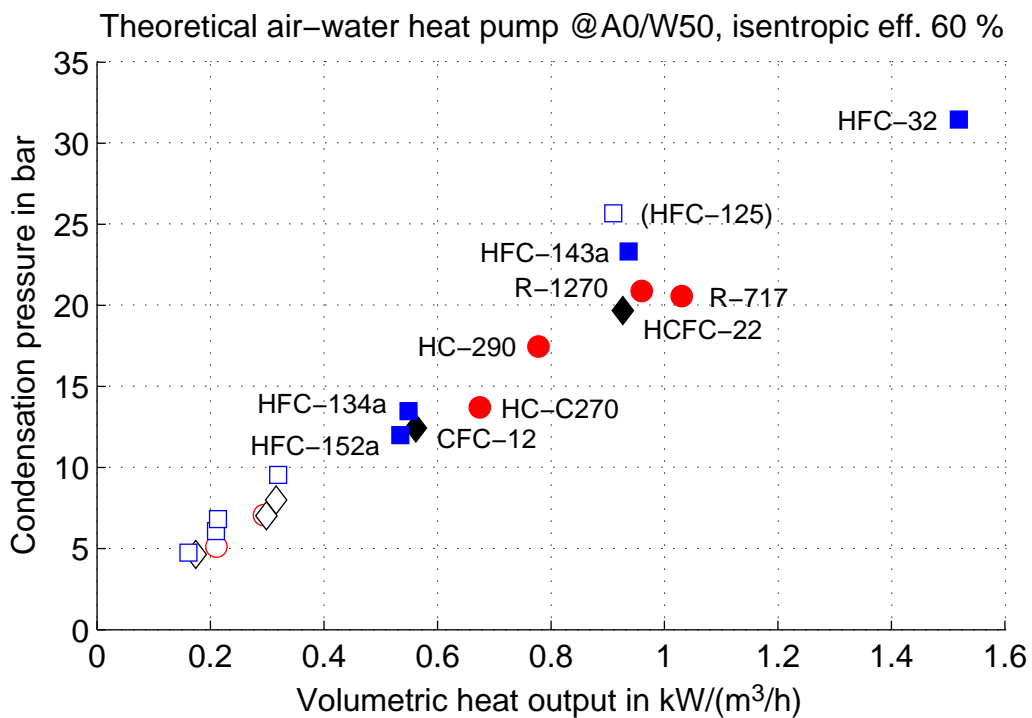


Figure 1.6: Pressure level vs Heat output / displacement volume (theoretical heat pump at air=0°C/water=50°C), pure refrigerants.

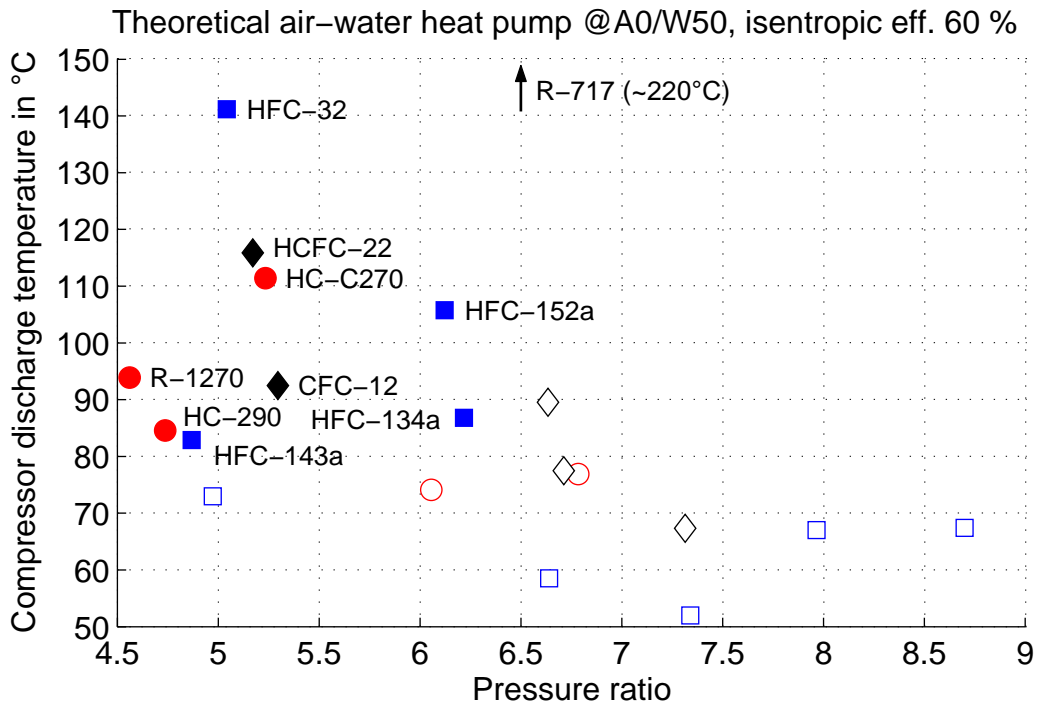


Figure 1.7: Compressor discharge temperature vs pressure ratio (theoretical heat pump at air=0°C/water=50°C), pure refrigerants.

Due to either their flammability or their ozone depletion potential, most of the pure (H)CFC and HC fluids represented in Figures 1.5-1.7 have on the market specific replacement counterparts, which either are pure HFC alternatives, or especially designed mixtures, made of HFC and HC. Calculated performance of these (chlorine free) mixtures are summarized in Table 1.2.

Table 1.2: Selected commercial refrigerant blends (HFC and HC), calculated performance data for heat pump at air=0°C/water=50°C

Refrigerant mixture name [by mass]	COP	Heat output kW/(m ³ /h)	T max. °C	P cond. bar	PR P _{cd.} /P _{ev.}
R-404A (HFC-125/143a/134a [44/52/4])	2.67	0.91	79.4	23.3	4.98
R-407C (HFC-32/125/134a [23/25/52])	3.00	0.95	98.6	21.2	5.30
R-407D (HFC-32/125/134a [15/15/70])	3.03	0.81	95.0	18.2	5.51
R-410A (HFC-32/125 [50/50])	2.81	1.35	107	30.7	5.00
R-413A (FC-218/HFC-134a/R-600a [9/88/3])	2.93	0.59	82.3	14.3	5.88
R-417A (HFC-125/134a/R-600 [46.6/50/3.4])	2.89	0.75	78.9	18.2	5.29
R-507A (HFC-125/143a [50/50])	2.63	0.91	78.6	23.9	4.96

1.3.3 Refrigerants in commercial products

Considering commercialized heat pumps (air/water, water/water and brine/water), the refrigerants used in tested units, see Figure 1.8, in the time period 2002-2003 are HFC-134a (16% of all units), R-404A (4%), R-407C (62%) and R-410A (18%). A few units have been operated with R-417A (in 2000/2001) and several with HC-290 (1994-2002). The phase out of HCFC-22 has been practically done within half of a decade (1993: 100%, 1997: 0%), although the last test with this refrigerant was performed in 1999. Considering only the air-water heat pumps of the period 2002/2003, out of the 18 published results, 14 used R-407C, 4 units were charged with R-404A and one unit with HC-290. The figure also shows, that the heat pump suppliers are ready to bring to the market concepts with alternative refrigerants. In some cases the availability of components (e.g. no compressor available for propane) has stopped the use of these refrigerants. Other refrigerants have been dropped due to lower efficiency or too high cost.

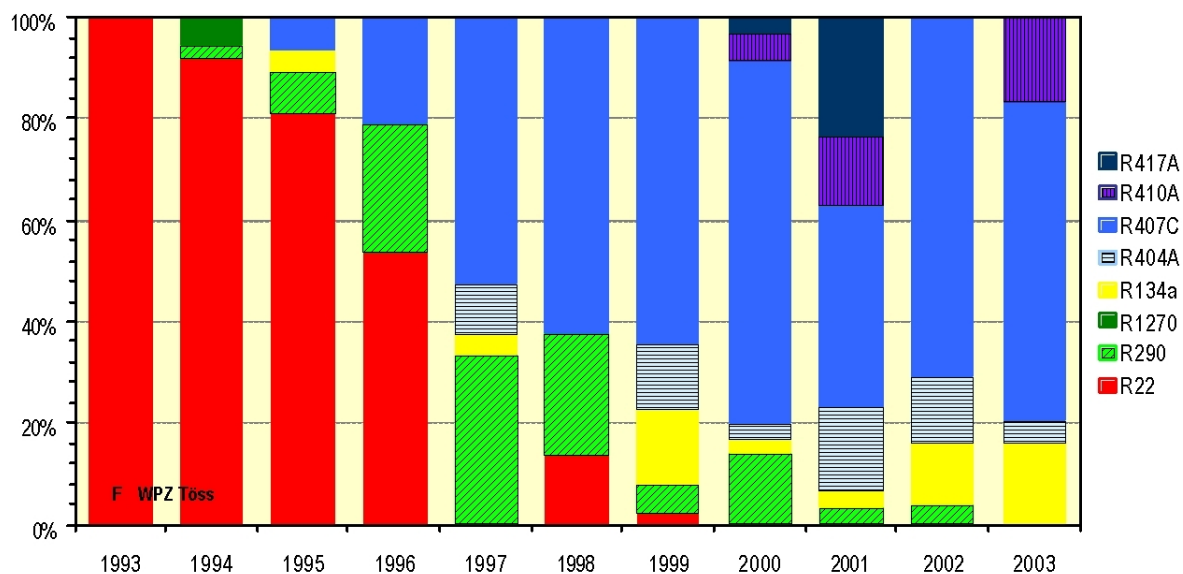


Figure 1.8: Refrigerants in use of tested heat pumps. Figure from Swiss Heat Pump Test Center, Bulletin 37 [WPZ, 1993-2003]

Comparing the simulated COP at the specified operating point A0/W50 of the commercially used refrigerants in residential heat pumps, shows that the commercial blend R-407C (COP=3.0) is one of the best performing refrigerants (excepting R-407D).

1.3.4 Research of new substitution blends for high temperature air-water heat pumps

For the screening of the best combinations of known refrigerants, two distinct objectives are chosen to run in the optimization routine: **COP and volumetric heat output (which corresponds to the ratio of heat output to the displacement of the compressor)**. This trade off has been set in order to reasonably choose between size of the components and efficiency. Observing the envelope of a saturation curve it can be shown, that the two objectives are in opposition (best COP is reached for cycles far from the critical point, having reduced throttling losses and the highest heat output is obtained at higher pressures and densities, therefore when the operating conditions approach the critical point).

All the locally best solutions (e.g. no better COP at one volumetric heat output and vice-versa), can be represented on a *Pareto-optimal frontier*, see [Leyland, 2002]. If we hypothetically limit the search on pure fluids (even if rigorously no optimization has been performed yet, but a simple selection), the Pareto-optimal frontier is composed by HC-C270, R-717 and HFC-32 (see Figure 1.5), followed on the second level (when the first Pareto-optimal points are removed) by HFC-142b, HFC-152a, HCFC-22 and R-1270. All of these fluids are classified as flammable according to the standard safety classification [ASHRAE, 2001], with the exception of HCFC-22, which is on the way to be phased out ($ODP > 0$).

The algorithm of the selected optimization tool uses the Pareto-optimal frontier to rank new evaluated points in relation of the existing population. Optimal points are kept and by combination new points will be created by a genetic type of algorithm. By this approach the Pareto-optimal curve evolves rapidly to a set of optimal solutions. A major attribute of the MOO optimizer, and distinguishing it from many other tools, is the ability to treat multi variable systems with a high degree of discontinuities (such is the case, when the algorithm changes the constituents of the mixture). By the nature of this approach it is impossible to know if (all) the optimal solutions have been identified. Selecting a large randomly composed initial population, increases the part explored in the space of the solutions.

Figure 1.9 visualizes an **example of three component blends, multi objective optimization restricting to the three common refrigerants, which are: HFC-125, HFC-134a and HFC-32**. Before running the optimization problem, a look on the performance chart in Figure 1.5, shows, that the two refrigerants HFC-134a and HFC-32 are clearly better performing (closer to the imagined Pareto-optimal curve) than HFC-125. It is therefore very likely, that the solution space will converge to a set of binary mixtures of the first two fluids. The line in the objective graphs represents the location of this couple with variable composition, including the limits of pure HFC-134a and pure HFC-32. This line is coinciding with the points found on the final Pareto-optimal frontier, as has been expected before. The rise of COP, comparing to the pure fluids, can be explained with

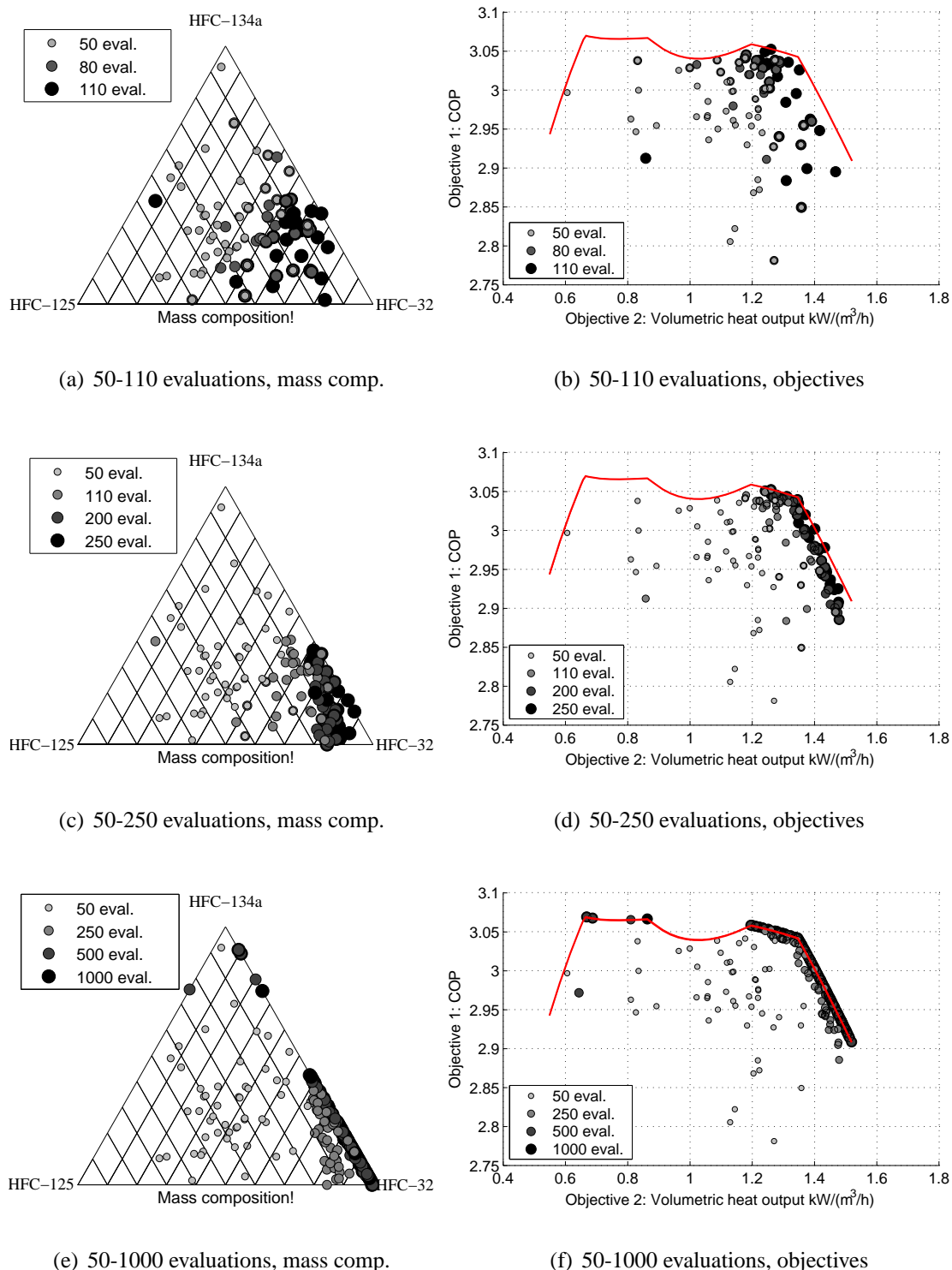


Figure 1.9: Example of a two-objective optimization (on COP and volumetric heat output of a heat pump at A0/W50) for the three component blend HFC-32/125/134a using MOO [Leyland, 2002]. graphs a+b and c+d represent intermediate results, e+f includes the final population. The line in the objective graphs represents the binary mixing from pure HFC-32 to pure HFC-134a and corresponds to the attended limiting curve for the optimization problem.

the adaptation of the saturation temperature glide of the non-azeotropic blend with the external flows. In the central part of this mixing line the COP is slightly lowered, when these temperature glides are becoming too important.

When observing the final set of solutions, the best COP is at 3.07 (corresponding to the mixture composition HFC-32/134a [9/91 by mass]) and the heat output is equivalent to 0.67 kW per m³/h displacement. About the double of heat is delivered with a mixture HFC-32/134a [76/24], with a COP on the same level (3.04 with 1.35 kW/(m³/h)). This increase of heating performance has to be paid with an important increase of the condensing pressure level (from 15 bar to 26 bar) and of the discharge temperature (90°C to 125°C). And the latter of these two mixtures is considered as flammable. The limit of flammability is given at max 42% of HFC-32 at 60°C, see [Didion, 1999]. The recommended mixture, taking into account of all these considerations, is represented at the point (COP=3.07, volumetric heat output=0.86 kW/(m³/h)), given by the mixture HFC-32/134a [25/75]. Comparing to the commercial R-407C (HFC-32/125/134a [23/25/52]) this represents a gain of 2% on the COP and a reduction of 9% on the heat output. Looking to the existing standard mixtures for these components, the most similar blend is R-407D (COP=3.03, volumetric heat output=0.81 kW/(m³/h)).

The optimization has then been applied for the total of 17 pure fluids: HC-170, HC-C270, HC-290, R-600, R-600a, HC-1270, HFC-32, HFC-125, HFC-134a, HFC-143a, HFC-152a, HFC-227ea, HFC-236ea, HFC-236fa, HFC-245fa, FC-218 and FC-C318. All CFC and HCFC fluids were not considered in this calculations. Neither to ammonia (R-717), due to its combination of negative attributes: toxicity, flammability and incompatibility with copper.

The thermodynamic properties of all these fluids are available in the refrigerant's properties calculation software, Refprop, Version 7 [Lemmon et al., 2002] and for the constitution of the blends, many binary interaction parameters are defined. The mixing parameters for the missing pairs are calculated based on an appropriate estimation, which is set by the software itself.

Several optimization runs were performed with up to 10'000 evaluations, for each problem. A **first run of the optimization problem has been initialized to study the optimal configurations** of mixtures with up to 4 components. As most of the high performance fluids are flammable, a **second evaluation has been started to show the impact of a limitation of the flammability of quaternary blends**. For this issue a very simple approach of calculating the lower flammability limit (LFL) of an arbitrary mixture has been applied, using the molar composition of the blend and the flammability values listed in Table 1.1 attributed to each component.

$$LFL_{mix} = \sum_i \varphi_i LFL_i \quad \text{with } \varphi_i = \text{molar fraction of component } i \quad (1.12)$$

The lower flammability limit of non flammable refrigerants has been set to 100%.

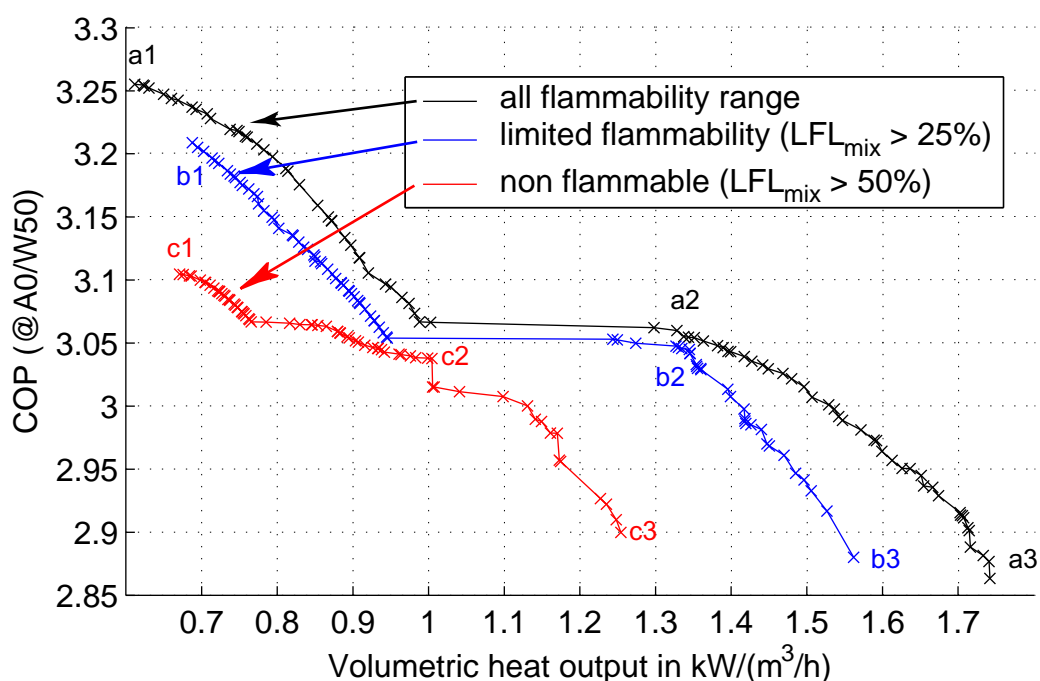


Figure 1.10: Pareto-optimal frontier for a multi objective optimization (COP and volumetric heat output, heat pump@A0/W50) of arbitrary refrigerant mixtures (max. 4 components, 17 selected pure fluids, using REFPROP 7). Frontiers for mixtures at distinct flammability degrees indicated.

Figure 1.10 with the extracted data in Table 1.3 shows the **importance of parameterizing the flammability limit**. In the **third optimization run, a minimum flammability limit of 50% (curve c1-c2-c3) for the mixture is set, using the eq. 1.12**. These fluids are considered to be non-flammable. The maximum attainable COP is at 3.10, which corresponds to a relative improvement of 3% compared to the reference fluid R-407C. The heat output is however sensibly reduced. Point c2 corresponds to the mixture HFC-32/134a, with the same mass composition, as in the run before. Performances of this mixture are very similar to R-407C. The other end of the Pareto-optimal curve

Table 1.3: Refrigerant mixture composition (mass perc.) for the selected solutions in Figure 1.10.

	Refrigerants	Composition	COP	Heat in kW/(m ³ /h)
a1	HC-C270/600	85/15	3.26	0.61
a2	HFC-32/134a/152a	3/80/17	3.06	1.32
a3	HFC-32/HC-1270/HFC-134a	82/15/3	2.88	1.74
b1	HC-C270/HFC-134a/245fa	55/18/27	3.21	0.69
b2	HFC-32/134a	76/24	3.04	1.35
b3	HFC-32/125/HC-1270/HFC-134a	60/20/10/10	2.88	1.56
c1	HFC-125/HC-C270/HFC-134a/152a	16/6/47/31	3.10	0.67
c2	HFC-32/134a	40/60	3.04	1.00
c3	HFC-32/125/236ea	37/58/5	2.90	1.26

is showing a ternary mixture with higher heat output but reduced COP.

Without any restriction in flammability, the end points of the Pareto-optimal frontiers represent best solutions in COP and in heat output, respecting the required saturation temperature range. The highest COP of 3.26 (+8% to R-407C) is given at the point a1. In this region all the solutions are mainly composed of the highly flammable hydrocarbon **cyclopropane (HC-C270)**, which has already been considered in some comparative studies before, see [[Ghodbane, 1999](#); [Granryd, 2001](#)], in the context of automotive air-conditioning systems. Measured efficiency comparison including cyclopropane are published by [[Kim et al., 1993](#)], showing improved efficiency of 6% - 7% compared to CFC-12 in a domestic refrigerator. The very low volumetric heat output of these mixtures require an increased component size, which is a major problem for designing systems with high safety requirements. On the opposing end of the performance graph, the major component of the found mixtures is **HFC-32**. The operation conditions result in the upper pressure range leading to increased wall thickness in the heat exchangers, which will have a negative impact on heat transfer characteristics.

The domain of highest COP has the advantage of lower pressure range. As shown in the diagram in Figure 1.11 (representing the solution HC-C270/600 [85/15]), the main inconvenience, besides the flammability, is the relatively high normal boiling point temperature, which restricts the application in colder climates.

This evaluation of new refrigerant mixtures for air-water heat pumps in residential applications shows the potential of improving the performances (COP and heat output) compared to standard refrigerants. The research of alternative mixtures is also motivated by the environmental aspect, in order to reduce the **total equipment warming impact (TEWI)** of the chosen heating system, [[Fischer et al., 1992](#)]. This warming impact is attributed in general for a minor part to the equipment

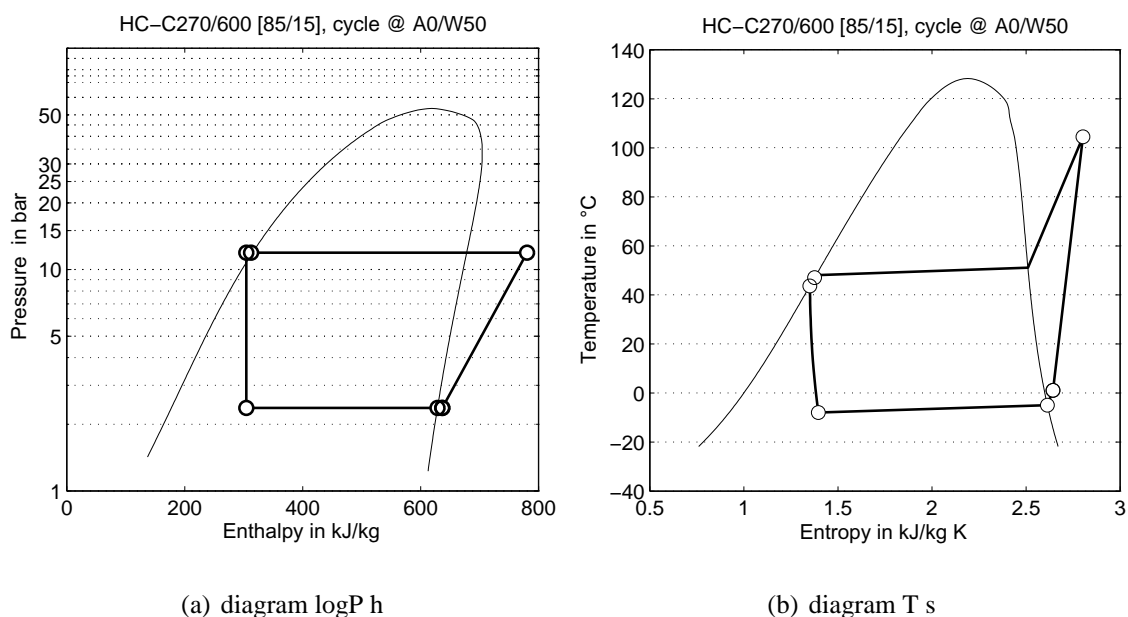


Figure 1.11: Simulated heat pump cycle at air=0°C/water=50°C with theoretical mixture HC-C270/600 [85/15], COP=3.26, $Q_{vol} = 0.61 \text{ kW} / (\text{m}^3/\text{h})$

and refrigerant leakage, and for a major part to the related energy consumption, depending on the electricity production. In order to reduce the refrigerant's contribution to the warming impact, policy makers in several countries are pushing on the use of 'natural refrigerants', which principally limit the selection to some hydrocarbons and their mixtures, ammonia and CO₂.

A calculation example shows the importance on the respective parameters, on the evaluation of the TEWI indicator.

$$\text{TEWI} = \text{GWP} \dot{L} n_{\text{years}} + \text{GWP} M_{\text{refr}} (1 - \alpha_{\text{recovery}}) + n_{\text{years}} E_{\text{el,ann}} \beta_{\text{em}} \quad (1.13)$$

The first two terms of eq. 1.13 are direct contributions (leakage and recovery losses), while the third term on the right hand side is an indirect contribution, related to the CO₂ emission of the energy source (here the electricity).

A residential heating application with an annual heat demand of $E_{th,ann} = 20'000 \text{ kWh}$, implementing a heat pump system, characterized by a seasonal COP of 2.5 and a refrigerant charge of $M_{\text{refr}} = 5 \text{ kg}$ ¹ and a running period of $n_{\text{years}} = 20$ years are assumed. Annual leakage rate is set to $\dot{L} = 1\%$ of the refrigerant charge² and refrigerant recovery is about $\alpha_{\text{recovery}} = 90\%$. With these assumptions, about 30% of the initial refrigerant charge is lost in the running period of the heat pump unit.

¹For residential heating air-water heat pumps, the typical refrigerant charge is about 0.5 kg/kWth, see [WPZ, 1993-2003].

²Ranging from 0.6% to 1.9%, see study CH4 in [Gilli et al., 1999].

Table 1.4: Direct and indirect CO₂ contributions for small size heat pump, unrecovered refrigerant 1.5 kg, annual electricity consumption 8'000 kWh with $\beta_{em} = 0.8$ kg CO₂/kWh (fossil power plant), 0.5 kg CO₂/kWh (European electricity mix), 0.025 kg CO₂/kWh (nuclear power). Considered time period 20 years.

TEWI _{direct/indirect}	with $\beta_{em} =$		
	0.8 kg CO ₂ /kWh	0.5 kg CO ₂ /kWh	0.025 kg CO ₂ /kWh
R-407C	2%/98%	3%/97%	36%/64%
Mix (Point b1)	<1%/99%	~1%/99%	16%/84%
HC-290	0%/100%	0%/100%	<1%/99%
TEWI _{total}	in T CO ₂ eq.	T CO ₂ eq.	T CO ₂ eq.
R-407C	130	82	6.28
Mix (Point b1)	129	81	4.75
HC-290	128	80	4.03

The CO₂ equivalent emission contributions of three refrigerants with distinct GWP₁₀₀ values are compared in Table 1.4 (GWP_{R-407C} = 1520 CO₂ eq.; GWP_{Mix Point b1}¹ = 500 CO₂ eq.; GWP_{HC-290} = ~20 CO₂ eq.). This theoretical evaluation shows the approximate COP gains which should be achieved in order to reduce the equivalent CO₂ emission. For fossil electricity production and for European electricity mix the direct emissions, caused by refrigerant losses, are negligible compared to the indirect emission from the power plants. Only for countries, whose electricity is mainly provided by nuclear-power (0.025 kg CO₂/kWh) and hydro-power (0.04 kg CO₂/kWh), the direct contributions are significant for all the HFC refrigerants and natural refrigerant contribute to a major reduction of the equivalent CO₂ reductions.

1.4 Market trends

Compared to the refrigeration sector the heat pump occupies still a niche market for companies acting worldwide in this segment. In some European countries, the choice to install a heat pump in new buildings in the residential sector has gained importance in the recent years, namely in Sweden (95%, 2000) and Switzerland (40%, 2002) the market share is already very high and sales increase continuously with a growing rate of 5% - 10%. Trends are highly positive in France (+87%, 1999) and Germany (+22%, 2000), pointing out some peak values according to [Rivoalen, 2001]. These extreme growth rates show, that some markets are highly unsaturated and further growth are expected for the future in all countries. The penetration in the renovation market is however still negligible and specific concepts and improved technologies have to be considered. For most

¹Composition of this mixture, see Table 1.3.

of the end consumers, profitability has to be considered, which can be expected with a favorable cost evolution of the primary energy source. While electricity price has been stable in the recent years for domestic use, the fuel oil price has been highly variable with peaks on the double level in September 2000, compared to the baseline corresponding to the end of the last century. The price evolution of fuel oil in the last 20 years (Fig. 1.12) illustrates this unstable situation, contributing to the substitution of fuel based systems by alternative heat pump systems allowing the use of renewable energy. The planned introduction of a CO₂-tax in several countries, in order to fulfill the CO₂ emissions reduction linked to the Kyoto protocol, might have an additional impact on the operating costs of fuel boiler based systems. In countries with electricity provided by nuclear and hydro-power, the CO₂ emission gain is very important, when converting fuel based to heat pump heating systems.

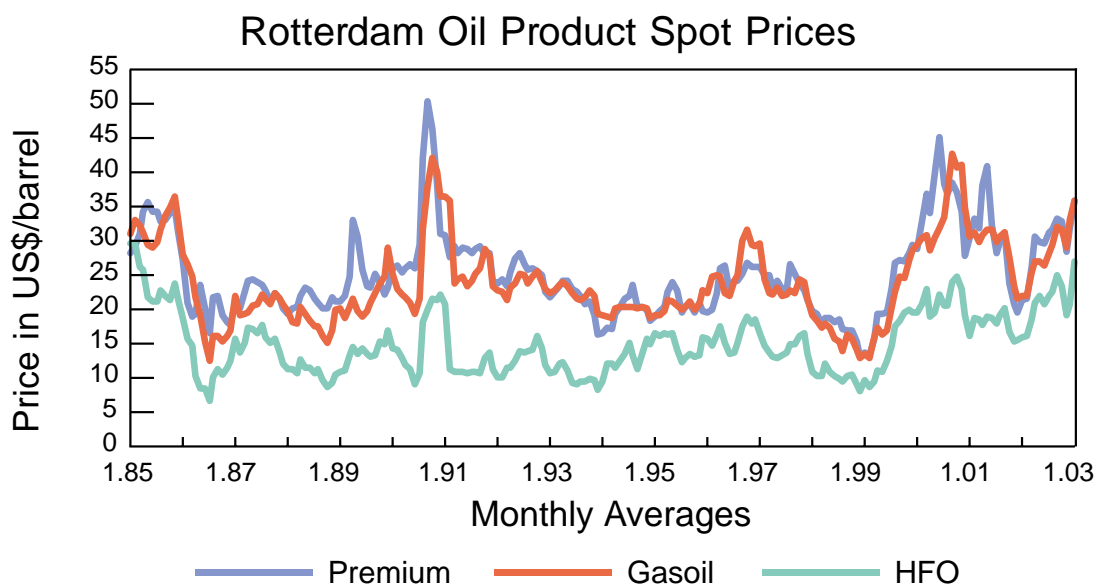


Figure 1.12: Oil price evolution for the period 1985 -2003, from [*International Energy Agency, 2003*]

1.5 Conclusions to the refrigerant selection

The presented optimization approach to evaluate new refrigerant compositions in high temperature lift air-water heat pumps for the residential sector, has demonstrated the performance increase potential on a semi theoretical simulation.

The following conclusions can be formulated:

- **Rise in COP**

An important elevation of the COP (+8% to R-407C) has been calculated at the operating point A0/W50. This improvement is mainly due to the highly flammable cyclopropane (HC-C270). The heat output intensity is however reduced by an important factor (-36% compared to R-407C). The mixture found for this calculated optimum is exclusively composed with hydrocarbons and results in a very low direct global warming impact. Reducing the flammability tolerance, then the mixtures found with high COP, have higher GWP values (point b1: $GWP_{\text{mix}} = 500$, c1: $GWP_{\text{mix}} = 1200$), which are values in the range of the HFC refrigerant class.

- **Rise in heat output**

On the other hand compact systems with a high volumetric heat output are obtained with the mixtures containing mainly HFC-32 (highest heat output + 83% to R-407C). Flammability, lower COP and higher operating pressures do not motivate the use of such refrigerants.

- **Global warming impact**

Residential heat pumps are in general compact systems with refrigerant leakage range tending to zero. The equipment warming impact, calculated for several refrigerants shows a negligible contribution related to refrigerant losses and are mainly depending on the seasonal coefficient of performance of the heating unit. One exception to this are heating systems, which are driven by 'CO₂ free' electricity (produced by nuclear or hydro, wind and solar power plants).

The application of this multi-objective optimization approach on the enhanced simulation model (see chapter 3) including real components with detailed heat transfer calculation, could not be applied due to the high calculation demands of the model and the time-frame attributed to this part. It is although proposed for future analysis to extend this general evaluation, including realistic compression efficiency and including cost based evaluations.

Bibliography

- ASHRAE. **ANSI-ASHRAE Standard 34-2001; Designation and Safety Classification of Refrigerants**, 2001.
- L. Borel. **Thermodynamique et Énergétique**. Presses Polytechniques et Universitaires Romandes, 3 edition, 1991.
- J. M. Calm. **Property, Safety, and Environmental Data for Alternative Refrigerants**. In *Earth Technologies Forum, Washington DC, oct. 26-28*, pages 192–205, 1998.
- D. A. Didion. **The Application of HFCs as Refrigerants**. In *20th Int. Congress of Refrigeration, IIR/IIF, Sydney, sept. 19-24*, volume Plenary Adresses, page Paper 728. Int. Institute of Refrigeration, 1999.
- T. Engler, L. Oellrich, G. Venkatarathnam, and S. Srinivasa Murthy. **Screening of Single Component Fluids for Compression Heat Pump Applications**. In *20th Int. Congress of Refrigeration, IIR/IIF, Sydney, sept. 19-24*, volume 2, page Paper 171. Int. Institute of Refrigeration, 1999.
- M. Erb, H. Eicher, and P. Hubacher. **Feldanalyse von Wärmepumpenanlagen**. In *8.Tagung des Forschungsprogrammes Umgebungs- und Abwärme, Wärme-Kraft-Kopplung (UAW) des Bundesamtes für Energie (BFE)*, 2001.
- D. Favrat and A. Tastavi. **Experience with 3.9 MWth Ammonia Heat Pumps**. In *IEA Heat Pump Programme, Annex 22: Compression Systems with Natural Working Fluids - Applications, Experience and Developments*, pages 81–86, 1995.
- S. Fischer, P. Fairchild, and P. Hughes. **Global Warming Implications of Replacing CFC's**. *ASHRAE Journal*, 34(4):14–19, 1992.
- M. Ghodbane. **An Investigation of R152a and Hydrocarbon Refrigerants in Mobile Air Conditioning**. *SAE Technical Paper Series, 1999-01-0874*, pages 1–16, 1999.
- P. Gilli, H. Halozan, W. Streicher, and G. Breembroek. **Environmental Benefits of Heat Pumping Technologies, Analysis Report HPC-AR6**. Technical report, IEA Heat Pump Centre, 1999.
- E. Granryd. **Hydrocarbons as Refrigerants - an Overview**. *Int. J. of Refrigeration*, 24:15–24, 2001.
- International Energy Agency. **Key World Energy Statistics**, 2003.

- N. Kattan. **Contribution to the Heat Transfer Analysis of Substitute Refrigerants in Evaporator Tubes with Smooth or Enhanced Tube Surfaces.** PhD thesis, École Polytechnique Fédérale de Lausanne, Lausanne, Switzerland, 1996. Thesis No. 1498.
- G. Kazachki and C. Gage. **Screening of Non-CFC Alternatives for High-Temperature Heat Pumps.** In *Commissions E2, E1, B2, IIR/IIF, Linz, sept. 28- oct. 1st.* Int. Institute of Refrigeration, 1997.
- K. Kim, U. Spindler, D. Jung, and R. Radermacher. **R-22/R-152a Mixtures and Cyclopropane (RC 270) as Substitutes for R-12 in Single-Evaporator Refrigerators: Simulation and Experiments.** *ASHRAE Transactions*, 99(1):1439–1446, 1993.
- E. Lemmon, M. McLinden, and M. Huber. **NIST Reference Fluid Thermodynamic and Transport Properties - REFPROP, Version 7.0.** National Institute of Standards and Technology, 2002.
- G. Leyland. **Multi-Objective Optimisation Applied to Industrial Energy Problems, Thesis No. 2572.** PhD thesis, Swiss Federal Institute of Technology (EPFL), Lausanne, Switzerland, 2002.
- T. Midgley and A. Henne. **Organic Fluorides as Refrigerants.** *Industrial and Engineering Chemistry*, 22:542–547, 1930.
- A. Molyneaux, G. Leyland, and D. Favrat. **A New, Clustering Evolutionary Multi-Objective Optimisation Technique.** *Third Int. Symposium on Adaptive Systems, Institute of Cybernetics, Mathematics and Physics, Havana, Cuba*, pages 41–47, 2001.
- H. Rivoalen. **Heat Pump Market Overview Europe.** *Webpage of the European Heat Pump Association*, 2001. URL <http://www.ehpa.org>.
- P. Vorster and J. Meyer. **Wet Compression versus Dry Compression in Heat Pumps working with Pure Refrigerants or Non-Azeotropic Binary Mixtures for different Heating Applications.** *Int. J. of Refrigeration*, 23:292–311, 2000.
- WPZ. **Published Results in Bulletin No. 1 - 37**, 1993-2003. URL www.wpz.ch.
- O. Zürcher. **Contribution to the Heat Transfer Analysis of Natural and Substitute Refrigerants Evaporated in a Smooth Horizontal Tube.** PhD thesis, École Polytechnique Fédérale de Lausanne, Lausanne, Switzerland, 2000.

2. Improved heat pump design concepts

2.1 Improving efficiency - ways to go

2.1.1 Acting on the heating system

As has been shown in the introduction chapter, the coefficient of performance (COP) of a heat pump cycle strongly depends on the temperature level of the external sources. The higher the heating temperature and the lower the cold source temperature, the more penalized are the system performances. The best way for improving efficiency in heat pump supplied residential heating systems is to **design heat distribution systems at temperatures as close as possible to the desired room temperature**. In existing buildings, this means, that the first step to consider in the procedure of implementing a new heating system is to reduce the heat losses, mainly by investing on the building envelope, including better windows. With the reduced heat demand, the heat distribution surfaces are over-sized and the heat distribution system can be operated on reduced temperatures, while maintaining the same comfort level. In addition, choosing a pump with higher mass flow rate in the hydronic loop, reduces the temperature difference between the supply and return line, which again allows further reduction of the heating temperature, although at the expense of increased pumping power.

Heat pumps for new buildings in the residential sector, are becoming more and more competitive to fuel based heating systems. If possible, geothermal brine-water heat pumps are installed, benefiting from stable external temperatures, and thus avoiding the low temperature power peak in cold winter days. Low temperature floor heating results in very efficient heating systems, if the heat is supplied by a heat pump. These favorable conditions are very close to the requirements of most air-conditioning devices (about the same temperature difference between the sources) and can be adapted with a relative ease to the heating application by simply choosing an adapted refrigerant. This fact explains the diversity of compact and efficient commercial low temperature heat pumps.

By contrast to these widely used air-conditioning units and low temperature heat pumps, the **market share for higher temperature lift heat pumps is still very low** and direct heating (*Joule effect*) and gas or fuel boilers are widely distributed in this sector. In retrofit, the main obstacle for market penetration of heat pump technology is related to the important installation costs. Available

space and consideration of noise emissions are other parameters, which have to be considered. Not to be neglected are the still remaining image problems of badly designed heat pumps in the issue of the second oil crisis in 1978.

2.1.2 Improving the thermodynamic cycle

Irreversibility losses in heat pump cycles, can be identified by an **exergy analysis**, as presented in [Liang and Kühn, 1991; Kruse, 1992]. For the high temperature heating application, using a one-stage compression heat pump, the most important cycle losses are located in the compression (in particular when operated at non adapted pressure ratio, in off design), in the condensation (high temperature difference in the desuperheating region) and in the expansion (throttling losses).

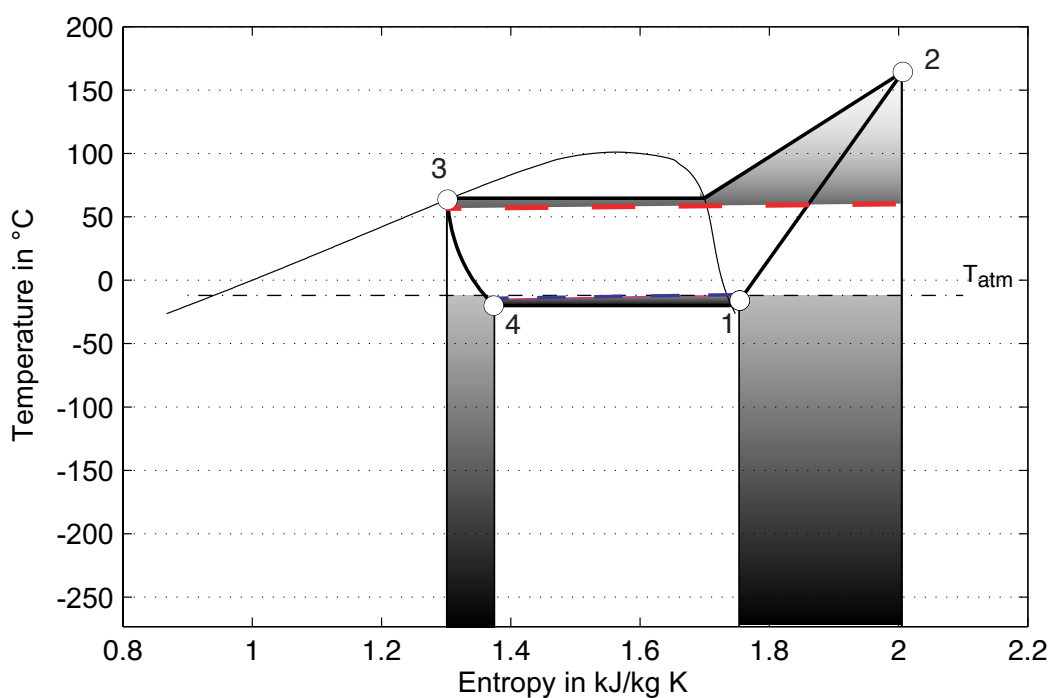


Figure 2.1: *T-s* diagram of the reversed Rankine cycle of an air-water heat pump at extreme operating conditions ($T_{atm} = -12^{\circ}\text{C}$, $T_{hot} = 65^{\circ}\text{C}$) and with indicated temperature evolution of the external sources. Grey surfaces indicate exergy losses corresponding to each transformation.

Looking to the simple configuration of a reversed Rankine cycle heat pump in Figure 2.1, the repartition of the main irreversibilities is shown graphically. A numerical application, including an inventory of exergetic losses in a two-stage and in a one-stage compression cycle, is provided in the Annex A.1.

The considered aspects consist of:

- **Appropriate compressor selection**

The most important transformation losses occur in the compression process. These can directly be reduced by implementing a more efficient compressor, which demonstrated the necessity to continuously optimize compressor design. For the considered high temperature lift application it is very important to select the appropriate compressor technology. Reciprocating piston compressors would for example represent the wrong choice, due to the high re-expansion losses in the higher pressure ratio applications. As will be shown later, hermetic scroll compressors are available with different built-in volume ratios, which defines the adapted application range.

- **Avoiding the high discharge line temperatures**

There are two reasons, why the the maximum system temperature should be reduced: **Thermal stresses** and **chemical degradation of the refrigerant-lubricant mixture**. These two effects can drastically reduce the life time of the heat pump. Temperature limits of about 120°C are generally set in the control unit of the heat pump, or by a mechanical security switch in the compressor. This is the main reason of a limited application range of the one-stage compression cycles in high temperature lift heat pump applications.

A very high temperature difference between the compressor exit and the saturation temperature, leads to important entropy creation (exergy losses) in the desuperheating part of the condenser, which indicates one efficiency gain potential.

There are two main approaches (supposing the same thermodynamic cycle) for reduced temperature. The first concerns the **choice of the appropriate refrigerant**, with a low value of the ratio of specific heats κ . The second concern the compression, which has already been mentioned in the previous point. Other concepts to reduce the discharge temperature consist of the design of integrated cooling (e.g. operating with high concentration of lubricating oil, as in some ammonia compressors). It has to be considered, that this heat, if not transmitted to the heating system, will have an impact on efficiency losses. The most effective approaches to lower the discharge temperatures are directly linked to the improved thermodynamic concepts, examined below in this text.

- **Valorization of the subcooling**

For low temperature glide heating systems the opportunities for the integration of several different thermal heat fluxes to approach the *desuperheating-condensation-subcooling* path of the refrigerant, are limited. Thus, **the valorization of the subcooling region represents an important potential of efficiency improvement**, when operated at high heating temperatures. **At the considered extreme operating point A-12/W60¹ the relative gain**

¹Air inlet and heating water outlet temperatures in °C.

in heat rate, valorizing the subcooling region from the saturation temperature to the room temperature, is about 30%! This relative increase, represent also the theoretical COP increasing potential, for the case, where this heat can directly be used for additional heat requirements, e.g. to maintain a minimal temperature in a room close to the location of the heat pump, by direct heat exchange. In most of the configurations this heat is exchanged, using a more sophisticated thermodynamic cycle, in order to increase the total heat rate, which is transmitted to the hydronic heating system. Such approaches could be tested, considering different solutions, and efficiency increases of 5%-10% in COP and 20%-35% of the heat rate, see sec. 2.3 could be measured.

Improved thermodynamic cycles have already been presented theoretically by [Granryd, 1992] and have been adapted for large size heat pumps with heating capacities up to 168 MW (6x28 MW), see [Bailer, 2002], which represents one of the largest heating plant using heat pumps. In such large size concepts temperature lifts of more than 80 K can be achieved with two or three-stage heat pump cycles (with a economizer-separator cycle), using centrifugal compressor technology. Another example is a 2400 kW, high efficiency heat pump, presented in [NEDO, 1993] and is designed with a multi stage condensing Lorenz cycle unit. These examples show, that some of the enhancement techniques are already applied in the upper range of system capacity. The downsizing of these solutions to small units suffers from the complexity and the induced costs. Therefore only the simplest options have been retained in the refrigeration technology for small sized units, e.g. the concept of using a refrigerant mixtures with adapted saturation temperature glide and the implementation of a suction line heat exchanger, which allows a better utilization of the evaporator surface, while maintaining the same degree of overhear at the compressor inlet. However, small capacity heat pump cycles are generally designed with the minimum of elements, in order to reduce the investment costs.

The two-stage compression cycle

To show the **potential of performance improvement by remodeling the thermodynamic cycle**, a simplified calculation **applied to a two-stage compression heat pump cycle** is shown hereby. Figure 2.2, shows the flow chart of the basic design with two compressors, connected in series. With additional bypass lines, a subdivision into three capacity levels in the heating mode could be easily achieved. The economizer flash tank is acting as a phase separator in the intermediate pressure, and consists of the easiest way to design a two-stage system (no risk of liquid plugs arriving into the second stage compressor), but is not the appropriate approach for refrigerant mixtures, due to a slow, but not negligible distillation.

Setting the compression efficiencies to a fixed value (70%), an optimum design in two-stage mode can be evaluated for different fluids, even for non-azeotropic refrigerant mixtures, supposing no distillation in the flash tank). The calculation results, shown in Figure 2.3, represent **the optimum**

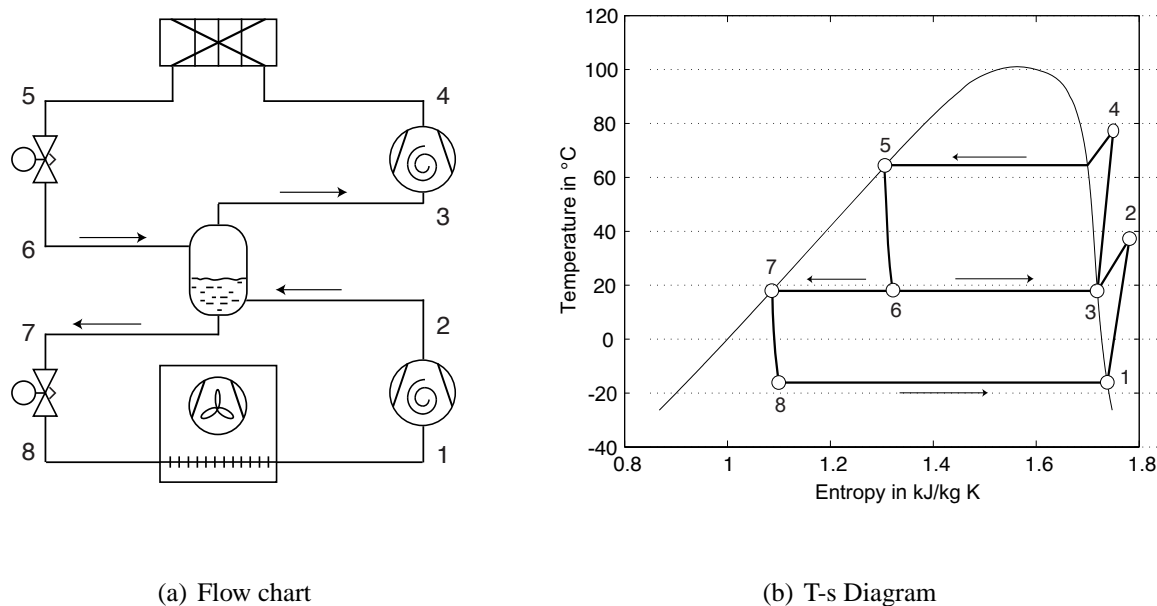


Figure 2.2: Flow chart and diagram of a two-stage heat pump with phase separator.

intermediate pressure level, which is clearly above the geometric average¹ of the evaporation and condensation pressures. For real compressor efficiency, however, the low pressure ratio region is highly penalized and the optimum mid-stage pressure level is shifted to equalized pressure ratios, see the simulation results in section 4.2.1.2 on page 158. The end points of the four curves indicate the level of the one-stage compression cycle efficiency. The relative **efficiency improvement are in the order of magnitude of 20%**, and are expected to be even higher in the real application, due to the better performance of compression in two-stage compression mode than in one-stage mode.

2.1.3 Facing the market

Main development efforts to improve heat pump efficiency and compactness, have been achieved in compressor technology (appearance of scroll compressors in 1987 by Copeland Corp., USA), in the design of brazed plate heat exchangers and in the electronic regulation, permitting an optimal control of the operating temperatures. Many progresses were also made in the system reliability, the design-tools and in the know-how of the installers.

For high temperature heating systems efficiency improvements, capacity gains and the extension

¹The geometric average is found to be the optimum intermediate pressure level, for refrigeration applications, which can be found in general textbooks of refrigeration. Approaching the critical point (for heat pumps) is resulting in a degradation of the upper cycle, shifting the optimum intermediate pressure closer to the condensation pressure.

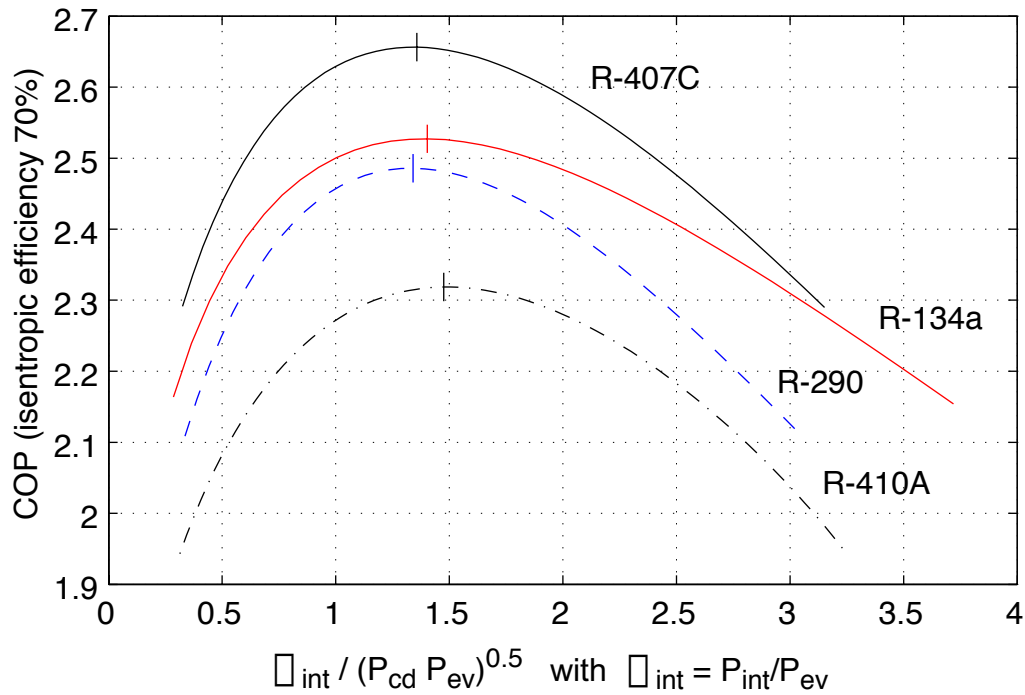


Figure 2.3: Optimum intermediate pressure for theoretical two-stage cycles. Constant compression efficiency.

of the application range have to be evaluated carefully in relation to the increased system cost. This selection among various schemes for additional performance increase can be made formally starting from a superstructure, including most components which could be considered in advanced heat pumps. The presented multi objective optimization tool, used in the first chapter to evaluate new refrigerant blends (sec. 1.3) can also be applied to this structure, in order to evaluate optimal configurations, based on several criteria of choice (such as cost).

2.2 Superstructure

The development of high efficiency solutions for small sized residential air-water heat pumps to replace oil or gas fired boilers in hydronic heat distribution systems, has concluded to a general form of **superstructure** in Figure 2.4, from which specific solutions are considered, and have been experimentally compared, within the framework of the *Swiss Retrofit Heat Pump*, which has been initiated and mainly funded by the *Swiss Federal Office of Energy*.

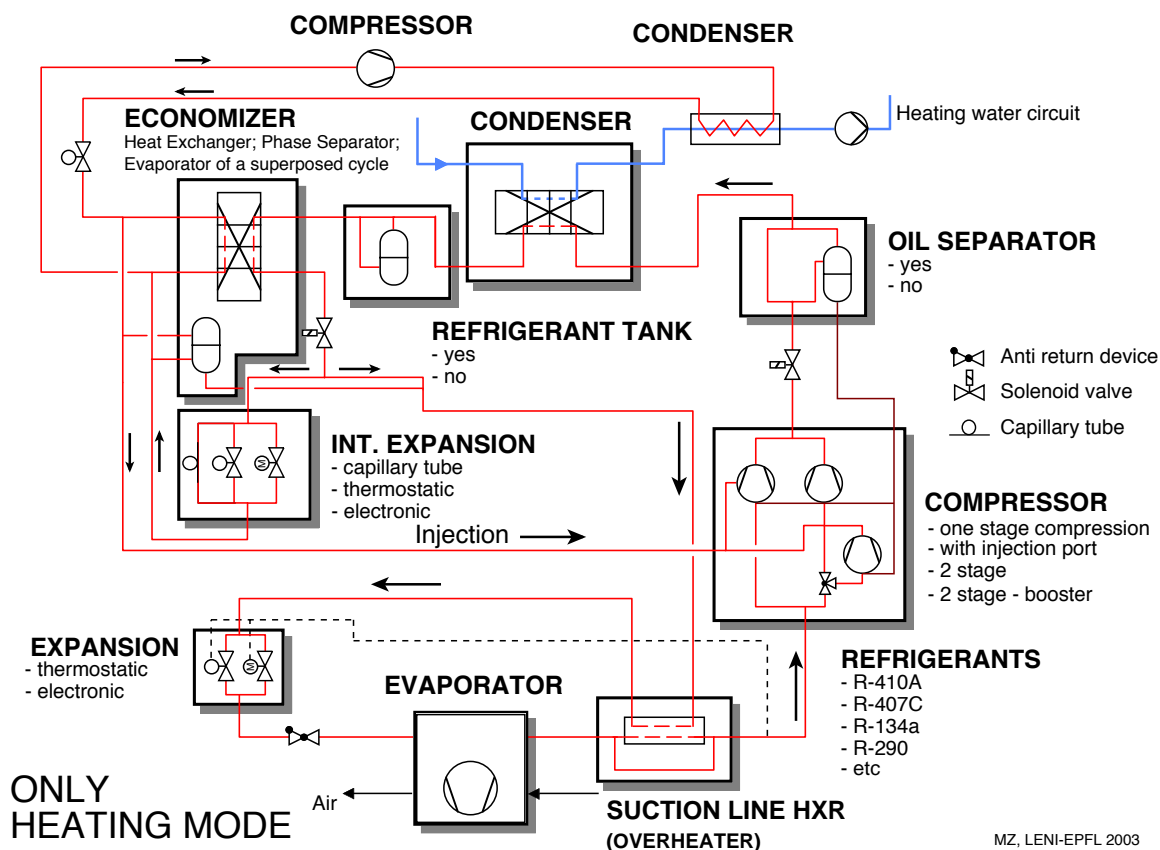


Figure 2.4: Superstructure for improved heat pump design concepts. Heating mode only.

The key elements of this structure are:

- **Compressor stage**

Four options are considered, representing the compression stage of the heat pump.

1. One-stage compression

The one-stage compression cycle represents the classical heat pump with limited application range. In the range of high pressure ratio applications, the use of reciprocating piston compressors is very restrictive, showing highly reduced volumetric efficiencies in reason of the re-expansion of the clearance volume. This is much less the case for

scroll type compressors, which show a slight decrease of the volumetric efficiency, which is proportional to the pressure ratio. Two series of hermetic scroll compressors, with distinct built-in volume ratios are available on the market and have been compared. Table 2.1 shows the performance comparison between a piston type compressor and the two scroll compressors at a pressure ratio of 5, corresponding to the operating point A0/W50 for R-407C.

Table 2.1: Comparison of compressor efficiencies (refrigerant side) at a pressure ratio of 5, representing the operating point A0/W50 for R-407C, based on an oil-free compression.

Brand Name	Type	Displacement @ 50 Hz	η_{is} [%]	η_{vol} [%]
Piston Bristol	Inertia H25A42QDBEA	12.2 [m ³ /h]	65	60
Scroll Copeland ZR	ZR49 K3 TFD 422 - VR _i = 1.8	11.7 [m ³ /h]	61	85
Scroll Copeland ZF	ZF15 K4E TFD - VR _i = 3.2	14.4 [m ³ /h]	66	90

This one-stage compression cycle is retained as the basic option and represents the simplest and cheapest heat pump configuration. The high built-in volume ratio compressor type will have to be selected. Heat capacity modulation can be realized by a tandem configuration (two compressors in parallel).

2. One-stage compression with intermediate (vapor) injection ports

A major extension of the application range is obtained by the most cost effective option using a compressor type with intermediate injection port. The injection can be combined with a direct injection through a capillary tube, using a part of the condenser exit flow, or with an economizer stage (heat exchanger or flash tank, see below in this text). Heat capacity can be modulated by enable/disable injection.

3. Two-stage compression cycle

Separating into two compression stages, each compressor works on a far more restricted range of pressure ratios and **could be optimally designed for a specific application.** This staged compression, **provides the highest flexibility in heat rate modulation** (theoretically 3 levels) and allows many intermediate pressure options. Unbalanced oil migration through the system represents a major drawback for small size heat pumps and particular efforts to improve the understanding of the oil migration phenomena are presented in chapter 5.

4. Restricted two-stage cycle with a booster compressor stage

To bypass these problems of unbalanced oil distribution, an intermediate configuration consists of using a so called *booster* compressor, which could be a low cost compressor with shorter life expectancy and with a flow path, as direct as possible, in

order to avoid oil accumulation. This compressor is only needed for an extension of the application range and to *boost* the heat rate during the coldest days of the heating season.

- **Oil separator**

The oil separator at the compressor outlet is an optional component of a heat pump system and is required for large capacity systems or in cycles with higher oil concentrations, which is especially the case in vapor compression cycles with ammonia. Higher migrating oil concentration lead to performance losses, due to increased pressure drop and reduced heat transfer performance. In small capacity heat pump cycles the total amount of accumulated and migrating oil throughout the system is reduced and an oil separator is mostly not necessary. Sufficient oil return to the compressor is obtained by appropriate design of the return line and by a careful selection of the appropriate oil (accounting to the miscibility between the oil and the refrigerant). In two-stage compression cycles, however, the oil separator might enable longer operating cycles, with balanced charge of lubricating oil in each compressor.

- **Condenser**

The choice of the condenser technology, is one of the less critical choice in heat pump technology. In air-water heat pumps, compact brazed plate heat exchangers are widely used.

- **Refrigerant vessel**

The refrigerant charge is function of the complexity of the heat pump cycle. Extended concepts and two-stage compression heat pumps present increased volume. For air source heat pumps, the evaporation pressure is highly variable and a compensation volume in the liquid line of the heat pump is recommended.

- **Economizer**

The concept of the *economizer* is to divide the expansion in two parts, and to recover some of the flashed vapor at the intermediate pressure stage. This represents a way to limit the exergy losses linked to the liquid expansion. This scope can be achieved by means of two approaches:

1. Economizer-separator (economizer flash tank)

The total mass flow is expanded to a intermediate pressure level. At the adiabatic expansion the fluid is flashed into a reservoir. This reservoir is connected at the vapor exit to the injection point in or between the compressor(s) and at the liquid exit to the second expansion device which is followed by the evaporator. A similar configuration, which is not represented in the Figure 2.4, is obtained in two-stage mode by the entire

de-coupling of the two compressors. The discharge line of the first compressor would then lead directly to the economizer-separator and the suction line of the second stage compressor would be fed with saturated vapor.

The **separator approach is unfortunately not adapted to zeotropic refrigerant mixtures** and will be eliminated for these types of fluids. A distillation is likely to happen and it will most probably lower the cycle efficiency.

2. Economizer heat exchanger

Only the part of flow which is injected into the compressor or which is mixed to the main flow between the two compressors is expanded to the intermediate pressure level. As the intermediate pressure saturation temperature is lower than the temperature of the condensate, the injection flow will recover heat from the subcooling of the main flow. The lower is the intermediate pressure, the more heat can be extracted from the main flow and the more work has to be put for the re-compression of the fluid. The intermediate pressure level resulting in a maximized COP has been evaluated by a theoretical approach (Fig. 2.3).

- **Auxiliary cycle with evaporation at intermediate temperature level.**

The energy of subcooling can also be valorized by evaporation of a refrigerant in a secondary loop which is alimented by its own compressor. **This auxiliary loop could be charged with a different refrigerant and offers the flexibility of deserving a second heat demand on a different temperature level** (hot water supply in parallel with the deliverance of the heat). The construction of an entire second cycle is relative cost intensive and the problem of a high pressure ratio in the main compressor still persists.

- **Expansion devices**

The expansion of the liquid can be done in a **capillary tube**, mechanically regulated with a **thermostatic valve** or with an **electrically regulated expansion device**. These options are presented in the respective cost order. The expansion device for the main expansion is generally a thermostatic expansion valve, regulated by temperature difference between the bulb sensor at the compressor suction line and the evaporation temperature after the expansion of the flow. Electric valves require additional regulation and capillary tubes are not adapted for the main flow in air-water heat pumps with highly variable operating conditions.

In the secondary expansion (at the injection flow) a capillary tube can be chosen in most cases, as has been experimentally demonstrated on different setup.

- **Evaporator**

Evaporator design is mostly restricted by the oil return concerns and the geometry of the air side flow has to meet the criteria of compactness and effectiveness. Performance gains in air-water heat pump systems are expected by improving the defrosting mode. Most of the actual defrost control systems are based on time-control and do not represent a high performance approach. [Bertsch and Ehrbar, 2002] compared the defrosting efficiency of hot-gas and reversing cycle defrosting modes and propose other non-conventional solutions, while [Kulik et al., 2003] proposes to act on a hydrophobic coating in order to maximize the contact angle of the droplets formed on the exchanger fins. The coated evaporator fins, however could not show a significant improvement in the test heat exchanger and further fundamental research is still required. In section 2.3.3, an alternative high performance defrosting is presented by the mixed approach, using available heat at low exergy, stored in the economizer flash tank.

- **Suction line heat exchanger**

The presence of this heat exchanger, more often referenced as the *overheater*, has two principle roles in a heat pump concept. The first is to finalize the required overheat of the refrigerant in the suction line before the compressor. The prevention of overheating the refrigerant in the evaporator has a direct impact on the system efficiency, using zeotropic refrigerants, with an important temperature glide during evaporation, which is equivalent or higher to the temperature difference between the air inlet and outlet. The second function is to sub-cool the high pressure liquid, and therefore to eliminate eventual vapor bubbles, which would partially block the expansion. This can occur in classical one-stage configuration (when all liquid line tubes are thermally isolated) and in the case of the economizer-separator configuration.

2.3 Selected configurations of high performance heat pump

2.3.1 Cycle with intermediate injection and heat exchanger

Scroll compressor with intermediate liquid injection port

The main issue of this setup has been to evaluate an, at that time, already available scroll compressor, with intermediate injection port, *Copeland - ZF series*. This compressor is used in the domain for low temperature refrigeration and is tested in a high temperature lift heat pump, which is equipped by an economizer heat exchanger. **This compressor is manufactured with a small diameter injection port, mainly for liquid intermediate injection flow**, allowing an important desuperheating during compression. This results to an extended application range and in a considerable increase of heat output on high temperature lift conditions. In addition the built-in volume ratio of this compressor series is higher than the ratio of the standard scroll compressors, leading to increased compressor efficiency at high pressure ratio applications.

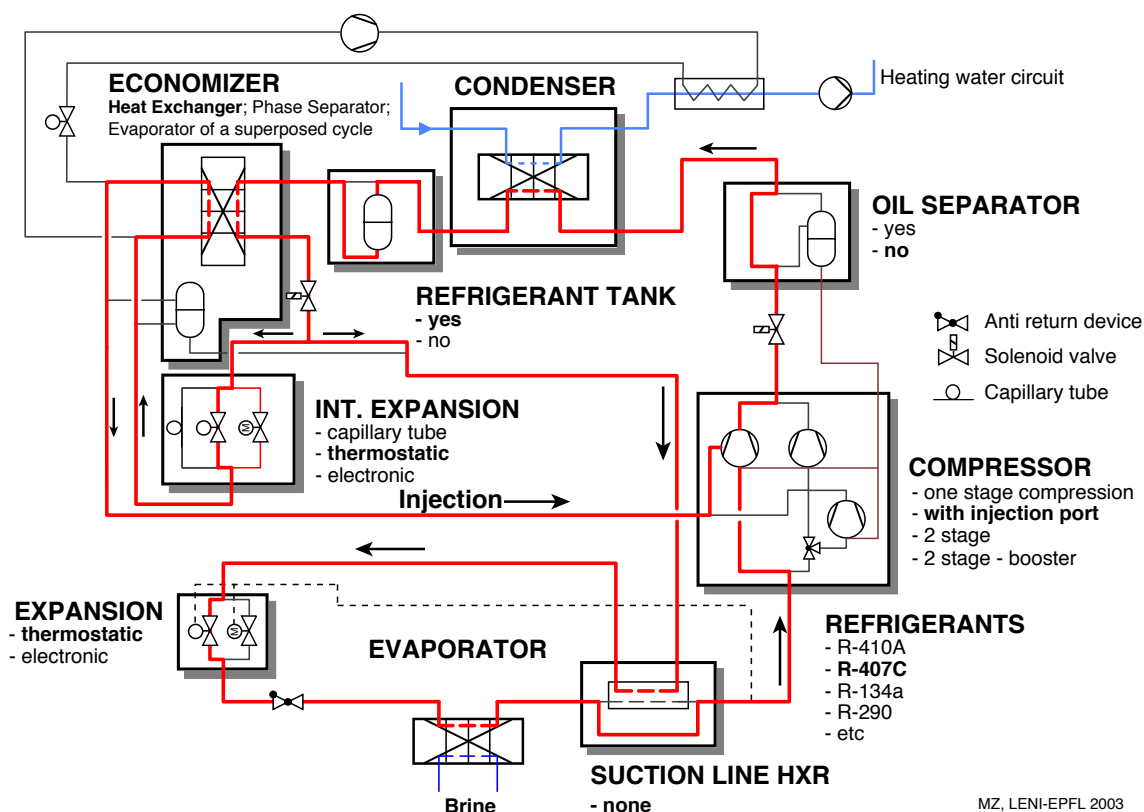


Figure 2.5: Economizer cycle, brine-water heat pump with intermediate injection port scroll compressor.

For simplification reasons, a brine-water prototype heat pump, was built by KWT AG, Belp and was tested in the Berne University of Applied Sciences, Burgdorf. Figures 2.5 and 2.8 are showing

the corresponding setup in the superstructure and the complete flow chart with indicated locations of measurement points. The complete listing of the implemented transmitters is given in the Annex [A.5.1](#).

The test points contain the operating conditions¹ B-5/0/5 and W35/50 and the extreme point B-10/W60. The performances of the heat pump at stationary conditions with and without injection flow have been measured and show an increase of the heat output of 15% at equivalent COP. The discharge line temperatures at the extreme operating conditions were reduced from 110°C down to 75°C. Increasing the injection flow rate showed the researched effect on the increase of the heat output, but from a certain flow rate limit the heat output stagnated (Fig. 2.6) and the COP diminished significantly. The evolution of the intermediate pressure level and the effective discharge line temperatures are shown in Figure 2.7. **The tested liquid injection port compressor is not perfectly adapted for the injection of saturated vapor**, as is the purpose of this setup. **The intermediate pressure level is highly correlating with injected mass flow rate**, which is due to the restricted flow channel until the injection port in the compressor. **This is negatively influencing the performances of the heat pump**. First, the potential of subcooling the refrigerant could not be exploited entirely, due to the high saturation temperature in the economizer, and second, the work of recompression has still to be done from a low pressure level, representing nearly the whole trajectory of compression. For very low injection flow rates, the resulting discharge line temperatures can even be higher than in the one-stage configuration. This fact is due to an important superheat of the injection flow in the economizer heat exchanger. Important oscillations in the discharge temperature have been observed. These can be strongly attenuated in connecting the heat exchanger in a self stabilizing co-current configuration.

¹B=brine inlet temperature, W=water output temperature in °C

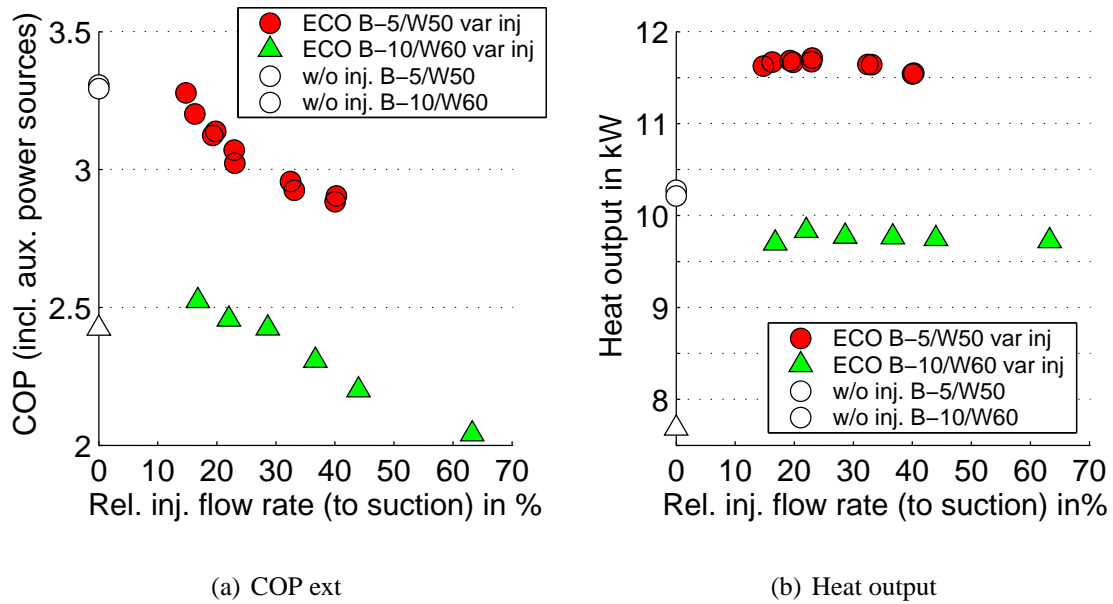


Figure 2.6: Evolution of COP and heat output with increasing injection mass flow rate. Brine-water heat pump with intermediate injection compressor in economizer cycle.

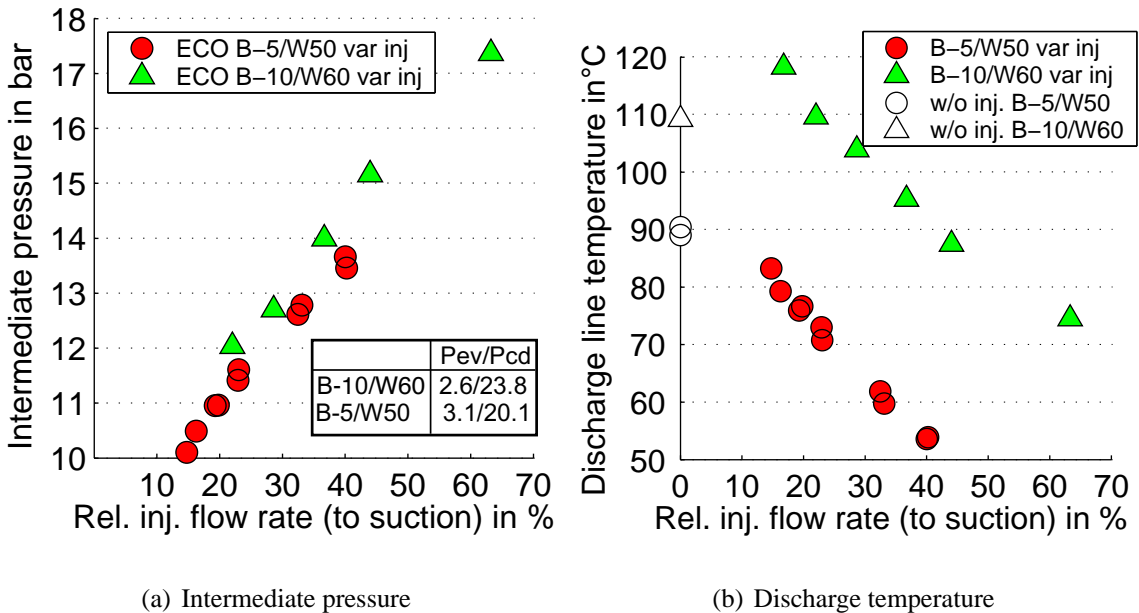


Figure 2.7: Evolution of the intermediate pressure level and discharge temperature with increasing injection mass flow rate. Brine-water heat pump with intermediate injection compressor in economizer cycle.

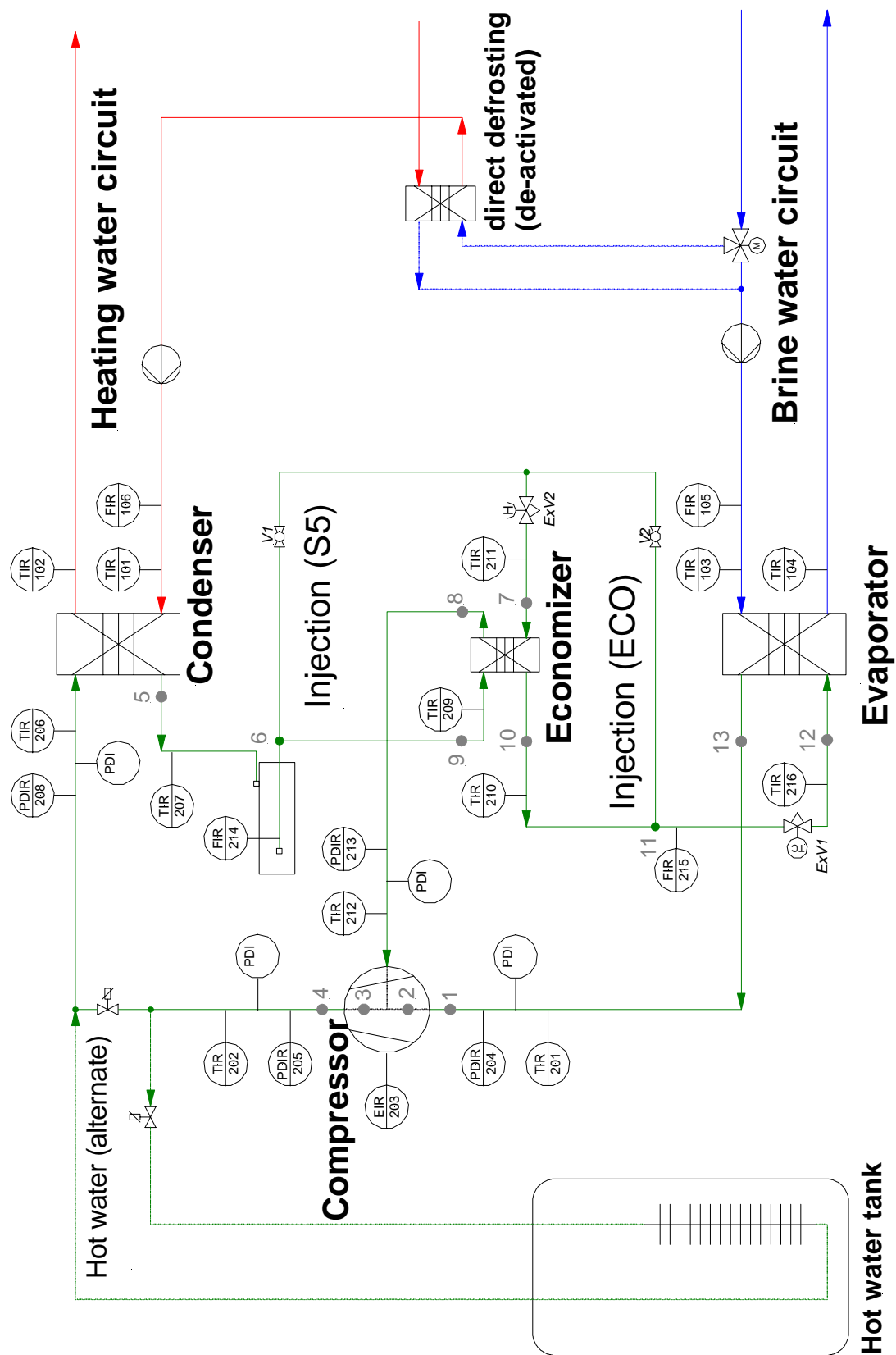


Figure 2.8: Flow chart and locations of measurement points for brine-water heat pump with intermediate injection compressor in economizer cycle.

High temperature heat pump with new vapor injection compressor

A first compressor prototype with modified injection port, allowing injection of saturated vapor, has been integrated in a economizer heat pump cycle and multiple injection mass flow rates have been tested, using an electrically driven intermediate expansion device¹. In a second phase of the project, a new compressor sample (prototype 2), based on the scroll geometry with higher built-in volume ratio, has been tested on the same heat pump prototype. See Figures 2.9 and 2.12 for the detailed setup, the complete listing of the implemented transmitters is given in Annex A.5.2. Two sizes of **capillary tubes have been evaluated for the injection flow control**, and automated 24 h operation tests with defrosting have been performed with the second setup, in order to test the durability of the heat pump at high load conditions.

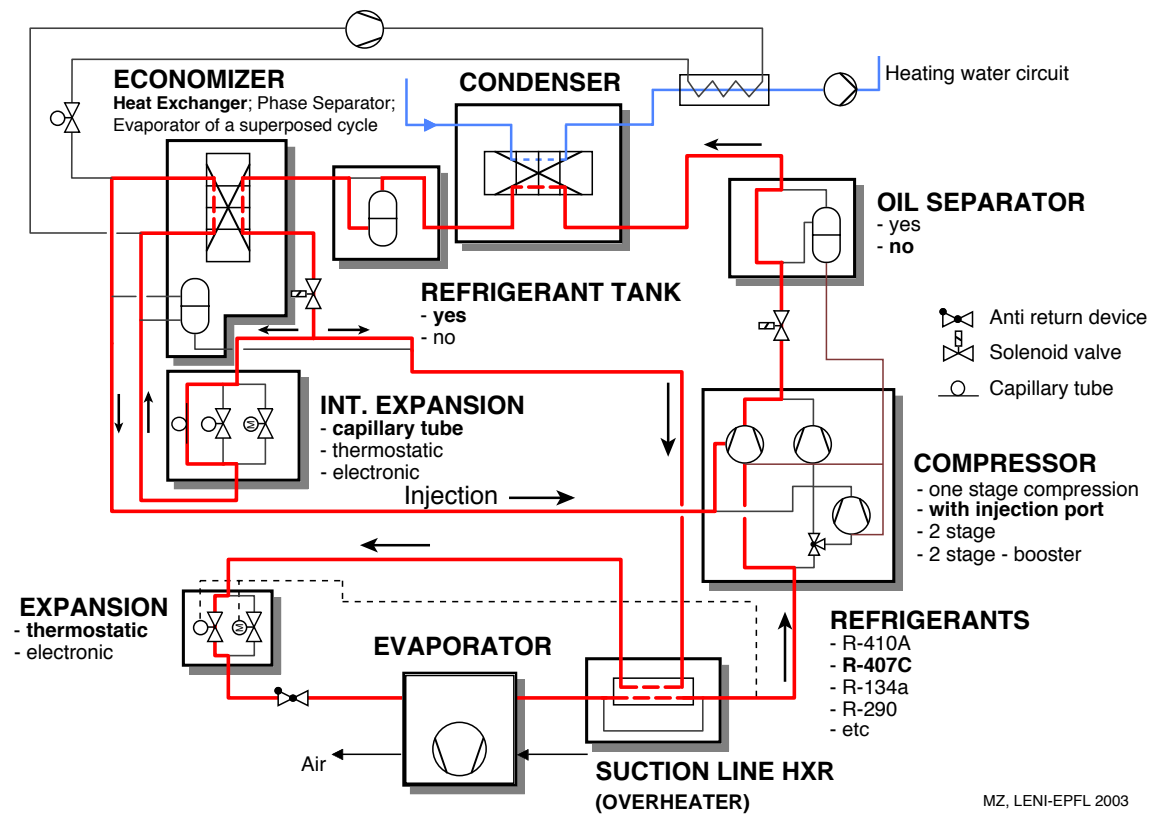


Figure 2.9: High temperature air-water heat pump with new compressor for saturated vapor or liquid intermediate injection.

Figures 2.10 and 2.11 summarize the main results, which have been obtained from the steady state heating tests, with the second compressor sample. The evolution of the COP and the variation of the discharge temperature are represented at multiple injection mass flow rates (given in relative value compared to the suction flow rate). Two distinct capillary tubes have been implemented in

¹This project, partly funded by the Swiss Federal Office of Energy, was a collaboration between Satag Thermotechnik AG, who provided the modified heat pump, Copeland Corporation, who manufactured the new compressor samples, Electricité de France, who made some of the compressor tests and the Laboratory of Industrial Energy Systems (LENI), who made the system tests and simulation.

the injection line, the first 2 m long with a diameter of 1.4 mm is perfectly adapted at A2/W50 and A-12/W50, corresponding to the optimal COP, but resulting in excessive¹ discharge temperature of 130°C at the extreme point A-12/W65! The second capillary tube, with a length of 1.4 m, leads to higher injection flow rates penalizing the COP in all operating conditions. However, the discharge temperatures are sensibly reduced to maximally 90°C, see Fig. 2.11.

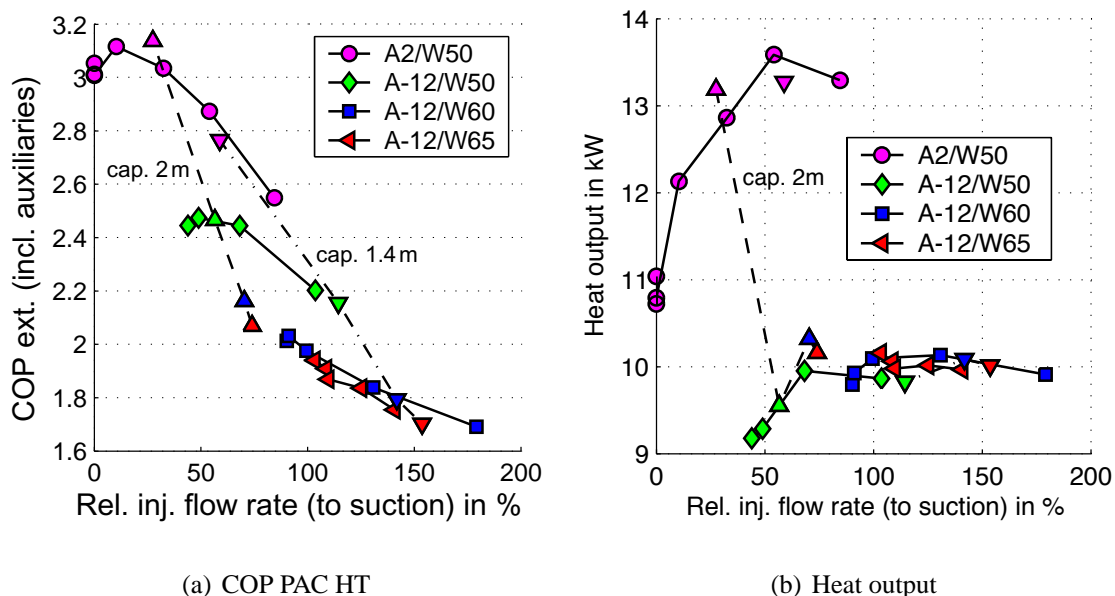


Figure 2.10: Measured performances of air-water heat pump with economizer heat exchanger and new compressor for intermediate vapor injection.

With this new compressor, the intermediate injection pressure level is considerably lowered, due to reduced frictional pressure losses in the admission channel and due to the earlier access to the compression chamber. For equivalent conditions (evaporation pressure and injection flow rate), the pressure level is reduced from 14.2 bar (liquid injection port), to 5.2 bar (new injection port)! This very important reduction results in a more efficient cycle and allows to extract more energy from the subcooling region.

¹The maximum allowed discharge mean temperature (measured in the refrigerant line at the compressor exit) in standard configurations is mostly set to 110-120°C.

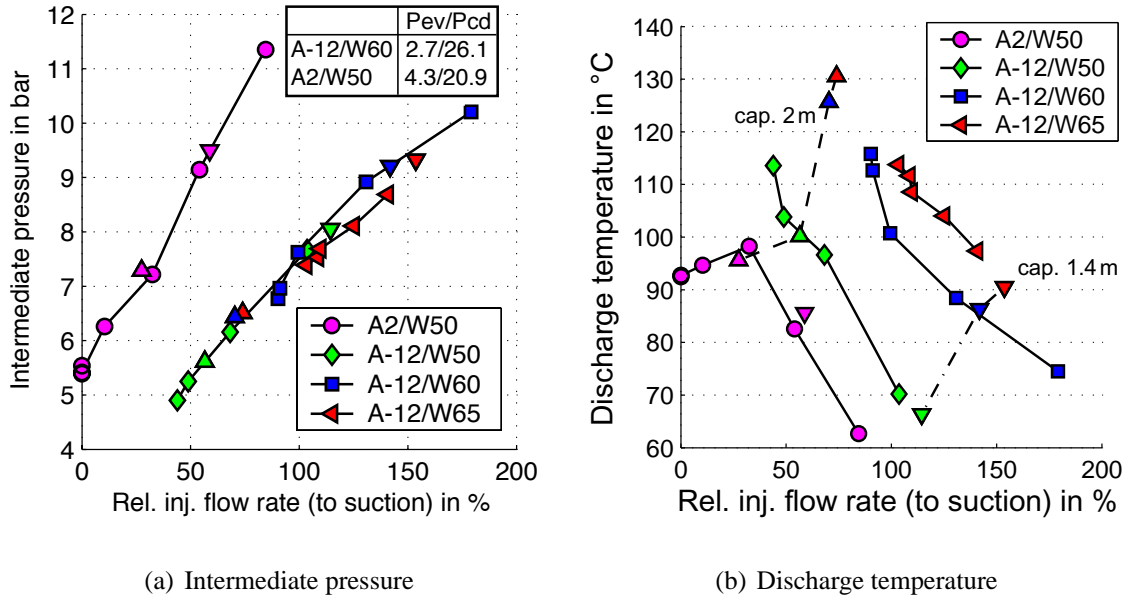


Figure 2.11: Measured pressure and discharge temperature of air-water heat pump with economizer heat exchanger and new compressor for intermediate vapor injection.

Table 2.2: Comparison of the performance of the economizer cycle with intermediate injection mean operating conditions and including the extreme operating point.

	A2/W50 (no inj)	A2/W50 (with inj)	A-12/W65 (min. req. inj)
COP (incl. aux.)	3.02	3.13	1.94
Heat output	10.8 kW	13.2 kW	10.2 kW
T_{dis}	93°C	96°C	114°C
P_{cd}	21.0 bar	20.7 bar	27.3 bar
$\Pi_{\text{tot}}(\Pi_{\text{L}}/\Pi_{\text{H}})^*$	4.8	4.8 (1.7/2.8)	10.3 (2.8/3.7)

*with $\Pi_{\text{L}} = P_{\text{int}}/P_{\text{ev}}$, $\Pi_{\text{H}} = P_{\text{cd}}/P_{\text{int}}$.

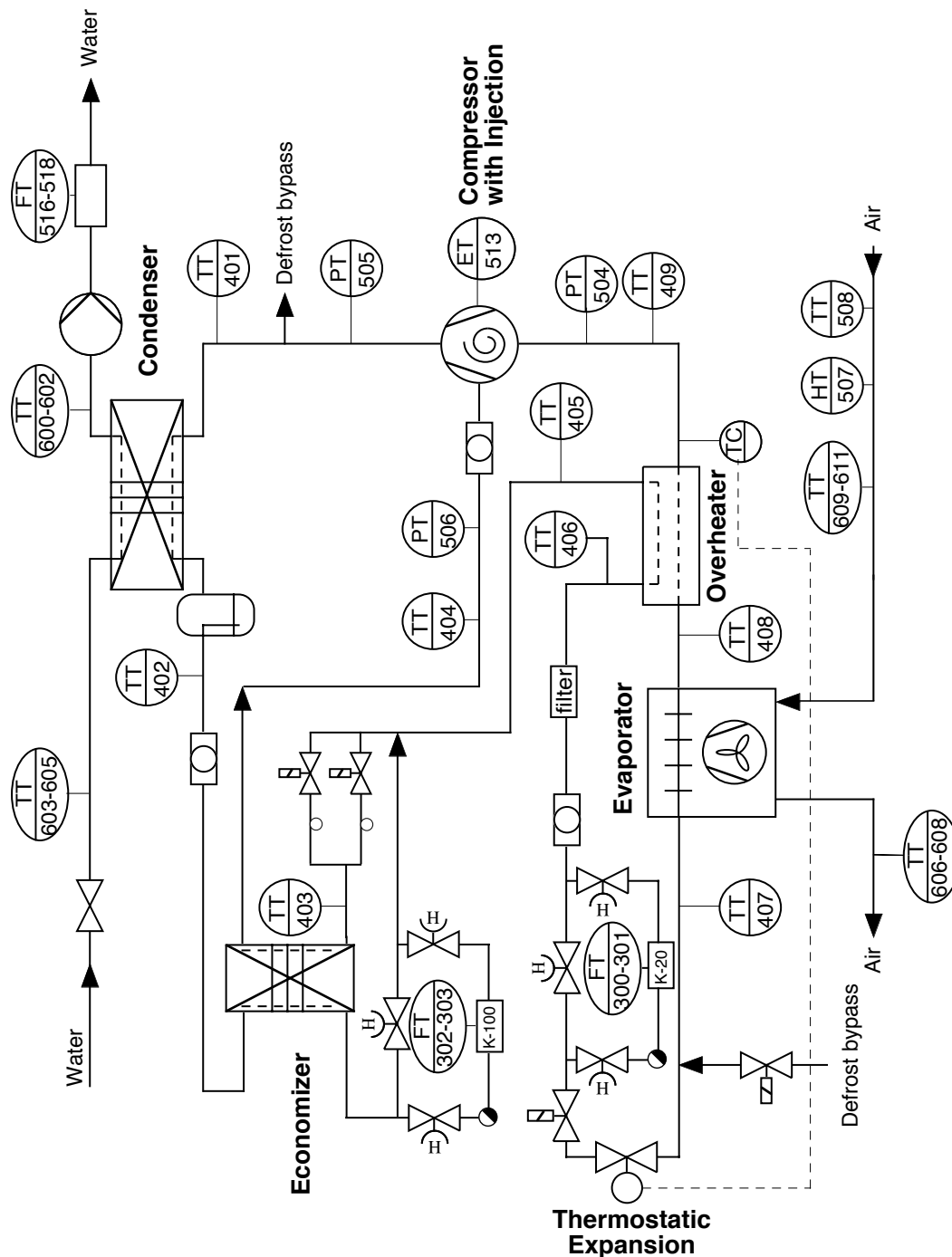


Figure 2.12: Flow chart of high temperature air-water heat pump with new compressor for saturated vapor intermediate injection.

This tested setup combines the simplicity (one single compressor, no injection control) with high performance over an extended application range. **The heat output at A-12/W65 with activated injection is 10.2 kW, which is very close to the heat output of the heat pump at A2/W50 without injection**, see Table 2.2. For traditional one-stage compression heat pump cycles only 60%-65% of the heat output would be delivered at the extreme point requiring additional heat supply.

Tests in a two-stage configuration **with an open scroll type, booster compressor have shown the possibility of doubling the heat output at the extreme operating conditions!** The setup and the test results of this configuration are shown in the section 2.3.3.

2.3.2 Heat pump with auxiliary cycle for liquid subcooling

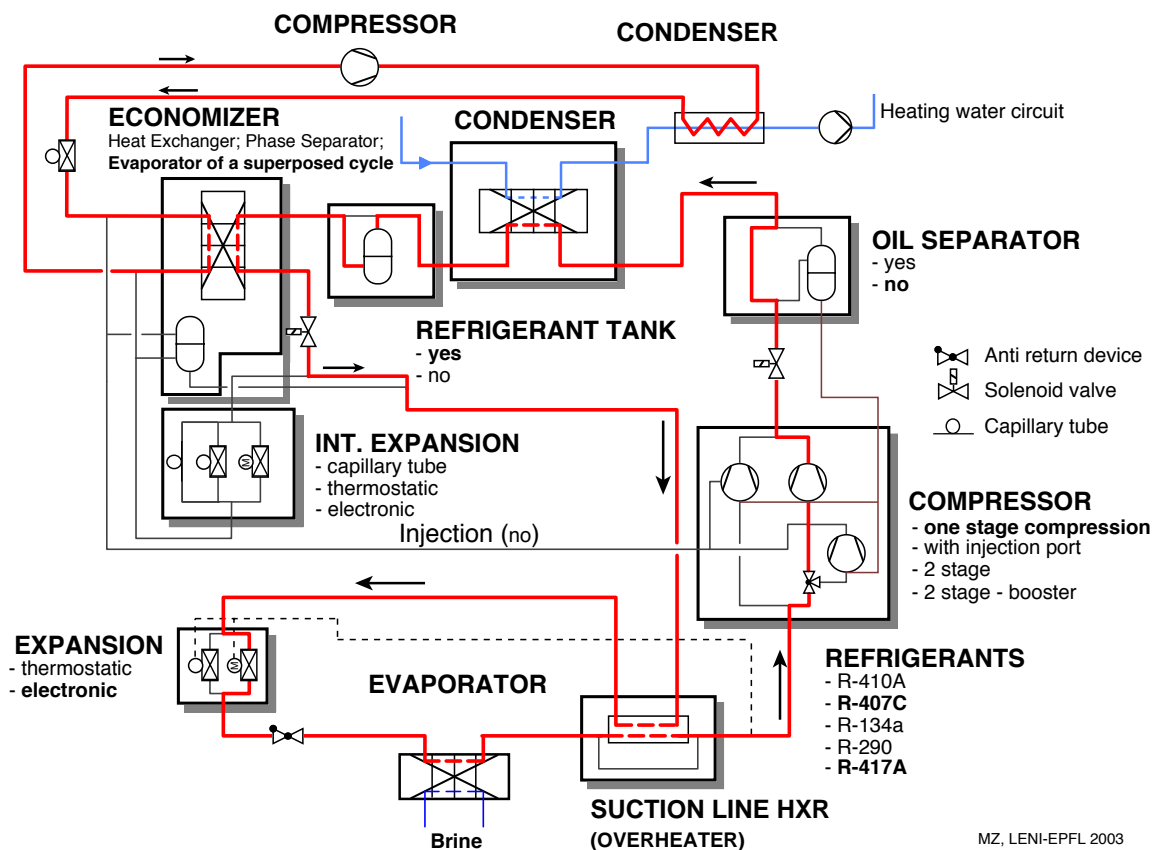


Figure 2.13: Brine-water heat pump with auxiliary cycle for liquid subcooling.

The valorization of the liquid subcooling is done by means of an auxiliary topping cycle, as shown in Figure 2.13. By the serial connection of an auxiliary condenser after the main condenser, this concept is most advantageous in heat distribution systems with a high temperature glide or in situations presenting heating needs on two distinct temperature levels (e.g. for parallel heating of a secondary heating circuit and hot water production), Figure 2.14. The present

evaluation although focused on the heating only application, with a moderate temperature glide of 10 K maximum in the heat distribution system. Under these conditions the required extreme point (B-10/W60) can only be operated with alternative fluids, like the R-417A, if a discharge temperature limit of 120°C in the refrigerant line is considered. The complete flow chart of the 9 kW heat pump (at B-2/W50, R-417A) is represented in Figure 2.16. The complete lists of the transmitters and of the main components of this setup are given in the Annex A.5.3.

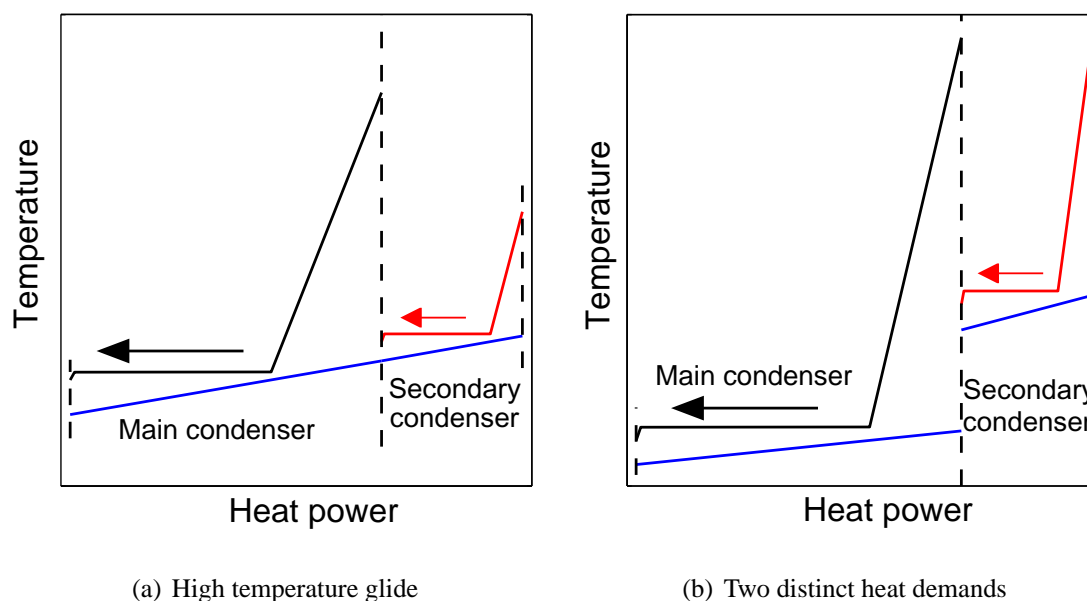


Figure 2.14: *Advantagous configurations with a double condenser heat pump cycle.*

The main results for this configuration, show a mean increase of the COP (Fig. 2.15) of 5% and of the heat output of 20% with the refrigerants R-407C and R-417A. The auxiliary cycle could not be designed in an optimal way and was principally restricted by the over-load limitation of the motor driving the piston compressor in the auxiliary cycle. In addition, and this is only related to the presented data, the selected heat exchangers were not properly adapted, resulting in higher temperature differences, penalizing the measured performances. A comparison of the efficiency between the two compressors, has shown a reduction of 15% in the maximum isentropic efficiency of the small sized auxiliary compressor, which had a displacement of 2.3 m³/h. In order to limit the temperature of the compressor shell, no thermal insulation has been mounted. All these contributions resulted in a moderate efficiency raise. In contrary to the small capacity heat pumps in residential application, the efficiency gains are more substantial in larger capacity heating applications (>20 kW_{th}), and especially in cases with a high temperature glide in the heating system, Fig. 2.14 (a), or in applications with parallel heat demand on well distinct temperature levels, Fig. 2.14 (b).

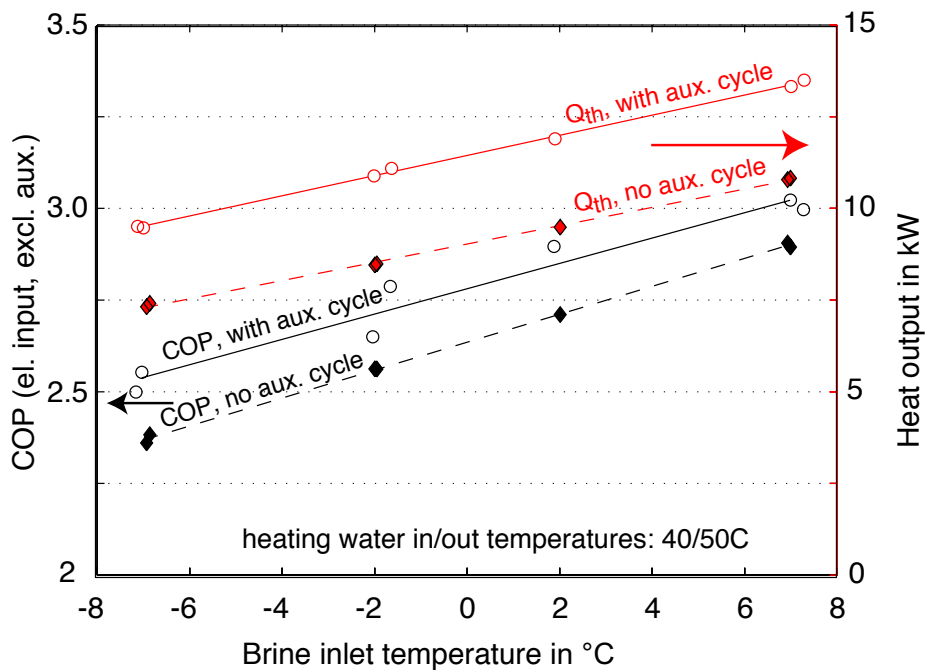


Figure 2.15: Brine-water heat pump with auxiliary subcooling cycle. Test runs with R-407C. Comparison of measured COP (based on el. power consumption of the compressor) and heat output for cycle with auxiliary subcooling and without.

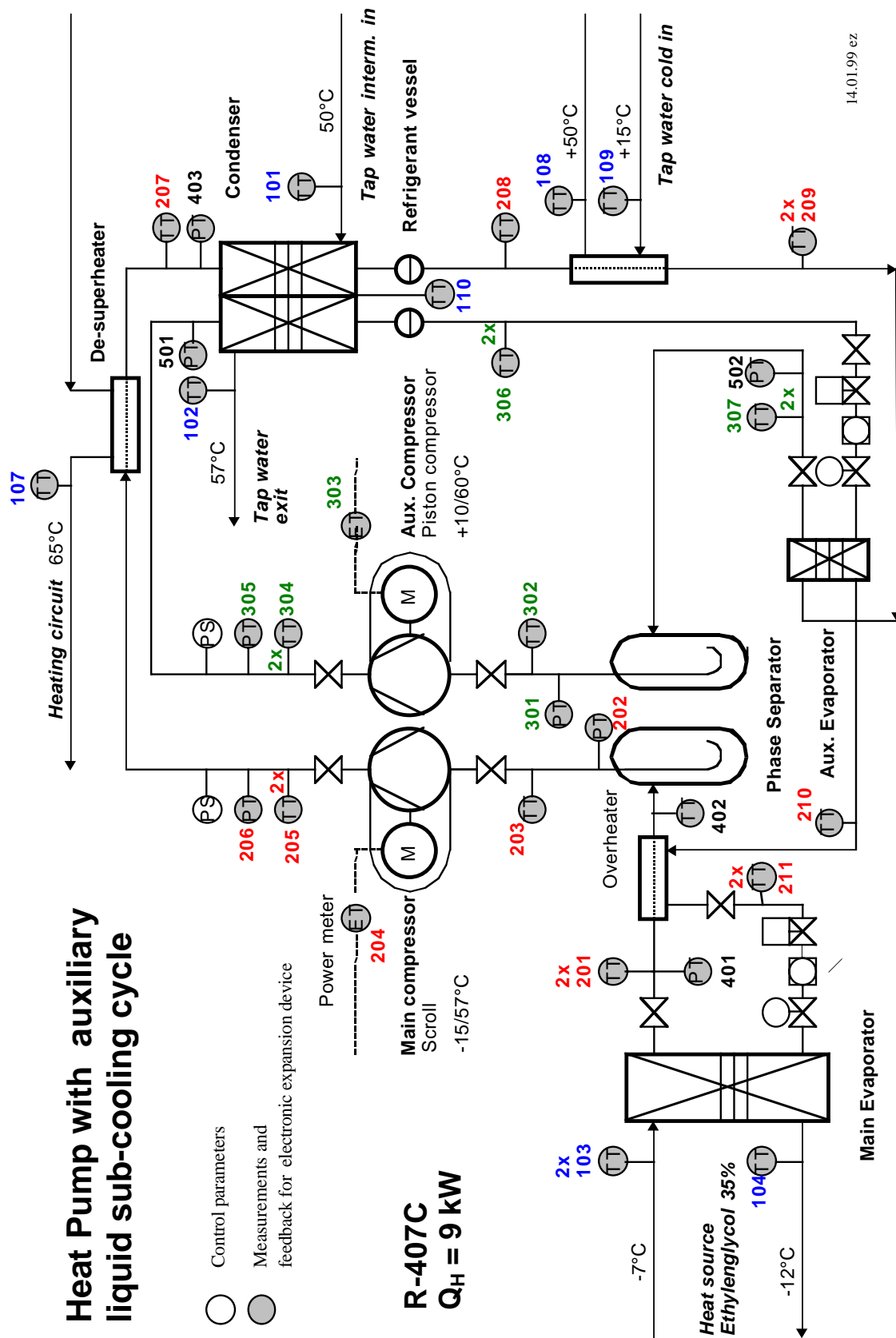


Figure 2.16: Flow chart, brine-water heat pump with auxiliary cycle for subcooling

2.3.3 The two-stage heat pump

Three different two-stage concepts have been experimentally evaluated at the Laboratory of Industrial Energy Systems.

Two-stage heat pump with combined economizer heat exchanger and phase separator



Figure 2.17: *Two-stage compression heat pump tests with an air-water test section, climatic air is produced in a separate circuit including the Igloo (big room at the right hand side of the picture).*

The project aim of this first two-stage compression cycle, was to evaluate the performances of a two-stage approach, which is adapted for pure refrigerants, as well as for zeotropic mixtures, coming on the market at that time. The project **combines the concepts of the economizer flash tank (15 ℓ)**, allowing a favorable defrosting with refrigerant stored at low exergy **and in order to avoid distillation in the flash tank, an (economizer) plate heat exchanger is added**, bypassing the flow through the tank. Initially the two-stage concept was designed with a new compressor type, with a discharge pressure housing permitting to connect the two compressors with an oil equilibration line. Unfortunately this compressor showed very low efficiency and had to be replaced by a piston compressor. This piston type compressor was driven by a frequency inverter, and tests were performed to show the capability of heat output modulation, in order to follow the heat demand avoiding on/off operating mode of the heat pump. Figures 2.18 and 2.19 show the combined configuration represented in the superstructure and the more detailed flow chart, including the different operating modes on this two-stage approach.

The benefit of the two-stage configuration, has been demonstrated by the relative increase of the two performance indicators, COP and heat output (Fig. 2.20) in steady state operation tests, according to normalized test conditions EN255 ([SNV, 1997]). An evaluation of the exergetic efficiency in Figure 2.21 shows, that the two-stage heating has increasing values at extreme operating conditions (A-11/W60) without attempting an optimum¹, while in one-stage heating mode, the location of the highest efficiency level is at the moderate external condition of A7/W50. Comparing the two heating modes, the efficiency curves cross between the operating conditions A2/W50 and A7/W50. At lower external temperature difference the compressors are operated in two-stage mode with a very low pressure ratio and their efficiency is dropping sensibly (see Fig. 3.8 (a)). The potential of subcooling the condensed liquid is reduced in lower temperature lift conditions. Oil migration from the higher stage to the lower stage compressor has been observed and was highly restricting the runtime of the two-stage compression cycle in steady state conditions.

¹No tests could be performed beyond this limiting temperatures. The air refrigeration unit was limited at about -11°C for steady state regulation and the main elements of the heat pump presented high pressure limits of 25 bar, which limited the water temperature to 60°C .

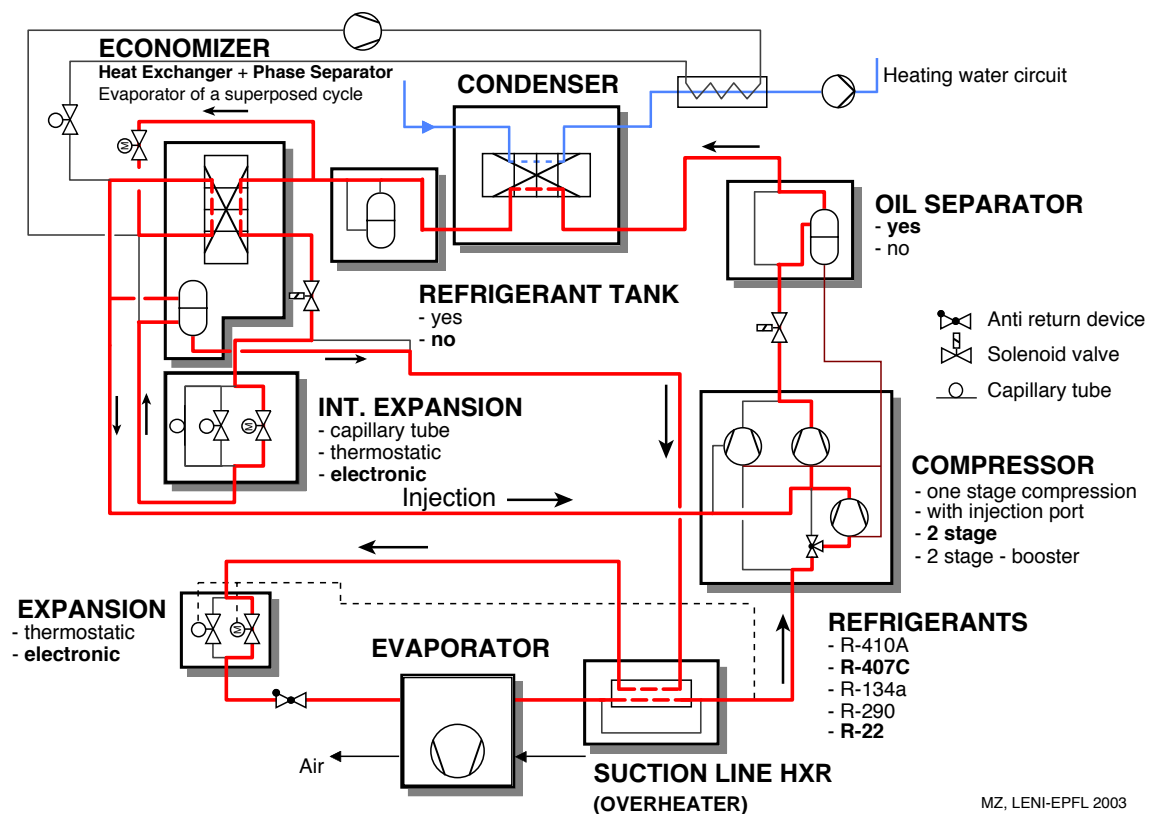


Figure 2.18: Two-stage compression air-water heat pump with economizer flash tank and economizer heat exchanger.

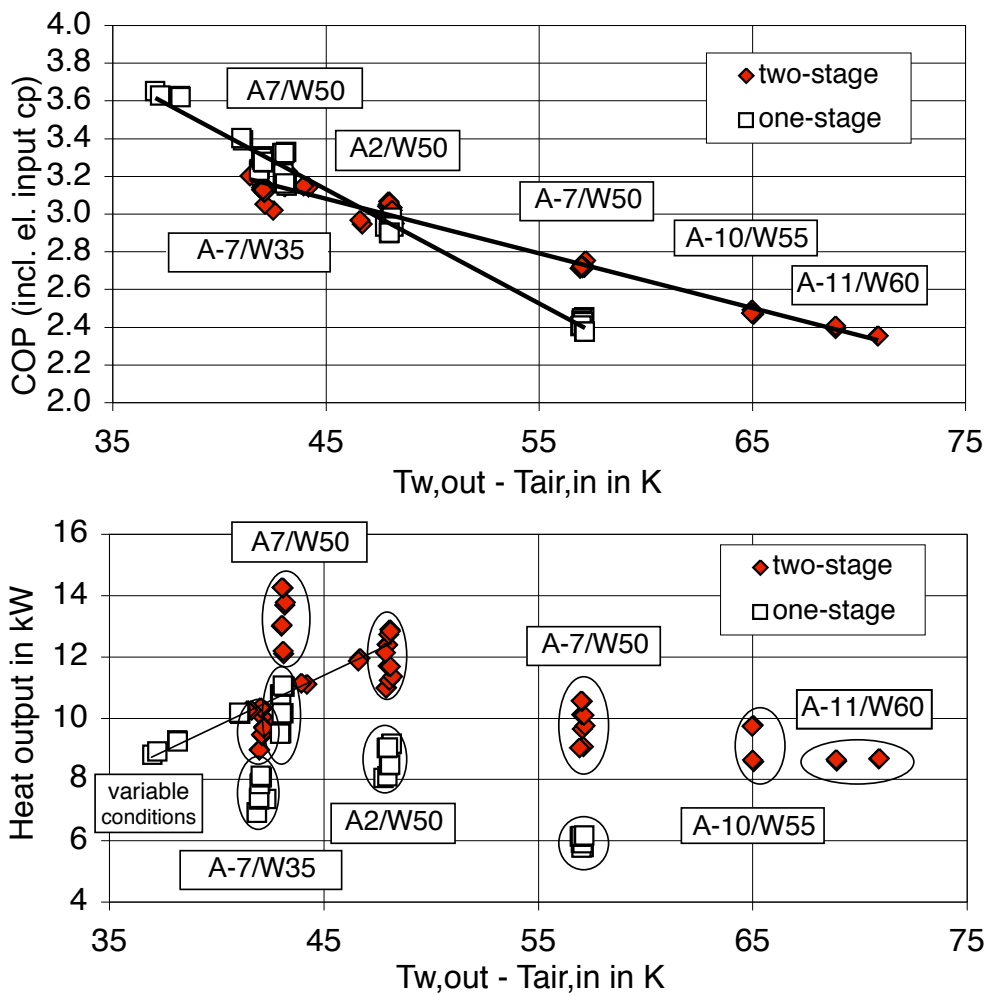


Figure 2.20: Two-stage heat pump with combined economizer flash tank and heat exchanger, inverter driven low stage piston compressor. Comparison of COP and heat output with R-22 in steady state conditions.

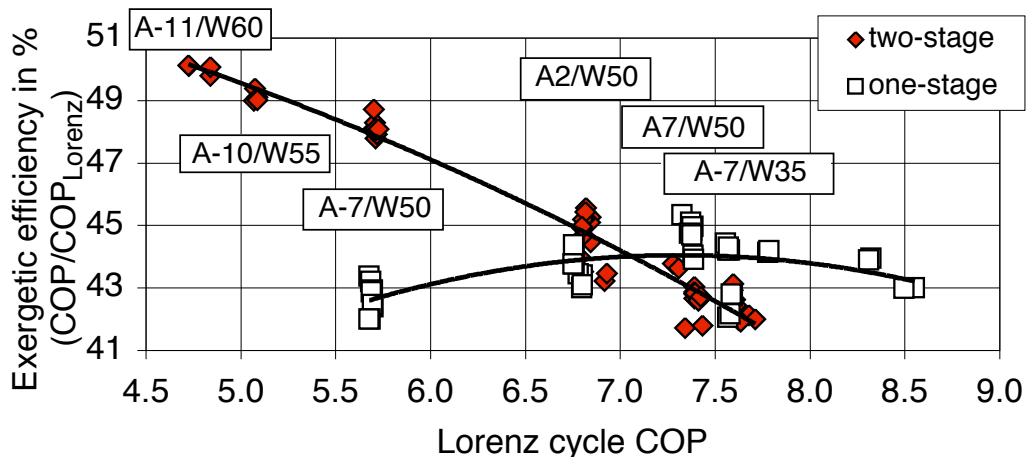


Figure 2.21: Two-stage air-water heat pump with economizer flash tank. Comparison of simplified exergetic efficiency (comparing to a Lorenz cycle with corresponding air and water inlet and outlet temperatures) of two-stage and one-stage steady state heating.

Defrost approach using low exergy heat from the economizer flash tank.

The mainly applied methods for defrosting the finned tube evaporator coil are not very satisfying, and are often poorly implemented in commercial air-water heat pumps. Published performance data ([WPZ, 1993-2003]) allow, by extrapolation from the measured operating conditions, to evaluate the impact of the defrosting on the performances of the heat pump. Figure 2.22 shows the ratings, separating into the two main defrosting techniques, **reversed cycle defrosting** (energy is partly extracted from the heating circuit, condenser acts as an evaporator) and **hot gas defrosting** (condenser is bypassed and all the heat to defrost the finned surface is provided by the compressor). Hot gas defrosting provides lower defrosting power and the defrosting mode has to be maintained for a longer time period. The reduction in the averaged heat output is therefore higher in hot gas defrosting than for units, which are operated by a reversing cycle defrosting. The evaluation has sorted out systems with lower refrigerant charge to those with higher charge, which show an increased impact on the heat output reduction. This fact might be explained by the higher thermal inertia, which absorbs part of the generated heat during the defrosting phase.

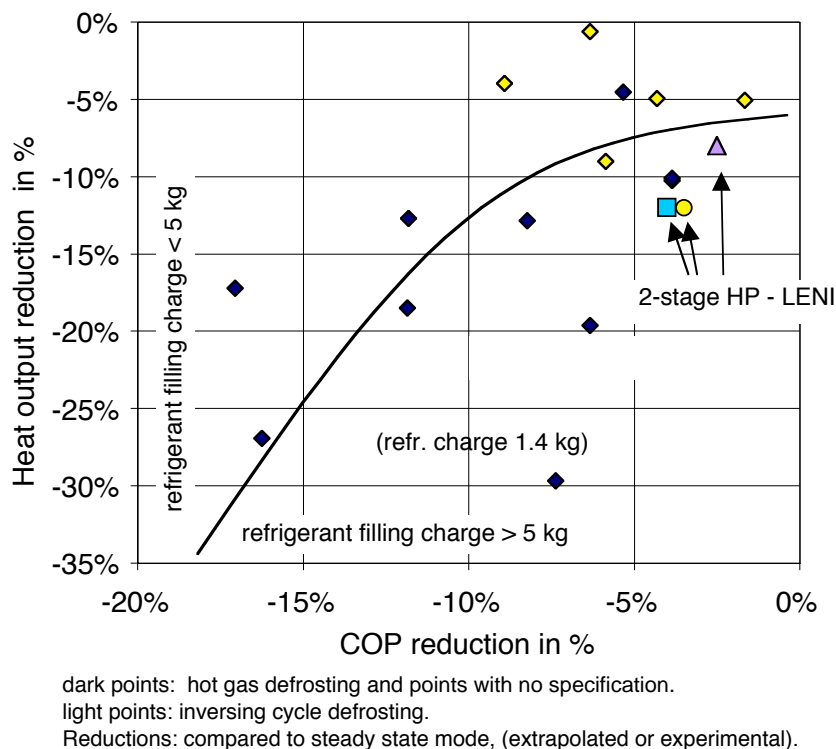


Figure 2.22: Defrosting, comparison to commercial products.

Tests with alternate defrosting modes have been performed (Fig. 2.22, from [Zehnder and Favrat, 1999]), relying on low exergy heat, which is extracted from the economizer flash tank. Figure 2.24, shows as an example, the evolution of the pressure and temperature levels during the defrosting, which has been performed according to the setup of Fig. 2.23 (a). Compared to a standard inversed

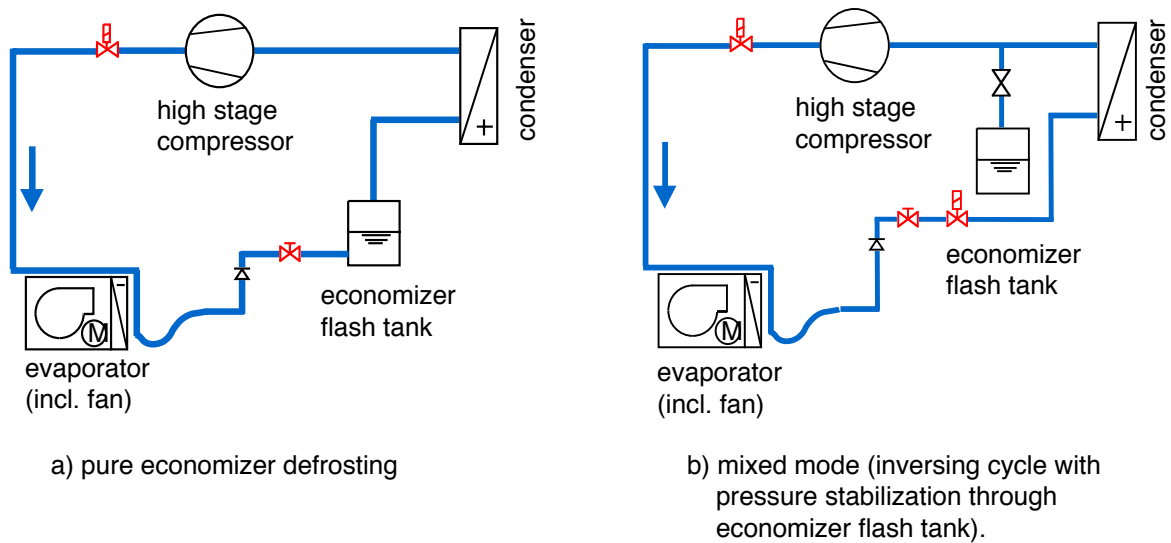


Figure 2.23: Alternative approaches for accelerated and high efficiency defrosting modes, referring to low exergy heat in the economizer flash tank.

cycle defrosting, the system pressures evolve much more smoothly. Considering the present case, the refrigerant mass content in the economizer tank is of ~ 9 kg.

During the defrosting sequence the high stage compressor¹ transports a cumulated refrigerant mass of 7.5 kg. Considering an isenthalpic flashing (no cooling from the returning fluid) from the initial tank pressure of 11 bar to the final pressure of 2.5 bar, 27% of the initial refrigerant mass is potentially liberated (which corresponds to 2.4 kg vapor, or 32% of the amount which is transported by the compressor). By means of adding a thermal inertia, which would accelerate the boiling of the stationary refrigerant, the low exergy contribution could be increased and the pressure level could be maintained at a high level, increasing defrosting power and efficiency.

In the combined reversed cycle defrosting with the connected economizer, the missing energy is delivered by the heating circuit and has resulted in the most efficient and the shortest defrosting.

¹ZR23-displacement of 5.4 m³/h.

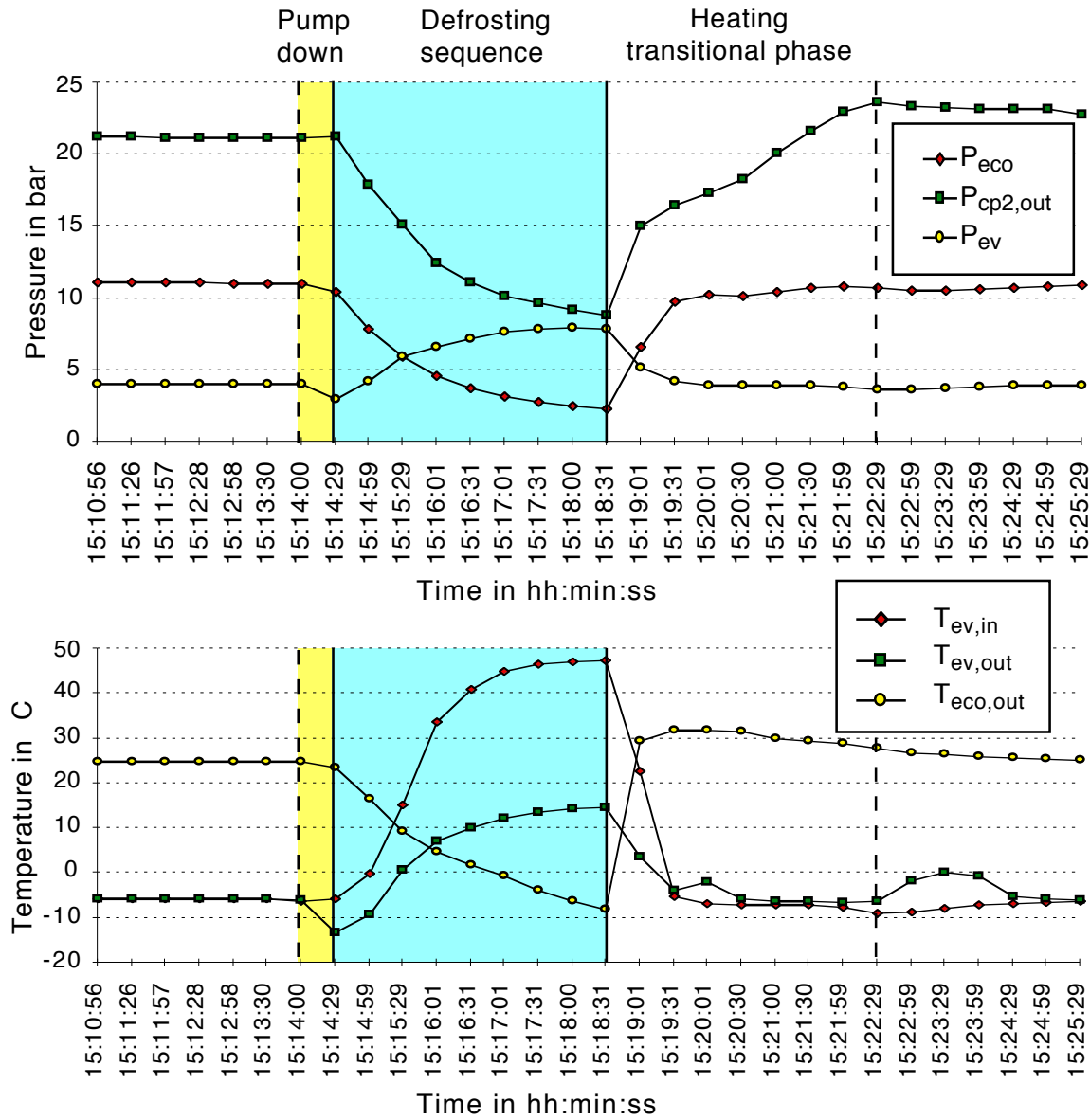


Figure 2.24: Defrosting sequence using low exergy heat source from the economizer; air inlet = -2°C , relative humidity 93%, heating water at 50°C . Two-stage compression heating mode.

Two-stage heat pump with oil migration control

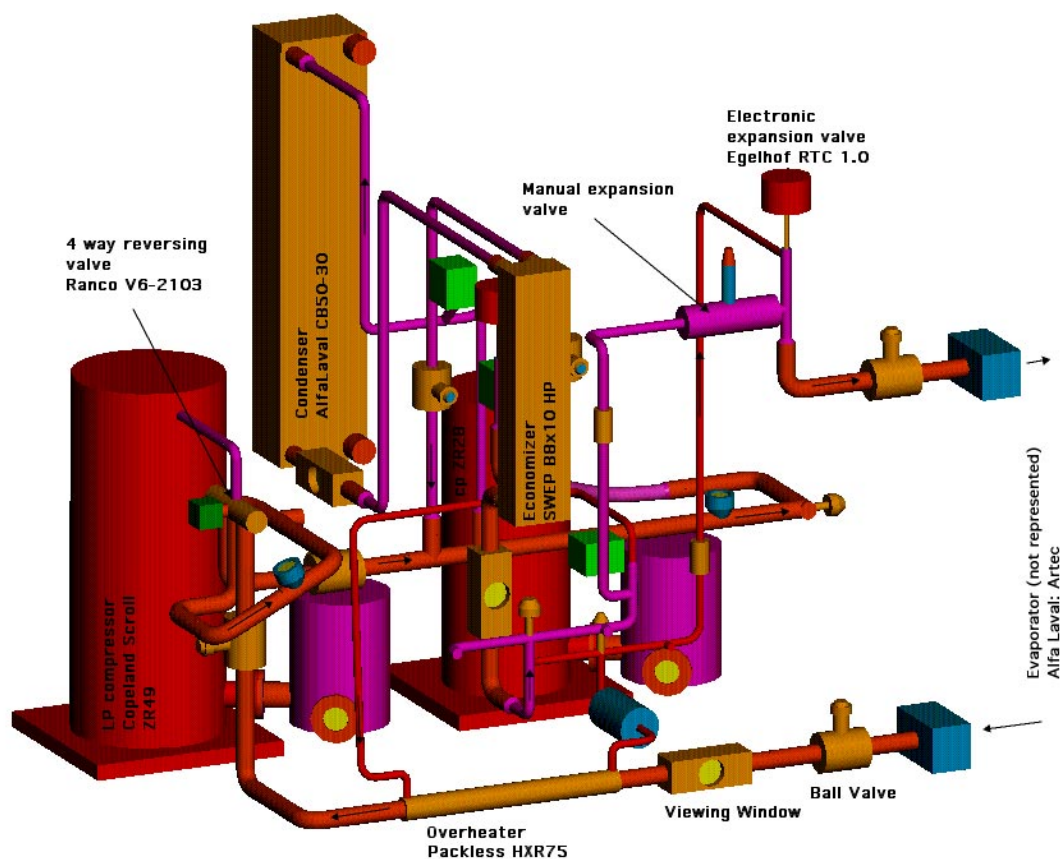


Figure 2.25: Three dimensional representation of the two-stage compression cycle with economizer heat exchanger. The evaporator block is not represented.

In order to show the amount of migrating oil through standard one-stage compression heat pumps and to find solutions enabling permanent two-stage heating mode for small capacity heat pumps, an experimental 10 kW air-water heat pump has been built and tested under standard conditions in the laboratory. Tests include one-stage and two-stage heating mode and some transitional regimes. The unit has been designed in order to avoid oil accumulation in the circuit (excepting the two compressors) and to ensure oil return by appropriate design of ascending vapor lines. The simplified configuration with indication of the two-stage heating mode, is represented in the Figure 2.26. The detailed setup including the measuring data points is shown in Figure 2.29.

As in the preceding performances of one-stage heating mode is compared to the two-stage mode with intermediate heat exchanger, enabling the heat pump to run at a highly extended application range. Figures 2.27 resume the main results and reconfirm the improvements shown in precedent works.

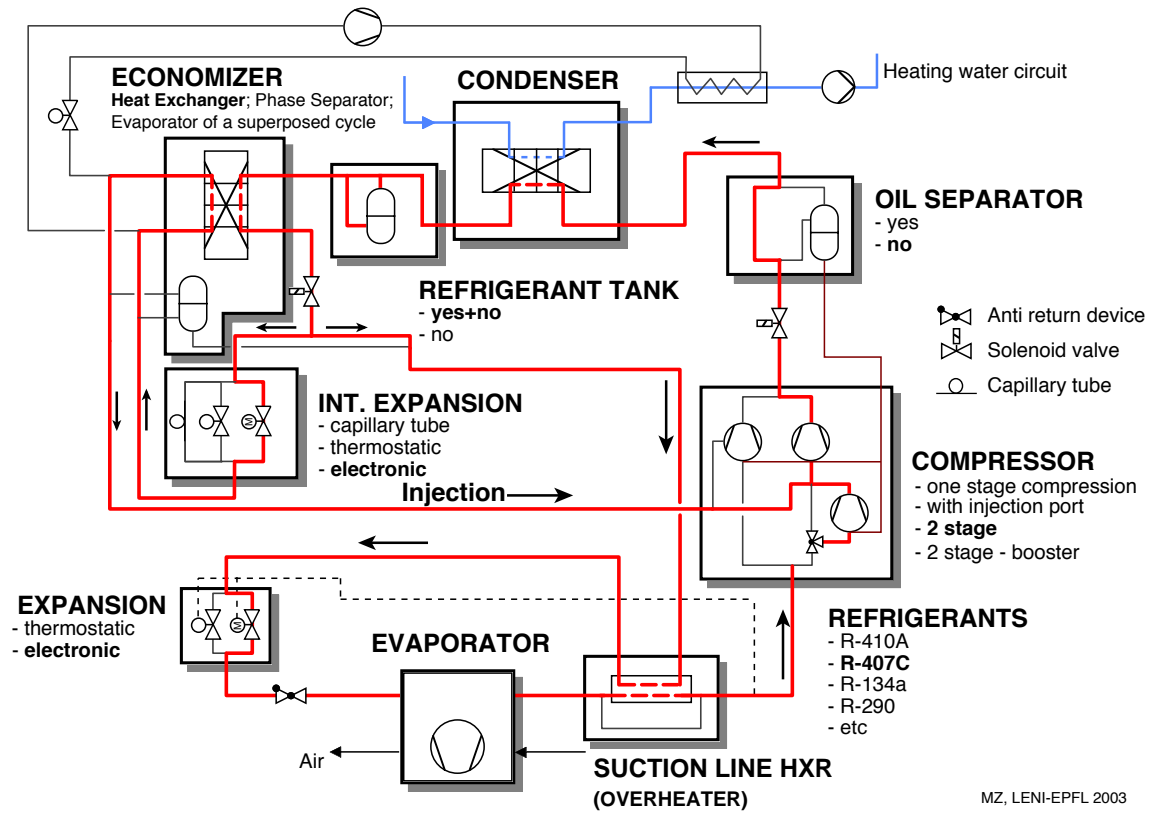


Figure 2.26: Two-stage compression air-water heat pump with economizer heat exchanger.

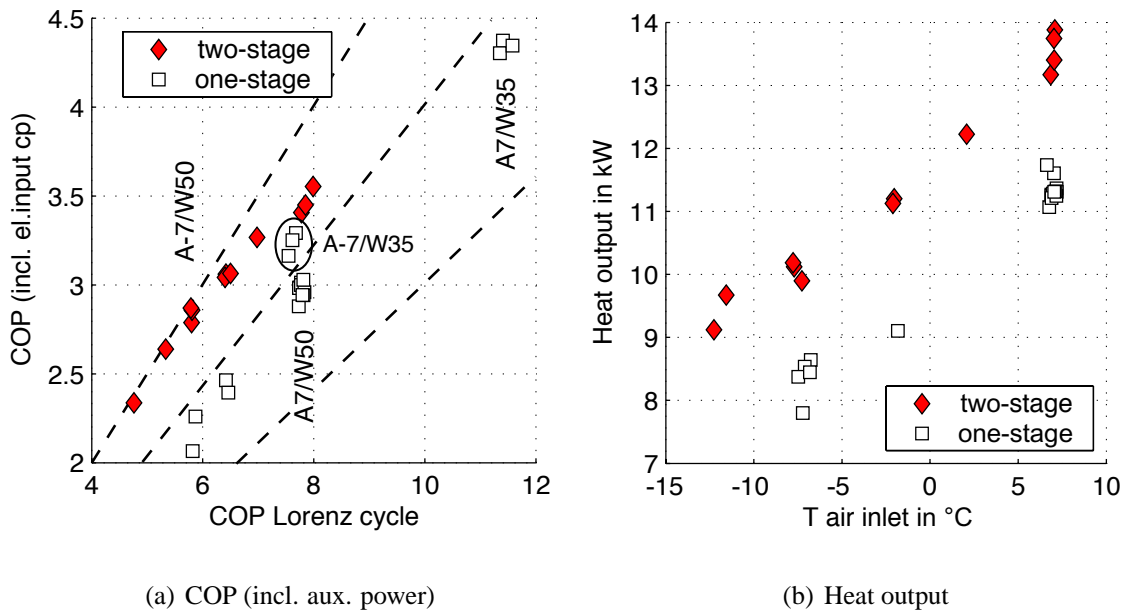


Figure 2.27: Two-stage heat pump with economizer heat exchanger. Comparison of measured COP and heat output with R-407C in steady state conditions.

The two compressor vessels have been equipped by an external sight tube in order to visualize the liquid (oil) level in each of the compressors. By means of electronic level detectors injection valves on the oil circuit were opened in order to re-align directly the low stage compressor with lubricating oil. An oil pump situated between the two compressor enabled the inverse operation, the transfer of oil from the low to the high pressure compressor. As already seen in the first of the two-stage heat pump concepts, a resulting oil flow from the high stage compressor to the low stage could be measured and the pump had to re-equilibrate permanently. Figure 2.28 is illustrating the evolution of the oil liquid level in the two compressor sight tubes.

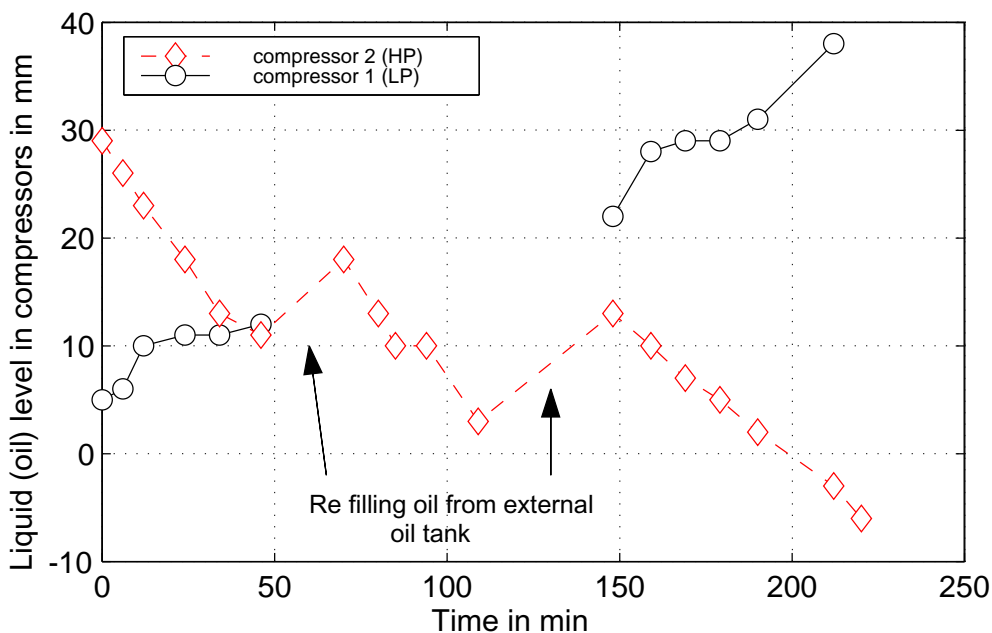


Figure 2.28: Measured evolution of oil levels in mounted external sight tubes in two-stage heating mode in the economizer heat exchanger heat pump.

In order to verify the oil concentration detected by an *Fourier Transform Infrared Spectrometer* in the liquid line of the heat pump, a syringe for injection of known oil packages has been mounted and connected at multiple injection points. Detailed description of the oil migration measurements in the one-stage and two-stage configuration are given in chapter 5.

Booster compressor with economizer heat exchanger

An alternate configuration of a two-stage compression heat pump, has been evaluated by measurements in a demonstration setup. This setup is represented by the *booster configuration* of the Figure 2.30. The booster compressor is intended to run only at a few days per years in order to increase the base heat output of the heat pump and thus to avoid the use of an electric heat supply. In order to avoid oil accumulation in the first stage compressor of this two-stage compression concept, some specific conditions are requested for this type of compressor. Compressor designs with limited oil retention volume and with high suction volume rate are requested. In order to

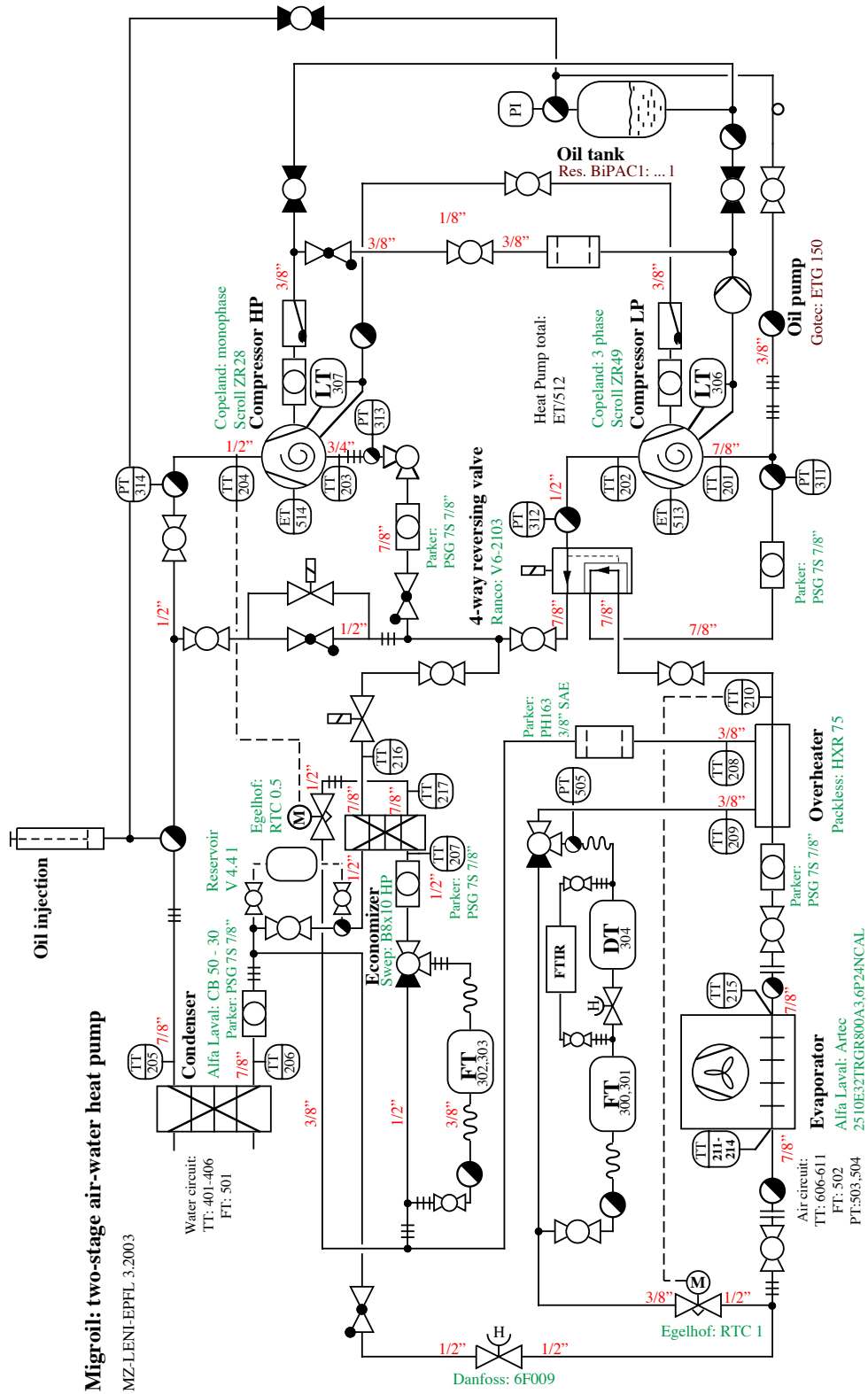


Figure 2.29: Flow chart, including oil equilibration parts for two-stage heat pump.

maintain the discharge temperature at the exit of the main compressor within reasonable limits, a desuperheat (by mixing the main flow stream with liquid or saturated vapor) has to be integrated into the concept. In the present setup, the economizer heat exchanger configuration is used.

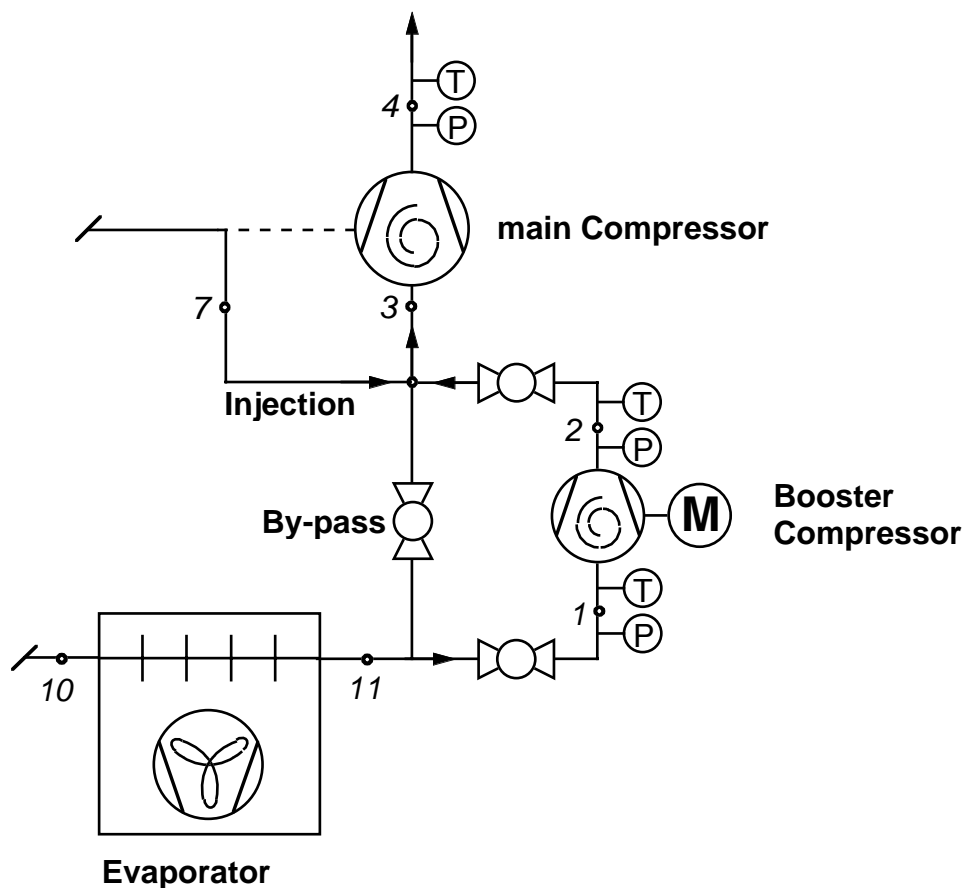


Figure 2.30: Alternative two-stage configuration, with scroll type main compressor, open type scroll compressor (booster) with high volumetric suction flow and low volume ratio, figure from [Zehnder et al., 2002].

The research of the booster compressor has included different types of compressors, as a hemispheric plate compressor, a roots turbo-compressor unit and an available scroll type automobile air-conditioning scroll compressor. A Sanden scroll compressor¹ was finally selected for the experimental evaluation and its geometry was adapted to the specific purpose (high displacement volume and lower built-in volume ratio).

The nominal characteristics of this compressor are listed in Table 2.3. In order to adapt the displacement volume of the compressor to the calculated needs, the booster compressor is alimented at the effective speed of 71 Hz.

With a global compression efficiency of $\sim 50\%$, the modified booster compressor is in a acceptable

¹Sanden International Corporation, <http://www.sanden.com>

Table 2.3: *Modified automotive air-conditioning scroll: Sanden, Type BBC QU112 M4 AZ.*

Compressor type	open type scroll compressor,
Displacement volume	15.3 m ³ /h @ 50 Hz
Rotational speed	71 Hz
Refrigerant	R-407C
Lubricant oil charge	0.15 ℓ
Total weight	3.8 kg

performance range¹. Steady state operating mode at A-11/W65 showed an **increased heat output of 15.7 kW compared to 7.4 kW in one-stage compression cycle at A-11/W60 on the same equipment**. COP of the booster configuration is slightly decreased, which is due to the lower evaporation pressure. Air flow was maintained at the same rate resulting in a higher temperature glide on the air side. Table 2.4 summarizes the obtained results.

Table 2.4: *Booster configuration, one-stage compression heat pump with and without intermediate injection. Steady state operation tests at air inlet -11°C and heat outlet temperature at 65°C (resp. 60°C in normal one-stage compression mode).*

	one-stage no injection	one-stage with injection	two-stage booster compressor
Air inlet	-11.1°C	-11.2°C	-11.4°C
Heating water outlet	59.0°C	64.6°C	64.6°C
Heat output	7.4kW	9.7kW	15.7kW
COP (incl. annex power)	2.08	2.02	1.89
Exergetic efficiency	43.9%	45.3%	42.6%
Discharge temperature	119.7°C	121.8°C	120.6°C
Condensation pressure	24.2 bar	26.9 bar	27.9 bar
Evaporation pressure	3.0 bar	2.8 bar	1.9 bar
Compression ratio (II)	8.1	9.6	3.9 / 3.8

The *booster* concept is very interesting for high temperature lift heat pump applications, allowing an extended application range, high heat output at the extreme operating conditions and enabling an adapted functionality at the more frequent temperature range, of the mid-winter season or for the hot water preparation. It can also be imagined as an optional feature to a standard or a intermediate injection heat pump. During several weeks of testing, no significant oil hold up could be detected. The concept as presented is viable, and different points can be further optimized to increase system

¹In contrary to the hermetic compressors, using an open type of compressor, the electro-mechanical motor losses are not recuperated by the refrigerant, and the generated heat is lost to the ambience.

efficiency: hermetic concept, in order to reduce to a maximum refrigerant leakage; two level speed fan, to reduce the air side temperature glide.

2.4 Conclusions

Different approaches for **improved thermodynamic concepts of high temperature lift heat pumps** are presented within this work and are experimentally compared to the classical one-stage heat pump in the context of high temperature heating applications, as typically occurring in existent, residential heating systems. While present and future heating design are orienting to low temperature floor heating or low energy air-air heating systems, environmentally friendly solutions for the large number of installations, which need to be retrofitted, have to be proposed as soon as possible. The use of emission free heat pumps enables a major contribution to the reduction of CO₂ emissions.

Considering air-water heat pumps, as the most probable candidate for the substitution of existing heat production systems, the thermodynamic process has been reviewed and efficiency improving concepts have been identified. The considered options are assembled in a **unifying superstructure**, which is further used to represent all the **experimentally realized concepts**, which are: **one-stage compression cycle with intermediate injection of saturated vapor**, **two-stage economizer cycle and booster concept** and **liquid subcooling through an auxiliary cycle**. Most of these approaches can be found as standard cycles in the refrigeration industry, while hardly any specific components could be found for heating heat pumps at the begin of this thesis work. The presented prototype heat pumps and related tests could be realized within the framework Swiss retrofit Heat Pump, funded by the Swiss Federal Office of Energy and in collaboration with several Swiss heat pump manufacturers (Axima, Cryotherm, Kälte-Wärme-Technik AG, Satag Thermotechnik AG, Termogamma) and the Berne University of Applied Sciences, Burgdorf.

With a target **heat output of 10 kW** at the base heating operation conditions, and considering a **monovalent heating** approach (the heat pump covers all the thermal needs), system **tests have successfully been performed at heating water temperatures up to 65°C at minimal external air temperatures of -12°C**. Direct evaluations in normal heating mode and with the implemented improved setup on the same unit, allowed to demonstrate the potential of performance increase. A cross evaluation between the specific concepts, is presented in Table 2.5. The internal cycle COP of the air/water concepts have been added, in order to suppress the contribution of fan power, which is the major contribution of annex power. Each configuration is represented by a mean operating point, comparing the cycle with and without improving addition, and on the considered extreme operating conditions. **Comparing COP values**, it reveals, that **the most important improvements**, compared to the standard setup, **are obtained by the two-stage cycle (@A-2/W50), and**

by the auxiliary cycle for subcooling (@B-2/W50), while the other comparisons could not show very high ameliorations. **The gain of 20%-35%! in heat output is considerable and has been measured equally on all concepts.** This gain is obtained, with the identical heat exchangers as in basic setup. The evaluation of **the booster solution has shown a enormous increase of 100%! (@A-12/W60), with nearly no decrease in COP.**

Table 2.5: Comparison of performance data for measured advanced heat pump concepts. A/W=air/water, B/W=brine/water, temperature in °C(air or brine inlet/water exit). COP int.=refrigerant side. / COP ext.= system side incl. annex power.

Cycle configuration	Operating point	COP	η_{II}^1 in %	Heat output	Size cp.
	A/W or B/W	(int./)ext.	(int./)ext.	in kW	in m ³ /h
One-stage with interm. injection (liquid port)	B0/W50 - no inj.	3.5	54	12.2	14.5
	B0/W50 - w. inj.	3.6	56	13.5	
	B-10/W60 - no inj.	2.4	50	7.7	
	B-10/W60 - w. inj.	2.5	53	9.8	
Aux. cycle for liquid sub- cooling	B-2/W50 - w/o aux.	2.6	42	8.5	11.8
	B-2/W50 - w. aux.	2.9	47	10.9	11.8&2.24
	B-7/W50 - w/o aux.	2.4	42	7.3	
	B-7/W50 - w. aux.	2.5	44	9.2	
One-stage with interm. injection (vapor port)	A2/W50 - no inj.	3.4/3.0	51/45	10.8	11.7
	A2/W50 - w. inj.	3.5/3.1	52/46	13.2	
	A-12/W60 - w. inj.	2.2/2.0	48/43	10.0	
Two-stage compression	A-2/W50 - 1-stage	2.5/2.1	40/34	9.4	11.7
	A-2/W50 - 2-stage	3.2/2.6	52/42	11.7	11.7&6.8
	A-12/W60 - 2-stage	2.4/2.0	52/43	9.0	
Two-stage booster	A-12/W65 - 2 stage	1.9	43	15.7	11.7&21.7

Considering economical aspects and the maturity of the tested approaches, **intermediate injection cycles are the most evident to be considered.** The present tests with a prototype vapor injection port compressor, have contributed to the development of an air-water heat pump, which in the meantime could be commercialized. The auxiliary cycle concept, could not go beyond the laboratory prototype phase. The system is considered to be far too complex, without really abating to the high discharge temperature and the high pressure ratio in the main compressor. Two-stage compression cycles have shown whether an excellent capacity improvement (booster solution) or a considerable improvement of both performance indicators, the COP, with relative improvements of 20%-30% (@A-2 and A-7/W50) and the heat output +25% for the economizer two-stage cycle. These improvements although are achieved, comparing to the one-stage cycle with a low built-in volume compressor, which certainly is not the appropriate technology for high lift applications in

¹Simplified exergetic efficiency: COP / COP_{Carnot} .

one-stage compression.

Experimental tests have although shown some difficulties, related to two-stage concepts in small capacity heat pumps. These are related to the oil migration, which is entrained with the refrigerant vapor out of the compressor and transits through the entire cycle. In all tested setups, the oil accumulates in the low stage compressor vessel, disabling a simple oil return management from one compressor shell to the other. In order to lift the oil into the high stage compressor shell, an oil pump is needed. A further investigation and propositions to resolve the oil migration problem is presented in chapter 5.

Bibliography

- P. Bailer. **Technischer Überblick über grosse Wärmepumpen in Europa.** In *9.Tagung des Forschungsprogrammes Umgebungs- und Abwärme, Wärme-Kraft-Kopplung (UAW) des Bundesamtes für Energie (BFE)*, 2002.
- S. Bertsch and M. Ehrbar. **Verbesserung des Abtauens bei luftbeaufschlagten Verdampfern, Phase 2: Bewertung der Abtauprozesse.** Final report. Swiss Federal Office of Energy, 2002. ENET-Nr. 220187.
- E. Granryd. **Energy Savings in Vapor Compression Refrigerating Systems.** In *Int. Symposium on the NTH Refrigerating Engineering, Trondheim*, pages 43–60, 1992.
- H. Kruse. **Refrigeration Cycles in Relation to Exergy Efficiency.** In *Int. Symposium on the NTH Refrigerating Engineering, Trondheim*, pages 21–41, 1992.
- G. Kulik, P. Hoffmann, and M. Zehnder. **Oberflächenbehandlung zur Vereisungsverringerung.** Final report. Swiss Federal Office of Energy, 2003. ENET-Nr. 230222.
- H. Liang and T. Kühn. **Irreversibility Analysis of a Water-to-Water Mechanical-Compression Heat Pump.** *Journal of Energy*, 16(6):883–896, 1991.
- NEDO. **Research and Development on Super Heat Pump Energy Accumulation System.** Final Report. New Energy and Industrial Technology Development Organization, Tokyo, 1993.
- SNV. **EN 255-2: Air Conditioners, liquid chilling Packages and Heat Pumps with Electrically Driven Compressors - Heating Mode - Part 2: Testing and Requirements for Marking for Space and Heating Units.** Swiss Association for normization and Standards, 1997.
- WPZ. **Published Results in Bulletin No. 1 - 37**, 1993-2003. URL www.wpz.ch.
- M. Zehnder and D. Favrat. **Pompe à chaleur biétagée à haute performance, Phase 2: Dégivrage par énergie à basse exergie.** Final Report. Swiss Federal Office of Energy, 1999. ENET-Nr. 194465.
- M. Zehnder, F. Maréchal, S. Guex, J. Schiffmann, and D. Favrat. **Pompe à chaleur air-eau à haute température, Phase 2: Cycle à injection optimisé, essais journaliers et compresseur booster; Analyse thermo-économique.** Final report. Swiss Federal Office of Energy, 2002. ENET-Nr. 220219.

3. Simulation model

A new **heat pump simulation tool** has been developed, in order to be able to simulate the previously evaluated **enhanced thermodynamic cycles for the high temperature lift applications**. This tool fills the gap between available programs, which simulate large scale, industrial heat pumps and those, which mainly apply to geothermal heat pumps or concerning air-conditioning units (an overview of the available software tools is provided in the next chapter). In this chapter, the different elements, which compose our simulation program are introduced and validated with available data.

The thermodynamic and physical properties of the refrigerants are calculated with the latest version of Refprop (Version 7.0 [Lemmon et al., 2002]). An in house developed fluid interface, called FLINT, includes the Refprop source code, which allows it to be compiled on any desired platform, as a fully featured Matlab executable interface (for Matlab (Version 6.5)).

The modular approach enables to extend this model easily to a much larger context. It is so far composed of a generalized description of the hermetic scroll compressors, including the new generation of intermediate injection compressors. A flow map based heat transfer model is implemented into the finned tube evaporators, including the impacts of eventually mixed oil. Generalized descriptions of the plate heat exchangers and the capillary tube allow to apply this program to a large number of heat pump cycles.

The simulation models have been developed considering the following **assumptions**:

1. Steady state conditions

Assuming only steady state conditions is one of the most restrictive assumptions, but is leading to considerable simplifications of the calculation needs and allows the most general approach, without entering too much into the geometrical specifications. In real operating conditions there are two main fluctuation levels to be considered. On the cycle level, the internal regulator (mostly a thermostatic expansion valve) induces a pulsated mass flow, with effects on the cycle temperatures and pressures. The pulsation length of this mode is in the order of 30 s to several minutes, depending on the complexity of the considered refrigerant cycle. On the heating system level, the cycling is mainly due to alternating on/off mode, with typical pulsation lengths of 20 min to 1 hour. The influence of this cycling on the system performances is highly depending on the implementation of the heat pump in the heating sys-

tem, on the regulation mode and on the electricity cut off conditions. Repetitive defrosting of the evaporator coil at colder external temperatures, approaching 0°C, is another transitional operating mode, which is specific to air source heat pumps. The impact of defrosting on the heat pump performances can be accounted for, by adopting a penalization approach.

2. Neglected pressure drop in the refrigerant lines

Pressure drop, related to the internal dissipation, is occurring in every flow conduct and has to be considered for the optimization of the specific elements, like in the heat exchangers, which have narrow flow sections and multiple bends. Gravitational, frictional and momentum pressure drop are not implemented, in this simulation model. Friction of flow is only considered in the capillary tube fluid flow and by way of the compression efficiency in the compressor.

3. Thermally insulated conducts and heat exchangers

All pipes and the heat exchangers are supposed to be perfectly thermally isolated to the outside. However, in order to meet the experimental results, thermal losses between the compressor shell and the ambiance have to be considered.

4. Influence of oil on two-phase heat transfer

Excepting specific configurations, where higher oil concentrations circulate with the refrigerant (e.g. in ammonia application, oil is needed to reduce compression discharge temperature) the oil amount is very low (<1%) and can reasonably be neglected in the energy balance. Oil is however affecting the boiling temperature curve in two-phase flow and influences the heat transfer mechanism as a result of modified thermo-physical properties of the refrigerant-oil mixture. Both effects have been included using an established refrigerant-oil mixture model.

5. Auxiliary power

To circulate the external flow, fans and pumps are needed, and their power consumptions have been integrated to calculate a realistic value of the coefficient of performance. Electric power consumption of the control board, the electromagnetic valves and the electric expansion device are not taken into account in the simulation balance, but are often part of the energy consumption in most of the experimental results presented in chapter 2.

Applying the basic laws of thermodynamics (energy conservation, entropy balance and equilibrium conditions in each point of the transformation) to a **homogeneous flow in steady state conditions**, the general set of equations for open flow systems can be written in the mass specific form:

$$\delta e^- + d\left(\frac{u^2}{2}\right) + gdz + \delta r = -vdP = -dh + \delta q^+ + \delta r = -dh + Tds \quad (3.1)$$

where

- δe^- is the mechanical work output, followed by the cinematic energy change $d\left(\frac{u^2}{2}\right)$, the gravitational term gdz and the specific internal dissipation δr .
- vdP represents the change of specific pressure energy.
- dh and δq^+ are the variations of specific enthalpy and the heat input and δr is (again) the specific internal dissipation.
- the term of heat and dissipation are equivalent to the variation of entropy times the temperature Tds .

In heat exchangers and in volumetric compressors the variations of the cinematic and the gravitational energy is negligible compared to the transferred heat or the compression work input.

3.1 Compressors

The compressor type selection is mainly driven by the power range of the heat pump, the requirements of cost and efficiency and the application range. For domestic heat pumps with a heat output range of 10 - 20 kW, the available types are: the scroll, reciprocating piston, rotary vane and rolling piston. The **scroll compressor** has replaced nearly all other heat pump compressors in the last decade, except for some specific applications with very small capacity or low pressure ratio. Exclusively **hermetic compressors are considered** in the simulation, although depending on the choice of the refrigerant also semi-hermetic or even open compressor types could be chosen.

A semi empirical simulation model, which is generally applicable to rotary volumetric compressors, but which has been specifically implemented for scroll type compressors, is presented in the following sections. This **extended model** matches experimental compression data over a wide range of pressure ratios and pressure differences, for the **simple compressor configuration, and for configurations with intermediate injection of saturated vapor and liquid**.

General definitions

Figure 3.1 presents the input-output model of a hermetic compressor. The compression part is supposed to be located at the top of the compressor shell and the lubricating oil is in the bottom part and is in contact with the aspirated refrigerant transporting a low quantity of oil.

The compression is characterized by the geometrical input data (displacement \dot{V}_{displ} , rotational speed n), the three efficiencies (η_{conv} , η_{cp} and η_{vol}) and the thermal shell losses \dot{Q}_{loss} .

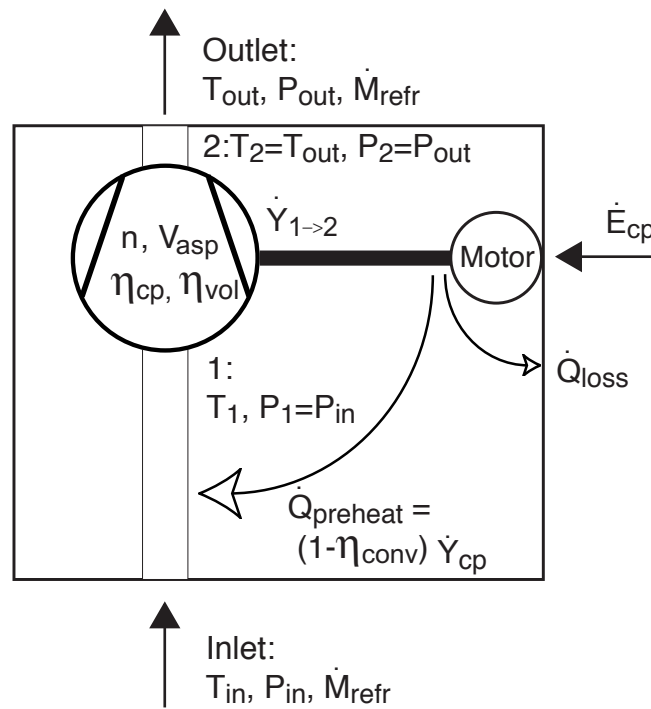


Figure 3.1: *Input-output model for compressor simulation*

The following **assumption** are applied to the compression unit:

1. Steady state operating conditions.
2. Conservation of mass and energy.
3. Adiabatic compression. (Heat transfer to the refrigerant is limited to the suction phase, but is neglected in the compression chamber.)
4. Kinetic and potential energy variation between the suction and the discharge line are neglected.

The global **energy (or instantaneous power) balance** is composed by the input of electricity (hermetic system) and the transformation output of the fluid:

$$\begin{aligned} \dot{E}_{cp} &= \dot{Y}_{cp} + \dot{Q}_{loss} \\ \text{with } \dot{Y}_{cp} &= \dot{M}_{refr}(h_{out} - h_{in}) \end{aligned} \quad (3.2)$$

where the thermal shell losses \dot{Q}_{loss} depend on the temperature difference of the shell to the ambient¹. The remaining compression power is divided into the two contributions, the preheating heat $\dot{Q}_{preheat}$ and the work of compression $\dot{Y}_{1 \rightarrow 2}$ as shown hereafter.

For **hermetic compressors, the electric and mechanical conversion losses are mainly transmitted** to the refrigerant (reduced by the shell losses). It is assumed, that all this generated heat of the transformation is transferred **to the refrigerant in the suction line**, by mass transfer via the lubricating oil to the oil sump and then by heat transfer (convection) to the refrigerant, preheating the entering vapor. An adiabatic transformation is assumed in the discharge line. Pressure drop in both, the suction and the discharge line within the compressor shell are neglected.

$$\dot{Q}_{preheat} = \dot{M}_{refr} (h_1 - h_{in}) = (1 - \eta_{conv}) \dot{Y}_{cp} \quad (3.3)$$

$$h_2 = h_{out} \quad (3.4)$$

With the above relations the **efficiency of the electric and mechanical transmission chain including the heat losses between the compressor housing and the ambience** is defined by the ratio

$$\eta_{conv} = \frac{\dot{Y}_{1 \rightarrow 2}}{\dot{E}_{cp} - \dot{Q}_{loss}} = \frac{\dot{Y}_{1 \rightarrow 2}}{\dot{Y}_{cp}} = \frac{\dot{M}_{refr} (h_2 - h_1)}{\dot{M}_{refr} (h_{out} - h_{in})} \quad (3.5)$$

Energy conversion efficiency for small to medium sized compressors are in the order of 90% (see [Afjei, 1993; Winandy et al., 2002]) to 80% [Hayano et al., 1988] in normal operating conditions. The amount of preheating cannot be measured from outside of the compressor shell. Measuring the refrigerant's temperature at the compression volume, or indirectly by heat transfer evaluations and the measure of the oil temperature in the shell, the part of the preheating could be evaluated more accurately, than the presented approach. As a first order approximation, the transmission losses are estimated to be proportional to compressor size (the displacement) only. A multiplying coefficient of proportionality is introduced to calibrate with experimental data. Other dependencies, as the rotational speed and the motor load should ideally be added to the model, allowing a more reliable extrapolation to the implementation of other refrigerants and operating conditions.

$$\dot{Q}_{preheat} = f_{transm} \dot{V}_{displ} \quad (3.6)$$

$$\text{with } \dot{V}_{displ} = V_{asp} n \text{ in m}^3/\text{s} \text{ and } f_{transm} = 0.09 \cdot 10^{-6} \text{ J m}^{-3}.$$

¹The heat losses are calculated on the base of experimental data, meeting the specific conditions of each setup (insulations). The measured loss rate varies between 0% – 20% of the electric power.

In the effective compression zone (1-2), the fundamental equation 3.1 (condensed form of the 1st and 2nd law of thermodynamics including Gibbs equation) resumes to the mass specific form:

$$\delta e^- + \delta r = -v dP = -dh + \delta q^+ + \delta r \quad (3.7)$$

And by integration of the first and second part

$$e^+ = \int_1^2 v dP + \int_1^2 \delta r \quad (3.8)$$

Equation 3.8 results to the **compression efficiency**, which is given by

$$\eta_{cp} = \frac{\int_1^2 v dP}{e^+} = \frac{\int_1^2 v dP}{h_2 - h_1 + q^-} \quad (3.9)$$

The compression efficiency equals to unity for an ideal compression without internal dissipation. The real trajectory can be approximated by a **polytropic transformation**. For this type of transformation, the specific pressure energy $\int v dP$ can be calculated with the expression 3.11, using the perfect gas approximation:

$$P v^n = Cst \quad (3.10)$$

$$\int_1^2 v dP = v_1 P_1 \frac{n}{n-1} \left[\Pi^{\frac{n-1}{n}} - 1 \right] \quad (3.11)$$

with $\Pi =$ Pressure ratio P_{cd}/P_{ev} , and $n =$ polytropic exponent

The **isentropic transformation** is used to characterize the reversible, adiabatic compression. The isentropic transformation is a specific polytropic transformation and equation 3.11 is also used for isentropic trajectory. The **polytropic exponent n is replaced by the isentropic exponent κ** , which is the ratio of volumetric and isobaric specific heat of the gas. Along the isentropic transformation, the compression work equals to the difference of enthalpy. The compression energy $\int v dP$ can therefore easily be evaluated for a real gas on the basis of the enthalpy difference Δh_{is} , which is readily available through thermodynamic property programs. In the literature, either the polytropic and isentropic transformation are used to characterize the quality of the compression.

The compression efficiency, expressed with the polytropic transformation is given by

$$\eta_{cp,poly} = \frac{\int_1^2 v dP}{e^+} \quad (3.12)$$

and can be approximated, using the perfect gas transformation (eq. 3.10):

$$\eta_{cp,poly} = \frac{\dot{M}_{refr} v_1 P_1 \frac{n-1}{n} \left[\Pi^{\frac{n-1}{n}} - 1 \right]}{\dot{Y}_{1 \rightarrow 2}} \quad (3.13)$$

When discussing test results, the compression efficiency is mainly expressed by the following expressions (adiabatic compression is assumed):

- Adiabatic compression \rightarrow Isentropic efficiency:

$$\eta_{cp,is} = \frac{\int_1^2 v dP}{e^+} = \frac{h_{2,is} - h_1}{h_2 - h_1} \quad (3.14)$$

- Total isentropic efficiency (including the mechanical and electric conversion):

$$\eta_{cp,tot} = \eta_{conv} \eta_{cp,is} \quad (3.15)$$

- External efficiency including the conversion losses and the thermal shell losses:

$$\eta_{cp,ext} = \frac{\dot{Y}_{cp}}{\dot{E}_{cp}} \eta_{cp,tot} \quad (3.16)$$

3.1.1 Scroll compressor model

The compression concept based on two symmetrically formed spirals, the scrolls, has already been patented by Léon Creux in 1905 ([Creux, 1905]), but could only mark its breakthrough in the 1980's with the appearance of computer aided machining tools.

The scroll compressor's specific features are the high efficiency, low noise emissions and no re-expanding clearance volume, resulting in high volumetric efficiency, even at high pressure ratios. Figure 3.2 shows a drawing of a hermetic scroll compressor illustrating the suction port, the electric motor, the compression part and the discharge port. The lubricating oil occupies the free space at the bottom and an eccentric channel in the center is working as oil pump.

The compression process, which is defined by the relative motion of the two spirals, is illustrated by Figure 3.3. Two symmetrical compression volumes are sealed simultaneously and gradually displaced towards the centrally located discharge port. With each revolution two new volumes are enclosed, defining the theoretical **aspiration volume** V_{asp} of the compressor. The ratio between the aspiration volume V_{asp} and the volume of the same compression chamber at the moment,

when it opens to the discharge port, V_{dis} , defines the **built-in volume ratio** $VR_i = V_{asp}/V_{dis}$ of the compressor.

Considering the theoretical performance characteristics of fixed built-in volume ratio compressors in adapted and non adapted compression, the **over-compression losses** (the discharge port opens, when the pressure in the compression volume is higher than the system pressure) and the **under-compression losses** (opening at lower inner pressure) with flow back from the system¹ are graphically represented as the additional areas in the P-V diagram of Figure 3.4. The analytical approach comparing the adapted transformation with the theoretical transformation of fixed built-in volume ratio compressors, has been presented by [Sauls, 1982] and has been widely applied to the scroll compressor models, see e.g. in [Afjei, 1993; Winandy et al., 2002].

Assuming perfect gas, the **adapted pressure ratio** for a given built-in volume ratio of the compressor, depends on the polytropic exponent n of the transformation, and **is therefore specific**

¹The return flow in under-compression situations is avoided with the implementation of dynamic valves, which has been recently introduced in the new compressor series for heat pump application.

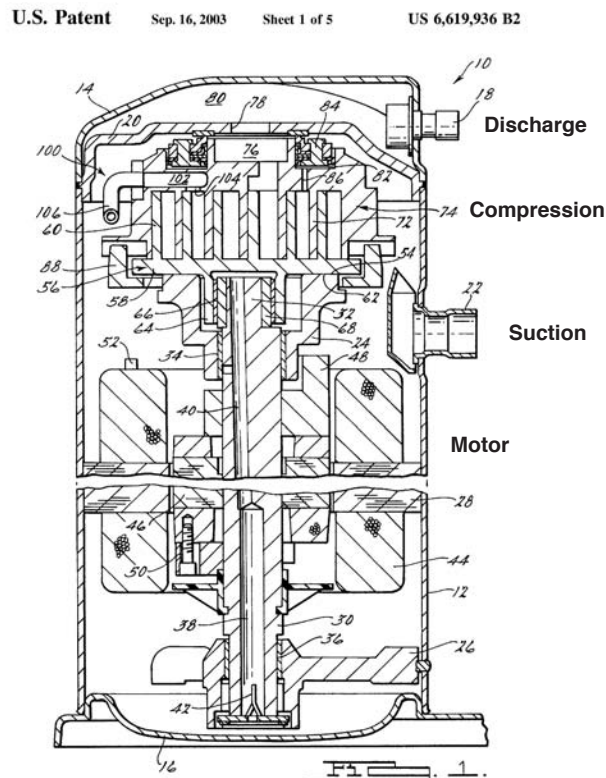


Figure 3.2: Drawing of a hermetic scroll type compressor, Copeland Corp. Sidney, Ohio, USA, US-Patent No. 6,619,936 B2, [Perevozchikov, 2003]

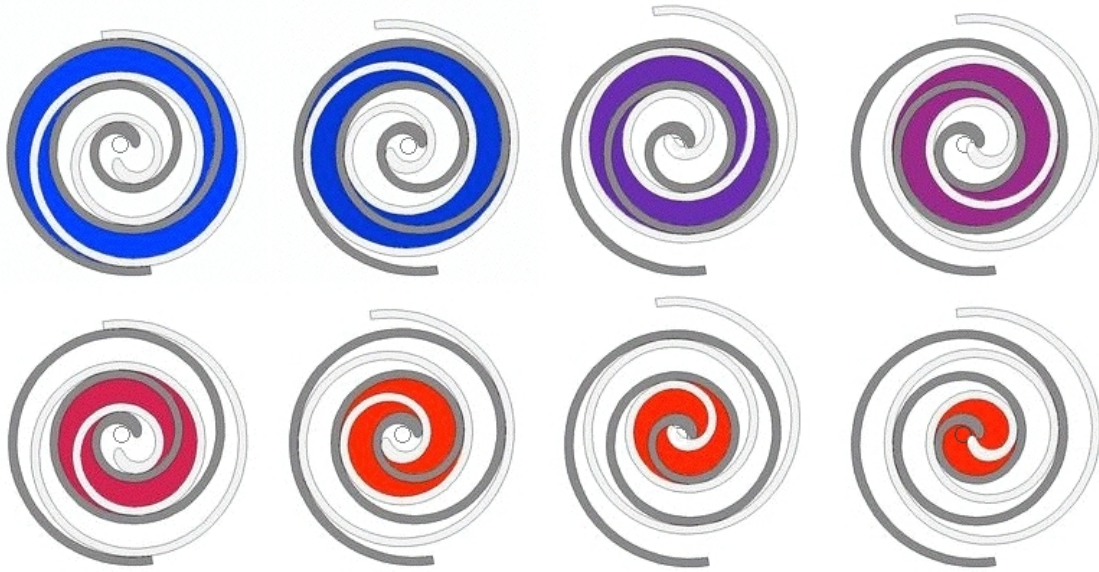


Figure 3.3: Scroll compressor in orbital mode, with representation of the discharge port in the center.

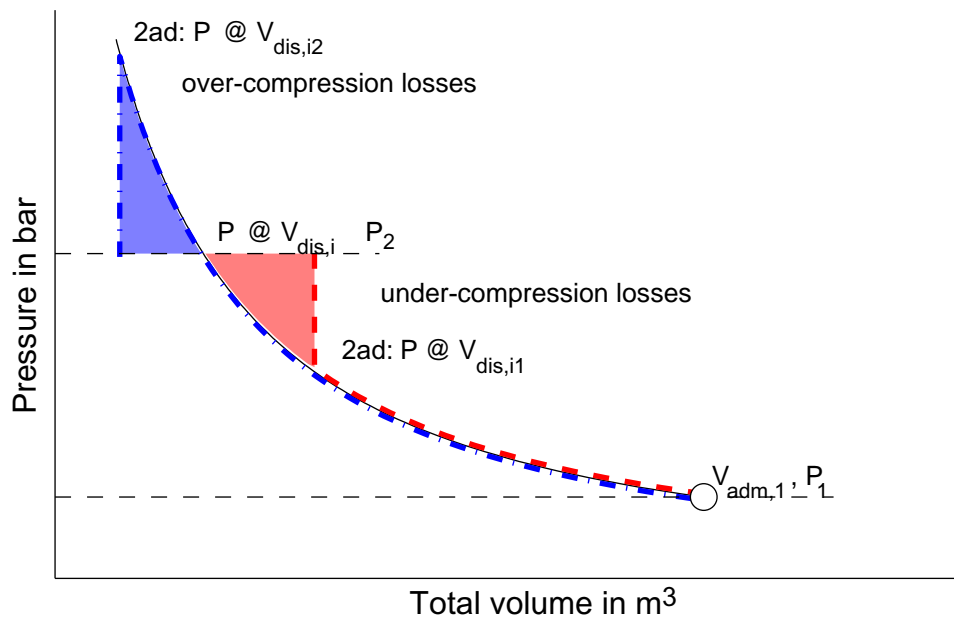


Figure 3.4: P-V diagram of a rotary volumetric compressor. Polytropic compression, over- and under-compression losses.

to the refrigerant and the thermodynamic point at suction. In fact, the transformation in non-adapted conditions, corresponds to a polytropic compression until the adapted discharge volume is reached in the compression chamber and a sudden pressure adaptation at constant total volume (compression or expansion, whether the system pressure is above or below the adapted discharge pressure). By separating the compression into the two zones, the thermodynamic state of the refrigerant is much more reliably predicted during the whole transformation.

Assuming no dissipation and no heat transfer, the theoretical (adapted) compression is assimilated to an isentropic transformation. The generalized form of the theoretical compression efficiency, accounting only for the non-adapted losses, is:

$$\eta_{cp,th} = \frac{\int_1^2 v dP}{\int_1^2 v dP} = \frac{\dot{M}_{refr} v_1 P_1^{\frac{\kappa}{\kappa-1}} \left[\Pi^{\frac{\kappa-1}{\kappa}} - 1 \right]}{\dot{M}_{refr} v_1 P_1^{\frac{\kappa}{\kappa-1}} \left[\Pi_i^{\frac{\kappa-1}{\kappa}} - 1 \right] + (P_2 - P_{dis}) V_{dis}}$$

$$= \frac{\kappa \left[\Pi^{\frac{\kappa-1}{\kappa}} - 1 \right]}{\frac{\kappa-1}{VR_i} \Pi + VR_i^{\kappa-1} - \kappa} \quad (3.17)$$

with $\Pi = \frac{P_2}{P_1}$, $\Pi_i = VR_i^\kappa$ and 1=in, 2=out

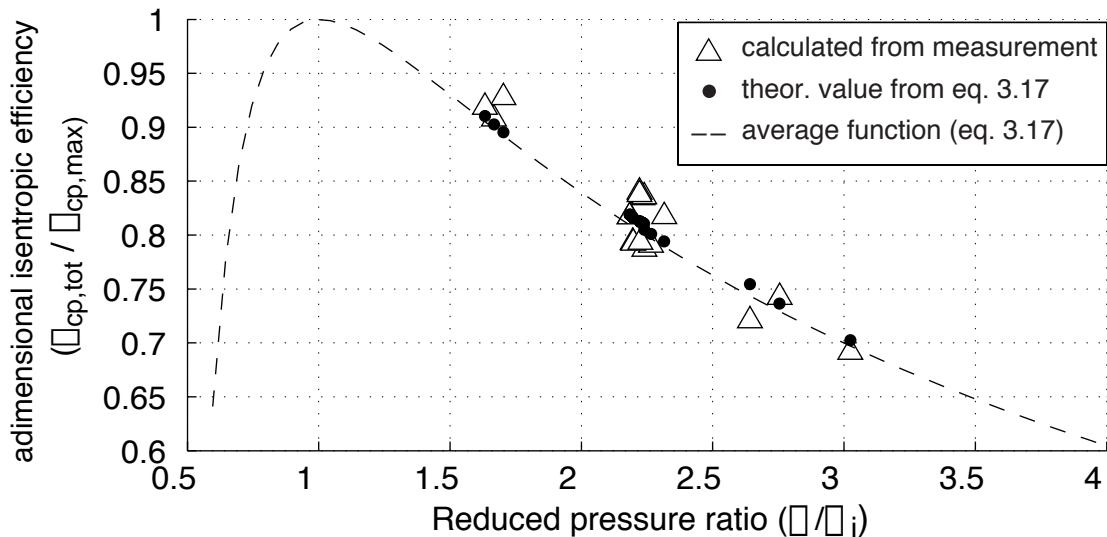


Figure 3.5: Shape of the theoretical compression efficiency for fixed built-in volume ratio compressor (cp#1) according to equation 3.17 and considering average entry condition. Comparison with experimental data, from [Zehnder and Favrat, 2003].

Measured isentropic efficiencies are very close to the theoretical average function defined by the previous relation, and are shown in Figure 3.5. Note, that the theoretical values (the dots), which are calculated with the specific entry conditions of the measured points, are not matching exactly the curve representing the average function (dashed curve). As the adapted pressure ratio is function of the entry conditions (variation of the isentropic exponent κ) the calculated points are marginally offset. By fitting with the experimental data, the maximum efficiency $\eta_{cp,max}^{meas}$ and the adapted volume ratio $VR_{i,meas}$, can be identified and can be applied to the compression efficiency model for the **global transformation in-out**. The identified $VR_{i,meas}$ provides a prediction of the built in volume ratio.

$$\eta_{cp,tot} = \eta_{cp,max}^{meas} \frac{\kappa \left[\Pi^{\frac{\kappa}{\kappa-1}} - 1 \right]}{\frac{\kappa-1}{VR_{i,meas}} \Pi + VR_{i,meas}^{\kappa-1} - \kappa} \quad (3.18)$$

The equation above represents a simple, but commonly adopted, approach to model the compression efficiency applicable for different refrigerants. This relation is however not appropriate to determine the thermodynamic state of the refrigerant during the transformation. Important deviations to this shape have been measured at off design conditions, for example at very low pressure difference measured on the same compressor model on a two-stage compression heat pump (see Fig. 3.6). These deviations are compensated by implementing a decomposed model approach, including the preheating of the refrigerant (transformation (*in* – 1) in Figure 3.7) during the aspiration and by separating the compression into the nominal (adapted) compression (1 – 2*ad*) and the sudden pressure adaptation at constant total volume (2*ad* – 2). The chosen setup of the compressor considers no heat exchange and no pressure losses from the discharge port to the compressor exit (2 = *out*).

The **decomposed compression model** is calculated with the following procedure:

1. Calculate the mass flow rate \dot{M}_{refr} , using the volumetric efficiency (eq. 3.21) in the expression 3.23, presented below in this section.
2. Resolve the set of equations, related to the transformations of the fluid:
 - **Suction preheat (*in* – 1):**
Calculate $\dot{Q}_{preheat}$ (eq. 3.6).
 - **Nominal compression (1 – 2*ad*):**
The nominal compression for the transformation 1 – 2*ad* is evaluated with the adapted isentropic efficiency:

$$\eta_{cp,is}^{nom} = \eta_{cp,is}^{max} f_{nom} \quad \text{with } f_{nom} = 1.11 \text{ (empirical)} \quad (3.19)$$

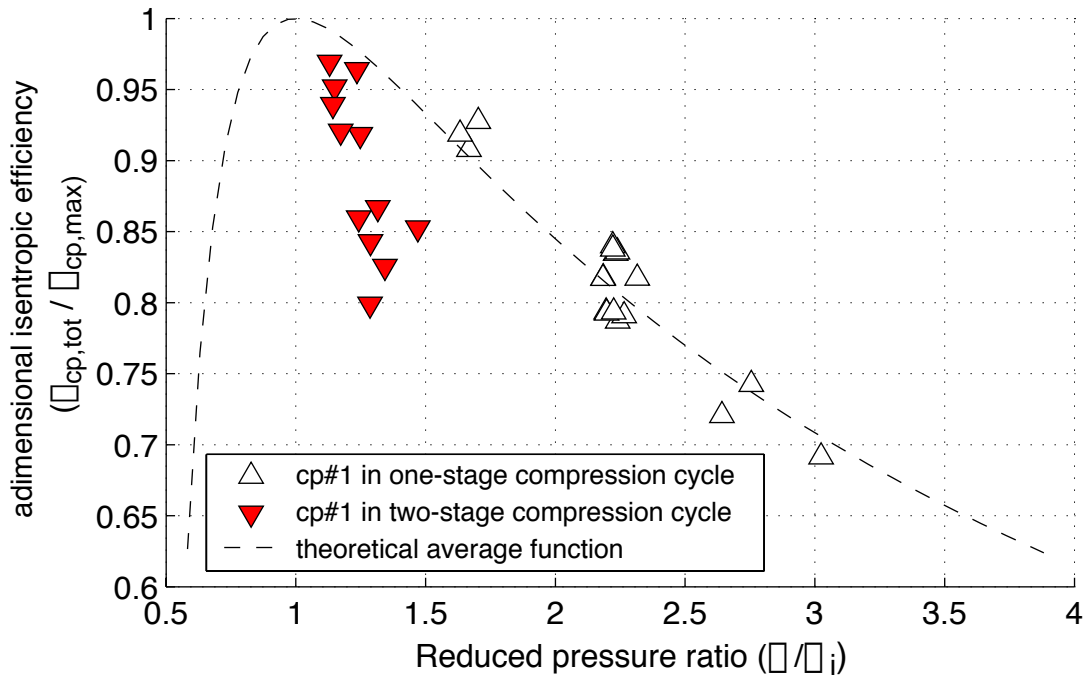


Figure 3.6: Comparison of the reduced compression efficiency of a compressor operated in a one-stage and two-stage compression heat pump cycle as the first stage compressor. Comparison to the theoretical function with average entry condition.

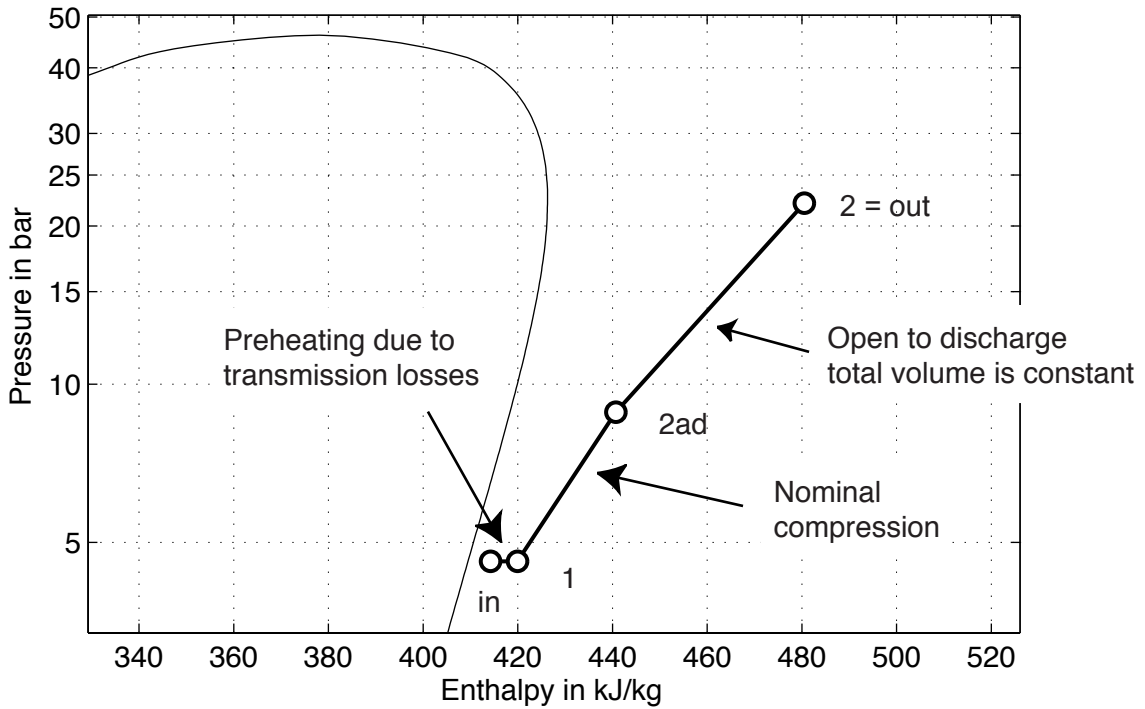


Figure 3.7: Schema of the compression zones corresponding to the simulation.

- **Pressure adaptation (2ad – 2):**

The compression chamber opens to the discharge port of the compressor. Sudden pressure adaptation is occurring and the corresponding specific work is given by:

$$\int_{2ad}^2 dh = h_2 - h_{2ad} = \frac{V_{dis}(P_2 - P_{2ad})}{\dot{M}_{refr}} \quad (3.20)$$

Note: If a dynamic discharge valve is implemented, the back-flow into the compression chamber is highly reduced and the compression is supposed to terminate with the nominal compression efficiency until the discharge pressure P_2 .

This model approach provides improved predictions of the compression work, the discharge temperature and the isentropic efficiency (Fig. 3.8), remaining within the simulation errors of $\pm 5\%$ for all available experimental data sets.

The second important characteristic of the compressor is the **volumetric efficiency**, which indicates the **ratio of the effective to the theoretical displaced volume**. The theoretical displacement is given by the sucked volume per revolution of the compressor and the rotation speed. The volumetric efficiency of scroll type compressors can be calculated by a linear function of the applied pressure ratio. Two series of compressors have been extensively tested and show clearly distinct evolutions. These are characterized by the following empirical coefficients:

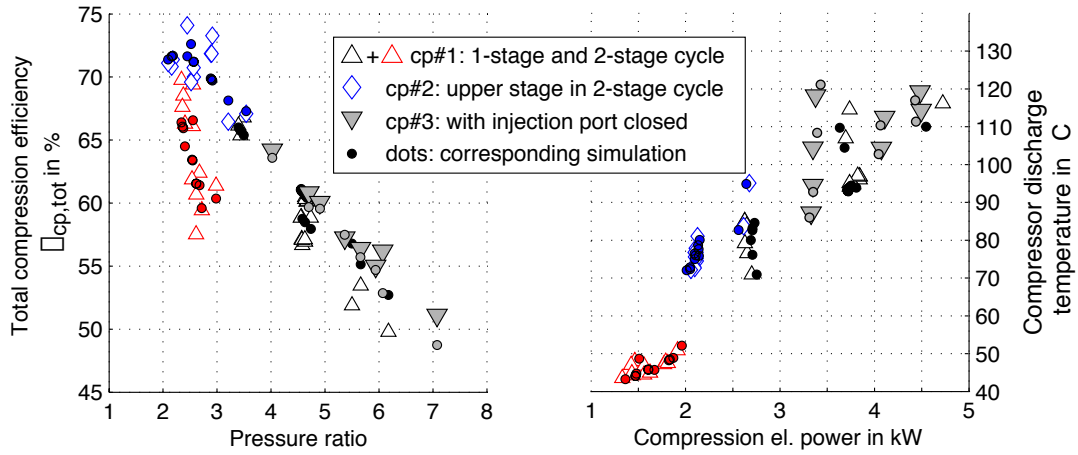
$$\text{lower installed volume ratio: } \eta_{vol} = 1.012 - 0.027\Pi \quad (3.21)$$

$$\text{higher installed volume ratio: } \eta_{vol} = 0.97 - 0.014\Pi \quad (3.22)$$

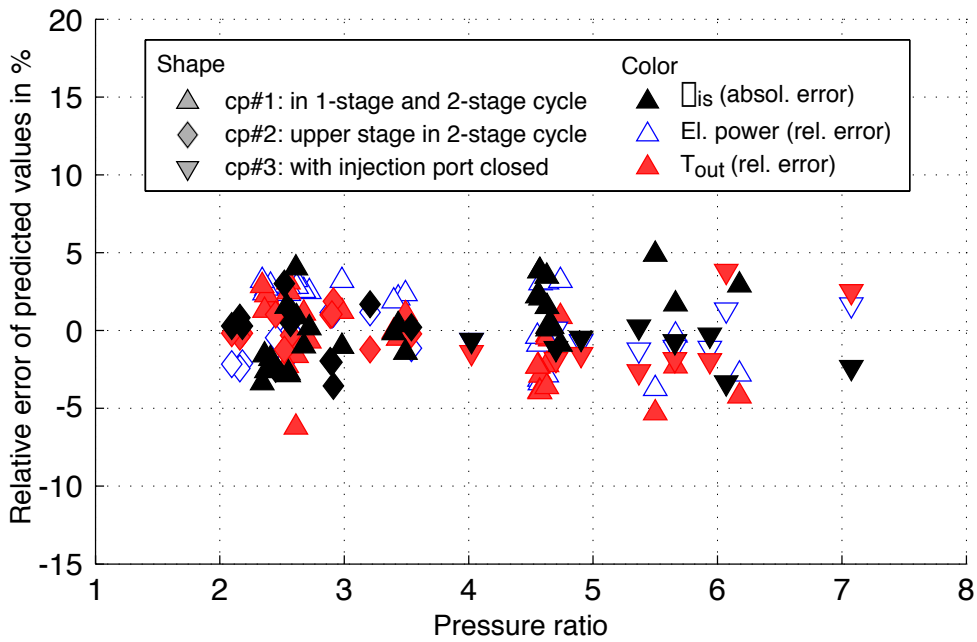
The absence of a clearance volume in rotary volumetric compressors, results in a very stable volumetric efficiency, even at high pressure ratio. This is the most important advantage of most rotary volumetric compressors, like the scroll, when comparing to the reciprocating compressor types. The practical implication of a loss in volumetric efficiency is that for a given heat rate a compressor with increased displacement would be required.

With the volumetric efficiency, the refrigerant mass flow is calculated by:

$$\dot{M}_{refr} = \eta_{vol} V_{asp} n \rho_{in} \quad (3.23)$$



(a) Comparison compression performances (corresponding simulation points are represented as dots in the figures above)



(b) Errors on isentropic efficiency, power and discharge temperature

Figure 3.8: Validation of the separated compressor model, on isentropic efficiency, discharge temperature and electric compression work. Single set of empirical coefficients $f_{transm} = 0.09 \cdot 10^{-6} \text{Jm}^{-3}$ and $f_{nom,cp} = 1.11$ for the tested hermetic scroll compressors.

3.1.2 Scroll compressor with intermediate injection port

The needs of small capacity refrigeration units, for deep freezing applications, has conducted to several patented intermediate injection configurations in hermetic scroll compressors. Searching the Worldwide Patents Databases the first applications of intermediate injection ports in scroll compressors, are dating from 1991/1992 ([Prenger and Seibel, 1991; Mizuno et al., 1992]). The injection possibility was mainly thought for liquid injection, allowing a cooling in the very low temperature range in the refrigeration sector. Only in 1999, due to a request for a high temperature heat pump project, a first **scroll prototype with adapted intermediate vapor injection port** [Brand et al., 2000; Zehnder et al., 2002b,a] has been tested at LENI-EPFL. After redesign and successful field tests, the vapor injection scroll has been patented by [Perevozchikov, 2003], and the public release of the new generation compressors is planned for fall 2004.

Intermediate injection during compression shows a great interest in large size refrigeration or heat pump systems using twin screw compressors. Its application to the small-medium capacity compressors, like the scroll, was not done until recently. The intermediate injection ports enable the following opportunities:

1. **Capacity reduction and modulation** with a possible communication channel to the suction zone.
2. **Injection of liquid refrigerant** to cool the fluid and the scroll members.
3. **Injection of lubricating oil** in order to cool and lubricate the scroll wraps.
4. **Injection of refrigerant vapor** to increase the capacity and the compression ratio of the scroll machine.

In this section a new simulation model is presented and the possible gains, due to liquid or vapor injection, on the performances of a heat pump system are evaluated and compared to measurements. The compressor simulation model should provide among others, the two following characteristics:

- **Discharge temperature:** What reduction of the discharge temperature can be obtained by intermediate injection of saturated or nearly saturated vapor.
- **Maximum injection mass flow rate:** What is the maximum mass flow rate of the injection, without entering the wet compression zone.

The impact of alternate injection designs on the system performances is analyzed in a global heat pump model, with a chosen intermediate expansion configuration (e.g. a capillary tube).

Simulation model

Basic definitions related to scroll compressor modeling are presented in section 3.1.1. This model has been extended to compressors with intermediate injection ports. Figure 3.9 represents the transformations used to model the global compression.

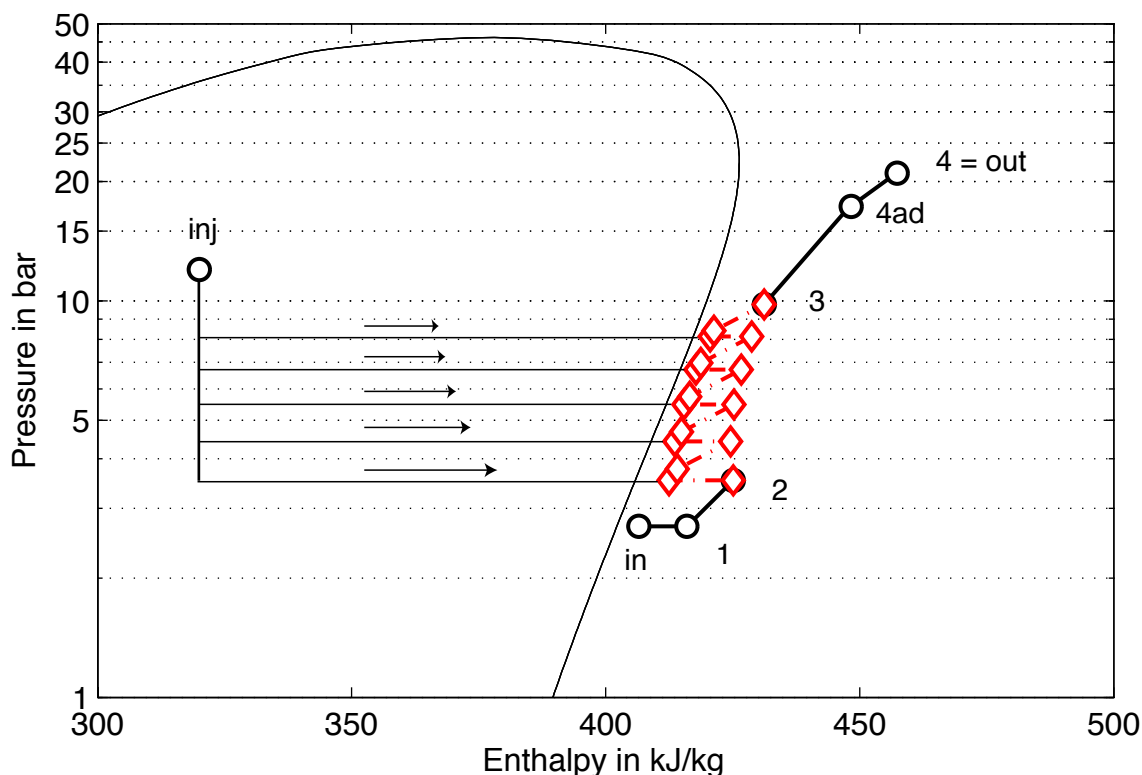


Figure 3.9: *Compression with intermediate injection. Definition of the transformations.*

The separated model is composed of:

1. Admission preheat ($in - 1$):

Preheating of the refrigerant in the suction line is calculated, using the selected compressor, supposing closed injection ports.

2. Adiabatic compression without injection ($1 - 2$):

Depending on the location and the geometry of the injection port, an injection-free compression is occurring before the starting point of the injection phase. A direct flow path from the injection port to the suction port is avoided, but injection is however influencing the inlet conditions (mainly originated by the increased leakage flow). It has been found, that the volumetric efficiency is affected in a significant manner during vapor injection, which was

not the case with the liquid injection port.¹

The empirical correction factor, proposed in the expression 3.24, is set proportional to the ratio of the injected and the theoretical admitted mass flow rate of the compressor. The volumetric efficiency is calculated for the external pressure ratio Π_{tot} .

$$\eta_{vol,inj} = f_{vol} \eta_{vol,noinj} \quad \text{with} \quad f_{vol} = 1 - 0.1323 \frac{\dot{M}_{inj}}{\dot{M}_{adm,th}} \quad (3.24)$$

The compression before and after the injection is characterized by the nominal isentropic efficiency $\eta_{cp,is}^{nom}$, which is evaluated in function of the external pressure conditions.

3. Intermediate injection (2&inj – 3):

The process of the intermediate compression is decomposed in appropriate calculation steps. The injection mass flow rate \dot{M}_{inj} is calculated with a **capillary tube equivalence** (tube diameter $D_{cap,inj}$ and a capillary tube length $L_{cap,inj}$, see section 3.3 for detailed description of the capillary tube modeling) adjusted to fit the experimental data. This mass flow rate is function of the pressure drop occurring in the injection line and is therefore conditioned by the position of the injection holes, respective to the position at compression start. The access of the injection port to one compression chamber is enabled during ideally one entire revolution of the orbiting scroll member. Considering the thickness of the tip of the spiral, which is covering the communicating port, this duration is reduced. A constant injection period of 270° is admitted in the simulation model. Figures 3.10 and 3.11 show a corresponding location of a selected injection geometry (composed of two injection ports). The accessibility period will be introduced into the model by the respective angular positions $\zeta_{inj,start}$ and $\zeta_{inj,end}$. In order to simplify the calculations, the two injection ports are treated as one injection port.

During the effective compression, the compression volume varies linearly with the angular position, as shown in Figure 3.11. The injection phase defines the partial volume ratios for the three considered zones during the compression: a) $VR_{i,1}$, b) $VR_{i,inj}$ and c) $VR_{i,2}$, for a) the pre-compression, b) the injection and the c) post-compression zone. **The injection phase is subdivided into the partial volumetric compression steps $dVR_{i,inj}$.**

The separated model has been developed to properly take into account injection mass distribution, mixing and partial compression, in order to follow as close as possible the real compression trajectory and to enable the evaluation of a critical injection mass flow rate, avoiding the wet compression zone, during which the compression efficiency is highly reduced². **Each injection step is decomposed into the following transformations** (see also Fig. 3.12):

¹A very low change of the rotational slip has been measured for a vapor injection case.

²Experimental result showing decreased efficiency, with controlled liquid injection in the suction line of an inverter driven scroll compressor are presented by [Afjei et al., 1992].

- **Isobaric mixing** (inj' & 2_i) $\rightarrow 3_i$: The rotation of the orbiting scroll member is virtually stopped and the two flows are mixed with the assumption of an isobaric transformation.
- **Isentropic adaptation** $3_i \rightarrow 3'_i$: The new pressure level of the mixed fluid is calculated by an isentropic transformation in order to fulfill the equilibrium conditions with the given total volume of the compression chamber at the considered angular position.
- **Differential compression** $3_i \rightarrow 2_{(i+1)}$: Nominal compression efficiency is applied during the partial compression and the transformation is calculated for a fixed volume change, which is corresponding to the partial volume ratio of:

$$dVR_{i,inj} = \frac{VR_{i,inj}}{k}$$
, with k = number of calculation steps.
 Experimental data show an important degradation of the compression efficiency, when entering the saturated region. In these conditions an efficiency correction is applied for each differential compression step during the injection phase.

$$\text{During wet compression: } \eta_{is,inj} = f_{corr,is} \eta_{cp,is}^{nom} \text{ with } f_{corr,is} = 0.5 \quad (3.25)$$

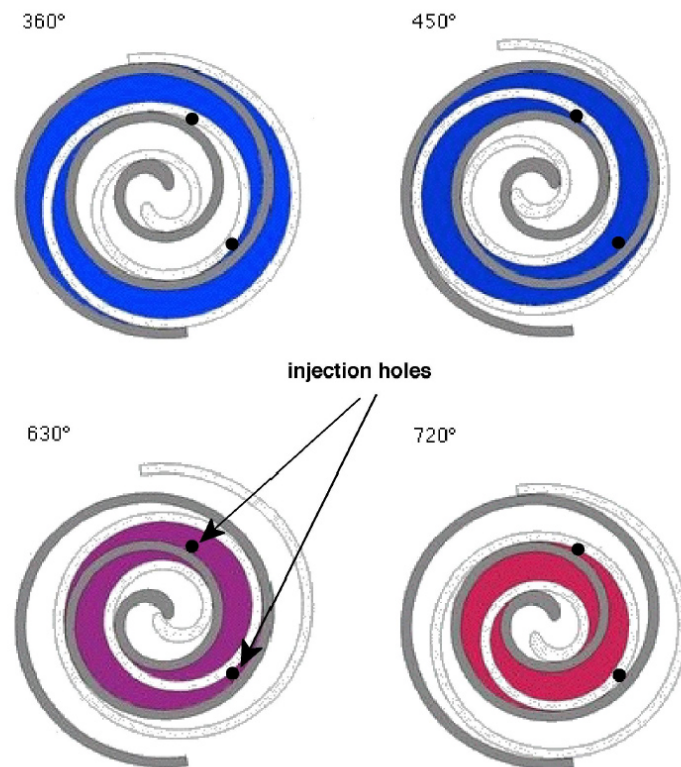


Figure 3.10: Schematic representation of a selected geometrical setup of the injection ports and their accessibility to the considered compression chambers.

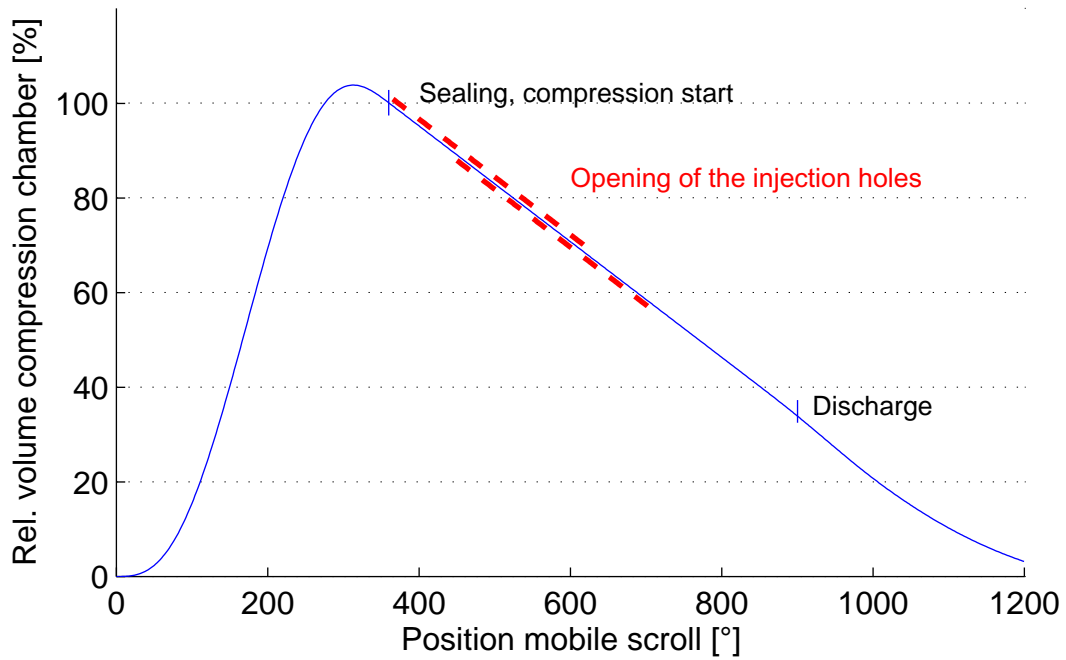


Figure 3.11: Evolution of the compression chamber volume in function of the rotation angle of the mobile scroll spiral. Indicated dashed red lines corresponds to the opening duration of the injection ports. In the presented case, see Figure 3.10, a 90° delay between the two injections is present.

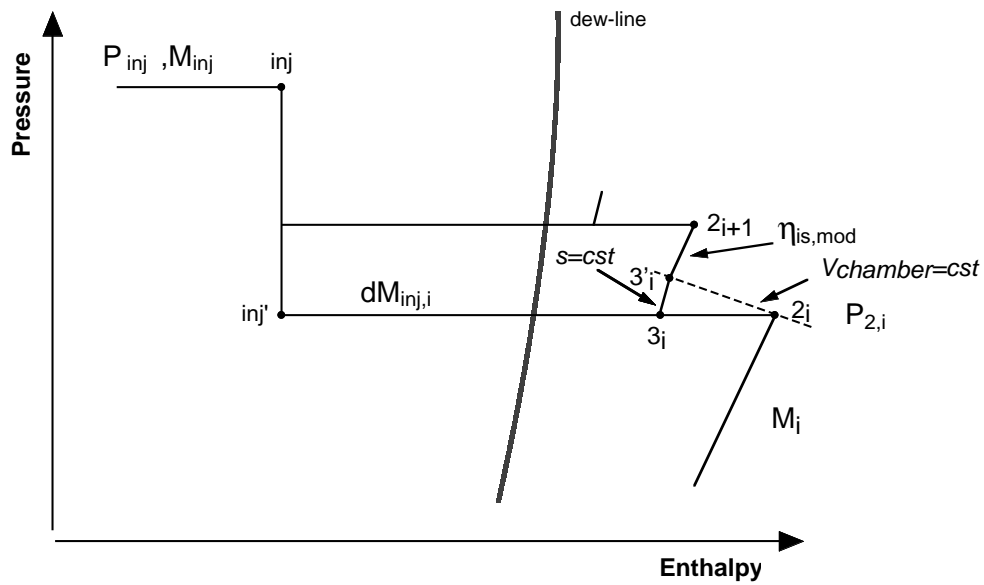


Figure 3.12: Simulation steps for intermediate injection in scroll compressors.

4. Adiabatic compression (2nd stage) (3 – 4_{ad}) and discharging (4_{ad} – 4):

These transformations are calculated, referring to the approach used for the compressor model without injection port (sec. 3.1.1).

Steps 1-4 can be simulated sequentially, but are interlinked with the volumetric efficiency adaptation (eq. 3.24) and the injection mass flow distribution, which has to be recalculated with the corresponding pressure difference of each differential injection step. By a single iteration step the transformations reached sufficient stability (< 1% variability).

Validation of the compression characteristics with intermediate injection:

Experimental data over a wide range of injection mass flow rates have been collected, using two prototype compressors, equipped by an adapted injection line for vapor injection, and comparing to the liquid injection model: *Copeland-ZF15K4E*. Figure 3.13 shows the evolution of the injected mass flow rate to the measured pressure level in the economizer line. The mass flow rate is related to the theoretical suction flow of the compression and the intermediate pressure is compared to the evaporation pressure. This representation allows, by linear regression, a direct evaluation of the injection mass flow rate and to bypass the time consuming calculation of the assumed capillary tube expansion in the injection line.

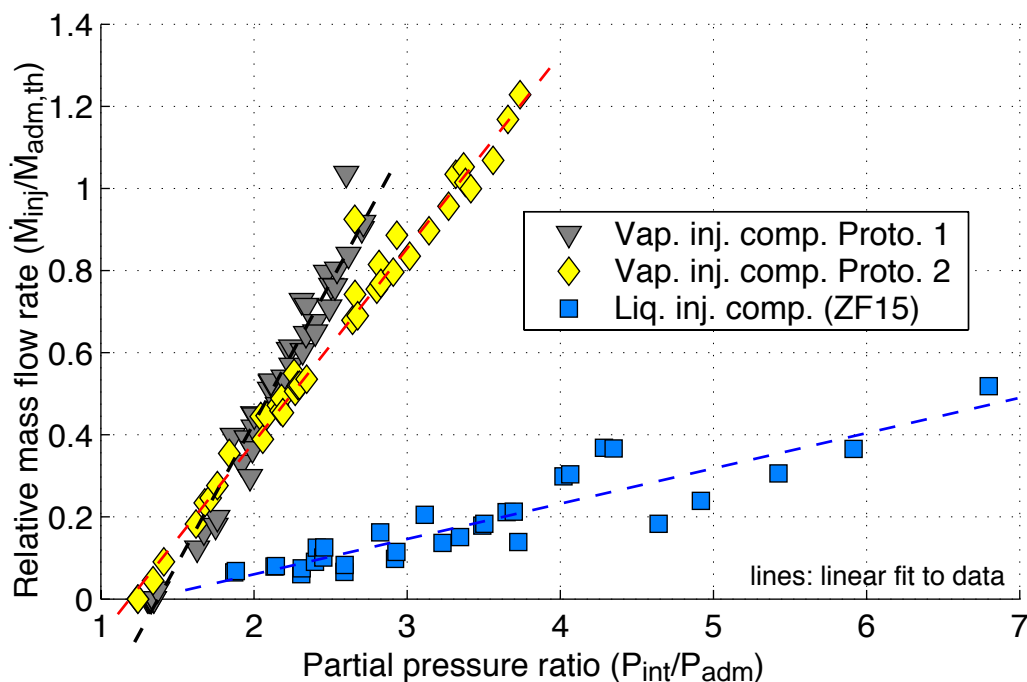


Figure 3.13: Comparison of injected mass flow rates into two vapor injection and one liquid injection compressor setup.

The proposed correlations for predicting the injection mass flow rates are:

$$\dot{M}_{inj} = \left(a + b \frac{P_{int}}{P_{ev}} \right) \dot{M}_{adm,th} \quad (3.26)$$

with Proto1: $a = -0.919$, $b = 0.675$

Proto2: $a = -0.566$, $b = 0.476$

ZF15: $a = -0.110$, $b = 0.0875$

Figure 3.13 also shows the significant increase of injected mass flow between the liquid injection configuration (ZF15) and the two prototype compressors, with adapted vapor injection port. For equivalent pressure drop in the injection line, the mass flow rate for the new configuration is 4-5 times higher, which is resulting in improved cycle efficiency (because of reduced re-compression work).

By estimation of the injection geometry an equivalent capillary tube geometry is identified to simulate the flow resistance in the injection line between the suction port and the injection hole accessing to the compression chamber. The geometrical setup is listed in Table 3.1.

Table 3.1: Injection geometry for capillary tube analogy.

Compressor	Diameter in mm	Tube length in mm
Vapor injection port #1	3.6	300
Vapor injection port #2	3.5	300
Liquid injection port (ZF15)	2.3	600

Using the capillary tube approach to calculate the injection rate, important deviations to experimental data are observed for low mass flow rates (Figure 3.14), showing the limitations of this approach at low mass flow range. These quite important relative errors in the predicted flow rate is a result of the simplified setup. The evaluated geometry has been adopted to minimize the prediction errors for an application range which is the largest possible. An uniform injection mass flow rate during the injection phase is assumed. A quadratic distribution with the pressure difference would be more logical, but resulted in a lower correspondence with the experimental data. In some flow conditions in the injection line, the flow reaches choked flow (Mach number=1) conditions.

In Figure 3.15 the measured **compression power** is compared to the simulation. Relative errors are situated in the band width of $\pm 10\%$, with the exception of a systematic over-prediction in the lower pressure ratio range for prototype compressor 2.

This systematic error is not mass flow related. The suction mass flow rate is well evaluated (errors $< \pm 5\%$) and even, when trying to calculate with the measured injection flow rates, the prediction is not significantly improved. The only way to improve the prediction capability consists in adapt-

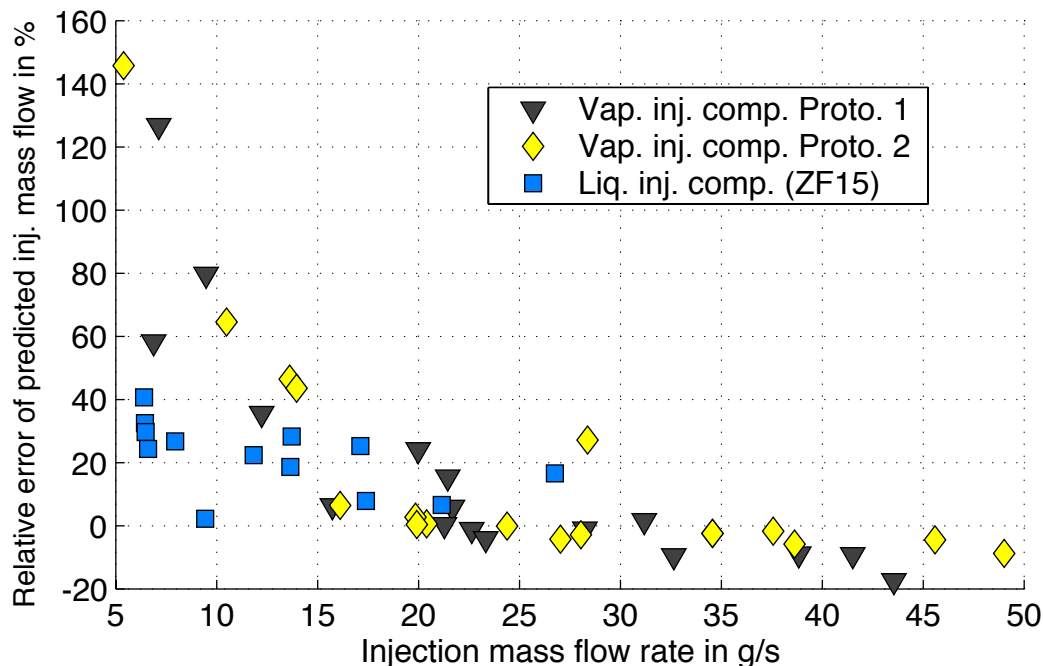


Figure 3.14: *Relative error of predicted injection mass flow rates, using capillary tube equivalence in the injection line of intermediate injection compressors.*

ing the nominal compression efficiency, which however would result in a reduced quality of the simulation model in the simple configuration with a closed injection line (see sec. 3.1.1).

Figure 3.16 represents the measured **discharge temperature** and the corresponding simulation output, for the three tested compressors. The calculated points reproduce in general the observed trends (with the same gradients between the specific points), but important absolute errors between the measured temperature in the discharge line and the calculated output are shown. For the prototype compressor 1, the simulated temperatures correspond to the experimental data, while those of the compressor 2 are clearly under-predicted (with considerable differences of ~ -20 K). The liquid injection compressor data is generally over-predicted by ~ 5 K. As many effects have a direct impact on the discharge temperature it is very difficult to improve the prediction, without losing precision on the other performance factors.

Conclusions:

While the concept of intermediate injection is well known in screw compressors and the geometry of these types of compressors allows a direct access to the compression volume, the setup for intermediate injection in hermetic scroll compressors is more complex. The injection flow path is very restricted, as can be observed on the existing compressor models. In order to simulate accurately the performances of the compressors with intermediate liquid or vapor injection, a one point mixing approach between the injected mass flow rate and the main flow passing through the

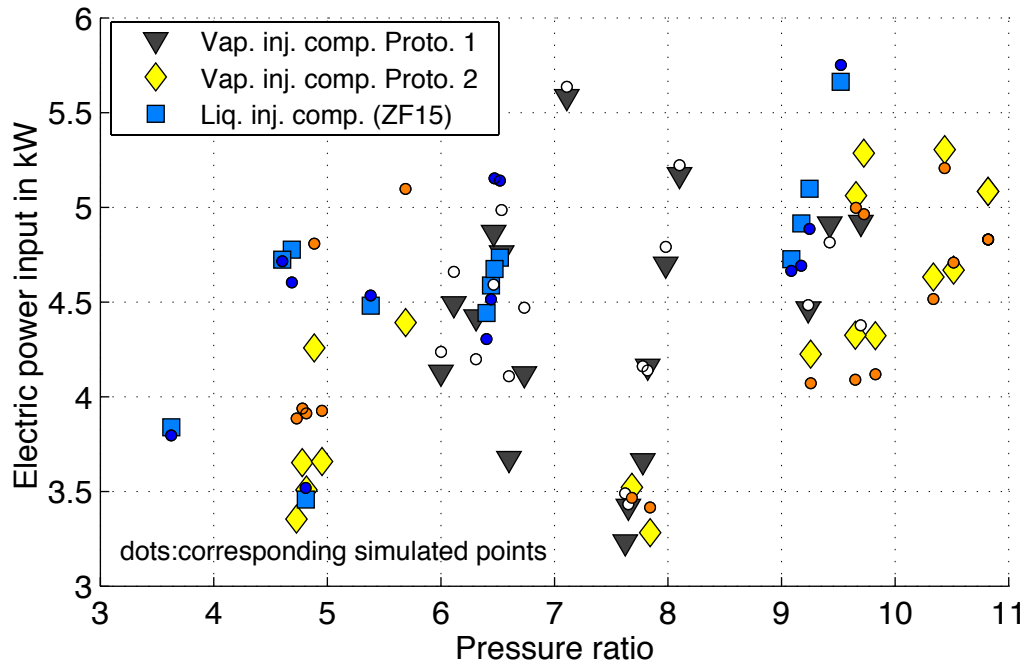


Figure 3.15: Comparison of measured and calculated electric power consumption for different types of compressors with intermediate injection port.

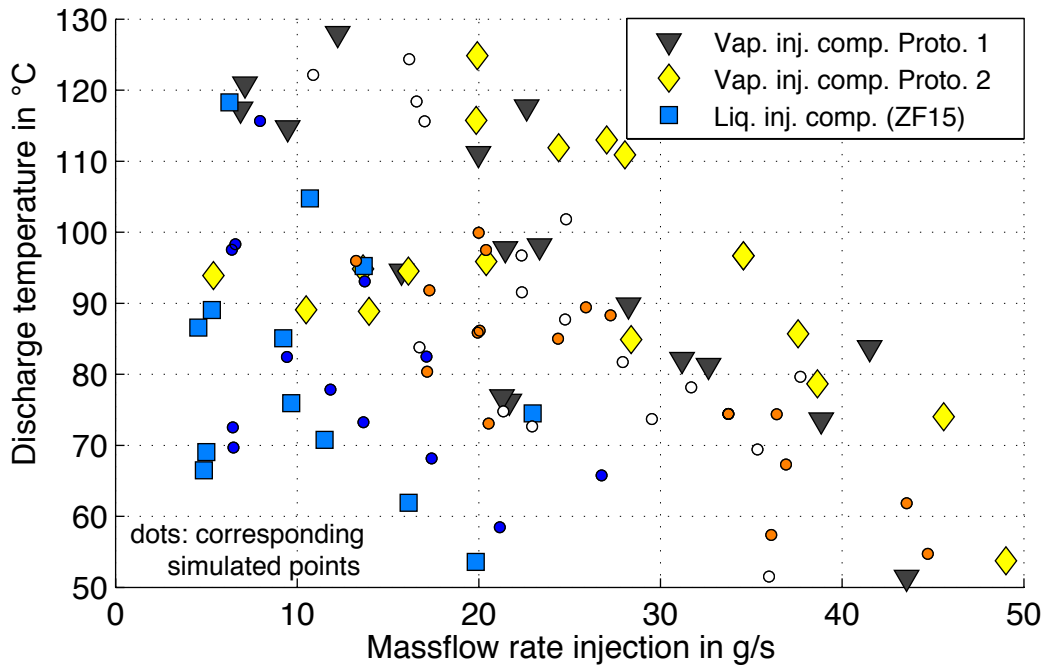


Figure 3.16: Comparison of measured and calculated discharge temperatures for different types of compressors with intermediate injection port.

suction port of the compressor, as proposed in [Winandy and Lebrun, 2002; Guoyuan et al., 2003], is not sufficient to predict the performance characteristics for a generalized simulation model.

The here proposed new approach, to model the intermediate injection, is composed of an equivalent injection channel, relating the total injection mass flow rate to the apparent pressure drop between the injection stage and the access point to the compression volume. The mixing with the compressed refrigerant vapor is done stepwise over the range of angular positions of the orbiting scroll member, at which the injection port is accessing the compression volume. With this generalized model, the performances of the compressor with intermediate liquid and vapor injection port can be predicted quite confidently in a large application range and enables a parametric analysis for system optimization.

3.2 Heat exchangers

While generalized **single-phase** heat transfer correlations in forced convection, remain in a relatively condensed form and predict data with an average accuracy between 5% - 10%, the **two-phase** heat transfer models involve highly complex flow patterns (see Fig. 3.17 for the evaporation case). Based on a highly physical model, a generalized method for two-phase heat transfer modeling is proposed by Thome and co-workers (including the diabatic flow pattern map, [Kattan et al., 1998a; Zürcher et al., 2002a; Thome and El Hajal, 2002; El Hajal et al., 2003a] and the related heat transfer models: [Kattan et al., 1998b; Zürcher et al., 2002b; El Hajal et al., 2003b]).

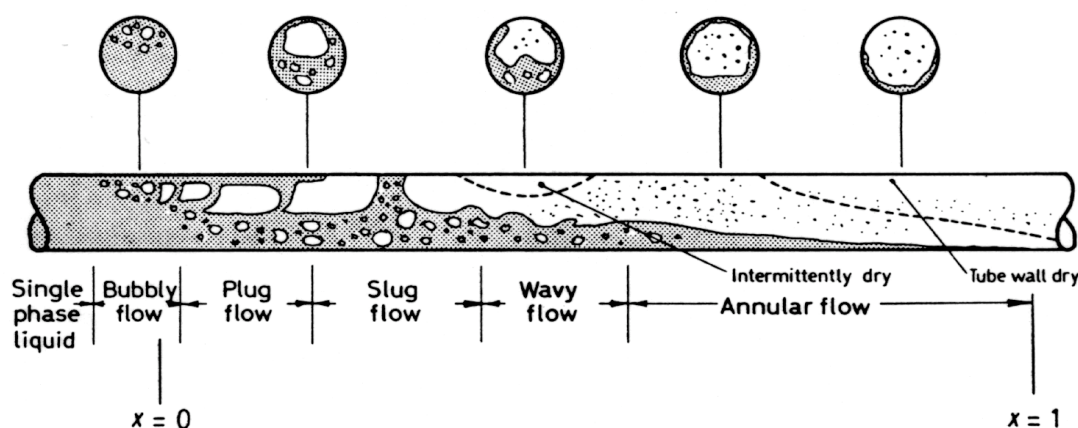


Figure 3.17: Representation of flow patterns in horizontal in-tube evaporation. Figure from [Collier and Thome, 1994].

3.2.1 Single-phase convective heat transfer

A generalized approach for in tube convective heat transfer was developed by [Wilson, 1915], the Wilson plot method, which is still widely applied to determine experimental heat transfer coefficients. This method is applied on the Dittus-Boelter (1930) equation for heating [Incropera and DeWitt, 1996], according to the equation:

$$Nu_D = 0.023 Re_D^{0.8} Pr^n \text{ for } Re > 10000 \quad (3.27)$$

with $n = 0.4$ for heating, and $n = 0.3$ for cooling

While Dittus-Boelter equation is applicable only for turbulent flow, the more accurate correlation proposed by Gnielinski (1976) [Incropera and DeWitt, 1996] is valid on an extended range,

including the laminar-turbulent transition zone.

$$Nu_D = \frac{(f/8) (Re_D - 1000) Pr}{1 + 12.7 (f/8)^{0.5} (Pr^{2/3} - 1)} \quad (3.28)$$

with the friction factor: $f = [0.79 \ln(Re_D) - 1.64]^{-2}$

valid in the range of $3000 < Re < 5 \cdot 10^6$ and $0.5 < Pr < 10^4$

3.2.2 The modified Kattan-Thome-Favrat flow pattern map

A two-phase flow pattern map for accurate prediction of flow transitions during evaporation in horizontal tubes, was originally proposed by [Kattan et al., 1998a]. Iterative resolution schemes and an incoherence of using different void fraction models have led to a simplified version presented in [Thome and El Hajal, 2002].

Void fraction

The void fraction ε , defines in two-phase flow the cross-sectional areas occupied by the vapor to the total area and determines the mean velocities of the liquid and vapor phase. The influencing choice of the void fraction models on the flow transitions and on the calculation of the heat transfer coefficients is discussed extensively in [Zürcher, 2000]. Three models of interest are shortly presented:

- **The homogeneous model**

In the homogeneous model, the velocity of each phase is assumed to be identical. This results in the highest void fraction prediction.

$$\varepsilon_h = \left[1 + \frac{1 - \chi}{\chi} \frac{\rho_{vap}}{\rho_{liq}} \right]^{-1} \quad (3.29)$$

- **The Taitel-Dukler model**

Taitel and Dukler (1976) proposed a void fraction model assuming same pressure gradient in a stratified flow regime, which permits to find (iteratively) the liquid height of the adapted flow regime, see section 3.10 in [Zürcher, 2000]. The liquid height and the void fraction are geometrically related by

$$\varepsilon_{td} = \frac{A_{vap}}{A_{tot}} = \frac{1}{\pi} \left[\arccos(\zeta_h) - \zeta_h \sqrt{1 - \zeta_h^2} \right] \quad (3.30)$$

with the liquid height factor: $\zeta_h = 2 \frac{h_{liq}}{D} - 1$

- **The Rouhani-Axelsson drift flux model**

The *Rouhani-Axelsson* (1970) void fraction is formulated for the drift flux flow model and is presented in the formulation of the VDI Heat Atlas [VDI, 1993].

$$\epsilon_{ra} = \frac{\chi}{\rho_{vap}} \left[\left(1 + 0.12(1 - \chi) \right) \left(\frac{\chi}{\rho_{vap}} + \frac{1 - \chi}{\rho_{liq}} \right) + \frac{1.18(1 - \chi) [g \sigma (\rho_{liq} - \rho_{vap})]^{0.25}}{G \rho_{liq}^{0.5}} \right]^{-1} \quad (3.31)$$

These three models result in important differences of the void fraction at low vapor qualities (Fig. 3.18), which is highly influencing the wetted perimeter and the liquid film thickness δ , used in the two-phase heat transfer correlations presented in the section 3.2.3.

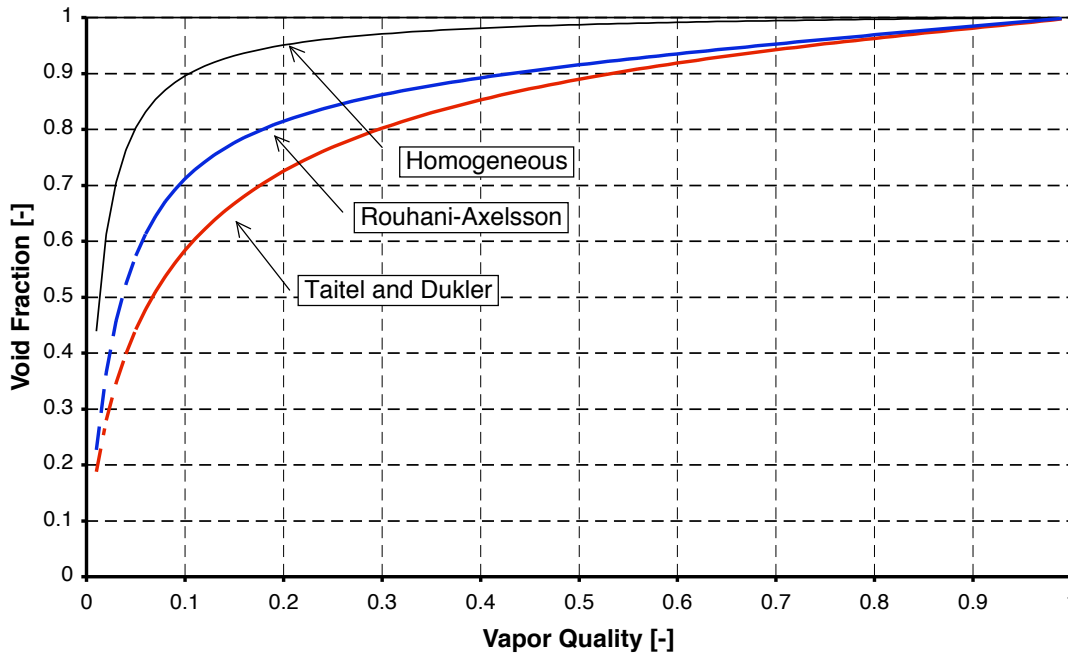


Figure 3.18: Comparison of Homogeneous, Rouhani-Axelsson and Taitel-Dukler void fractions for R-134a with $D=14$ mm, $G=100$, $T_{sat}=4^{\circ}\text{C}$.

Accurate heat transfer calculations in two-phase flow, require the prediction of the flow pattern, which is done by representing the local flow conditions in a corresponding flow map, Fig. 3.19. The flow pattern transitions are determined for a horizontal in-tube evaporation with the set of equations 3.32-3.35.

Stratified - stratified wavy flow

$$G_{strat} = \left[226.3^2 \frac{A_{liq,d} A_{vap,d}^2 \rho_{vap} (\rho_{liq} - \rho_{vap}) \mu_{liq} g}{\pi^3 \chi^2 (1 - \chi)} \right]^{1/3} + 20 \chi \quad (3.32)$$

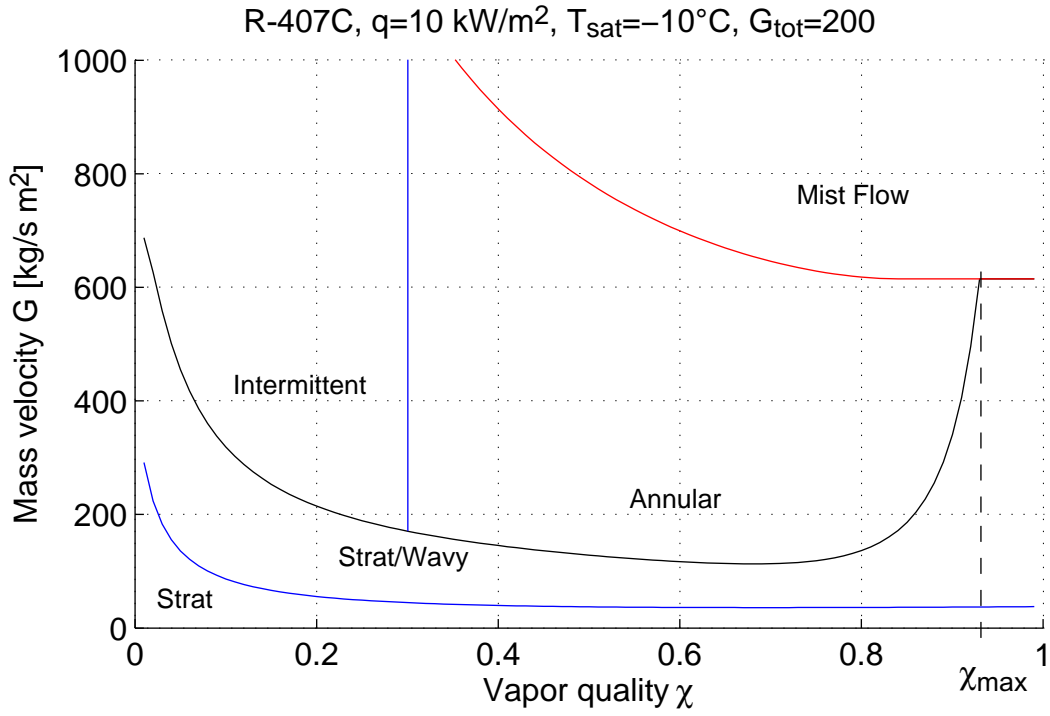


Figure 3.19: Evaporation flow pattern map for R-407C in horizontal smooth tubes - updated version [Thome and El Hajal, 2002].

Stratified wavy - annular flow

$$G_{wavy} = \left\{ \frac{16A_{vap,d}^3 g D \rho_{liq} \rho_{vap}}{\pi^2 \chi^2 \sqrt{1 - (2h_{liq,d} - 1)^2}} \left[\frac{\pi^2}{25 h_{liq,d}^2} (1 - \chi)^{-F_1(\dot{q})} \left(\frac{We}{Fr} \right)_{liq}^{-F_2(\dot{q})} + 1 \right] \right\}^{0.5} + 50 - 75 \exp^{-\frac{(\chi^2 - 0.97)^2}{\chi(1-\chi)}} \quad (3.33)$$

Intermittent - annular flow

$$\chi_{I-A} = \left\{ \left[0.2914 \left(\frac{\rho_{liq}}{\rho_{vap}} \right)^{-\frac{1}{1.75}} \left(\frac{\mu_{liq}}{\mu_{vap}} \right)^{-\frac{1}{7}} \right] + 1 \right\}^{-1} \quad (3.34)$$

Annular - mist flow

$$G_{mist} = \left\{ \frac{7680 A_{vap,d} g D \rho_{liq} \rho_{vap}}{\chi^2 \pi^2 f} \left(\frac{Fr}{We} \right)_{liq} \right\}^{0.5} \quad (3.35)$$

Equations 3.32 to 3.35 use the additional parameters:

- The void fraction is calculated from eq. 3.31, and the angle θ_{strat} for the stratified flow pattern is geometrically defined by

$$(1 - \varepsilon) = \frac{1}{2\pi} [(2\pi - \theta_{strat}) - \sin(2\pi - \theta_{strat})] \quad (3.36)$$

Eq. 3.36 is an implicit formulation to find θ_{strat} . An accurate explicit approximation is proposed by [Biberg, 1999]:

$$\theta_{strat} = 2\pi\varepsilon + 2 \left(\frac{3\pi}{2} \right)^{\frac{1}{3}} \left[1 - 2\varepsilon - (1 - \varepsilon)^{\frac{1}{3}} + \varepsilon^{\frac{1}{3}} \right] \quad (3.37)$$

- The reduced geometrical dimensions are calculated with the relations, according to a stratified flow regime (Fig. 3.20) :

$$A_{liq,d} = \frac{A(1-\varepsilon)}{D^2} = \frac{\pi}{4} (1 - \varepsilon), \quad A_{vap,d} = \frac{\pi}{4} \varepsilon, \quad P_{int,d} = \sin\left(\frac{2\pi - \theta_{strat}}{2}\right)$$

and $h_{liq,d} = \frac{h_{liq}}{D} = 0.5 \left[1 - \cos\left(\frac{2\pi - \theta_{strat}}{2}\right) \right]$

- The ratio of the liquid Weber and Froude number: $\left[\frac{We}{Fr} \right]_{liq} = \frac{g D^2 \rho_{liq}}{\sigma}$

- The friction factor: $f = \left[1.138 + 2 \log\left(\frac{\pi}{1.5 A_{liq,d}}\right) \right]^{-2}$

- The empirical correction functions to account for the onset of dry-out in the G_{wavy} boundary:

$$F_1(\dot{q}) = 646.0 \left(\frac{\dot{q}}{\dot{q}_{crit}} \right)^2 + 64.8 \frac{\dot{q}}{\dot{q}_{crit}} \quad \text{and} \quad F_2(\dot{q}) = 18.8 \frac{\dot{q}}{\dot{q}_{crit}} + 1.023$$

with the critical heat flux: $\dot{q}_{crit} = 0.131 \rho_{vap}^{0.5} h_{lat} [g(\rho_{liq} - \rho_{vap}) \sigma]^{0.25}$

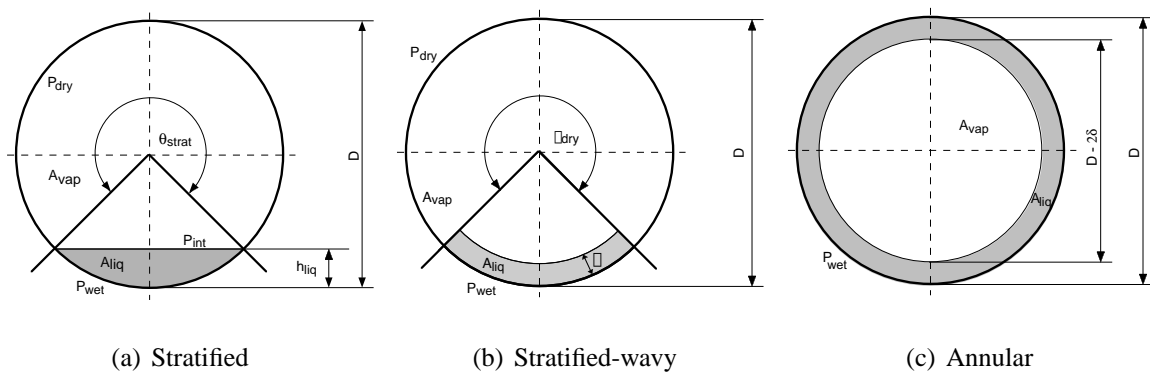


Figure 3.20: Liquid and vapor phase distribution for stratified, stratified-wavy and annular flow.

Figure 3.19 shows the flow pattern map, according to the presented transitions of the latest version of the *Kattan-Thome-Favrat* for evaporating R-407C in horizontal, smooth tubes. This map allows to design the tubing of the evaporator in order to obtain the aimed flow pattern. Aiming, for example, an annular flow in a heat pump evaporator, which is typically working in the vapor quality range of 30% - 100%, the inferior limit of mass velocity can be extracted from the flow map. In practice, however, internally grooved microfin tubes are employed, which have a wetting effect and thus an enhanced heat transfer coefficient at reduced flow speed.

3.2.3 Evaporating heat transfer model

The developed flow pattern map, originally proposed by [Kattan et al., 1998a], will be used in its *latest version* [Thome and El Hajal, 2002] to calculate the corresponding flow pattern in horizontal tube evaporation.

The liquid and vapor heat exchange contribution is calculated with the respective surfaces (or perimeters) applying the **linear mixing model**:

$$\alpha_{tp} = \frac{P_{wet} \alpha_{liq} + P_{dry} \alpha_{vap}}{\pi D} \quad (3.38)$$

The **liquid phase heat transfer α_{liq}** is calculated with the **asymptotic approach** proposed by *Steiner and Taborek* (1992), combining the liquid convective and the nucleate boiling contributions.

$$\alpha_{liq} = (\alpha_{nb}^3 + \alpha_{conv}^3)^{1/3} \quad (3.39)$$

[Kattan, 1996] collected heat transfer data for 5 refrigerants, resulting in the formulation of the **convective boiling correlation**:

$$\alpha_{conv} = 0.0133 Re^{0.69} Pr^{0.4} \frac{\lambda_{liq}}{\delta} \quad (3.40)$$

The **nucleate boiling** contribution, referring to the liquid heat transfer, is given by the *Cooper* (1984) correlation

$$\alpha_{nb} = 55 P_{red}^{0.12} (-\log P_{red})^{-0.55} \check{M}^{-0.5} \check{q}^{0.67} \quad (3.41)$$

Nucleate boiling effect occur only if the applied heat flux is above the **onset of nucleate boiling** limit, which is calculated with the approach proposed in [VDI, 1993].

$$\dot{q}_{ONB,\chi} = \frac{2 \sigma T_{sat} \alpha_{conv,crit}}{r_{crit} \rho_{vap} h_{lat}} \quad (3.42)$$

with $r_{crit} = 0.38 \cdot 10^{-6} \text{ m}$

and $\alpha_{conv,crit}$ evaluated with eq. 3.40 using largest film thickness for

$$\text{stratified and intermittent flow}^1: \delta_{crit, strat} = h_{liq} = \frac{D}{2} \left[1 - \cos \left(\frac{2\pi - \theta_{strat}}{2} \right) \right] \quad (3.43)$$

$$\text{strat-wavy and annular flow: } \delta_{crit, ann} = \delta = \frac{\pi D (1 - \varepsilon)}{2(2\pi - \theta_{dry})} \quad (3.44)$$

Comment: The critical liquid film thickness in the stratified-wavy flow has been presented as a form of the two supplementary angles, the *half wetting angle* and the *moon angle*, see [Zürcher, 2000]. In this work the geometry will be kept as simple as possible and the film thickness in the stratified-wavy and annular region is considered to be uniform. In intermittent flow, the critical film thickness corresponds to the stratified.

The **vapor heat transfer coefficient** α_{vap} is calculated with the Dittus-Boelter (1930) correlation:

$$\alpha_{vap} = 0.023 Re_{vap}^{0.8} Pr^{0.4} \frac{\lambda_{vap}}{D} \quad (3.45)$$

Reynolds numbers are calculated with the respective flow velocities of each phase and the uniform liquid film thickness.

$$u_{liq} = \frac{G(1-\chi)}{\rho_{liq}(1-\varepsilon)} \quad u_{vap} = \frac{G\chi}{\rho_{vap}\varepsilon} \quad (3.46)$$

$$Re_{liq} = \frac{4G(1-\chi)\delta}{(1-\varepsilon)\mu_{liq}} \quad Re_{vap} = \frac{G\chi D}{\varepsilon\mu_{vap}}$$

$$\text{with } \delta = \frac{\pi D (1 - \varepsilon)}{2(2\pi - \theta_{dry})} \quad (3.47)$$

The dry angle θ_{dry} is given in the stratified and in the annular flow regime, while in the stratified-wavy and in the annular flow with partial dry-out, this angle will be calculated by vertical and

¹Applied to all flow regimes in the quality range inferior to the intermittance boundary χ_{I-A} (eq. 3.34)

horizontal linear interpolation, using the upper and lower boundaries of the stratified/stratified-wavy and the stratified-wavy/annular transitions and the maximum quality χ_{max} located at the intersection of the annular and the mist flow boundaries, as illustrated in Figure 3.19:

$$\text{if } \chi \leq \chi_{max} : \quad \theta_{strat-wavy} = \theta_{strat}(\chi) \frac{G_{annular}(\chi) - G}{G_{annular}(\chi) - G_{strat}(\chi)} \quad (3.48)$$

$$\text{else :} \quad \theta_{dry-out} = (2\pi - \theta_{strat-wavy}(\chi_{max})) \frac{\chi - \chi_{max}}{1 - \chi_{max}} + \theta_{strat-wavy}(\chi_{max}) \quad (3.49)$$

Correction for zeotropic mixtures:

A correction factor to account for the mass diffusion effect of zeotropic mixtures during evaporation is proposed by [Thome, 1987] and suggested by [Kattan, 1996]. This correlation has only been verified for smooth tubes and caution should be applied for using it with enhanced tube surfaces.

$$F_c = \left\{ 1 + \frac{\alpha_{nb}}{\dot{q}} \Delta T_{glide} \left[1 - \exp\left(\frac{-\dot{q}}{\rho_{liq} h_{lat} \beta_L}\right) \right] \right\}^{-1} \quad (3.50)$$

with the mass transfer coefficient $\beta_L = 0.0003 \text{ m/s}$

Comparison with measured local heat transfer coefficients:

Figures 3.21 and 3.22 show the well predicted evolutions of the two-phase heat transfer test data (from [Kattan, 1996]) and the implemented heat transfer model for both, the pure R-134a refrigerant and the zeotropic mixture R-407C. The model still over predicts significantly the heat transfer in stratified wavy flow. In the work of [Zürcher, 2000], the stratified wavy/annular transition has been remodeled in order to take into account extensive test data at lower mass velocities and the prediction is in very good agreement with the presented data. The implemented heat transfer model although does not include Zürcher's modified transition, in order to be congruent with the most recent flow map.

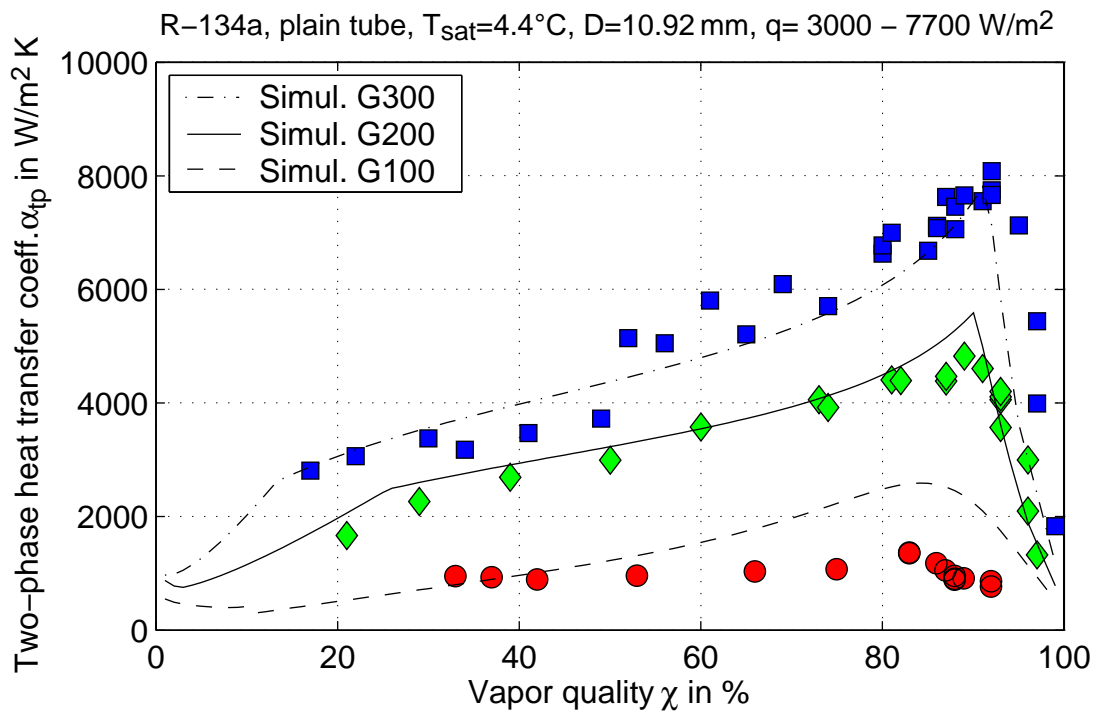


Figure 3.21: Comparison of experimental heat transfer data, from [Kattan, 1996], with simulation for horizontal plain tube evaporating flow with R-134a.

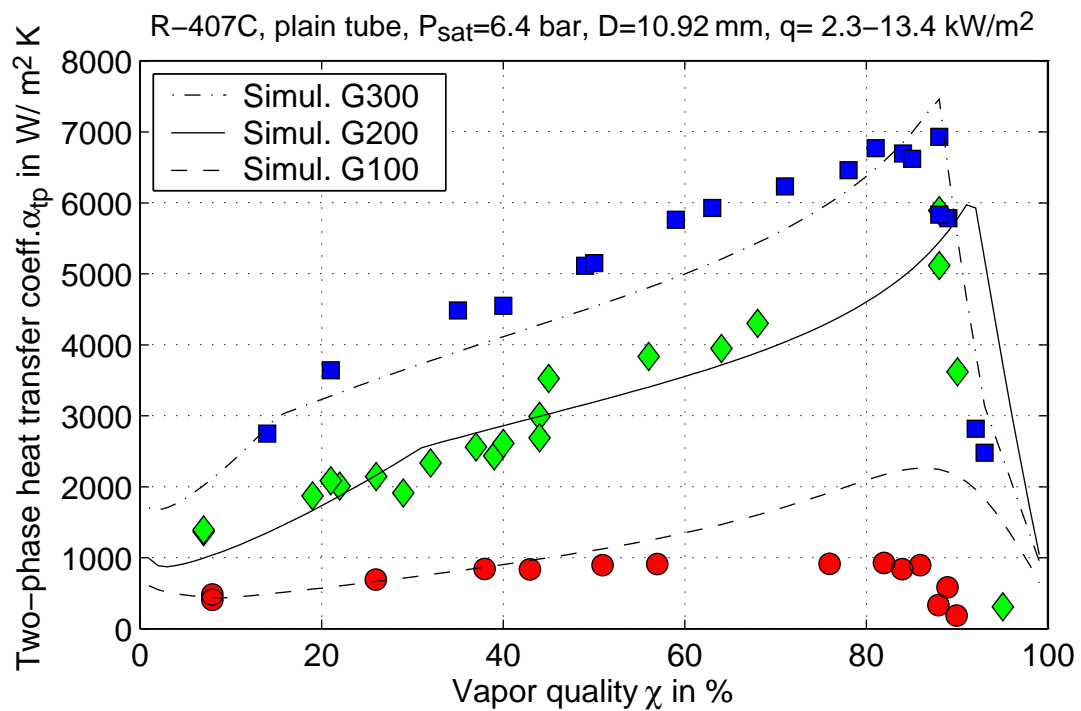


Figure 3.22: Comparison of experimental heat transfer data, from [Kattan, 1996], with simulation for horizontal plain tube evaporating flow with R-407C.

Microfin tubes, enhancement model:

Evaporator tubes with enhancing internal microfin structures are becoming the standard in industry. The spiral microfins tend to guide the liquid up-wards along the grooves and annular like flow regime result, even in stratified flow conditions. Correlations to determine, the enhancement effect of the microfins in evaporating heat transfer are proposed by [Kattan, 1996], according to:

$$\alpha_{tp,mf} = E_{mf} \left[\alpha_{nb}^3 + (E_{rb} \alpha_{comv})^3 \right]^{1/3} \quad (3.51)$$

$$\text{with } E_{rb} = \left\{ 1 + \left[2.64 Re_{liq}^{0.036} \left(\frac{e_{mf}}{D_{mf}} \right)^{0.212} \left(\frac{p_{mf}}{D_{mf}} \right)^{-0.21} \left(\frac{\phi_{mf}}{90^\circ} \right)^{0.29} Pr_{liq}^{-0.024} \right]^7 \right\}^{1/7} \quad (3.52)$$

$$\text{and } E_{mf} = 1.89 \left(\frac{G}{G_0} \right)^2 - 3.7 \frac{G}{G_0} + 3.02 \quad \text{with } G_0 = 500 \text{ kg/m}^2 \text{ s} \quad (3.53)$$

The geometric properties of the microfin tube are (with values given in [Kattan, 1996]): Max. inside tube diameter: $D_{mf} = 11.9 \text{ mm}$, fin height: $e_{mf} = 0.25 \text{ mm}$, axial pitch: $p_{mf} = 1.6437 \text{ mm}$ and helix angle: $\phi_{mf} = 18^\circ$

The Reynolds number is given for annular flow, using eq. 3.46 at the diameter D_{mf} .

3.2.4 Condensation heat transfer model

Heat transfer in condensation applied to heat pump heat exchangers, is analyzed for forced vertical down-flow conditions. The liquid is mainly generated by film-wise condensation. Compact plate heat exchangers are standard solutions, combining compactness and efficiency, for heat pump design. In these types of condensers, the two-phase flow can be assimilated to a highly turbulent annular flow pattern. Two simple approaches to calculate local film condensation heat transfer in annular flow are proposed in the literature. These methods apply for circular tubes and are presented in [Collier and Thome, 1994]:

$$\text{Akers (1959): } Nu_D = C Re_{eq}^n Pr^{1/3} \quad \text{with } Re_{eq} = DG_{eq}/\mu_{liq} \quad (3.54)$$

using $C = 0.0265$ and $n = 0.8$ for $Re > 50000$

$C = 5.03$ and $n = 1/3$ for $Re < 50000$

and with the mass velocity for an equivalent mass flow rate:

$$G_{eq} = G \left[(1 - \chi) + \chi \left(\frac{\rho_{liq}}{\rho_{vap}} \right)^k \right] \quad (3.55)$$

The exponent k takes a fixed value of 0.5.

$$\text{Shah (1979): } Nu_D = 0.023 Re_{liq}^{0.8} Pr_{liq}^{0.4} \left[(1 - \chi)^{0.8} + \frac{3.8 \chi^{0.76} (1 - \chi)^{0.04}}{P_{red}} \right] \quad (3.56)$$

with the reduced pressure $P_{red} = \frac{P}{P_{crit}}$

While the above mentioned correlations are found through empirical adaptations of the single phase convective flow, [El Hajal et al., 2003a,b] presented a derivation of their evaporation flow pattern map and heat transfer model to the condensation. This general method is summarized here below.

A generalized flow pattern map based method for tube condensation.

Restricting the analysis to the **turbulent annular flow**, where the dry angle θ_{dry} equals to zero, **only the convective condensation part of this general method is presented in this work.**

Compared to the evaporation model, this method includes the new definition of the **logarithmic mean void fraction model**, a composition of the Rouhani-Axelsson correlation (eq. 3.31), reflecting the separated drift flux model, and the homogeneous void fraction model (eq. 3.29), which is more adapted for high reduced pressures, where the liquid and vapor densities are similar. This new model is given with the relation

$$\varepsilon_{ln} = \frac{\varepsilon_h - \varepsilon_{ra}}{\ln\left(\frac{\varepsilon_h}{\varepsilon_{ra}}\right)} \quad (3.57)$$

The convective condensation heat transfer correlation, obtained for turbulent film condensation, equals to

$$\alpha_{conv} = C Re_{liq}^n Pr_{liq}^m \frac{\lambda_{liq}}{\delta} f_i \text{ for } Re_{liq} > 1800 \quad (3.58)$$

The three constant numbers are set statistically to $C = 0.003$, $n = 0.74$ and $m = 0.5$, replacing the values of the Dittus-Boelter equation (eq. 3.27). The Reynolds number is given for the mean velocity in the liquid film with:

$$Re_{liq} = \frac{4G(1 - \chi)\delta}{(1 - \varepsilon)\mu_{liq}} \quad (3.59)$$

The liquid film thickness in annular flow is analytically defined by

$$\delta = \delta_{annular} = \frac{D}{2} (1 - \sqrt{\varepsilon}) \quad (3.60)$$

An interfacial roughness correction factor f_i has been introduced to account for the formation of interfacial waves on the liquid film. The analytical expression is given in eq. 3.61, where the respective velocities are found in eq. 3.62.

$$f_i = 1 + \left(\frac{u_{vap}}{u_{liq}} \right)^{0.5} \left(\frac{(\rho_{liq} - \rho_{vap}) g \delta^2}{\sigma} \right)^{0.25} \quad (3.61)$$

$$u_{liq} = \frac{G(1 - \chi)}{\rho_{liq}(1 - \varepsilon)} \quad u_{vap} = \frac{G\chi}{\rho_{vap}\varepsilon} \quad (3.62)$$

Based on this model, a first extension to include heat transfer effects with zeotropic mixtures has been investigated by [Del Col et al., 2004].

Condensation with zeotropic mixtures

While in the literature, the models of condensation with zeotropic mixtures are referring to the simplified approach of *Bell and Ghaly* (1973), this model has been modified by [Del Col et al., 2004] to include interfacial roughness and non equilibrium effects. The new model is an extension of the condensation heat transfer model of [El Hajal et al., 2003a], presented in the paragraph before.

As the saturation temperature of the zeotropic mixture changes during the condensation process, sensible heat and mass transfer effects have to be considered. Complete mixing during the condensation is presumed and overall equilibrium is maintained.

With the Bell and Ghaly concept the heat transfer coefficient for zeotropic mixtures is calculated by

$$\alpha_{conv,mix} = \left[\frac{1}{\alpha_{conv,pure}} + \chi c_{p,vap} \frac{(\Delta T_{sat}/\Delta h_{lat})}{\alpha_{vap,0}} \right]^{-1} \quad (3.63)$$

The heat transfer coefficient $\alpha_{vap,0}$ in equation 3.63 is calculated for the vapor flowing alone in the duct and standard single-phase correlations can be applied, using the corresponding Reynolds number for the vapor phase: $Re_{vap,0} = \rho_{vap} u_{vap} D / \mu_{vap}$ using u_{vap} from eq. 3.62. [Del Col et al., 2004] introduces the interfacial roughness correction to the Bell and Ghaly approach by replacing $\alpha_{vap,0}$ with $\alpha_{vap,f} = \alpha_{vap,0} f_i$, with f_i proposed in eq. 3.61.

The generalized model for condensation heat transfer in horizontal tubes has good perspectives to become a new base for the development of new heat transfer correlations to more complex geometrical configurations. The application of this method to the corresponding flow geometry

in compact plate heat exchangers, which are commonly used in heat pump applications, could not be applied reasonably and other semi-empirical approaches have been selected to model the condensers (section 3.2.6). The modified Bell and Ghaly correction for zeotropic mixtures could although be integrated into the cycle simulation mode, using an appropriate correlation for the vapor phase heat transfer coefficient in eq. 3.63.

3.2.5 Finned tube evaporator

Considering air-water heat pumps, a finned tube evaporator model is implemented, using the general equation 3.64 to calculate the total exchanged heat rate.

$$\dot{Q}_{ev} = k_{ev} \Delta T_{ln} S_{refr} \quad (3.64)$$

The overall heat transfer coefficient k_{ev} for the evaporator is the result of the three main resistances (refrigerant convection, conduction through the tube wall and the fin, air side convection), with the option of a homogeneous frosting layer covering the fins.

In order to simplify the notation of the subsequent equations, the three types of diameters involved are: d = internal tube diameter, D = external tube diameter, $D^* = D + 2f_s$ = air side tube diameter, covered with fin, see Figure 3.23.

$$k_{ev} = \left[\left(\frac{1}{\alpha_{air}} + \frac{\delta_{ice}}{\lambda_{ice}} \right) \frac{A_{int,tube}}{A_{ext,tot}} + \frac{d \ln \frac{D^*}{D}}{2 \lambda_{fin}} + \frac{d \ln \frac{D}{d}}{2 \lambda_{tube}} + \frac{1}{\alpha_{refr}} \right]^{-1} \quad (3.65)$$

The refrigerant side heat exchange is modeled by the general heat transfer model presented in section 3.2.3. The air side heat exchange is based on the model proposed in [VDI, 1993]. The corresponding setup is shown in Figure 3.23.

The fin efficiency η_{fin} , which is defined by the ratio of the average temperature difference between the fin surface and the air temperature to the difference between the tube surface and the air, is used to calculate the air side heat transfer.

$$\alpha_{air} A_{ext,tot} = \alpha_{av} [A_{tube,ext-free} + \eta_{fin} A_{tube,ext-tot.}] \quad (3.66)$$

with the fin efficiency

$$\eta_{fin} = \frac{\tanh X}{X} \quad \text{with } X = H' \sqrt{\frac{2 \alpha_{av}}{\lambda_{fin} f_s}} \quad (3.67)$$

for staggered tube arrangement and connected fins:

$$H' = \frac{D^*}{2} (\varphi' - 1) (1 + 0.35 \ln \varphi') \quad \text{with } \varphi' = 1.27 \frac{f_w}{D^*} \sqrt{\frac{f_h}{f_w}} - 0.3$$

and the average heat transfer coefficient for the tubes and fins is

$$\alpha_{av} = 0.38 Re_{air, D^*}^{0.6} \left(\frac{A_{ext, tot}}{A_{tube, ext}} \right)^{-0.15} Pr_{air}^{1/3} \frac{\lambda_{air}}{D^*} \quad (3.68)$$

The Reynolds number in the above correlation is calculated by geometry, with the air velocity at the narrowest flow area and the characteristic flow dimension D^* . Frost formation on the surfaces generates a supplementary reduction in the flow area, increases the air-side pressure drop and adds

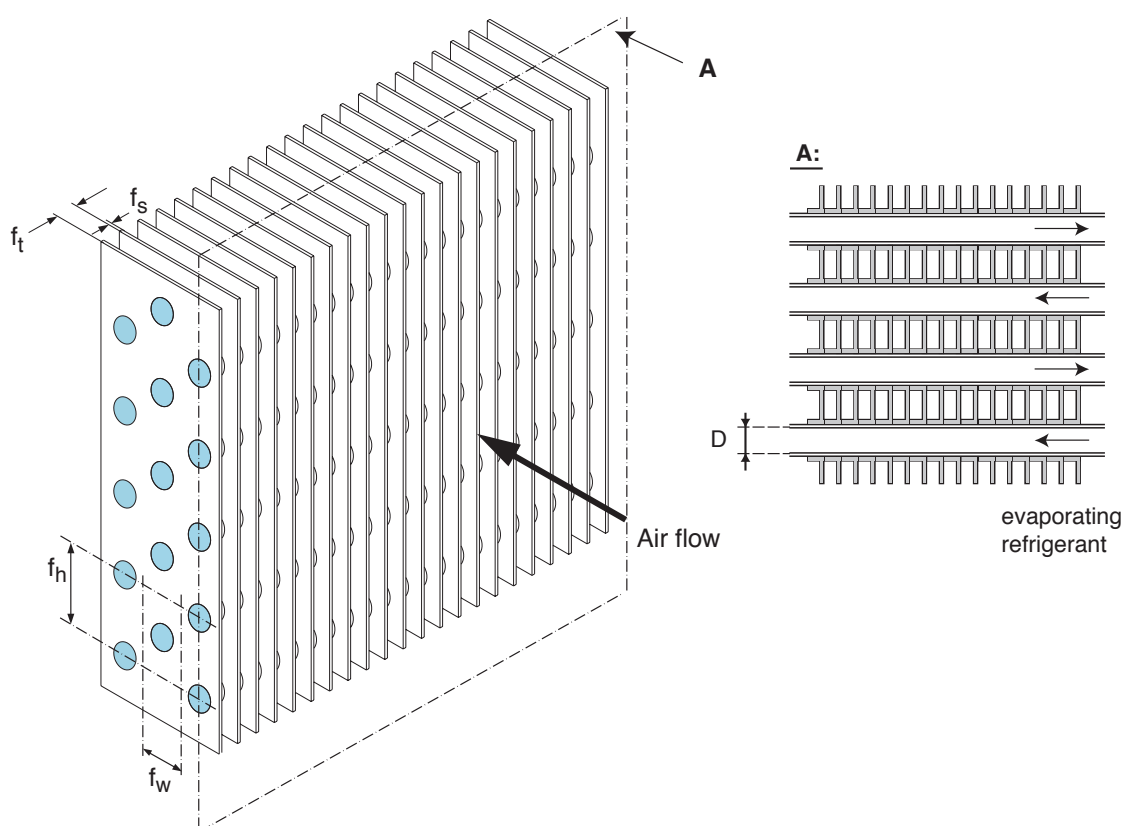


Figure 3.23: Geometrical setup for finned tube evaporator.

a thermally isolating layer, which will be accounted with the equivalent thickness δ_{ice} .

The refrigerant side modeling of the heat transfer coefficient is described in detail in sections 3.2.2 and 3.2.3. In order to take into account the variation of the local heat transfer coefficient during the evaporation process, the evaporator coil model is split into equally distributed surfaces (according to the number of passes of the fluid). This also permits to consider the temperature evolution of the air in counter-current flow. Air is considered as humid air (modifying the specific heat of the air), which also allows an estimation of the condensation rate or the frost formation rate on the coil.

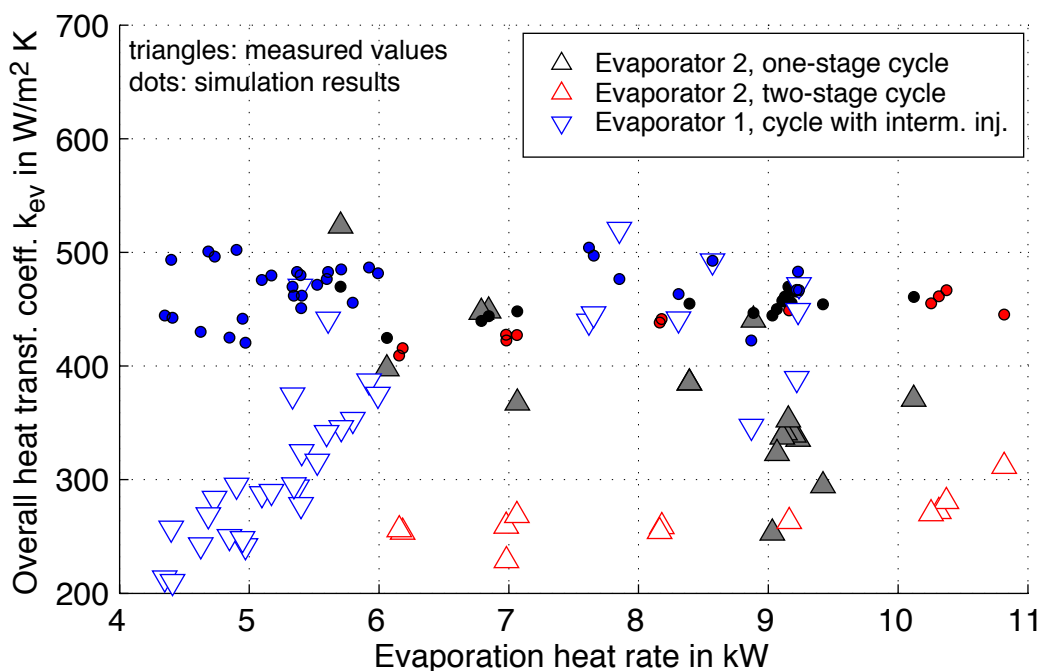


Figure 3.24: Comparison of the simulated overall heat transfer coefficient (dots) for two distinct fin and tube evaporator models with measured data (triangles). Evaporating R-407C in microfin tube ($d=10$ mm), air $T = -12^{\circ}\text{C}$ to 7°C , straight fins with surface increase of factor ~ 10 . Mass velocity of the refrigerant $G = 30 - 60$, air flow rate $3000 - 4000$ m^3/h for evaporator #1 (see flow chart on Fig. A.4) and $G = 20 - 35$, air flow rate $4000 - 5000$ m^3/h for evaporator #2 (see flow chart on Fig. A.6).

Two types of finned tube evaporator coils with 10 mm microfin tubes, have been tested in laboratory conditions under different cycle configurations (one-stage, two-stage and cycle with intermediate injection). The experimental overall heat transfer coefficient is calculated with the traditional logarithmic mean temperature difference approach (eq. 3.64). The logarithmic mean temperature difference is composed of the measured air inlet and exit (3 transmitters on each side) and the refrigerant inlet and the calculated saturated vapor temperature, based on the value of the pressure at the compressor inlet (the contribution of eventual overheat is not included). The total heat rate is known from the refrigerant mass flow rate (Coriolis flow meter) and the enthalpy difference of the inlet point (isenthalpic expansion) to the exit conditions (estimated backwards from the com-

pressor inlet and the suction line heat exchanger). The listings of the transmitters are provided in the Annex [A.5](#).

Simulations were performed with given flow inlet conditions (mass flow rates and temperatures), leading to an evaluation of the global heat transfer coefficient on idealized conditions, which consist of the following assumptions: homogeneous air flow over the entire flow section, no frosting layer, steady state conditions and no cycling due to regulation effects on the refrigerant side, no oil hold up in the evaporator and perfect flow division into the parallel refrigerant circuits. In addition it is assumed, that the entire surface is contributing to the heat transfer.

In Figure [3.24](#) the measured heat transfer coefficients are represented as triangles. The quite important scatter of the values in comparable test conditions, shows the difficulty to perform overall heat exchanger rating tests on such complex setups. The main factors, which reduce the heat transfer coefficient, are: a) Air flow distribution: With the use of only three temperature transmitters on each air section, the flow inhomogeneities of the air cannot be detected very accurately, which can lead to important errors on the effective heat transfer surface and the measured mean temperature difference on the air side. b) Presence of frosting layer: In repeated frosting-defrosting cycles, locally compact ice layers are formed, which lead to an increase of the total heat transfer resistance. c) Fluctuating flow conditions: The experimental heat transfer coefficient is a result of the mean operating conditions over a time period of 10 to 20 min. Due to partial shifting of the overheat into the evaporator, a fluctuating regulation mode leads to a reduced portion of wetted surface in the evaporator, which reduces its capacity.

The simulation results show a much more limited bandwidth of the global heat transfer coefficient, than seen by the experiments. All the simulated points remain between a value of 400 - 500 W/m² K, which corresponds to the upper limit of the experimental range. The very low experimental values could not be predicted by the model due to the assumptions made. As the heat transfer resistance is the most important on the air side, it is recommended for future work to investigate thoroughly the air flow, in particular at the exit of the evaporator (much better coverage by thermocouples over the flow section).

3.2.6 Plate heat exchangers

To transfer heat from two-phase to liquid or from liquid to liquid flow, the **plate heat exchangers**, Fig. [3.25](#), are the most compact solution and are as consequence used in heat pumps as condensers, evaporators or for intermediate heat exchange (economizers).

The state of knowledge in generalized modeling of compact plate heat exchangers is still poor and the diversity of geometries limits the capacity of empirical correlations proposed. While chevron-

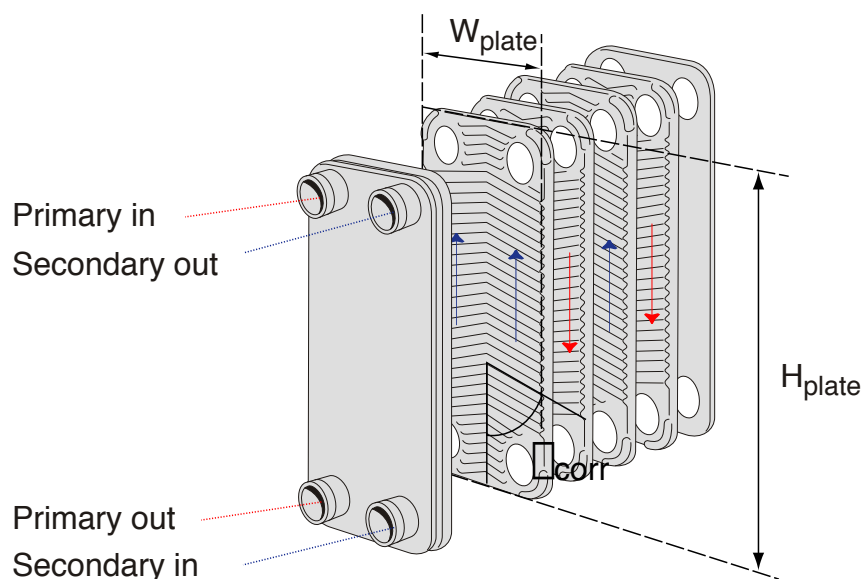


Figure 3.25: Plate heat exchanger configuration

type¹ plates are the usual type of plate heat exchangers, main modifications in the heat transfer characteristics are due to the influence of the corrugation angles β_{corr} , which differ from one exchanger to another.

A generalized model to predict heat transfer and pressure drop characteristics, related to the corrugation angle, has been proposed by [Martin, 1996] for single phase flow. This model, however shows important deviations to the empirical correlations of [Le Pellec, 1997; Yan et al., 1999] (Fig. 3.26). The last model will be applied in the cycle simulation code for the **liquid heat transfer coefficient in the plate heat exchangers** (eq. 3.69) and the model of [Martin, 1996] is used to adapt the heat transfer coefficient to other corrugation angles used in our tests.

$$Nu_{liq} = 0.2121 Re_{liq}^{0.78} Pr_{liq}^{1/3} \quad (3.69)$$

The impact on heat transfer and pressure drop with two different corrugation angles (30° and 60°) has also been measured by [Würfel and Ostrowski, 2004], who tested water and n-heptane in condensation mode, over a large range of Reynolds numbers. As in [Yan et al., 1999], who exclusively correlated R-134a data, the proposed **empirical correlations for the condensation**

¹Also known as the herringbone-type heat exchangers.

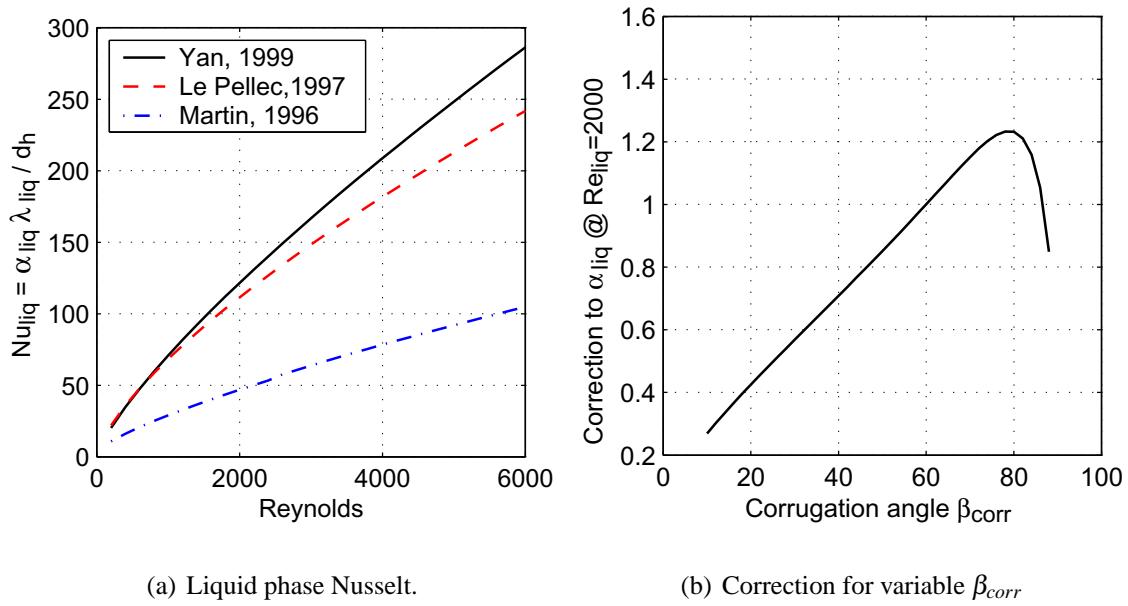


Figure 3.26: Comparison of the empirical correlations to calculate liquid heat transfer coefficient, using Water at $T = 50^\circ\text{C}$, with hydraulic diameter $d_h = 6.6\text{ mm}$ and for $\beta_{corr} = 60^\circ$.

heat transfer are based on the Akers equation, see eq. 3.54, with:

$$Nu_D = C Re_{eq}^n Pr^{1/3} \quad \text{with} \quad Re_{eq} = DG_{eq} / \mu_{liq} \quad (3.70)$$

$$\text{and} \quad G_{eq} = G \left[(1 - \chi) + \chi \left(\frac{\rho_{liq}}{\rho_{vap}} \right)^k \right]$$

using the parameters of Table 3.2.

Table 3.2: Correlations for film condensation, modified parameters of the Akers equation (to insert in eq. 3.70).

	β_{corr}	C	n	k
Akers, 1959	(in tubes)	5.03	1/3	0.5
Yan et al., 1999	60°	4.118	0.4	0.5
Würfel, 2004	30°	0.325	0.62	0.4
	60°	3.77	0.43	0.14

Figures 3.27 (a+b) show a comparison of the condensation models, using the setup of [Yan et al., 1999]. Deviations of the two correlations, which are adapted for plate heat exchangers are important and the prediction of the heat transfer for other geometries and fluids is not expected to be very accurate. For this reason the heat exchanger will only be subdivided to consider transition points, as in a classical condenser application the refrigerant traverses desuperheating (gas flow),

condensation (two-phase) and subcooling (liquid). Figure 3.27 also compares the heat transfer prediction of [El Hajal et al., 2003b], which is given for in-tube condensation. As only annular flow is assumed, the assumption of a turbulent film is not always verified and the transition point, of the supposed validity limit is indicated on the graph. It is interesting to remark, that the generalized model for in-tube flow shows the same trends for varying vapor quality and for variable Reynolds number as found in the correlation of [Würfel and Ostrowski, 2004]. The heat transfer in plate heat exchangers is in the order of 2-3 higher according to these results.

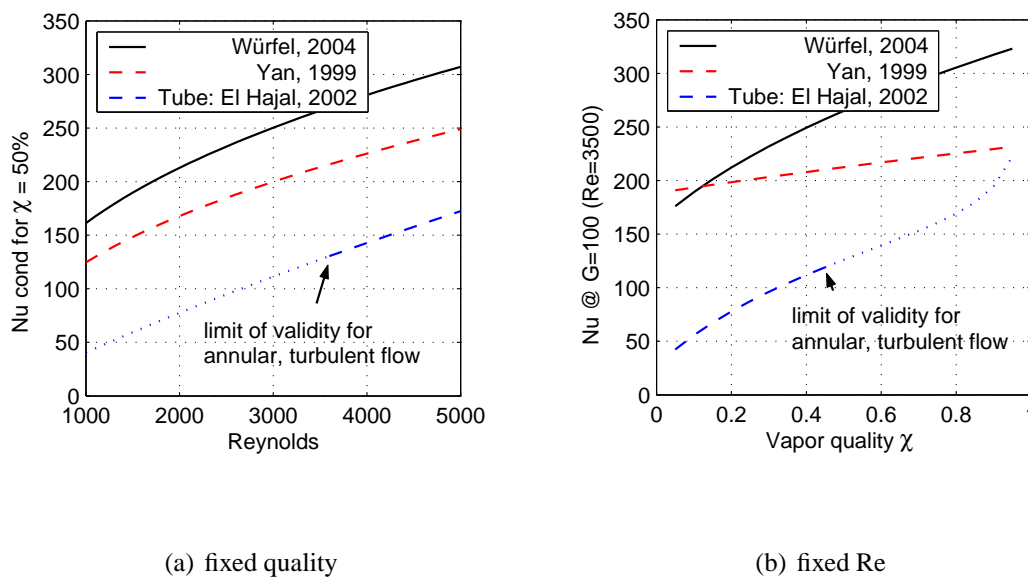


Figure 3.27: Comparison of the empirical approaches to calculate condensation heat transfer coefficient for R-134a at 8 bar ($T_{sat} = 31^\circ\text{C}$), hydraulic diameter $d_h = 6.6\text{ mm}$ for $\beta_{corr} = 60^\circ$ corrugation angle.

Far less published work is available for the evaporation in plate heat exchangers. A proposition to calculate evaporation heat transfer is given by [Yan and Lin, 1999]. [Lottin et al., 2003] compared their data (using the refrigerant R-410A) with two in-tube evaporation models, as the Gungor and Winterton (1986) and the Bivens and Yokozeki (1994) models. Both in-tube correlations have been predicting their data with satisfying precision, as they state. The single phase heat transfer coefficient has been replaced by Yan's correlation (eq. 3.69). As using the in-tube correlations to predict the evaporation heat transfer in plate heat exchangers is often mentioned, we have tried to couple the evaporation model presented in section 3.2.3 with the use of the convective heat transfer coefficient from [Yan et al., 1999], but with very low success. Therefore **the Bivens and Yokozeki equation [Bivens and Yokozeki, 1994] has finally been adopted to predict the evaporation**

heat transfer coefficient in plate heat exchangers:

$$\alpha_{evap} = (\alpha_{pool}^{2.5} + \alpha_{conv}^{2.5})^{1/2.5} \quad (3.71)$$

with the boiling correlation by Cooper (1984)

$$\alpha_{pool} = 55 P_{red}^{0.12} (-\log(P_{red}))^{-0.55} \check{M}^{-0.5} \check{q}^{0.67} \quad (3.72)$$

$$\alpha_{conv} = C \alpha_{liq} (0.29 + X_{tt}^{-1})^{0.85} \quad (3.73)$$

with $C = 2.838 Fr^{0.2}$ if $Fr < 0.25$, else $C = 2.15$

using the standard definitions of the dimensionless numbers, the Lockhart-Martinelli X_{tt} parameter and the Froude number Fr . The liquid heat transfer coefficient is calculated with the correlation for plate heat exchangers, eq. 3.69.

The overall heat exchange in a plate-heat exchanger (PHE) is given as

$$k_{PHE} = \left[\frac{1}{\alpha_{circuit,1}} + \frac{\delta_{wall,plate}}{\lambda_{wall}} + \frac{1}{\alpha_{circuit,2}} \right]^{-1} \quad (3.74)$$

and has to be applied for each flow zone separately.

Plate heat exchangers are employed for different purposes, in a air-water heat pump cycle:

Table 3.3: Use of plate heat exchangers for air-water heat pump.

Function	Primary flow	Secondary flow
Condenser	water (liquid)	refrigerant (gas, two-phase: condensing)
Economizer	refrigerant (liquid)	refrigerant (two-phase: evaporating)
Secondary evap.	refrigerant in cycle 1 (liq.)	refrigerant in 2 nd cycle 2 (two-phase: evap.)
Tap water heater	water (liquid)	refrigerant (liquid or gas)

Several complications arise when comparing the models with the collected data. The overall heat transfer coefficient, which is calculated by the measured entry and exit conditions cannot be decomposed into the contributions of the different flow zones and the relative heat transfer surfaces can only be estimated (by simulation). In the plate condenser, for example, an internal measurement would be needed to calibrate the transition of the desuperheating to the saturation flow region. The problem in the economizer heat exchanger is however of different nature. For the given small heat exchange rate, no correctly sized plate heat exchangers could be identified and the available exchange surface is well oversized. Therefore, the validation of the used correlations cannot be performed correctly.

3.2.7 Coaxial tubular suction line heat exchanger

The model of the internal suction line overheater consists of a tubular concentric counterflow heat exchanger. On the inner tube, the subcooled liquid is further cooled and the Gnielinski correlation is applied (eq. 3.28). In the low pressure suction line, the refrigerant enters at high vapor quality. The evaporation process is finalized and is followed by the superheating process in this heat exchanger. The heat exchanger is normally mounted in horizontal position, in order to ensure oil return to the compressor. The remaining liquid is flowing on the outer, thermally isolated, wall. The prediction of the overall heat transfer coefficient of this counterflow heat exchanger can thus be performed with a single phase approach also for the annulus.

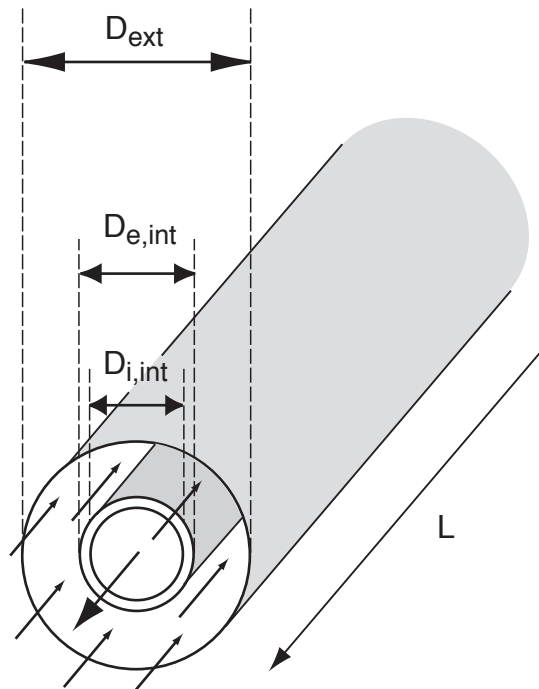


Figure 3.28: Geometrical setup for concentric suction line heat exchanger

The hydraulic diameter of the external flow D_h is equal to the difference of the internal diameter of the external tube D_{ext} and the external diameter of the internal tube D_{int} .

The flow in the annulus is in transitional or turbulent flow for $Re_{ann} > 2300$. If these conditions are reached (which will be supposed in the further development of the relations), the Nusselt values are expressed in the adapted form derived from the circular tube heat transfer, also calculated with the Gnielinski correlation.

$$\frac{Nu_{annulus}}{Nu_{tube}} = 0.86 \left(\frac{D_{ext}}{D_{int}} \right) \quad (3.75)$$

The overall heat transfer coefficient between the subcooling liquid (subc.) and the vapor in the annulus is given with

$$k_{concentric} = \left[\frac{1}{\alpha_{subc.}} + \frac{D_{i,int} \ln \left(\frac{D_{e,int}}{D_{i,int}} \right)}{2 \lambda_{wall}} + \frac{D_{i,int}}{D_{e,int} \alpha_{annulus}} \right]^{-1} \quad (3.76)$$

3.2.8 Influence of oil in heat transfer

The presence oil diluted oil in the refrigerant affects the heat transfer by these main contributions:

1. Preferential evaporation of the refrigerant:

Typical lubricating oil have saturation pressures 10^5 times lower than those for the refrigerants. During phase change, nearly all the oil remains in the liquid phase, leading to increased oil concentrations and higher saturation temperatures at the end of the evaporation process.

2. Increase of the viscosity:

The most important influence on heat transfer and pressure drop characteristics, is the change of the bulk viscosity of the remaining liquid refrigerant-oil mixture. The increased viscosity results in a lower convective heat transfer coefficient and in an elevation of the friction factor.

3. Non-equilibrium during the boiling process:

Oil rich layers may be formed at the interfaces (liquid-vapor or liquid-solid), resulting in an increased resistance to heat and mass transfer.

4. Foaming:

A heat transfer increasing effect has been attributed to the foaming of refrigerant-oil mixtures, which occur during flashing (pressure reduction), or in highly turbulent flow. An increased liquid-vapor interface surface is the main explication for the gain in heat transfer.

5. Flow pattern changes:

With the modified physical properties of the refrigerant-oil mixture, the transition curves may be shifted with important local effects on heat transfer coefficient. As shown in [Thome et al., 1996] on plain tube evaporation tests with R-134a/oil mixtures, important increase of the heat transfer coefficient (max. +65%) at medium vapor qualities and at the lowest mass velocities ($G=100$) were measured. This increase is mainly attributed to the change of the flow pattern from stratified-wavy flow to intermittent and annular flow. Tests with a microfin tube showed at very low global oil concentrations of 0.5% an important reduction of the heat transfer coefficient of 40%. In this case the effect of the internal fin structure to lift the refrigerant to the top of the tube is reduced at low mass velocities, where the interfacial shear

from the vapor to the liquid is not sufficient to transport the liquid film to the top of the tube. This effect is also resulting in a global oil holdup in the evaporator. Foaming was observed in R-407C/oil mixtures, preventing such a drastic reduction of the heat transfer coefficient compared to the pure refrigerant tests.

The **thermodynamic correct modeling of the refrigerant-oil equilibrium conditions** relies on the use of fugacity coefficients, which require the formulation of an equation of state or it can be evaluated by means of the Gibbs free energy formulation, which is further described in [Arnemann, 1993; Martz et al., 1996; Mermond et al., 1999]. For reliable results, the molecular structure (or a good estimation of the bulk molecule) of the lubricant should be known, which is difficult to define, considering, that the oil is a complex mixture, containing several additives. A second mainly adopted approach is to refer to experimentally evaluated solubility charts for the specific refrigerant-oil combination. This method was mainly used due to the absence of good models. [Youbi-Idrissi et al., 2003] proposes to use this approach (and produces his own database), but such informations are not available for our mixture. **In this work a fitting mixture model is used**, which is based on the approach proposed by [Thome, 1995], for the saturation temperature and the latent heat of evaporation.

An overview of other refrigerant-oil mixing properties, which are used for the heat transfer calculation, is provided by [Conde, 1996].

3.2.8.1 Pure oil properties

General indications

The list below resumes the available technical information of the used synthetic polyolester lubricant:

- Brand name: Mobil EAL Arctic 22 CC
- Viscosity
 - @40°C 23 cSt (= mm²/s)
 - @100°C 4.8 cSt
- Viscosity index 130
- Density at 15°C: 0.991kg/l
- Lower miscibility limit (10% oil) with R-134a at -54°C, with R-407C at -38°C.
- Heat capacity at 15°C: 1.96 kJ/kg K

The physical and thermodynamic properties of the lubricant are modeled, using, where existing, correlated data. The remaining properties are evaluated through expressions found in literature (see [Conde, 1996; Skripov et al., 2003; Zhelezny et al., 2003]).

Critical and normal boiling point

The oil properties at the critical and the normal boiling point are basically needed in some of the proposed correlations from the literature. The used lubricant is a complex mixture of the polyolester molecules and several additives (e.g. anti-foaming agents), and critical point can hardly be evaluated experimentally, since at high temperature high degradation of the mixture composition and chemical interaction are expected.

An original approach to evaluate pseudo-critical properties of refrigerant-oil mixtures including Mobil EAL Arctic 22 oil is proposed in [Skripov et al., 2003], using a pulse heating method. Critical point properties and normal boiling point temperature can only roughly be extracted from the presented graphs. Numerical values have fortunately been found in a later publication of one of the co-authors [Zhelezny et al., 2003].

$$\begin{aligned} T_{crit} &= 820 \text{ K} \approx 550^\circ\text{C} \\ T_{nb} &= 780 \text{ K} \\ P_{crit} &= 6.5 \text{ bar} \end{aligned} \tag{3.77}$$

In addition two correlations to estimate boiling or critical temperature are given by [Conde, 1996]. These expression are:

$$T_{crit} = 15.2762 S^{0.2985} T_{nb}^{0.62164} \tag{3.78}$$

$$T_{crit} = 189.8 + 450.6 S + (0.4244 + 0.1174 S) T_{nb} + (0.1441 - 1.069 S) \frac{10^5}{T_{nb}} \tag{3.79}$$

$$\text{with } S = \text{specific gravity} = \frac{\rho \text{ at } 16^\circ\text{C}}{999 \text{ kg/m}^3}$$

The resolution of these expressions, shows, however, a normal boiling temperature of the oil well below the experimentally determined temperature. The calculated temperature is:

$$T_{nb,oil} = 612 \text{ K} = 339^\circ\text{C} \tag{3.80}$$

The experimental value of 780 K is however used in the calculations.

Density

Density is correlated from tabulated values in the temperature range of 0 to 120°C. The liquid oil is considered to be compressible. The oil density has been experimentally verified at ambient temperature 20°C.

$$\rho_{oil} = 1000.7 - 0.6976 T \quad \text{with } T \text{ in } ^\circ\text{C} \quad (3.81)$$

Figure 3.29 compares the refrigerant (R-134a and R-407C) liquid densities with that of POE-oil over a range of temperature, corresponding to the liquid temperatures in the heat pump. At the higher end of this range, oil and refrigerant densities are approaching and density based oil concentration evaluation will be very difficult to perform.

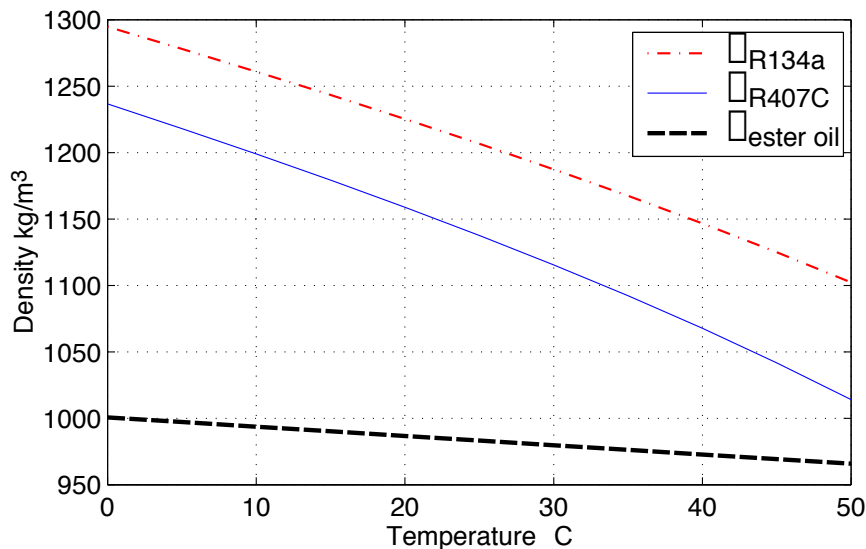


Figure 3.29: Comparison of oil density (EAL Arctic 22 CC) and refrigerant liquid density (R-134a, R-407C) at the corresponding bubble point.

Kinematic viscosity

Lubricant oil viscosity changes exponentially with temperature. The general expression 3.82 is fitted with tabulated data provided by the oil manufacturing company:

$$\nu = e^{f(T)} \quad \text{with } f(T) \text{ being a polynomial function of } T \quad (3.82)$$

The degree of the polynomial regression has been chosen in the 3rd degree, in order to obtain a prediction within errors of < 3%:

$$\nu = e^{-1.7999 \cdot 10^{-6} T^3 + 5.0048 \cdot 10^{-4} T^2 - 0.0683 T - 8.6126} \quad \text{with } T \text{ in } ^\circ\text{C} \quad (3.83)$$

Thermal conductivity

The conductivity of the oil is regressed by a linear law from provided tabular data. The used correlation is:

$$\lambda = 0.1637 - 1.631 \cdot 10^{-4} \text{ with } T \text{ in } ^\circ\text{C} \quad (3.84)$$

Liquid specific heat

The specific heat of liquid oil is calculated by the proposed correlation of *Liley and Gambill*, proposed in the chemical handbook of [Perry and Green, 1997].

$$c_{oil} = 4.186 \frac{0.388 + 4.5 \cdot 10^{-4}(1.8T + 32)}{\sqrt{S}} \text{ with } T \text{ in } ^\circ\text{C} \text{ and } c_{oil} \text{ in kJ/kg K} \quad (3.85)$$

with $S = \text{specific gravity} = \frac{\rho \text{ at } 16^\circ\text{C}}{999 \text{ kg/m}^3}$

Surface tension

No data is available to evaluate the surface tension of the oil. this property will be used in heat transfer calculations. Equation to estimate this properties are presented in [Conde, 1996]. The equation of *Brock and Bird*, which has been adapted by *Miller* has shown the best prediction for other oil types, and will be used in this work.

$$\sigma_{oil} = 4.642 \cdot 10^{-4} Q P_{crit}^{\frac{2}{3}} T_{crit}^{\frac{1}{3}} \left(1 - \frac{T}{T_{crit}}\right)^{11/9} \text{ in mN/m} \quad (3.86)$$

with $Q = 0.1196 \left[1 + \frac{\frac{T_{nb}}{T_{crit}} \ln\left(\frac{P_{crit}}{P_{atm}}\right)}{1 - \frac{T_{nb}}{T_{crit}}}\right] - 0.279$

3.2.8.2 Refrigerant-oil mixing models

The modeling of refrigerant-oil mixture properties is based on the works of [Bošnjaković and Knoche, 1997; Thome, 1993; ASHRAE, 1998] and have recently been reviewed by [Shen and Groll, 2003].

Mixture density

Ideal mixing density is found by the expression:

$$\rho_{mix}^0 = \frac{1}{\frac{w_{oil}}{\rho_{oil}} + \frac{1-w_{oil}}{\rho_{refr}}} \quad (3.87)$$

The mixture of vapor, can be considered (in absence of chemical reaction) as an ideal mixture and the relation above is well suited. In liquid mixture, the molecules of the components are highly compressed and ideal law can result in considerable errors. To account for the real behavior, but without entering into molecular considerations, an excess volume v^E is defined to characterize the departure from the ideal law. This deviation, can be either positive, negative or even change sign, when traversing the entire mixture range of a considered mixture. The departure from ideal mixture density for R-407C/oil and R-134a/oil mixtures has been evaluated experimentally, in the range of interest (0-10% oil mass concentration, see Fig. 3.31).

$$v^E = v_{mix} - v_{mix}^0 = (A - 1) v_{mix}^0 = f(T, P) \quad (3.88)$$

In some textbooks (e.g. in [ASHRAE, 1998]), the departure from ideal state is characterized by the **density correction coefficient** A and to show the order of magnitude the example of the R-22/mineral oil mixture is shown in Fig. 3.30.

With the second formulation the real mixture density is calculated with:

$$\rho_{mix} = \frac{1}{\frac{1}{\rho_{mix}^0} + v^E} = \frac{\rho_{mix}^0}{A} \quad (3.89)$$

Density measurements with controlled oil concentration are presented in the paragraph 5.2.3.2 on page 192. These measurements, however, show a strong limitation of resolution in the higher temperature range of 30°C and above.

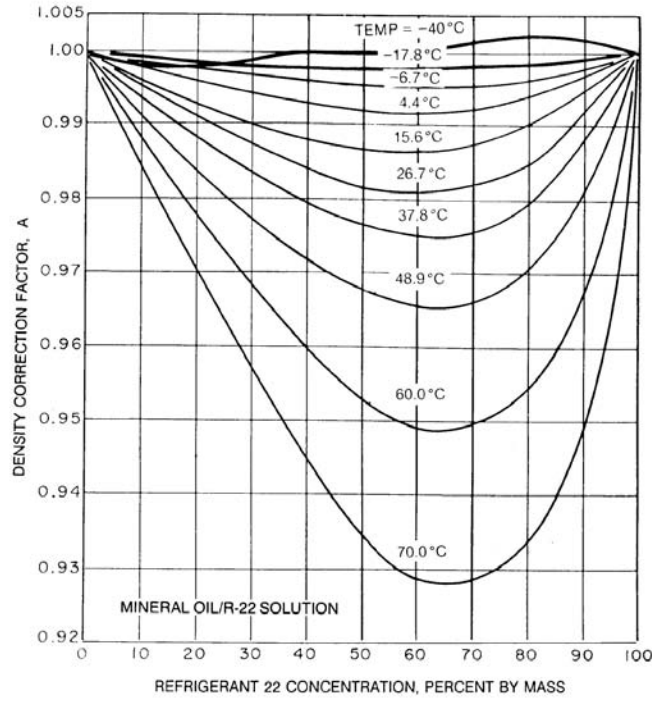


Figure 3.30: Density correction coefficient for R-22 and mineral oil mixture. From [ASHRAE, 1998].

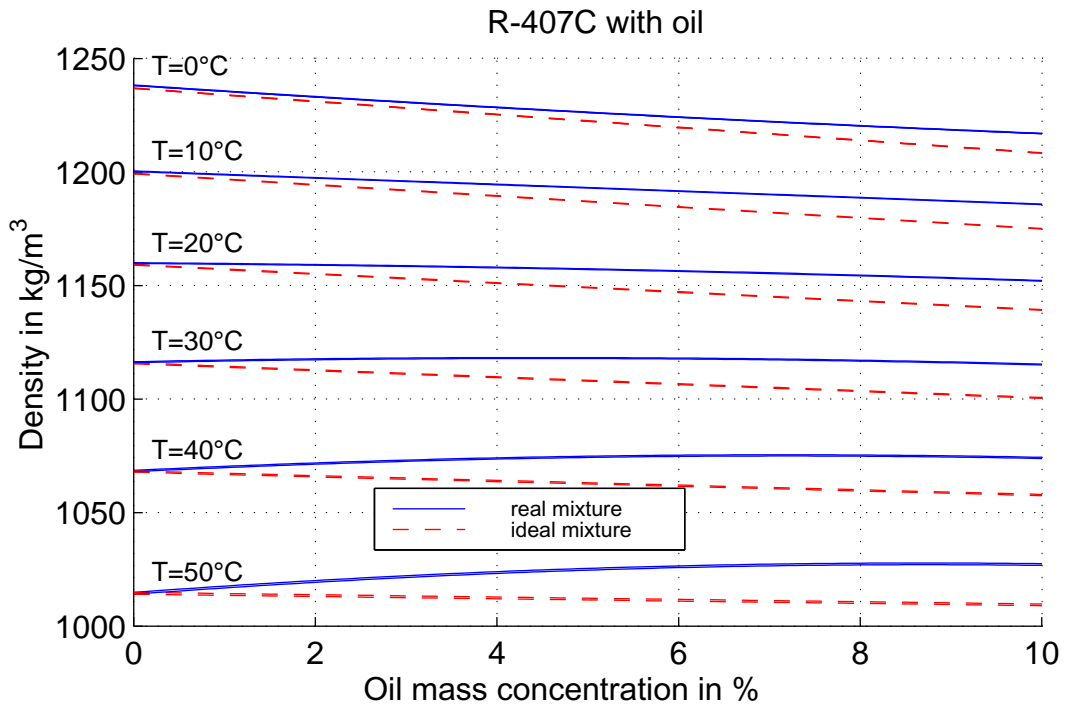


Figure 3.31: Mixture density of R-407C/EAL Arctic 22 CC mixture. Solid lines: extrapolated trends from measured density. Dashed lines: ideal mixture density.

Viscosity

Mixture viscosity, is a subject which has resulted in a series of proposed mixing laws. The thesis work of [Arnemann, 1993] includes 24 approaches to calculate the bulk viscosity of a refrigerant-oil mixture! In the work of [Thome et al., 1996], the use of the logarithmic law by Arrhenius is proposed, and was finally adopted in the simulation model.

With local oil mass concentration w_{local} , and by an appropriate choice of the empirical exponent m , the final form of the viscosity mixing law, proposed by [Thome et al., 1996] is given with:

$$\mu_m = \mu_{refr} \left[\frac{\mu_{oil}}{\mu_{refr}} \right]^{m w_{local}} \quad (3.90)$$

with $m = 0.26$ and $w_{local} = \frac{w_{in}}{(1 - \chi)}$

During the evaporation of the refrigerant-oil mixture, the local oil mass concentration is gradually increasing, until converging to the value of unity.

Liquid specific heat

The specific heat of mixture is calculated directly by the mass fractions

$$c_{liq,refr-oil} = w_{local} c_{oil} + (1 - w_{local}) c_{refr} \quad (3.91)$$

3.2.8.3 Saturation temperature or solubility of refrigerant-oil mixtures

A brief literature review of works who handle refrigerant-oil properties and equilibrium conditions is proposed at the beginning of this section. In absence of an extensive knowledge about the specific composition of the used oil, the calculation of the mixing saturation temperature is performed according to the approach proposed by Takaishi and Ogushi (1987) for the mixture R-22 with benzene oil. The correlation has later been generalized by [Thome, 1995] to be used for any refrigerant-oil combination.

$$T_{sat} = \frac{A}{\ln P_{sat} - B} \quad \text{T in K and P in MPa} \quad (3.92)$$

with $A = a_0 + a_1 w_{oil} + a_2 w_{oil}^3 + a_3 w_{oil}^5 + a_4 w_{oil}^7$
 $B = b_0 + b_1 w_{oil} + b_2 w_{oil}^3 + b_3 w_{oil}^5 + b_4 w_{oil}^7$

The coefficients $a_1 - a_4$ and $b_1 - b_4$ depend on the specific refrigerant-oil mixture, but for low local oil concentrations the induced errors become very low and major deviations may occur on a

concentrated range at high local oil concentrations. The default values are:

$$a_1 = 182.52 \quad a_2 = -724.21 \quad a_3 = 3868 \quad a_4 = -5268.9$$

$$b_1 = -0.7221 \quad b_2 = 2.3914 \quad b_3 = -13.78 \quad b_4 = 17.066$$

The coefficients a_0 and b_0 of the equation 3.92 can be evaluated by least square regression, applying the equation to the known bubble line.

Using this correlation, the (equilibrium) bubble point temperature of R-407C with the synthetic POE EAL Arctic 22 CC oil at typical evaporation conditions, has been calculated for several inlet oil mass concentrations (see Fig. 3.32).

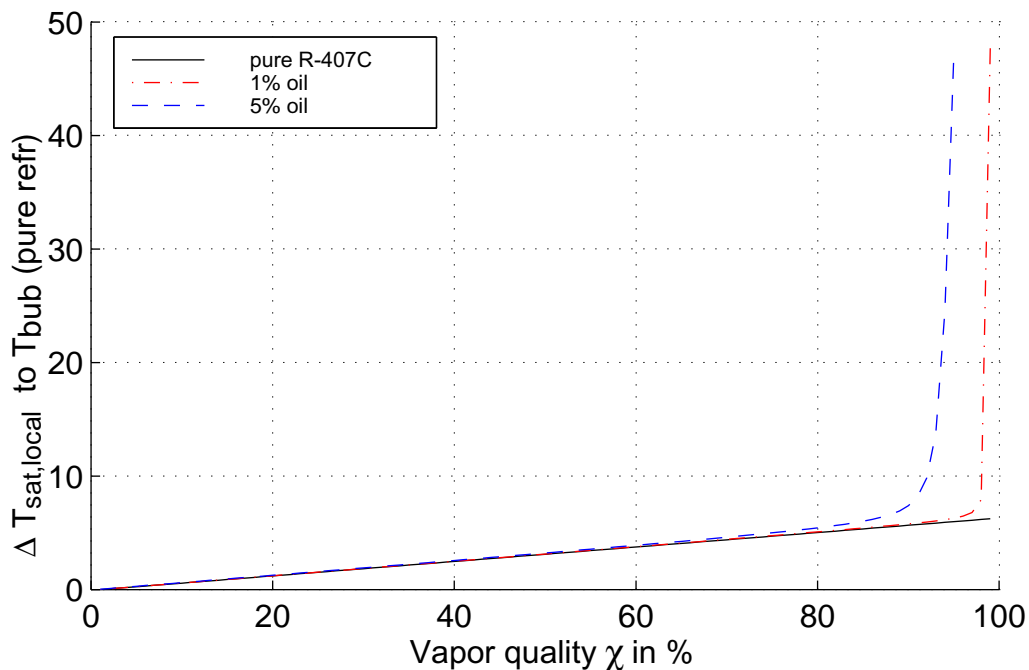


Figure 3.32: Calculated evolution of the saturation temperature of the mixture R-407C with POE EAL Arctic 22 CC oil.

The saturation temperature of the mixture is practically equal for the major part of the evaporation path, but highly deviates at higher vapor qualities. This results in a reduced temperature difference between the refrigerant-oil mixture to the external flow. At the low oil concentrations of <1%, this influence on the heat transfer has a negligible impact.

The evolution of the equilibrium temperature curve for the refrigerant-oil mixtures lets inversely conclude to the liquid composition (or the solubility) of the used mixture. As an example of calculation, the R-407C/oil equilibrium at 4 bar evaporation pressure and 10 K superheating, the liquid is composed of 74% of oil (by mass). This is estimated to be approximately the composition of the liquid in the lower stage compressor during heating mode.

Due to saturation pressures, which are 10^{-5} times lower for the oil, according to the formulation of *Raoult's Law*, which is **valid for an ideal mixture** vapor liquid equilibrium, the quantity of oil in the vapor phase can be neglected and will be supposed to be zero.

Raoult's Law

$$P_i = \varphi_{vap,i} P_{tot} = \varphi_{liq,i} P_{sat,i}(T) \quad (3.93)$$

3.2.8.4 Enthalpy of vaporization

As the oil remains entirely in the liquid phase, the enthalpy change during evaporation is composed of the latent heat of vaporization of the refrigerant and of the sensible heat of the liquid phase, which is composed of the refrigerant and the oil and of the coexisting refrigerant vapor. Both, refrigerant liquid and vapor composition are assumed at bulk composition, which is an approximating assumption:

$$dh = \Delta h_{lat} + (1 - \chi) dT_{bub} c_{liq,refr-oil} + dT_{bub} c_{p,vap} \quad (3.94)$$

As the enthalpy change vary with the oil concentration, modified plots of the *Mollier* diagram (logP-h diagram), have been presented by different authors [Hughes et al., 1983; Youbi-Idrissi et al., 2003], showing the distortion of the isothermal lines.

In a classical mechanically controlled heat pump operation, the superheat at the compressor inlet is generally set to a differential value between the evaporator inlet saturation temperature and the compressor inlet temperature. Figure 3.32 shows, that with increased inlet oil concentration, the exit vapor quality at equal superheat is reduced and has thus a reducing impact on the enthalpy change and the exchanged heat rate.

3.2.8.5 Modified heat transfer coefficient

A short review of the estimated impacts of oil onto the heat transfer mechanisms during the evaporation of refrigerant-oil mixtures has been effectuated at the beginning of this section and the cited experimental results show the high degradation effects of very small oil concentrations in microfin tubes. These high impacts could not be effectively integrated into the existing heat transfer models and need further investigations and basic work. The here proposed approach to take into account oil effects on the evaporation flop map and the heat transfer model, uses a modified bulk viscosity (eq. 3.90), as is suggested by [Thome et al., 1996].

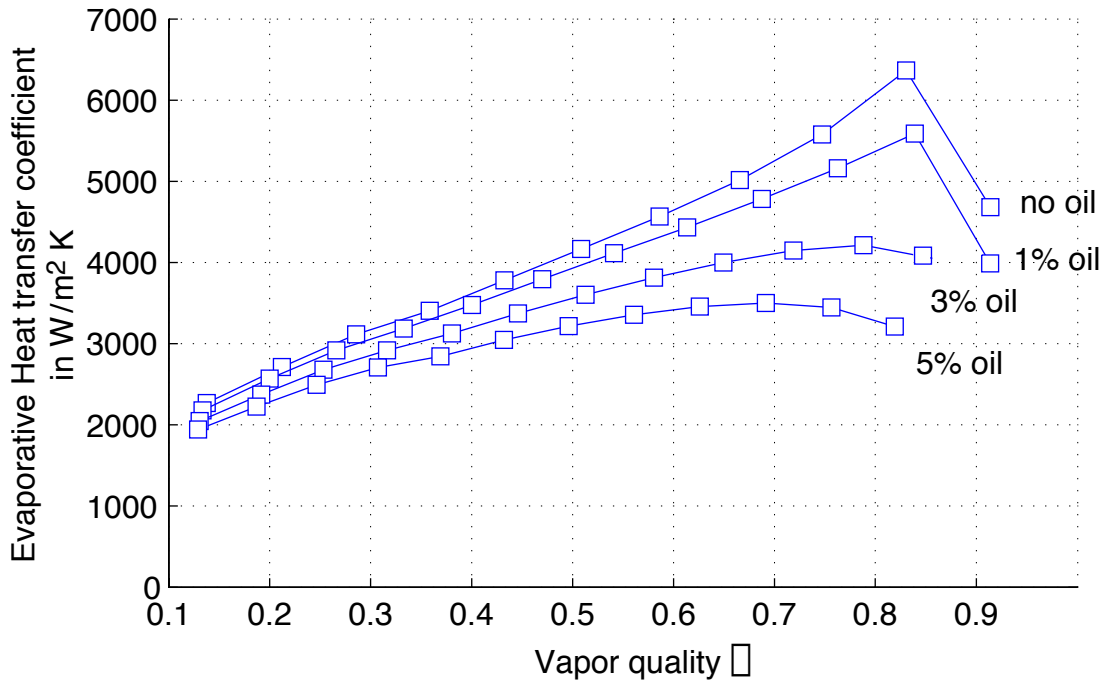


Figure 3.33: Impact of variable inlet oil mass concentration on evaporative heat transfer coefficient, applied to microfin tube heat exchanger and with R-407C and POE EAL Arctic 22 CC oil. $T_{bub} = -10^{\circ}\text{C}$, $G = 50$.

By variation of the inlet oil mass concentration between 0% to 5%, the calculated mean value of the overall heat transfer coefficient is reduced by 4% at the highest oil concentration. Considering the evaporative heat transfer coefficient (which is represented in Figure 3.33) the oil impact is apparent and reduces the mean value by 10% per 1% of added oil. The simulation model is only considering the physical impact and the consequences on the flow map. Annular flow is forced until dry-out, because microfin tubes are implemented in the heat exchangers. The real impact is estimated to be higher, using microfin tubes, see text above.

As the measured oil concentration is very low, its impact on the heat transfer is neglected, allowing highly reduced calculation time to compute the comparative cycle evaluation.

3.3 Expansion devices

Capillary tubes

The simulation model of expansion flow in capillary tubes is generally the last component to implement in a heat pump cycle simulation code, but in the present case the capillary expansion model will be used as well as for the expansion of the intermediate injection flow and also for the calculation of the injection mass flow into the compressor through the injection port.

With the proposed calculation scheme pressure drop and temperature evolution are modeled for capillary tubes and the resulting mass flow rate is determined. The literature review shows the different types of models proposed, starting with the basic *homogeneous, adiabatic one dimensional two-phase flow* model proposed by [Goldstein, 1981; Stoecker and Jones, 1982]. This basic model, was extended for entrance and subcooled region, to refrigerant mixtures and taking into account oil miscibility and metastable subcooling zone [Jung et al., 1999; Wongwises and Pirompak, 2001; García-Valladares et al., 2002b,a; Fukuta et al., 2003]. Other model extensions treat non-adiabatic flow [Xu and Bansal, 2002; Sinpi boon and Wongwises, 2002] or consider a non-homogeneous approach for the flow modeling [Fischer, 1995; Liang and Wong, 2001].

The friction models presented in the literature have to be considered separately for liquid flow and for two-phase flow. In the **liquid flow** the most generally applicable friction model is given by the *Blasius relationship* for laminar and by the *Colebrook equation* (solution found by iteration, but including pipe roughness) for turbulent flow.

In the **two-phase flow** regime the calculations depend on the flow model (homogeneous, separated flow or drift-flux).

3.3.1 Basic equations

- **Mass conservation (continuity)**

For steady state the continuity equation is written as

$$\dot{M} = \rho u S = cst \quad (3.95)$$

for the further mathematical formulations, the *mass velocity* is used as:

$$G = \frac{\dot{M}}{S} = \rho u \quad (3.96)$$

Within the capillary tube the cross-sectional area is constant. For *subcooled liquid* the density change is negligible and therefore the flow speed is constant.

- **Energy and momentum equation**

For *horizontal* fluid flow the equation 3.1 is reduced to:

$$d\left(\frac{u^2}{2}\right) + \delta r = -v dP = -dh + \delta q^+ + \delta r = -dh + T ds \quad (3.97)$$

By integration of the first and third part of the equation the **energy conservation in adiabatic flow** can be written in the form

$$h + \frac{u^2}{2} = cst \quad (3.98)$$

The **momentum** equation is resulting from the first and second part of equation 3.97

$$v dP + d\left(\frac{u^2}{2}\right) = -\delta r = -f \frac{u^2}{2 D_h} dx \quad (3.99)$$

using the appropriate definition of the friction factor f applied to a hydraulic diameter $D_h = \frac{4S}{P}$.

3.3.2 The flow regions

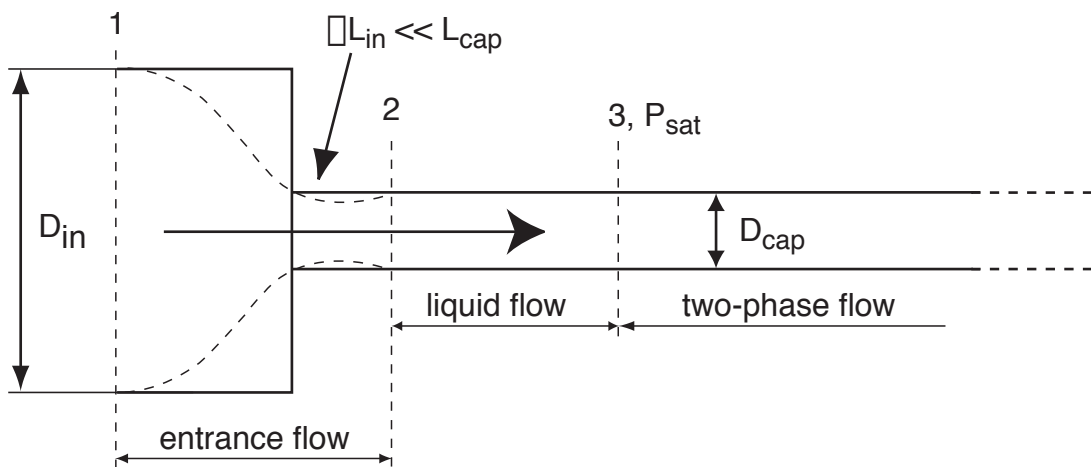


Figure 3.34: Geometrical setup and flow regions in a capillary tube.

3.3.2.1 Entrance region

At the entrance of the capillary tube the flow passes a singular area contraction. A single phase liquid flow (or a homogeneous two-phase flow at low vapor quality) in turbulent flow conditions is assumed. The momentum equation 3.99 is expressed for the singular pressure drop formulation (adapted from [Collier and Thome, 1994]), with the mass velocity G with the capillary tube section. This expression will be adapted in a first approximation also to the two-phase region with higher inlet vapor quality, admitting a mean value for the density.

$$\Delta P_{in} = k \rho \frac{u^2}{2} = k \frac{G^2}{2 \rho} \quad (3.100)$$

with $k = f(S_1/S_2) = (1/0.586 - 1)^2 (1 - S_1/S_2)$

3.3.2.2 Liquid phase region

For subcooled liquid flow conditions at the inlet of the expansion device the fluid is incompressible. At constant section, the variation of flow speed is very small and can be neglected.

The pressure drop, calculated with the momentum equation, takes the form:

$$\frac{dP}{dx} = -f \frac{\rho_{liq} u^2}{2 D_h} \quad (3.101)$$

In **adiabatic flow** the local enthalpy is constant and the length $L_{liq,phase}$ is given by the difference of the inlet pressure P_2 and the saturation pressure P_{sat,T_2} of the entrant liquid:

$$L_{liq,phase} = (P_2 - P_{sat,T_3}) \frac{2 D_h}{f \rho_{liq} u^2} = (P_2 - P_{sat,T_3}) \frac{2 \rho_{liq} D_h}{f G^2} \quad (3.102)$$

with P_{sat,T_3} = bubble point saturation pressure at $T_3 = T_2$
 f friction factor, using the *Colebrook* equation.

The expression 3.102 above, which is formulated for adiabatic flow, can be adapted for **non-adiabatic conditions**, by calculating the temperature change between the inlet (point 2) and the exit of the liquid flow region, using the following relations.

$$d\dot{Q}(\ell) = \dot{M} \delta q = k \Delta T_{ln} dA \quad (3.103)$$

the energy balance for the liquid flow is

$$\delta q = dh = c_p dT \quad (3.104)$$

and referring to the tube diameter of the capillary, the local temperature change is found as

$$dT = \frac{4k\Delta T_{ln,\ell} d\ell}{GD_{int} c_p} \quad (3.105)$$

By integration of the equation 3.105, over the adiabatic length (eq. 3.102), the new outlet temperature T_3 is found by iteration. The new liquid length is then evaluated with the modified saturation pressure P_{sat,T_3} .

In all of the considered situations, heat transfer is neglected in the liquid flow region of the capillary tube, and therefore, no detailed heat transfer calculation is presented.

Two-phase region

The homogeneous approach of calculating the two-phase flow, consists of calculating the thermodynamic properties of the bulk by mixing the properties of the corresponding saturated liquid and vapor phase.

For a given quality χ , these bulk properties are calculated with the following set of equations:

$$h = h_{liq} + \chi (h_{vap} - h_{liq}) = h_{liq} + \chi h_{lat} \quad (3.106)$$

$$v = v_{liq} + \chi (v_{vap} - v_{liq}) = v_{liq} + \chi v_{v-l} \quad (3.107)$$

$$s = s_{liq} + \chi (s_{vap} - s_{liq}) = s_{liq} + \chi s_{v-l} \quad (3.108)$$

With the explicit form of the mixture properties and the integrated form of energy balance for **adiabatic flow** between the inlet point of the two-phase region in,tp and the position ℓ , the equation takes the form:

$$h_{in,tp} + \frac{G^2 v_{in,tp}^2}{2} = h_{liq} + h_{lat} \chi(\ell) + \frac{G^2}{2} (v_{liq} + \chi(\ell) v_{v-l})^2 \quad (3.109)$$

This is a quadratic equation to evaluate the quality χ at each point of the tube (with the correspond-

ing saturation pressure), and the solution is

$$\chi(\ell(P)) = -\frac{v_{liq}}{v_{v-l}} - \frac{h_{lat}}{G^2 v_{v-l}^2} + \frac{\sqrt{(G^2 v_{liq} v_{v-l} + h_{lat})^2 - G^2 v_{v-l}^2 \left[G^2 (v_{liq}^2 - v_{in,tp}^2) + 2(h_{liq} - h_{in,tp}) \right]}}{G^2 v_{v-l}^2} \quad (3.110)$$

For **non-adiabatic flow** the equation 3.110 can be formulated in a finite difference form (point $i \rightarrow i+1$):

$$\chi_{n+1} = -\frac{v_{liq}}{v_{v-l}} - \frac{h_{lat}}{G^2 v_{v-l}^2} + \frac{\sqrt{(G^2 v_{liq} v_{v-l} + h_{lat})^2 - G^2 v_{v-l}^2 \left[G^2 (v_{liq}^2 - v_i^2) + 2(h_{liq} - h_i) - G^2 \int_i^{i+1} \delta q \right]}}{G^2 v_{v-l}^2} \quad (3.111)$$

The conservation of momentum is expressed for the two-phase region by

$$dL = -\frac{2 D_h}{G^2 v^2 f} \left[v dP + d \left(\frac{u^2}{2} \right) \right] \quad (3.112)$$

with $d \left(\frac{u^2}{2} \right) = d \left(\frac{G^2 v^2}{2} \right) = G^2 v dv$, equation 3.112 can be written in the alternative form, using the thermodynamic properties of the bulk flow:

$$dL = -\frac{2 D_h}{f} \left[\frac{dP}{v G^2} + \frac{1}{v} dv \right] \quad (3.113)$$

The friction factor of the homogeneous two-phase flow is calculated by the *Colebrook* formula.

Vapor Phase Region

Vapor phase flow in a capillary tube may occur in the intermediate injection admission line of such types of compressors. The flow model is based on a compressible adiabatic flow, using the conservation equations of continuity (eq. 3.95), energy (eq. 3.98) and momentum (eq. 3.99). In saturated flow, the density and the enthalpy are expressed, both, by the quality and the local pressure, which allows a direct evaluation of the final state, using the energy conservation. In vapor flow, the final state is found iteratively, and is located between the isenthalpic and isochoric expansion for adiabatic flow.

3.3.3 Friction factor

The friction factor model for single phase and homogeneous two-phase flow is proposed for turbulent flow by *Colebrook*

$$\frac{1}{\sqrt{f_{turb}}} = 1.14 - \log \left[\frac{e}{D_h} + \frac{9.34}{Re \sqrt{f_{turb}}} \right] \quad (3.114)$$

with Reynolds number: $Re = \frac{\rho u D_h}{\mu} = \frac{G D_h}{\mu}$

e : Surface rugosity of the tube

D_h : Internal capillary tube diameter

The above equation is given for turbulent flow ($Re > 3500$) but will also be calculated for the transition zone between the laminar and turbulent zone. In case the flow in the capillary tube is laminar ($Re < 2300$) the friction factor takes the simple form:

$$f_{lam} = \frac{64}{Re} \quad (3.115)$$

Two-phase viscosity used for Reynolds number is provided by Refprop.

3.3.4 Resolution model

The purpose of this model is to calculate the **massflow** passing through an existing capillary tube (given length) at given thermodynamic conditions at the entrance (and considering the outlet pressure).

Input variables: Inlet P and h (or T) of the refrigerant (pure fluid or mixture), capillary tube diameter D and length L .

Calculation procedure:

1. Calculate the pressure drop at the tube entrance with equation 3.100.
2. If the fluid is in the subcooled region then calculate liquid length with equation 3.101.
3. If (liquid length < total length) and calculated pressure drop < external pressure difference, calculate two-phase flow. Divide the remaining tube length in segments with a nonlinear

distribution, as proposed by [Escanes et al., 1995].

$$\Delta L_i = \frac{L_{(2-ph)}}{\tanh(k)} \left[\tanh\left(k \frac{i}{n}\right) - \tanh\left(k \frac{(i-1)}{n}\right) \right] \quad (3.116)$$

with $L_{(2-ph)}$: resulting length of the tube for the two-phase flow regime.
 k : numeric concentration factor, e.g. $k = n/10$
 n : number of steps to be calculated.

For each step ΔL_i a one level iteration on the pressure drop allows to calculate the new quality $\chi_{(i+1)}$ and the new properties $h_{(i+1)}$, $v_{(i+1)}$ and $s_{(i+1)}$.

If the calculated entropy is not increasing the flow is choked (see Fanno curve) and the fluid is flowing at speed of sound.

Regulated expansion valve

The regulated expansion valves behave as a variable flow resistance and would only be of interest to be integrated into the simulation for non steady state conditions. The mass flow in a regulated expansion device (electronic expansion or mechanically controlled thermostatic expansion) is resulting from the control variable, which generally is the superheat at the inlet of a compressor.

3.3.5 Validation of the capillary tube model

The adiabatic and homogeneous model of [Stoecker and Jones, 1982] and the related data are mainly used as the academic reference to calculate the adiabatic expansion in a capillary tube. Stoecker presented its data for flow conditions reaching choked conditions at the exit of the tube. He used the Blasius friction model and R-22 as refrigerant. In the reference, the fluid viscosity model is also indicated, which is deviating from the data calculated by Refprop program. Figures 3.35 (a+b) compare the model results using the Stoecker's original model (with some of his tabulated data) with 2 adaptation steps: 1) Refprop viscosity model, and 2) Colebrook friction model. The last most general approach is used in the simulation program.

As the flow speed in the presented simulation case approaches the speed of sound, small deviations in the model have an important impact on the pressure drop calculations, as seen in the comparison of Figure 3.35.

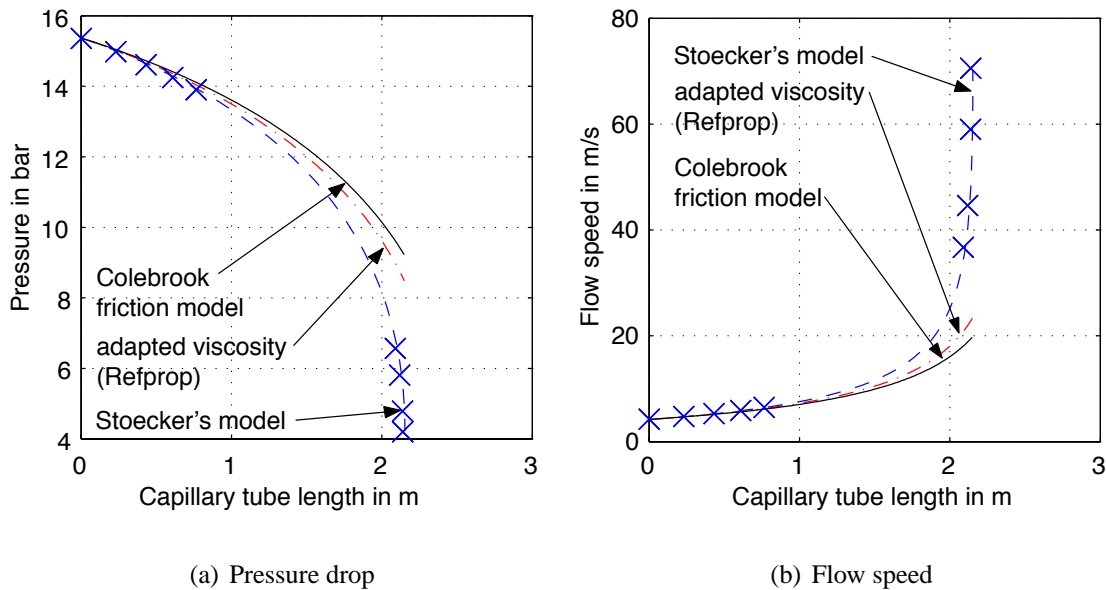


Figure 3.35: Capillary tube expansion model for R-22 at liquid saturated conditions at the tube inlet. Comparison of Stoecker's original model [Stoecker and Jones, 1982] with the implementations of the Refprop viscosity and the Colebrook friction model. Mass flow rate 10 g/s, Tube diameter 1.63 mm, tube length 2.1 m.

3.4 Conclusions to the simulation model

A generalized simulation model has been developed to predict the performances of different high performance heat pump cycles, which mainly have been presented in chapter 2 and which are adapted for high temperature lift applications (as found in high temperature residential heating systems). The model is mainly composed of a new developed compressor model, applied to a new generation of scroll compressors with intermediate injection ports. A flow map based heat transfer model for the main evaporator of the heat pump has been linked to the in house developed fluid calculation interface (FLINT), which includes Refprop, an accurate fluid properties calculation software. Oil effects and an air-side heat transfer model enable to calculate the performances of selected finned-tube air-refrigerant evaporator models and to compare with measured data. Generalized models for the plate heat exchangers and the tubular counter-current heat exchanger are also integrated to this model, as well as a general model for the expansion flow in a capillary tube, which is mainly applied to the injection flow path of the used compressors.

Compared to the experimental data, the compressor model predicts quite accurately the measured performances over the whole application range. The evaporation model, is composed of two complex heat transfer models, which cannot be validated separately with the collected data. The overall heat transfer coefficient is overpredicted with errors up to 100%. As the resistance to the heat trans-

fer is most important on the air side, the air side flow and heat transfer model should be analyzed in more detail. The refrigerant side modeling, is based on a complex, flow map based model including the two extensions to consider the zeotropic fluids and the presence of a small quantity of oil. The proposed model has been validated for horizontal evaporation in plain tubes and a correction is applied to take into account the enhancement effects of micro-fin tubes. This correction, however, reduces the model precision for calculating the evaporative heat transfer coefficient

The modeled components are formulated for steady-state operating conditions only and pressure drop in the heat exchangers and in the piping of the heat pump have not been integrated into this model description and could be added, if requested, for future works.

The linking of these elements to the complete heat pump cycle(s) and the simulation results, including a comparison of the different setups, are presented in the next chapter.

This completely extensible and generally applicable simulation model for enhanced heat pump cycles is programmed in the Matlab environment and can easily be used on different computer platforms. The graphical user interface of the Matlab environment is used to visualize the simulation results and the main characteristics of all the components and of the entire cycle are saved into specific data structures.

Bibliography

- T. Afjei. **Scrollverdichter mit Drehzahlvariation**. PhD thesis, Eidgenössische Technische Hochschule Zürich, Zurich, Switzerland, 1993. Thesis No. 10069.
- T. Afjei, P. Suter, and D. Favrat. **Experimental Analysis of an Inverter-Driven Scroll Compressor with Liquid Injection**. In *Proceedings of the International Compressor Engineering Conference at Purdue*, pages 541–550, 1992.
- M. Arnemann. **Methoden zur Bestimmung thermophysikalischer Eigenschaften von Öl-Kältemittel-Gemischen**. PhD thesis, Universität Hannover, 1993.
- ASHRAE. **ASHRAE Handbook 1998 Refrigeration**. ASHRAE, 1998.
- D. Biberg. **An Explicit Approximation for the Wetted Angle in Two-Phase Stratified Pipe Flow**. *The Canadian J. of Chemical Engineering*, 77:1221–1224, 1999.
- D. Bivens and A. Yokozeki. **Heat Transfer Coefficients and Transport Properties for Alternative Refrigerants**. In *Proceedings of the International Refrigeration Conference at Purdue*, pages 299–304, 1994.
- F. Bošnjaković and K. Knoche. **Technische Thermodynamik**. Darmstadt: Steinkopff, 1997.
- F. Brand, M. Zehnder, and D. Favrat. **Pompe à chaleur à haute température, Phase 1: Solution avec compresseur à injection vapeur**. Final report. Swiss Federal Office of Energy, 2000. ENET-Nr. 200090.
- J. Collier and J. Thome. **Convective Boiling and Condensation**. Oxford University Press, 3 edition, 1994.
- M. Conde. **Estimation of Thermophysical Properties of Lubricating Oils and their Solutions with Refrigerants: an Appraisal of existing Methods**. *Applied Thermal Engineering*, 16(1): 51–61, 1996.
- L. Creux. **Rotary Engine**. Technical report, United States Patent Office, 1905.
- D. Del Col, A. Cavallini, and J. Thome. **Condensation of Zeotropic Mixtures in Horizontal Tubes: New Simplified Heat Transfer Model Based on Flow Regimes**. *Journal of Heat Transfer*, page in review, 2004.

- J. El Hajal, J. Thome, and A. Cavallini. **Condensation in Horizontal Tubes, Part 1: Two-Phase Flow Pattern Map.** *Int. J. of Heat and Mass Transfer*, 46:3349–3363, 2003a.
- J. El Hajal, J. Thome, and A. Cavallini. **Condensation in Horizontal Tubes, Part 2: New Heat Transfer Model Based on Flow Regimes.** *Int. J. of Heat and Mass Transfer*, 46:3365–3387, 2003b.
- F. Escanes, C. Pérez-Segarra, and A. Oliva. **Numerical Simulation of Capillary-Tube Expansion Devices.** *Int. J. of Refrigeration*, 18(2):113–122, 1995.
- R. Fischer. **Calculation of the Discharge Characteristic of an Orifice for Gas-Liquid Annular-Mist Flow.** *Int. J. of Multiphase Flow*, 21(5):817–835, 1995.
- M. Fukuta, T. Yanagisawa, T. Arai, and O. Y. **Influences of Miscible and Immiscible Oils on Flow Characteristics through Capillary Tube- Part I: Experimental Study.** *Int. J. of Refrigeration*, 26:823–829, 2003.
- O. García-Valladares, C. Pérez-Segarra, and A. Oliva. **Numerical Simulation of Capillary-Tube Expansion Devices Behaviour with Pure and Mixed Refrigerants Considering Metastable Region. Part I: Experimental Validation and Parametric Studies.** *Applied Thermal Engineering*, 22:379–391, 2002a.
- O. García-Valladares, C. Pérez-Segarra, and A. Oliva. **Numerical Simulation of Capillary-Tube Expansion Devices Behaviour with Pure and Mixed Refrigerants Considering Metastable Region. Part I: Mathematical Formulation and Numerical Model.** *Applied Thermal Engineering*, 22:173–182, 2002b.
- S. Goldstein. **A Computer Simulation Method for describing Two-Phase Flashing Flow in Small Diameter Tubes.** *ASHRAE Transactions*, 2(87):51–60, 1981.
- M. Guoyuan, C. Qinhu, and J. Yi. **Experimental Investigation of Air-Source Heat Pump for Cold Regions.** *Int. J. of Refrigeration*, pages 12–18, 2003.
- M. Hayano, H. Sakata, S. Nagatomo, and H. Murasaki. **An Analysis of Losses in Scroll Compressor.** In *Proceedings of the International Compressor Engineering Conference at Purdue*, pages 189–197, 1988.
- D. Hughes, J. McMullan, and R. Morgan. **Influence of Lubricating Oil on Heat Pump Performance.** Technical report, New University of Ulster, N. Ireland, 1983.
- F. Incropera and D. DeWitt. **Fundamentals of Heat and Mass Transfer.** John Wiley&Sons, 4th edition, 1996.
- D. Jung, C. Park, and B. Park. **Capillary tube selection for HCFC22 Alternatives.** *Int. J. of Refrigeration*, 22:604–614, 1999.

- N. Kattan. **Contribution to the Heat Transfer Analysis of Substitute Refrigerants in Evaporator Tubes with Smooth or Enhanced Tube Surfaces.** PhD thesis, École Polytechnique Fédérale de Lausanne, Lausanne, Switzerland, 1996. Thesis No. 1498.
- N. Kattan, J. Thome, and D. Favrat. **Flow Boiling in Horizontal Tubes: Part 1-Development of a Diabatic Two-phase Flow Pattern Map.** *Transactions of the ASME*, 120:140–147, 1998a.
- N. Kattan, J. Thome, and D. Favrat. **Flow Boiling in Horizontal Tubes: Part 2-New Heat Transfer Data for Five Refrigerants.** *Transactions of the ASME*, 120:148–155, 1998b.
- C. Le Pellec. **Etude expérimentale et modélisation d'échangeurs à plaques frigorigène-caloporteur.** PhD thesis, Ecole des Mines de Paris, Paris, France, 1997.
- E. Lemmon, M. McLinden, and M. Huber. **NIST Reference Fluid Thermodynamic and Transport Properties - REFPROP, Version 7.0.** National Institute of Standards and Technology, 2002.
- S. Liang and T. Wong. **Numerical Modeling of Two-Phase Refrigerant Flow through Adiabatic Capillary Tubes.** *Applied Thermal Engineering*, 21:1035–1048, 2001.
- O. Lottin, P. Guillemet, and J.-M. Lebreton. **Effects of Synthetic Oil in a Compression Refrigeration System using R410A. Part II: Quality of Heat Transfer and Pressure Losses within the Heat Exchangers.** *Int. J. of Refrigeration*, 26:in press, 2003.
- H. Martin. **A Theoretical Approach to Predict the Performances of Chevron-Type Plate Heat Exchangers.** *Chem. Eng. and Processing*, 35:301–310, 1996.
- W. Martz, C. Burton, and A. Jacobi. **Local Composition of the Thermodynamic Properties of Refrigerant and Oil Mixtures.** *Int. J. of Refrigeration*, 19(1):25–33, 1996.
- Y. Mermond, M. Feidt, and C. Marvillet. **Propriétés thermodynamiques et physiques des mélanges de fluides frigorigènes et d'huiles.** *Int. J. of Refrigeration*, 22:569–579, 1999.
- T. Mizuno, N. Hagita, K. Nagata, and A. Amata. **Scroll Compressor and Scroll-Type Refrigerator.** Technical report, United States Patent Office, Hitachi, Ltd., Tokyo (Japan), 1992. US-5,103,652.
- M. Perevozchikov. **Scroll Compressor with Vapor Injection.** Technical report, United States Patent Office, Copeland Corporation, Sidney, Ohio (USA), 2003. US-6,619,936 B2.
- R. Perry and D. Green. **Perry's Chemical Engineer's Handbook.** Mc Graw Hill, 7 edition, 1997.
- W. Prenger and S. Seibel. **Compressor with Liquid Injection.** Technical report, United States Patent Office, Copeland Corporation, Sidney, Ohio (USA), 1991. US-5,076,067.

- J. Sauls. **Performance Characteristics of Fixed Volume Ratio Compressors.** In *Proceedings of the International Compressor Engineering Conference at Purdue*, pages 201–207, 1982.
- B. Shen and E. Groll. **A Critical Review of the Influence of Lubricants on the Boiling of Refrigerants.** In *21th Int. Congress of Refrigeration, IIR/IIF, Washington, D.C.*, page ICR0032. Int. Institute of Refrigeration, 2003.
- J. Sinpiboon and S. Wongwises. **Numerical Investigation of Refrigerant Flow through Non-Adiabatic Capillary Tubes.** *Applied Thermal Engineering*, 2002.
- P. Skripov, A. Starostin, D. Volosnikov, and V. Zhelezny. **Comparison of Thermophysical Properties for Oil/Refrigerant Mixtures by use of the Pulse Heating Method.** *Int. J. of Refrigeration*, 26:721–728, 2003.
- W. Stoecker and J. Jones. **Refrigeration and Air-Conditioning.** McGraw-Hill Book Company, 2nd edition, 1982.
- J. Thome. **Enhanced Boiling of Mixtures.** *Chem. Eng. Science*, 42(8):1909–1917, 1987.
- J. Thome. **Thermodynamic and Transport Properties of Refrigerant and Lubricating Oil Mixtures.** Technical report, Swiss Federal Office of Energy, 1993.
- J. Thome. **Comprehensive Thermodynamic Approach to Modeling Refrigerant-Lubricating Oil Mixtures.** *ASHRAE HVAC&Research*, 1(2):110–126, 1995.
- J. Thome and J. El Hajal. **Two-Phase Flow Pattern Map for Evaporation in Horizontal Tubes: Latest Version.** In *1st Int. Conference on Heat Transfer, Fluid Mechanics and Thermodynamics*, page TJ2, 8-10 April, Kruger Park, South Africa 2002.
- J. Thome, D. Favrat, O. Zürcher, and E. Nidegger. **Heat Transfer and Pressure Drop in the Dryout Region of Intube Evaporation with Refrigerant/Lubricant Mixtures.** Technical report, École Polytechnique Fédérale de Lausanne, ASHRAE Project 800-RP, 1996.
- VDI. **VDI Heat Atlas.** Verein deutscher Ingenieure, VDI-Verlag GmbH, 1993.
- E. Wilson. **A Basis for Rational Design of Heat Transfer Apparatus.** *Transactions of the ASME*, 37:47–70, 1915.
- E. Winandy and J. Lebrun. **Scroll Compressors using Gas and Liquid Injection: Experimental Analysis and Modelling.** *Int. J. of Refrigeration*, pages 1143–1156, 2002.
- E. Winandy, C. Saavedra, and J. Lebrun. **Experimental Analysis and Simplified Modelling of a Hermetic Scroll Refrigeration Compressor.** *Applied Thermal Engineering*, 22:107–120, 2002.

- S. Wongwises and W. Pirompak. **Flow Characteristics of Pure Refrigerants and Refrigerant Mixtures in Adiabatic Capillary Tubes.** *Applied Thermal Engineering*, 21:845–861, 2001.
- R. Würfel and N. Ostrowski. **Experimental Investigations of Heat Transfer and Pressure Drop during the Condensation Process within Plate Heat Exchangers of the Herringbone-Type.** *Int. J. of Thermal Sciences*, in press, 2004.
- B. Xu and P. Bansal. **Non-Adiabatic Capillary Tube Flow: A Homogeneous Model and Process Description.** *Applied Thermal Engineering*, 22:1801–1819, 2002.
- Y. Yan and T. Lin. **Evaporation Heat Transfer and Pressure Drop of Refrigerant R-134a in a Plate Heat Exchanger.** *Transactions of the ASME*, 121:118–127, 1999.
- Y. Yan, H. Lio, and T. Lin. **Condensation Heat Transfer and Pressure Drop of Refrigerant R-134a in a Plate Heat Exchanger.** *Int. J. of Heat and Mass Transfer*, 42:993–1006, 1999.
- M. Youbi-Idrissi, J. Bonjour, C. Marvillet, and F. Meunier. **Impact of Refrigerant-Oil Solubility on an Evaporator Performances working with R-407C.** *Int. J. of Refrigeration*, pages 284–292, 2003.
- M. Zehnder and D. Favrat. **Analyse de la migration d’huile dans les pompes à chaleur mono- et bi-étagées.** Final report. Swiss Federal Office of Energy, 2003. ENET-Nr. 230161.
- M. Zehnder, D. Favrat, H. Hohl, C. Olivier, and M. Perevozchikov. **High Performance air-Water Heat Pump with Extended Application Range for Residential Heating.** In *7th Heat Pump Conference, Beijing*. Int. Energy Agency, 2002a.
- M. Zehnder, F. Maréchal, S. Guex, J. Schiffmann, and D. Favrat. **Pompe à chaleur air-eau à haute température, Phase 2: Cycle à injection optimisé, essais journaliers et compresseur booster; Analyse thermo-économique.** Final report. Swiss Federal Office of Energy, 2002b. ENET-Nr. 220219.
- P. Zhelezny, V. Zhelezny, and V. Skripov. **Determination of the Pseudocritical Parameters for Refrigerant/Oil Solutions.** *Fluid Phase Equilibria*, 212:285–302, 2003.
- O. Zürcher. **Contribution to the Heat Transfer Analysis of Natural and Substitute Refrigerants Evaporated in a Smooth Horizontal Tube.** PhD thesis, École Polytechnique Fédérale de Lausanne, Lausanne, Switzerland, 2000.
- O. Zürcher, D. Favrat, and J. Thome. **Development of a Diabatic Two-Phase Flow Pattern Map for Horizontal Flow Boiling.** *Int. J. of Heat and Mass Transfer*, 45:291–301, 2002a.
- O. Zürcher, D. Favrat, and J. Thome. **Evaporation of Refrigerants in a Horizontal Tube: An Improved Flow Pattern Dependent Heat Transfer Model Compared to Ammonia Data.** *Int. J. of Heat and Mass Transfer*, 45:303–317, 2002b.

4. Heat pump cycle simulation results

The purpose of this chapter is to present the specific external operating conditions of the so called retrofit application in residential heating systems. On this basis the presented high performance heat pump cycle approaches are evaluated to consider their application limits and to compare the calculated performances for optimized configurations. The simulation will specifically consider the system parameters for a selection of nine refrigerants, which are considered to be the most adapted for the aimed application. Then the features and an optimization of the new type scroll compressor with intermediate injection port are analyzed in detail. The compressors of the two-stage compression cycles are dimensioned and system performances are compared to the one-stage compression cycle. Finally the concept of a combined cycle with auxiliary cycle for liquid subcooling is implemented for higher temperature glides on the heating water side.

4.1 External conditions

In order to perform a comparison of the performance of the proposed improved heat pump cycles, it is necessary to define the considered study case.

Following assumptions are made:

1. Hydronic heating system, through radiators.
2. Air as external heat source.
3. Constant mass flow rate in the heat distribution with maximum 10 K temperature difference between condenser exit and inlet temperature of the heated water.

4.1.1 Climatic conditions

Daily mean temperature occurrences (since 1995) for an important number of cities worldwide are published at [University of Dayton, 1995-2004]. Figure 4.1 represent the climatic fingerprint of selected cities, which are well adapted for the use of heating only heat pumps. Heating days represent the sum of all days with a mean temperature below the **heating limit**, which is selected at

15°C. The climates can be characterized by the **degree-days (DD)** number, which is the cumulation of the daily temperature difference between the **room temperature** (20°C) and the atmosphere.

The temperature frequency of the represented sites gives an important help for system and cost optimization of the heat pump heating system. For the case of Zurich, temperatures below -7°C occur very rarely and peak heat output can be completed by an additional (electric) heating supply. The minimum external temperature $T_{ext,min}$ is -12°C, which is setting the extreme operating point of the heat pump in permanent heating mode. While peak heat rate is occurring at the lowest external temperature, the integrated heat energy, corresponding to the external temperature distribution, is highest at medium temperatures (Fig. 4.2). In the selected example, about 50% of the electricity consumption correspond to the external temperatures between -1°C and 3°C. System optimization has therefore to be performed at these mean conditions, while an important heat rate is still required at very low external temperature.

4.1.2 Heat load and heat curve

The thermal heat losses of the building are function of the temperature difference between the room temperature T_{room} and the external ambient air temperature $T_{air,ext}$. Solar input is assumed to compensate the heat losses between the upper heating limit and the room temperature.

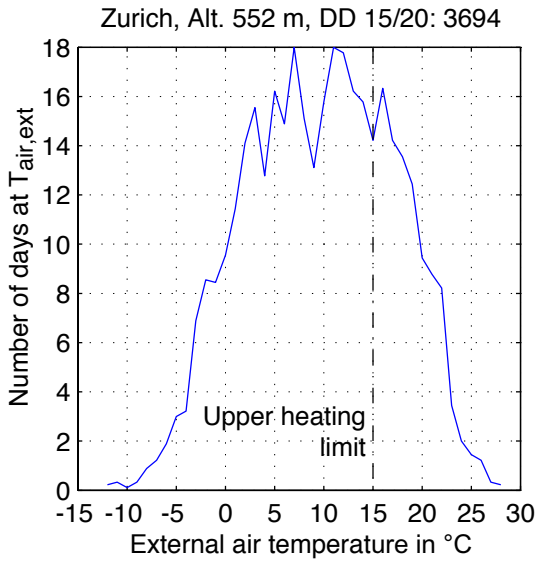
The **heat load** is chosen to be a linear function defined by

$$\dot{Q}_{heat} = \dot{Q}_{base} \frac{T_{heating,limit} - T_{air,ext}}{T_{heating,limit} - T_{air,min}} \quad (4.1)$$

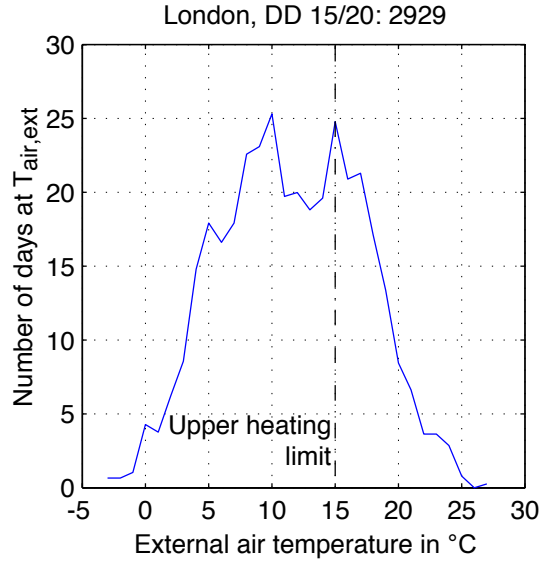
Using the definition of the heating degree-days number (DD), according to [SIA, 1982], the seasonal heating energy is calculated with

$$Q_{heat,season} = \frac{\dot{Q}_{base} 24 h}{T_{heating,limit} - T_{air,min}} DD_{15/20} \quad \text{in kWh} \quad (4.2)$$

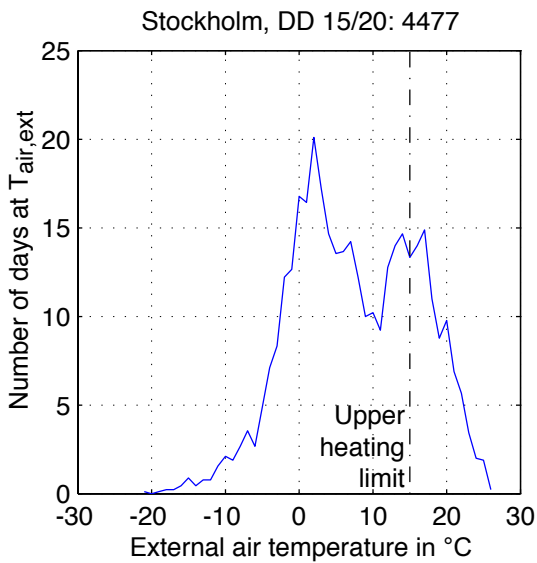
Note: The external heating limit has been adapted from the standard value of 12°C to 15°C, in order to consider the lower quality of the thermal insulation in existing buildings.



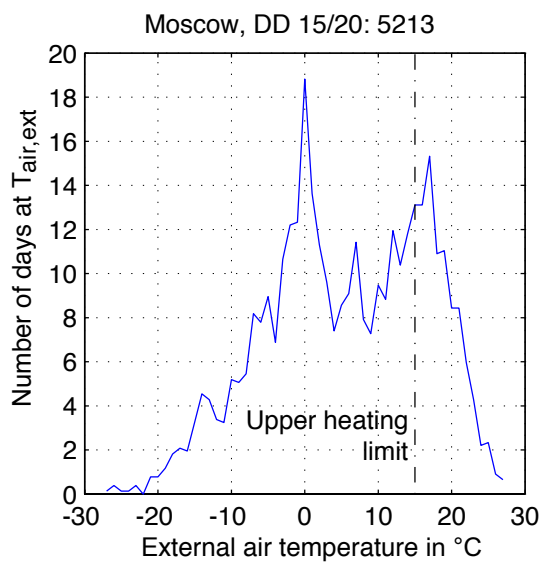
(a) Zurich, CH



(b) London, E



(c) Stockholm, SWE



(d) Moscow, Ru

Figure 4.1: Representation of the climatic temperature distribution for selected town, where heating only applications, e.g. heat pumps are well suited. Data from <http://www.engr.udayton.edu/weather/citylistWorld.htm>

The heat curve, is characterizing the required temperature by the heating system to the circulating heating water. The heat curve is defined with the following normalized equation (from [SIA, 1988]) applied to the nominal external temperature $T_{air,0}$ and nominal heating water output temperature $T_{w,out,0}$.

$$T_{w,out} = T_{room} + \frac{\Delta T_{w,0}}{2} \frac{T_{room} - T_{air,ext}}{T_{room} - T_{air,0}} + \left(\frac{2 T_{w,out,0} - \Delta T_{w,0}}{2} - T_{room} \right) \left[\frac{T_{room} - T_{air,ext}}{T_{room} - T_{air,0}} \right]^{1/m} \quad (4.3)$$

with temperatures in °C and the emission coefficient $m = 1.33$ for radiators.

The temperature lift, between the supply and the return line of the heat distribution system, is function of the volume flow rate of the water and the building's heat losses. A maximum temperature difference $\Delta T_{w,0} = 5$ K is assumed for the calculation. This temperature lift is directly proportional to the heat demand.

The temperature difference over the condenser of the heat pump is function of the heat rate delivered by the heat pump, which is minimum at the extreme operating conditions. Assuming a

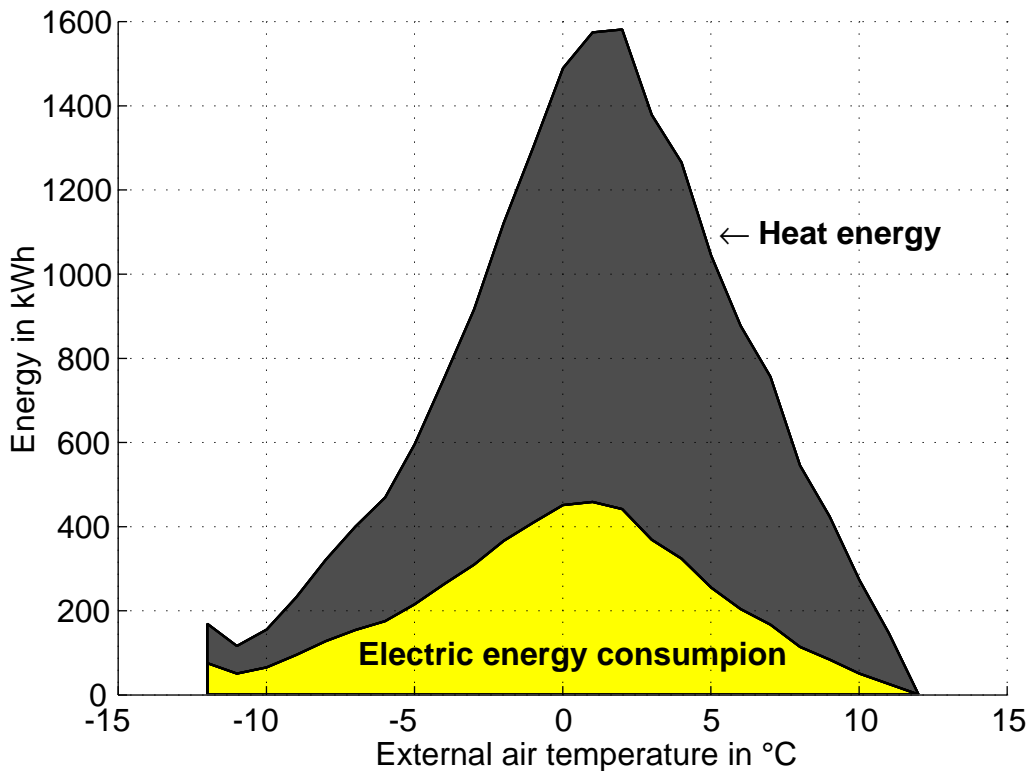


Figure 4.2: Seasonal distribution of the heat requirements and electricity consumption, using a heat pump, based on a selected daily mean temperature frequency, which corresponds to that of Zurich, CH.

constant mass flow rate of the heating water and a monovalent heating¹, the condenser exit temperature is higher than the required supply temperature of the heat network (see Fig. 4.3). Heat pumps with multi-stage heat output present a considerable advantage, to one level systems, as shows in the evolution of the condenser exit temperatures.

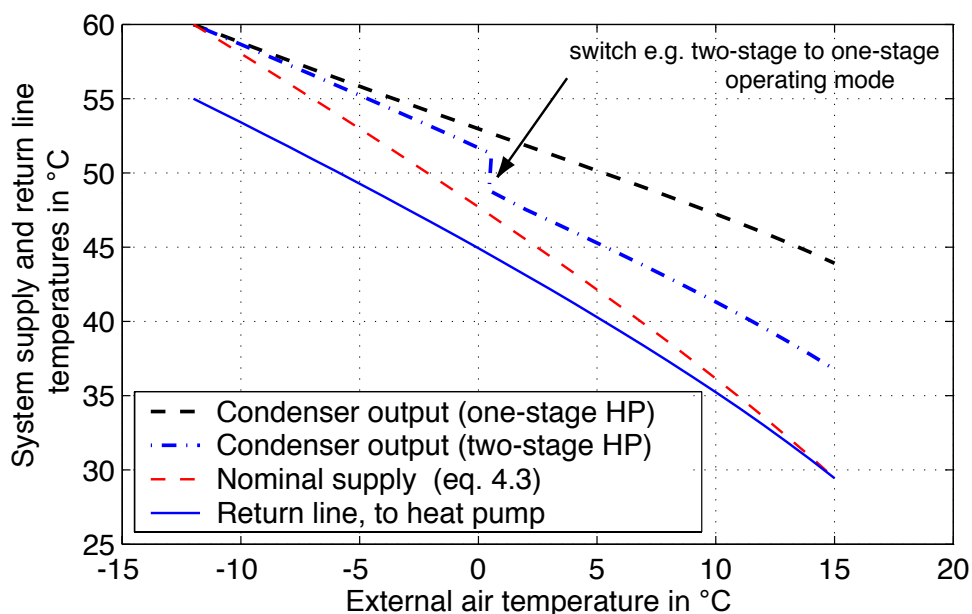


Figure 4.3: Definition heat curve. System temperatures and heat pump condenser inlet and exit conditions. Comparison one-stage heat pump with e.g. two-stage heat pump.

4.1.3 Frosting/Defrosting

On air-water heat pumps, defrosting is an important factor, which has to be considered for optimal system design. The energy required to defrost the evaporator during the heating mode penalizes considerably the system performances. According to [Bertsch and Ehrbar, 2002] the impact on the seasonal COP is about 2%. Tentatives of reduction of the frost formation with hydrophobic surface treatment of the evaporator fins, have shown limited success (see e.g. [Kulik et al., 2003]), but are an important issue for the future. An additional approach to the traditional defrosting modes is presented in section 2.3.3, referring to low exergy heat, used for defrosting the evaporator coil.

¹ Monovalent heating = The heat pump provides the totality of the annual heating demand and no complementary heating device is needed.

4.1.4 Hot Water Preparation and Integration

High temperature heat pump concepts are perfectly adapted to be used for combined tap water preparation (at temperatures between 50°C and 65°C), which can be provided in parallel to the heating mode or in alternating production mode. Furthermore, the use of air source heat pumps result in increased annual efficiency, due to the higher source temperatures in the summer.

4.1.5 Auxiliary power

Auxiliary power contributions are calculated for the ventilation of the air through the evaporator and the auxiliary tubing (the air channels in in-house installations) and for the pumping of the water through the condenser. This corresponds to standardized contributions¹, which are calculated as follows.

Fan power:

$$\dot{E}_{fan} = \dot{V}_{air} \frac{\Delta P_{air}}{0.3} \quad (4.4)$$

using for air side pressure drop $\Delta P_{air} = 50 \text{ Pa}$.

Pumping power:

$$\dot{E}_{pump} = \dot{V}_w \frac{\Delta P_w}{0.2} \quad (4.5)$$

using water pressure drop in the condenser of $\Delta P_w = 20 \text{ kPa}$.

The auxiliary power represents about 5% of the electric power consumed by the heat pump at nominal conditions. Constant values are admitted for the overall performance evaluations.

4.2 Cycle performances and system parameters

The theoretical evaluation for the selection of refrigerants applied to high temperature lift heat pumps in classical one-stage compression cycle (see section 1.3 on page 9), has sorted out the most promising pure fluids and refrigerant mixtures (among the commercially available or new mixtures), using a multi objective optimization tool. The flammability issue has been shown to be an important aspect. The restriction to non-flammable fluids, shows a status-quo of COP improvement, while the admission of flammable fluids leads to improved COP of 10% compared to the today employed refrigerants.

¹European standard EN-255, [SNV, 1997], defined for heat pump rating tests.

In this section, a selection of refrigerants is used to evaluate the performances, using an enhanced heat pump cycle simulation program, which has entirely been developed by the author, integrating all the efficiency improvement configurations of the superstructure (section 2.2, Fig. 2.4 on page 33).

4.2.1 The enhanced heat pump cycle simulation program.

A collection of available refrigeration and heat pump simulation tools is given at the *IEA Heat Pump Centre*¹. Most of the referenced tools apply to the **(industrial) refrigeration applications** and are design aids for refrigeration equipment suppliers (**FrigoSim**, **CoolTool**). The program **KmKreis**² is more specifically oriented on the refrigerant cycle calculation and all industrial one-stage and two-stage vapor compression cycles are proposed. However, specifically for heating heat pump, only the one-stage cycle is adopted in that reference. Refrigerant data are calculated through their own code proposing most of the available refrigerants, or through a Refprop interface, which can be integrated on demand. A second major class of applications are design and simulation tools applied to **ground coupled heat pumps**, and are extended to air-water heat pump applications. To our knowledge, cycle design is limited to one-stage heat pump cycles. An interesting application for **compact air-conditioning units**, is proposed in the DOE/ORNL Heat Pump Design Model (Mark VI Version), which is available on-line³. The **enhanced heat pump model** we propose here is intended to fill the gap of designing heat pumps with enhanced cycle configurations, which are:

- Classical one-stage configuration with optional suction line heat exchanger.
- Compression with intermediate injection and with economizer heat exchanger.
- Two stage compression cycle with economizer heat exchanger cycle.
- Single stage main cycle with additional subcooling cycle.

Thermodynamic properties are calculated through Refprop (latest version 7.0, [Lemmon et al., 2002]), with an in house developed fluid interface (called FLINT). This interface has been compiled as a Matlab MEX-function on Mac OS X, Linux and Windows environments. The interface provides thermodynamic and physical data from Refprop and allows as in the original application to define new fluids and blends with up to 20 constituents. This universal fluid interface, also handles other fluid models, such as perfect gas, Lee-Kesler or Reynolds.⁴

¹See, <http://www.heatpumpcentre.org/tools/listfull.htm>

²Version 6.0, from FKW - Research Centre for Refrigeration Technology and Heat Pumps in Hannover, Germany.

³See, <http://www.ornl.gov/~wlj/hpdm/MarkVI.html>

⁴The latter two have not been updated to the last version of the interface, due to lack of interest and due to the much more complete fluid library, which is available through the newest version of Refprop.

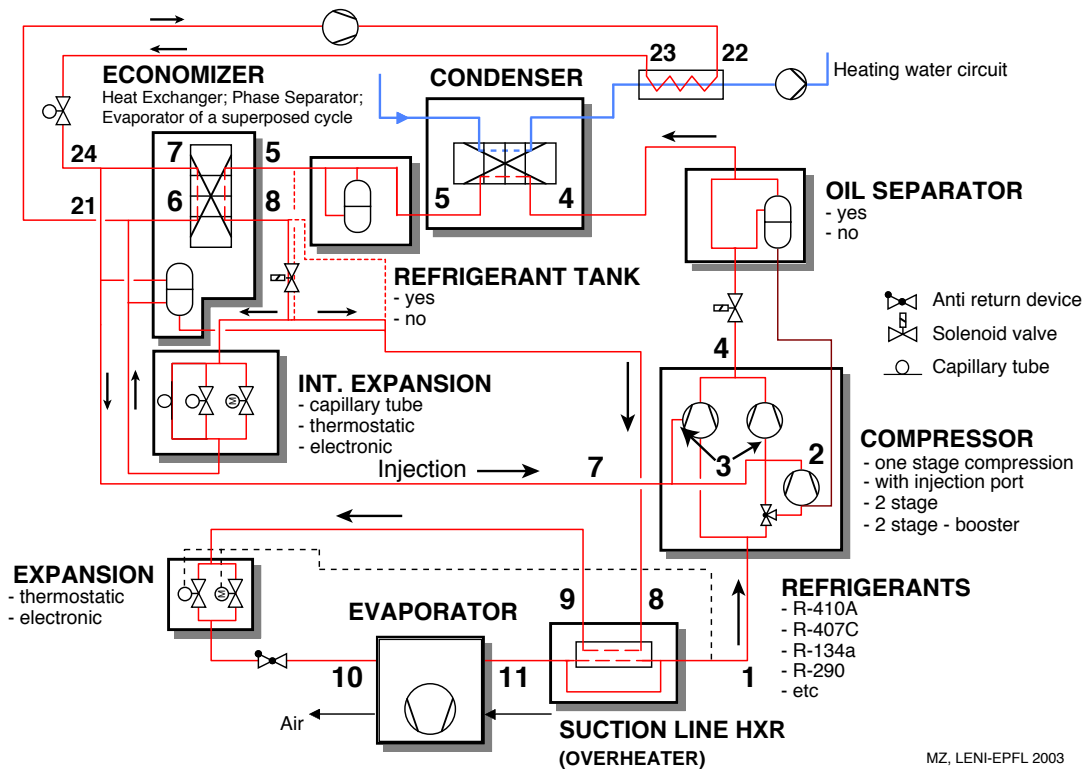


Figure 4.4: Superstructure for enhanced air-water heat pump simulation model. Numbers indicate the stream locations.

The components of this simulation code are independent modules and can be arranged according to the configurations proposed in the superstructure in Figure 4.4. A set of variables, composed of the thermodynamic state of the fluid and the mass flow rate is defined at each connection. The entire cycle is resolved through a non linear, multi dimensional equation solver provided by the *Optimization Toolbox* in Matlab. The selected mode of calculation (theoretical components, pinch based calculation or real components) defines the convergence criteria (e.g. pinch, heat exchange surface and energy balance) for the implemented solver. Figure 4.5 represents the system input variables for the example of a two-stage compression heat pump cycle, which are controlled simultaneously by the solver. For the chosen example, the resolution is acting on the three cycle pressure levels and on the inlet enthalpy of the 2nd stage compressor.

The convergence criteria are:

1. Minimum temperature difference on the heat exchangers:

The minimum local temperature difference (or pinch) between the hot stream and the cold stream has to be positive, in order to agree with 2nd Law of thermodynamics. The pinch point calculation approach can be used to by-pass the time consuming heat transfer calculation. For all simulations of this section, which refer to the *pinch calculation mode*, the following conditions are applied:

- Inlet flow temperatures: air inlet: -12/0/12°C, heating water inlet: 55/45/33°C
- Temperature glides: air side: 3/4/5 K, water circuit: 5/7/9 K
- Minimal temperature difference in exchangers:
 - evaporator: 2 K, condenser: 2 K, economizer: 2 K, (overheater: 2 K)
 - superheat at compressor inlet: 6 K
 - subcooling at condenser exit: 1 K

2. Real heat exchanger surfaces:

Facing real heat exchangers, two approaches are applied in this simulation model:

- a) Based on the flow inlet conditions and the target heat rate (e.g. known, because the refrigerant exit conditions are specified by the superheat in the evaporator or by the subcooling in the condenser) the heat exchange surface is recalculated with the heat transfer model and is compared with the real surface of the real heat exchanger. The surface difference is a return value to the solver.
- b) With the known inlet flow temperatures and the total heat transfer surface the exchanged heat rate is calculated and an internal iteration level is only needed in counter-flow conditions.

3. Energy balance on the intermediate flow:

One additional constraint has to be fixed for cycles with an intermediate pressure level. The enthalpy of the economizer exit point or the 2nd stage compressor inlet point are mainly selected, in order to ensure a correct energy balance of the heat pump cycle.

4.2.1.1 One-stage compression cycle

The optimization which has been performed to evaluate new candidates of refrigerant mixtures in high temperature lift heat pump cycles, has shown different solutions, which will be further considered in the following simulations. The key characteristics of all the considered refrigerants are listed in Table 4.1.

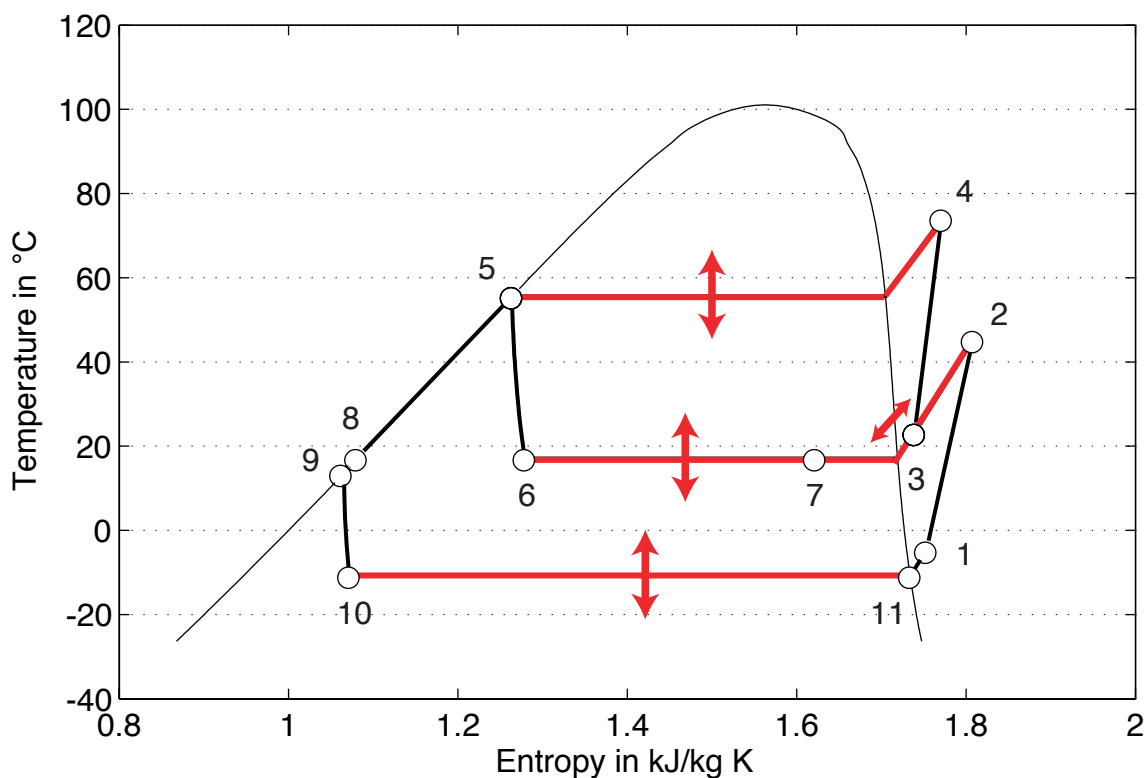


Figure 4.5: Iteration input variables, which are controlled by the implemented multi-dimensional equation solver for the case of a two-stage compression heat pump cycle.

Table 4.1: Selected refrigerants in simulation results.

Name [by mass]	sat. T_{glide} at 0°C	T_{crit} in °C	T_{nb} in °C	$P_{\text{sat,vap}}$ in bar at 65°C
R-134a	pure fluid	101.1	-26.1	18.9
R-290	pure fluid	96.7	-42.1	23.4
R-152a	pure fluid	113.3	-24.0	16.9
R-1270	pure fluid	92.4	-47.7	28.0
R-407C	6.2	86.0	-40.2	28.4
R-32/125/134a [23/25/52]				
R-407D	5.9	91.4	-36.0	24.5
R-32/125/134a [15/15/70]				
R-417A	4.0	85.9	-37.3	25.2
R-125/134a/600 [46.6/50/3.4]				
Mix_a1	3.5	128.2	-27.9	16.3
R-C270/600 [85/15]				
Mix_b1	5.8	126.1	-28.1	17.7
R-C270/134a/245fa [55/18/27]				

Theoretical compression cycle

The theoretical comparison is performed with a fixed isentropic efficiency and using the corresponding conditions for the pinch calculation mode (see above).

The simulation input parameters for the theoretical compression are set to:

- Total (isentropic) efficiency of 60% ($= \Delta h_{is} / \Delta h_{in-out}$).
- Volumetric efficiency of 100%.
- No heat losses.
- A suction line heat exchanger is implemented for all fluids.

The evolution of the performances for the selected operating mode, implementing nine of the selected refrigerants is shown in Figures 4.6 to 4.8. Note that the present input parameters have been modified from the simulation setup of the refrigerant selection optimization approach of section 1.3¹.

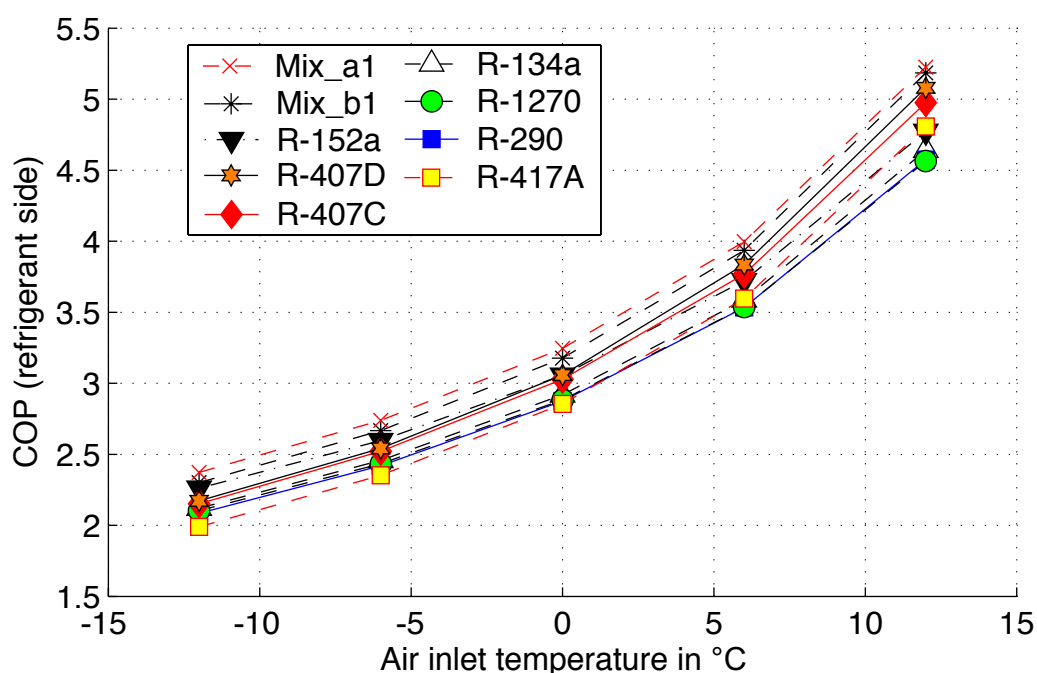


Figure 4.6: Coefficient of performance in a theoretical one-stage compression cycle (with a fixed isentropic efficiency of 60%, a minimum temperature difference in the heat exchangers of 2 K and a temperature difference in the external flows (3-5 K air-side, 5-9 K heating water)).

This theoretical evaluation shows that the selected new mixtures dominate as far as the coefficient of performance is concerned and which are appropriate for higher condensing temperatures. The

¹Redefined pinch temperatures and temperature differences in the external heat exchangers

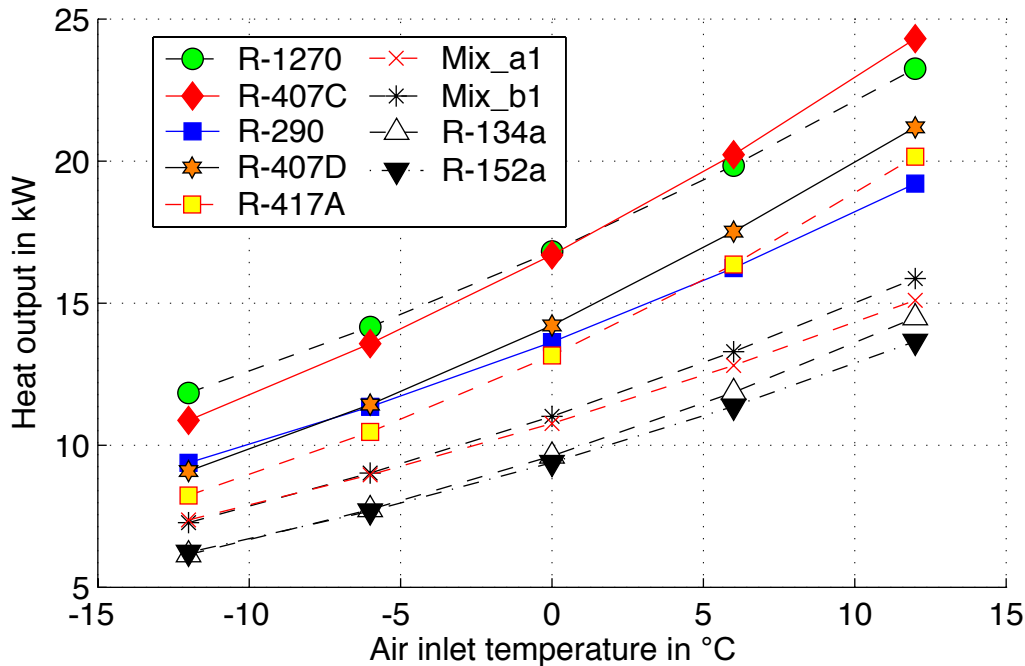


Figure 4.7: Heat output with the same compressor size for all refrigerants. Theoretical one-stage compression cycle (with a fixed isentropic efficiency of 60%, a minimum temperature difference in heat exchangers of 2 K and a temperature difference in the external flows (3-5 K air-side, 5-9 K heating water)).

two proposed new mixtures Mix_a1 and Mix_b1 (identified by the optimization process), are situated in the lower density range and need larger displacements for the same heat duty. They show advantageous lower absolute pressure levels, but result in relatively high discharge temperatures. Pressure ratios are in the same range as for R-407C. The refrigerants R-152a (very high discharge temperature and pressure ratio and lowest capacity) and R-407D (similar to R-407C, lower pressure) result in the same order of COP as the reference fluid R-407C.

One-stage compression cycle with real components

In order to obtain a similar heat output of 10 kW at the extreme operating condition A-12/W60¹, corresponding (existing) hermetic compressors have been selected for each refrigerant. The selected compressors are listed in Table 4.2. In order to meet the required water temperature difference of 5 K in the condenser, the water mass flow rate is calculated with the calculated effective heat rate at the indicated operating point.

Three typical operating points (out of the chosen heat curve) are calculated with real compressors and heat exchangers for the one-stage compression heat pump. The comparison of the isentropic compression efficiency shows distinct performance rates, represented by two groups, the high pres-

¹A=ambient air inlet in °C, W=heating water outlet in °C.

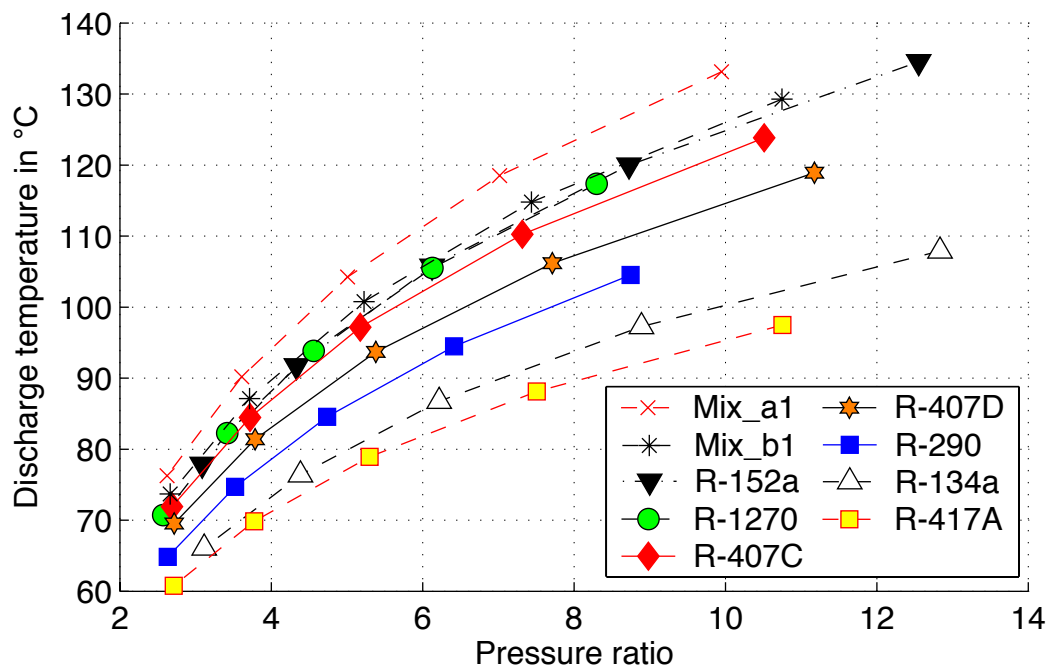


Figure 4.8: Comparison of the discharge temperatures and pressure ratios in a theoretical one-stage compression cycle (with a fixed isentropic efficiency of 60%, a minimum temperature difference in heat exchangers of 2 K and a temperature difference in the external flows (3-5 K air-side, 5-9 K heating water)).

sure refrigerants and the low pressure ones, including the two new mixtures, R-134a and R-152a. An efficiency degradation of 7% is calculated, comparing peak to peak efficiency (Fig. 4.9). Even if this difference appears to be quite important, it is of the same order, as the measured difference showed by experimental data, where a unique fluid is compressed at different suction line conditions, see Fig. 3.8.

Note: Compressors within a common series are performing in a similar way¹. Based on one or two reference models, the other sizes are set up by scaling, preserving the same efficiency ratings.

¹This can to a certain extent be verified by recalculating the performances, using catalog data.

Table 4.2: Compressor selection in one-stage compression cycle for target heat rate of 10 kW at A-12/W60. Complementary specifications of the compressor models are provided in the Annex A.4.

Compressor	Displacement	Refrigerants
ZB75	28.8 m ³ /h	R-134a, R-152a, Mix_a, Mix_b1
ZB56	20.9 m ³ /h	R-290, R-407D, R-417A
ZB45	17.2 m ³ /h	R-1270, R-407C

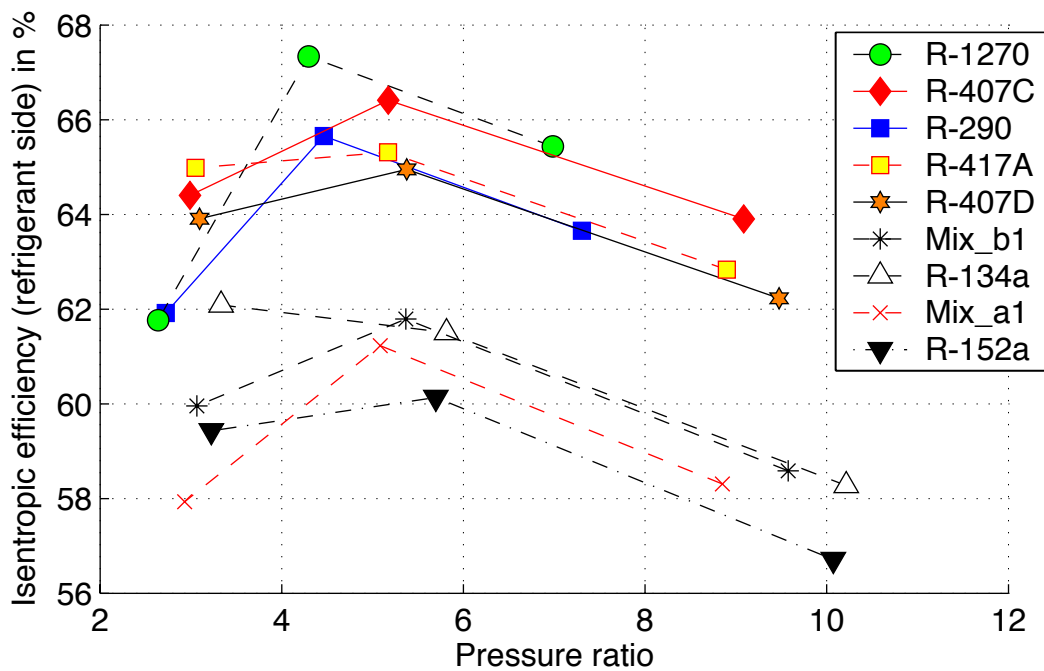


Figure 4.9: Isentropic compression efficiency, comparison of nine selected refrigerants, heat pump cycle simulation at specified operating points (A-12, A0 and A12), water inlet: corresponding to the heating return line temperature.

The maximum compressor discharge temperatures at A-12/W60 are very close to those of Figure 4.8, and are not reprinted here for the performed simulation.

On the evaporator side, the most efficient refrigerants are found to be the lighter hydrocarbon molecules. A difference of 25% between the mean values of the two-phase evaporative heat transfer coefficients is calculated, see Figure 4.10. This gain is unfortunately not corresponding in the overall heat transfer coefficient. Maximum gain is only 2.6%, due to the air side heat transfer, which is not depending on the the refrigerant selection.

Comparing the simulated cycle efficiency, with real components and in one-stage compression setup, the refrigerants Mix_a1, R-407C, R-1270 and R-407D show the best COP on both operating points at air inlet temperature of -12°C and 0°C , while R-417A and R-134a result in up to 10% lower values. The advantage of the theoretically determined refrigerants Mix_a1 and Mix_b1 compared to R-407C is partly to completely lost as a result of the lower calculated compression efficiency. Better heat transfer performances can not compensate these losses.

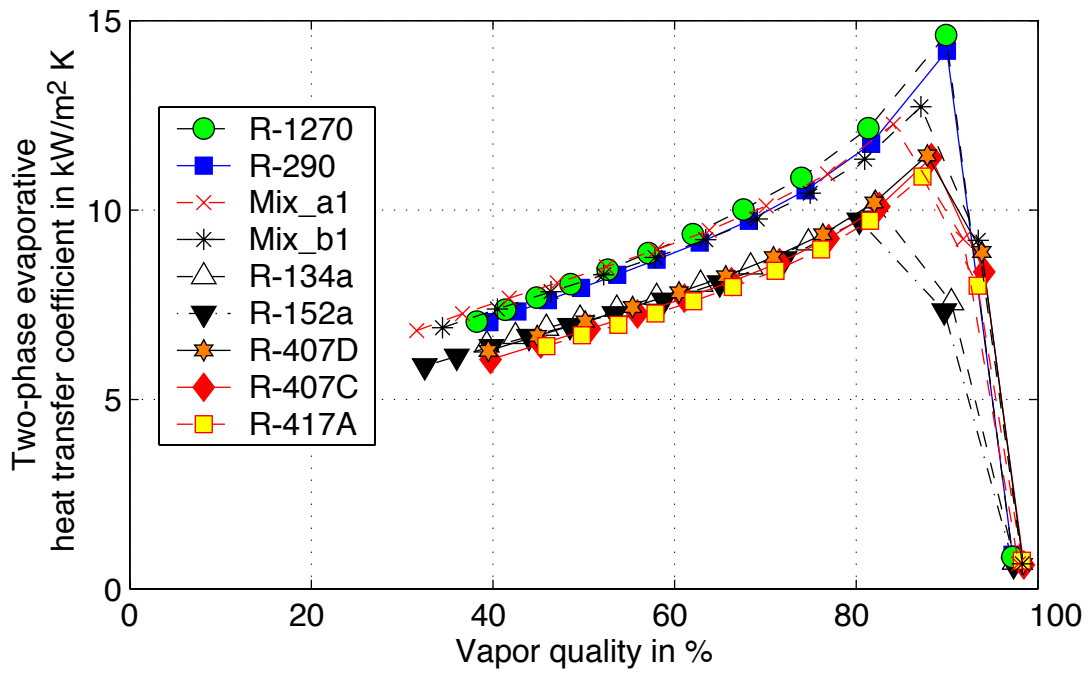


Figure 4.10: Simulated evaporative two-phase heat transfer coefficient, microfin tube with inner diameter of 9.5 mm, evaporation mean saturation temperature $\sim -6^\circ\text{C}$, mass velocity $50\text{-}110\text{ kg/s m}^2$, heat flux $=2000\text{ W/m}^2$.

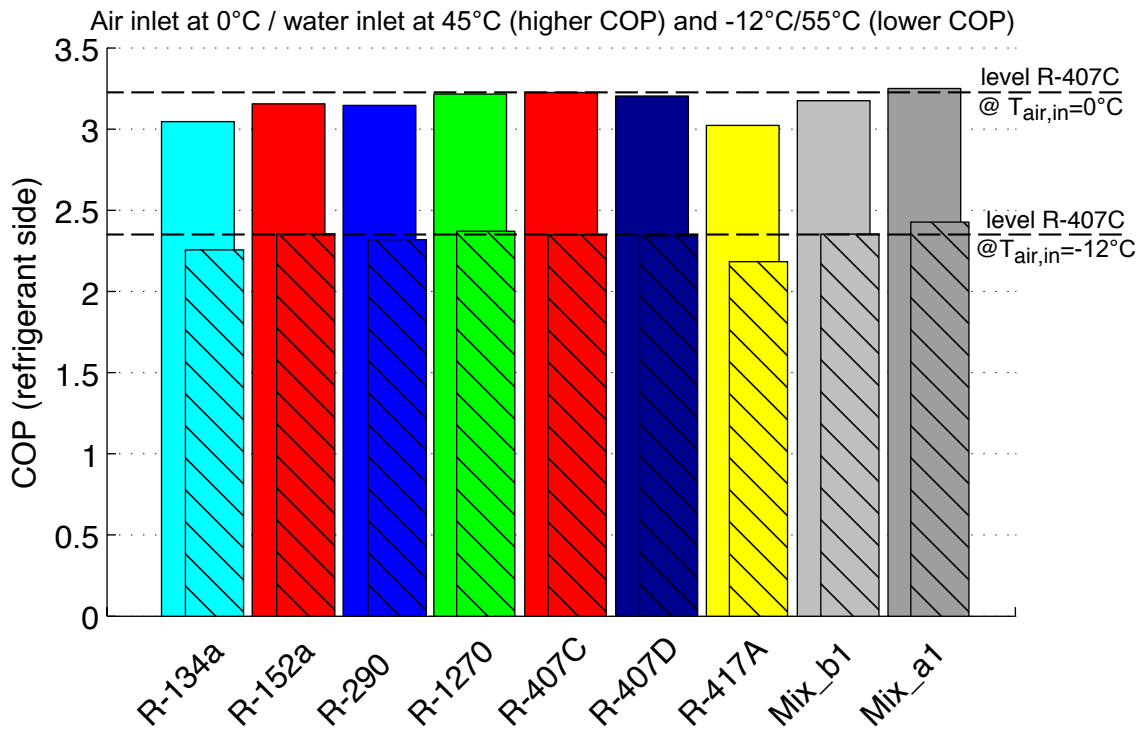


Figure 4.11: One-stage compression cycle at air inlet $=-12^\circ\text{C}$ and 0°C , evaporator #1 ($S_{ev}=5.04\text{ m}^2$), condenser #2 ($S_{cond}=4.68\text{ m}^2$) and compressors, see Table 4.2.

One-stage compression with intermediate injection.

A **parametric analysis** is performed at first with the refrigerant R-407C, using a specific high built-in volume ratio compressor with intermediate injection port (prototype compressor 2), which has been dimensioned for vapor injection. The purpose of this analysis is to find the ideal operating conditions for a given setup, by variation of the injection mass flow rate. Then in a second evaluation one geometric parameter is varied and the impacts on the system performances and on the potential of discharge temperature reduction are shown.

Figures 4.12 (a-d) show the simulation results corresponding to a configuration with a **variable injection mass flow rate**, which reflects the use of a controlled intermediate expansion device. With increased injection flow rate, the intermediate pressure level is adapting according to the characteristics of the injection flow path, which is described in section 3.1.2. An operating point at air inlet temperature of -12°C and water outlet of 60°C has been chosen, in order to show the evolution of the discharge line temperature, the heat rate and the COP at the extreme operating point. The evolution paths show a discontinuity, at a mass flow rate of 28 g/s, which is in the order of magnitude of the mass flow rate in the suction line (30 g/s). This discontinuity is due to a significantly reduced compression efficiency attributed to the wet compression (see the simulation model in section 3.1.2 for a more detailed description). This calculated discontinuity is however very difficult to be verified experimentally, because of highly pulsating flow conditions throughout the installation. The calculated evolution in the dry compression zone corresponds to that found by the experiments.

According to the simulations, the COP is optimum for injection rates of 50% of the suction rate at the operating point A-12/W60. This optimum is shifted to lower injection rates at higher air inlet temperatures (Figure 2.10 on page 43). The heat output gains, compared to the one-stage compression mode without injection, are important and in the order of 30%! The evolution of the heat output is weakly decreasing at higher injection rates, including a minor step at the dry to wet compression limit.

With increasing injection rate, the discharge temperatures are also increasing until reaching a maximum value. This maximum is situated close to the calculated optimum of the COP and the heat output of the calculated cycle. For higher injection flow rates the discharge temperature is highly reduced. This inversion of the evolution can be explained as follows: At low injection rates, the intermediate pressure is closer to the evaporation pressure and the refrigerant is highly superheated in the economizer heat exchanger. The pinch point is located at the injection exit point. When this injected vapor is mixed to the partially compressed refrigerant in the compression chambers, it contributes to a temperature increase of the compressed flow. With increasing mass flow rates this heating effect is increased until the pivot point is reached, at which the pinch point in the economizer changes from the injection exit to the injection inlet. By further increasing the mass flow

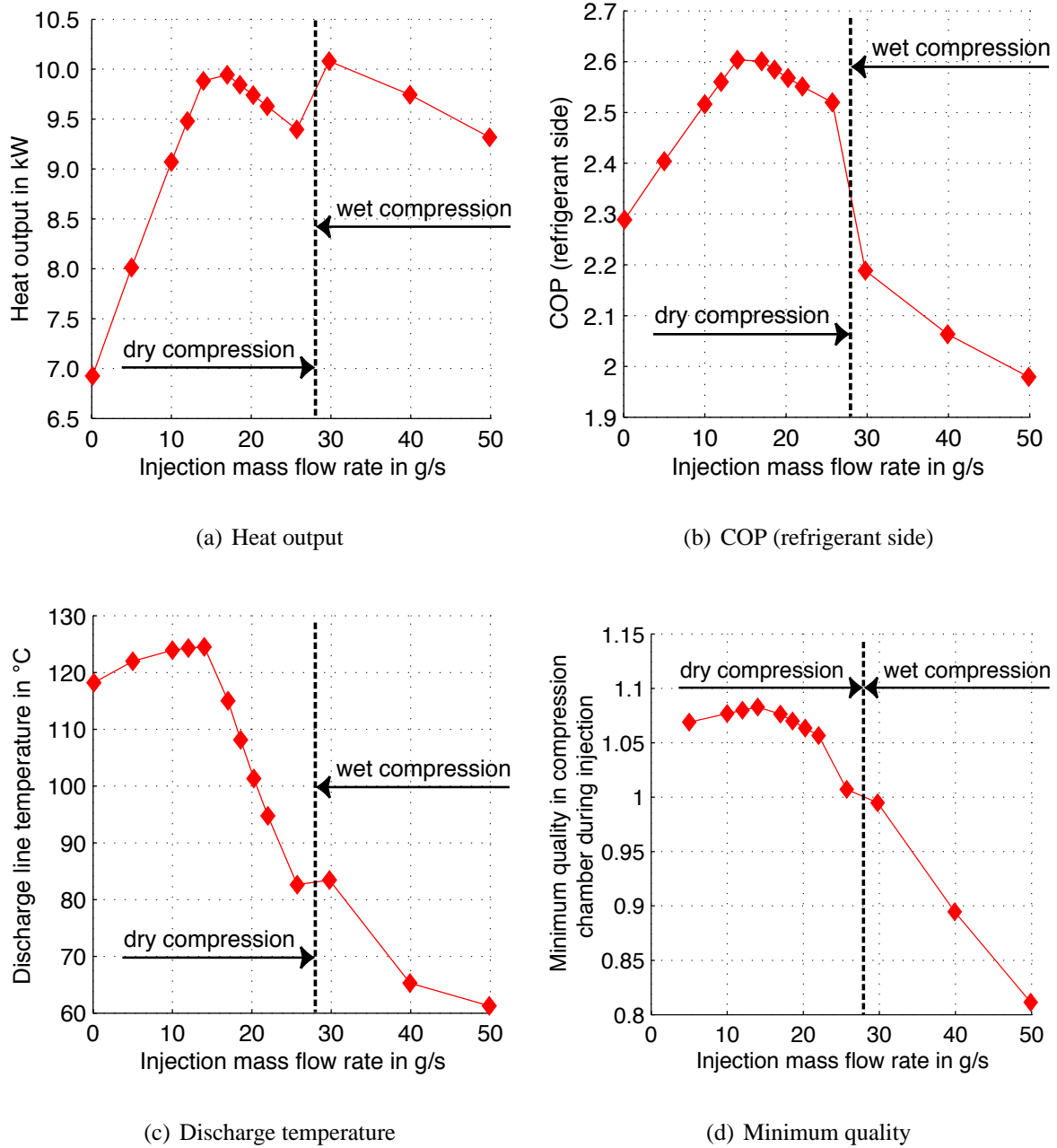


Figure 4.12: Controlled injection flow rate for R-407C (at air inlet=-12°C/water exit=60°C). Refrigerant mass flow rate in the suction line = 30 g/s, injection start at sealing of the compression chamber. Heat exchangers with fixed, pre-calculated minimum temperature difference. Fixed external mass flow.

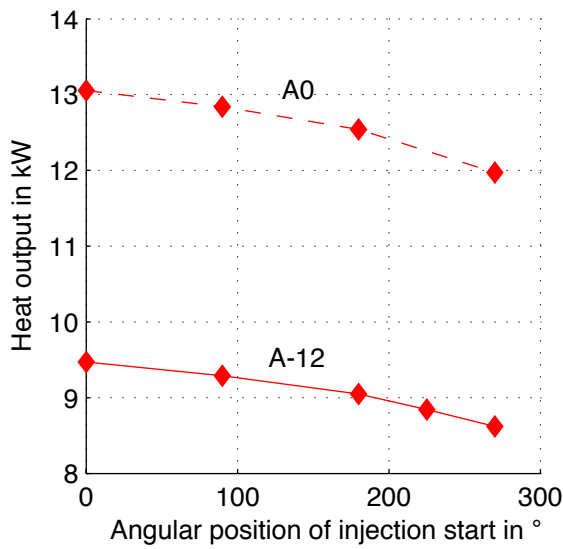
rate, the temperature of the injection flow is rapidly decreasing, until remaining saturated at the economizer exit. As long as the compression remains in the dry compression zone, the COP value remains at a high level. The proximity of the compression curve, which included the mixing steps, to the saturation curve is represented as the minimum quality in the compression chamber. Quality numbers, which are > 1 correspond to the ratio of the enthalpy difference of the considered point to the bubble point enthalpy divided by the latent heat of evaporation.

In the parametric study, the influence of the location of the injection port to the system performances is analyzed. The position of the injection port(s) is characterized by the angular position of the orbiting scroll member, where the access to the compression chamber is opened. Using the original geometry (diameter and length of the equivalent capillary tube, which represents the complex injection flow path), the position of the injection port has a direct impact on the intermediate pressure level and the resulting mass flow rate in the intermediate stage of the heat pump cycle. Its position can be varied from 0° to 270° . The simulations are performed with maximum injection flow rate, but remaining entirely in the dry compression zone. Two operating points, the extreme point at A-12/W60 and the mean condition at the air inlet temperature of 0°C are compared.

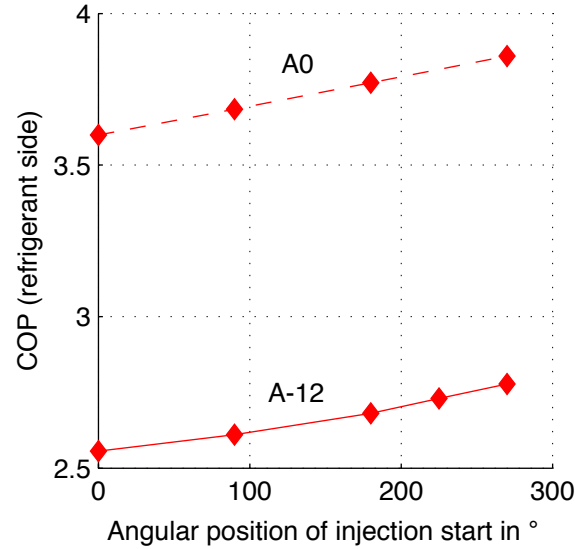
The represented calculated evolutions (Figures 4.13 (a-d)) indicate for both operating conditions a clear increase of the COP and a reduction of the delivered heat rate and of the discharge temperature level, with the placement of the injection port at higher angular positions. The estimated gain in COP is about 10% compared to the actual setup. The very low discharge temperatures allow to run the heat pump in a very large application range and at reduced thermal stresses, acting on the scroll members.

4.2.1.2 Two-stage compression cycles

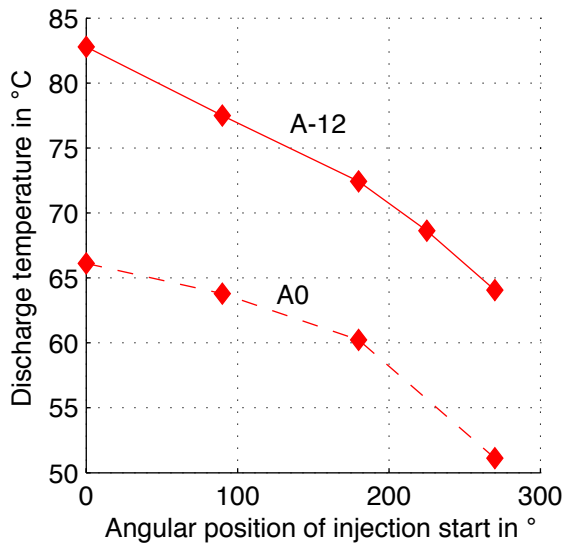
Due to their highly extended application range, their increased efficiency and the possibility of heat output modulation, the two-stage compression cycles are the most adapted solution for high temperature lift applications. The concept of an economizer cycle allow a sensible reduction of the discharge line temperatures and allow to operate at a very high temperature lift between the cold source and the hot utility. This advantage has been experimentally shown (sec. 2.3.3 on page 50) and has been calculated in the example before. The operating conditions for the aimed application vary over a large range of evaporating and condensation temperatures, inducing a total pressure ratio, which typically varies from 3 to 10 (see Figure 4.8). The division into two compression steps allows to operate the compressors close to their design conditions. For the heating season with moderate external temperatures, one compression stage can be stopped, presenting the advantage to adapt the heat output closer to the demand. Comparing to the one-stage compression cycle, the two-stage approach with an economizer heat exchanger results in increased efficiency, due to the internal valorization of the liquid subcooling. The irreversibilities of the intermediate flow



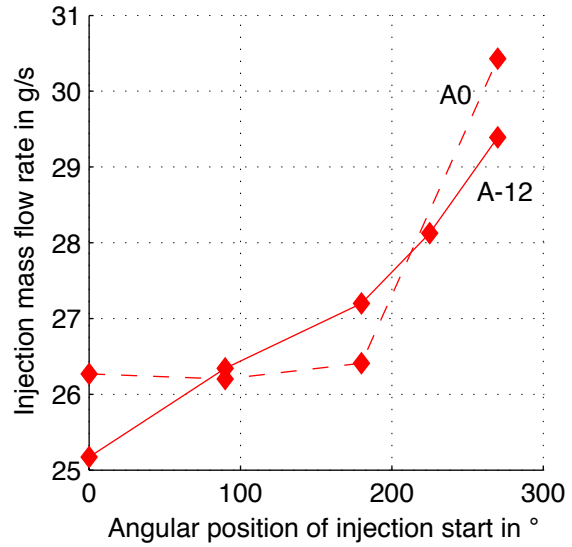
(a) Heat output



(b) COP (refrigerant side)



(c) Discharge temperature



(d) Injection mass flow rate

Figure 4.13: Evaluation of limit injection flow for R-407C, avoiding wet compression. Influence of the angular position of the access start of injection port to the compression chamber, calculated with corresponding injection geometry (capillary tube). Mass flow rate at the suction port = 30 g/s and 48 g/s for air inlet (A) -12°C and 0°C . Heat exchangers with fixed minimum temperature difference. Fixed external mass flow.

are highly reduced, when comparing with the intermediate injection solution, which has a highly restricted flow path in the injection line.

Nevertheless, system complexity (leading to increased cost), higher refrigerant charge and the limitations, which have been identified by the oil migration through the cycle have to be considered in the selection of such potentially high performance approaches.

Two-stage compression cycle with economizer heat exchanger.

A two-stage compression cycle, with economizer heat exchanger and suction line overheater is simulated. Flow separation is done before the economizer (dashed lines between the condenser and the economizer, in Fig. 4.4), in order to avoid additional iterations in the resolution of this cycle. The standard setup (represented by the hard line connections, Fig. 4.4), is theoretically the better solution, allowing an improved utilization of the subcooling energy, due to the higher mean temperature between the hot and cold flow. It is also the more stable configuration for the intermediate expansion device.

Using the pinch temperature approach in the heat exchangers, the optimal size of the second stage compressor has been evaluated at the extreme operating point at A-12/W60 and for mean operating conditions at A0/W52 (see Figures 4.14 and 4.15).

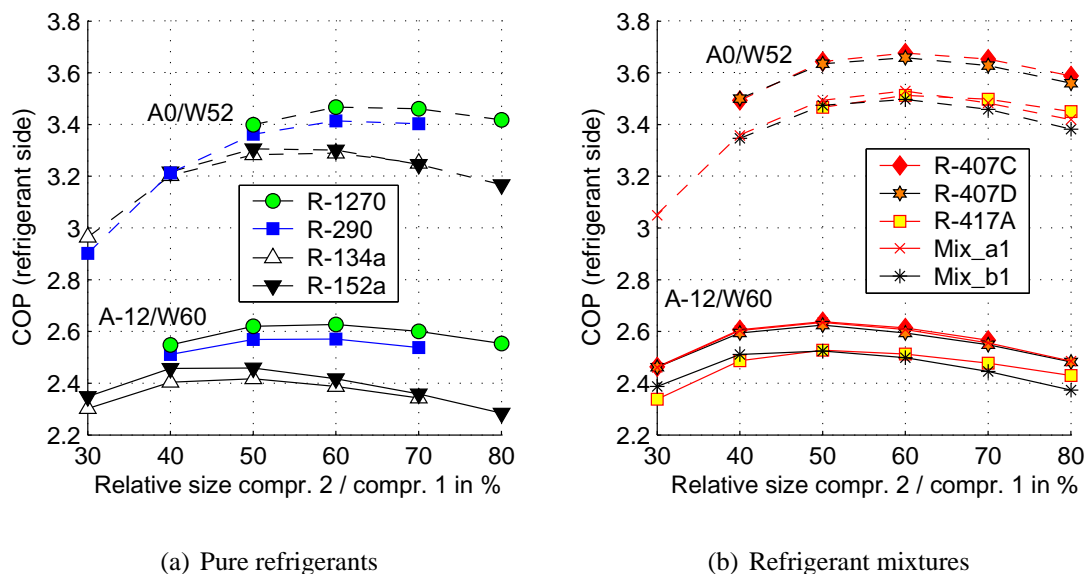


Figure 4.14: Two-stage compression cycle, evolution of COP with relative compressor size of the second stage compressor. Simulation with fixed minimum temperature difference in the heat exchangers. External temperatures (air inlet/water outlet) at A0/W52 and A-12/W60.

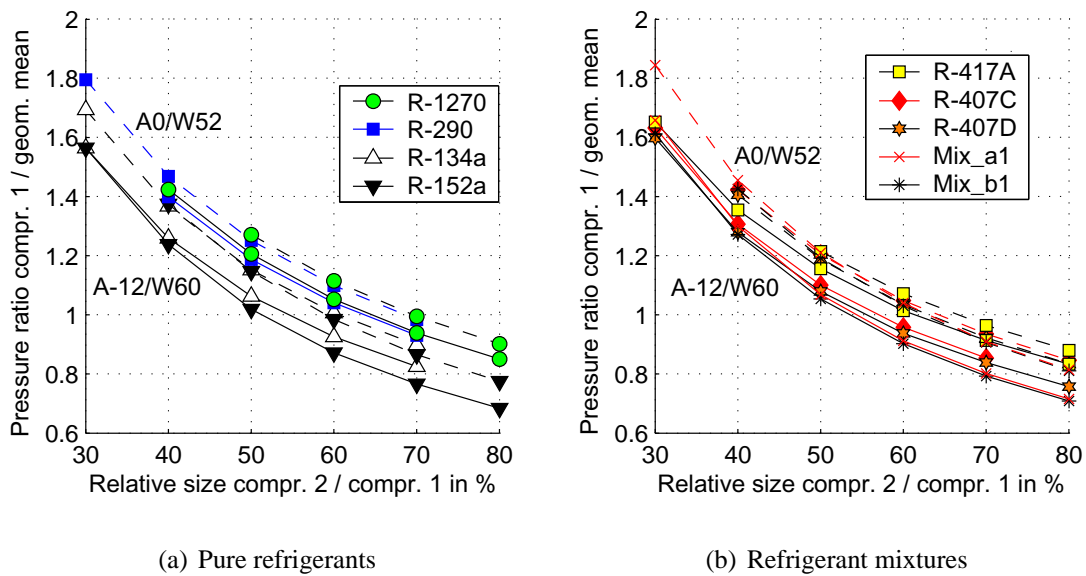


Figure 4.15: Two-stage compression cycle, first stage pressure ratio, compared to the geometric mean intermediate pressure. Simulation with fixed minimum temperature difference in the heat exchangers and with variable sized second stage compressor. External temperatures (air inlet/water outlet) at A0/W52 and A-12/W60.

This approach allows an optimal selection of both compressors, in order to achieve the highest COP over a wide range of operating conditions. Best relative compressor size of the 2nd stage compressor is $\sim 50\%$ at A-12/W60 and $\sim 60\%$ at A0/W52. The compressors are selected from available models, in order to meet the heat output requirement of 10 kW at external air temperature of -12°C , and to be close to the optima in Figures 4.14 (a+b). Table 4.3, lists the final compressor selection, used for the comparison with real components, and the refrigerant specific optimal configurations.

The simulation results of the two-stage compression cycle, using the selected compressors and real heat exchanger characteristics, show the COP and the maximum cycle temperatures, for each refrigerant. These temperatures are (compared to the one-stage compression cycle without intermediate injection) highly reduced, and are no more a critical system parameter, allowing to extend the application range to very high temperature lifts. In this case, condensation pressure level is limited either by the component design, or by a decrease of the system performance, in the region close to the critical point or above. Among the selected fluids, R-134a, R-152a and the evaluated mixtures Mix_a1 and Mix_b1, could be considered to condensation temperatures up to $\sim 90^{\circ}\text{C}$, respecting a pressure limit of 30 bar.

First stage and second stage pressure ratios remain within a highly reduced range (Fig. 4.18) and would allow an optimal compressor design for this type of application.

Table 4.3: Two-stage compression cycle, optimal compressor selection criteria.

Refrigerant	Optimal size of 2 nd stage compr.		Heat output in kW	Size of main compr. in m ³ /h	Target size of 2 nd stage in m ³ /h	Sel. model ¹⁾ , size in m ³ /h
	@A0	@A-12	@A-12			
R-134a	57%	47%	10.3	19.2	10.0	9.4
R-152a	54%	47%	9.6	19.2	9.8	9.4
R-290	62%	55%	11.2	14.4	8.35	8.0
R-1270	64%	57%	10.9	11.5	6.9	6.8
R-407C	60%	50%	10.2	11.7	6.4	6.8
R-407D	59%	50%	10.8	14.4	7.9	8.0
R-417A	62%	52%	11.1	14.4	8.2	8.0
Mix_a1	58%	50%	10.7	19.2	10.4	11.5
Mix_b1	58%	49%	10.7	19.2	10.4	11.5

1) Available compressor sizes, see catalog data in Annex A.4.1.

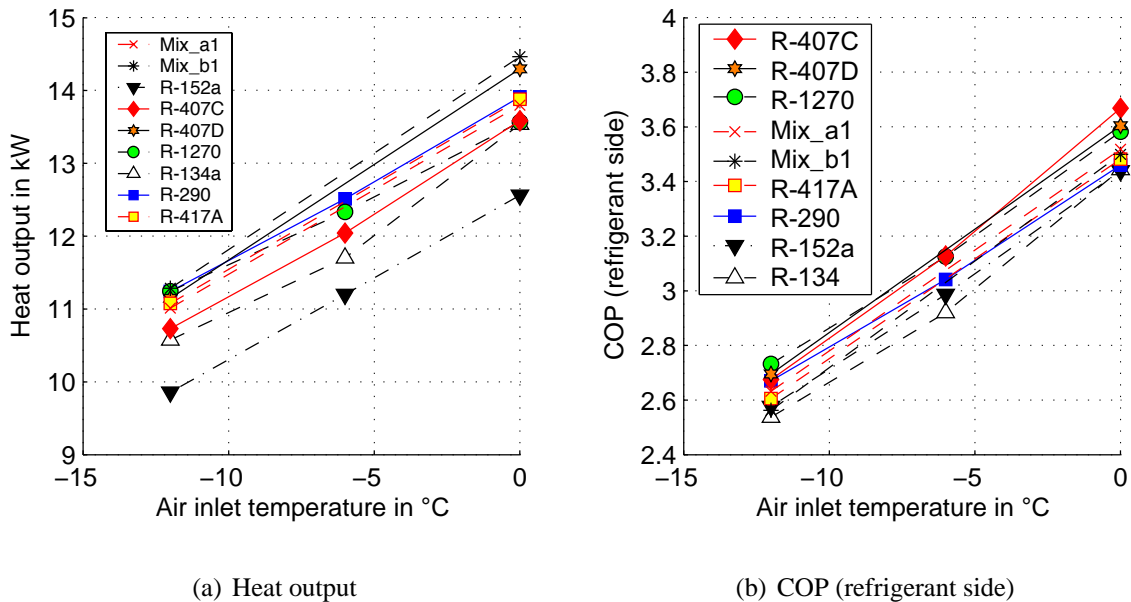


Figure 4.16: Two-stage compression cycle with optimally selected compressors. COP and discharge temperature of the second stage compressor, for a heating heat pump with ~10 kW base heat output.

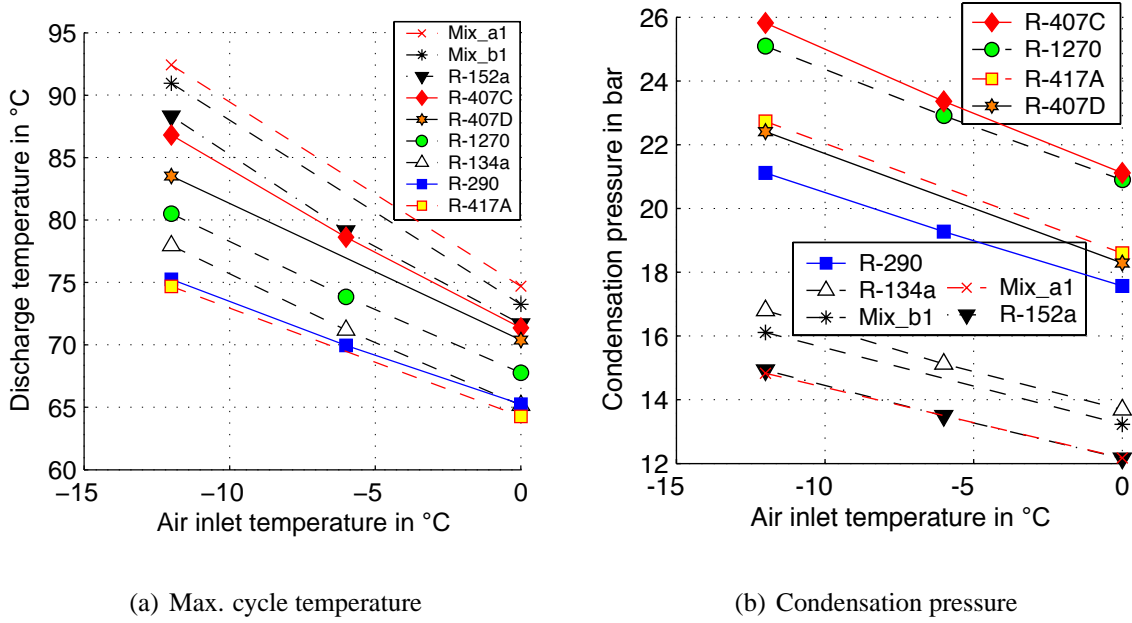


Figure 4.17: Two-stage compression cycle with optimally selected compressors. COP and discharge temperature of the second stage compressor, for a heating heat pump with ~10 kW base heat output.

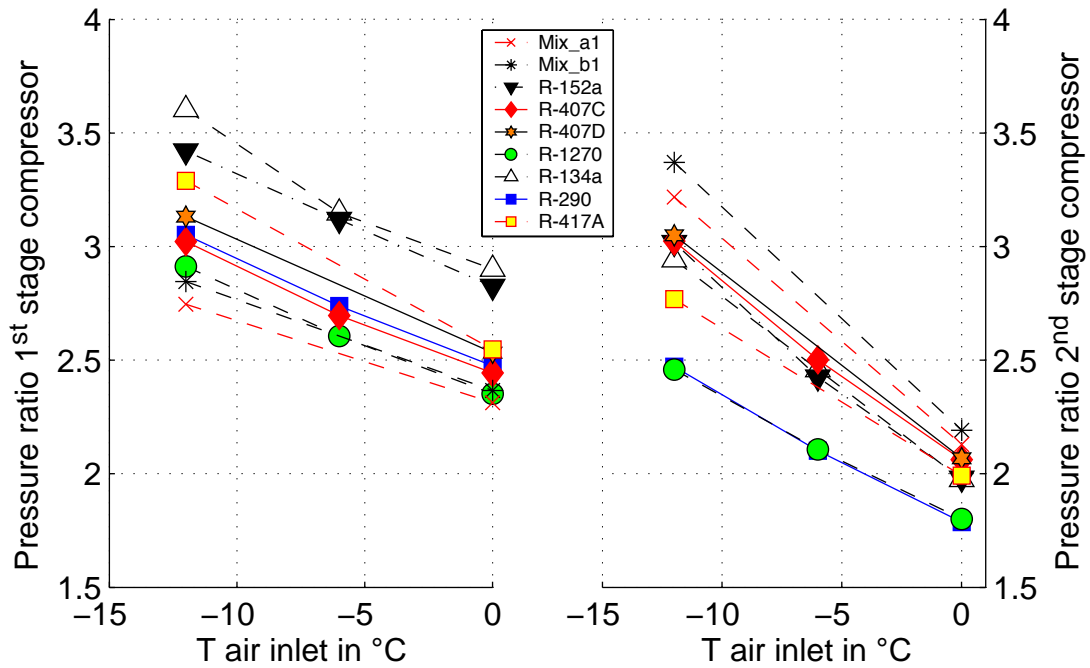


Figure 4.18: Corresponding range of pressure ratio on the main and the auxiliary compressor, in two-stage compression cycle.

As the two-stage cycle allows to switch from the two-stage compression to the one-stage compression operating mode, it is interesting to compare the performances of the two modes over the entire application range. The external flow rates of the air and the heating water are maintained equal. In order to complete the analysis, the results of the one-stage heat pump are added to the following graphs. The zeotropic refrigerant R-407C is used in this comparison.

The differences between the setups of the two one-stage compression cycles 'One-stage heat pump' and 'only first stage' are principally found in a different selection of the compressor. In the **one-stage heat pump**, the used compressor, is one with a **higher built-in volume ratio**, while the **first stage compressor of the two-stage heat pump**, is one with a **lower built-in volume ratio**. At the extreme operating conditions, the first-stage compressor, operated alone, does not provide the full heat rate and using the same external flow rates as in two-stage mode, the temperature changes of the air and the water flow are also reduced. These advantages are largely compensated by the reduced compression efficiency at lower air inlet temperatures.

For increasing external air temperatures, the COP curve of the first-stage compression cycle is gradually approaching and finally crossing the two-stage curve (Figure 4.19 (b)). This behavior is the result of several effects, which are:

1. Reduced heat output in one-stage mode: With a reduced heat output, the temperature change of the heating water is also reduced and the heat supply temperature is therefore lower, comparing to the two-stage mode. For the same reason the air exit temperature in the evaporator is higher. Both effects contribute to a higher COP of the heat pump.
2. Reduced thermodynamic benefits: The thermodynamic advantages of the economizer cycle of the two-stage compression cycle are less important at lower temperature lift.
3. Off design compression: The compressors, in two-stage mode, work in a non-adapted, very low pressure ratio range. For moderate external conditions, the one-stage compression is situated closer to the design conditions.

According to the Figure 4.20 (a), there is an application range, in which a one-stage compression with the first-stage compressor alone results in discharge temperature which exceed the temperature limit of 120°C. The important difference in the evolution between the curves (only first stage and one-stage HP) is mainly due to the different compressor series (lower and higher built-in volume ratio).

According to these simulation results, the switch between the two-stage to the one-stage operating mode should be performed very late in the heating season (at air inlet temperatures of $>10^{\circ}\text{C}$). In order to reduce the number of on/off-cycles of the heat pump, this switching point is probably shifted to a lower temperature. The first stage compressor should not be operated alone at air temperatures below -3°C .

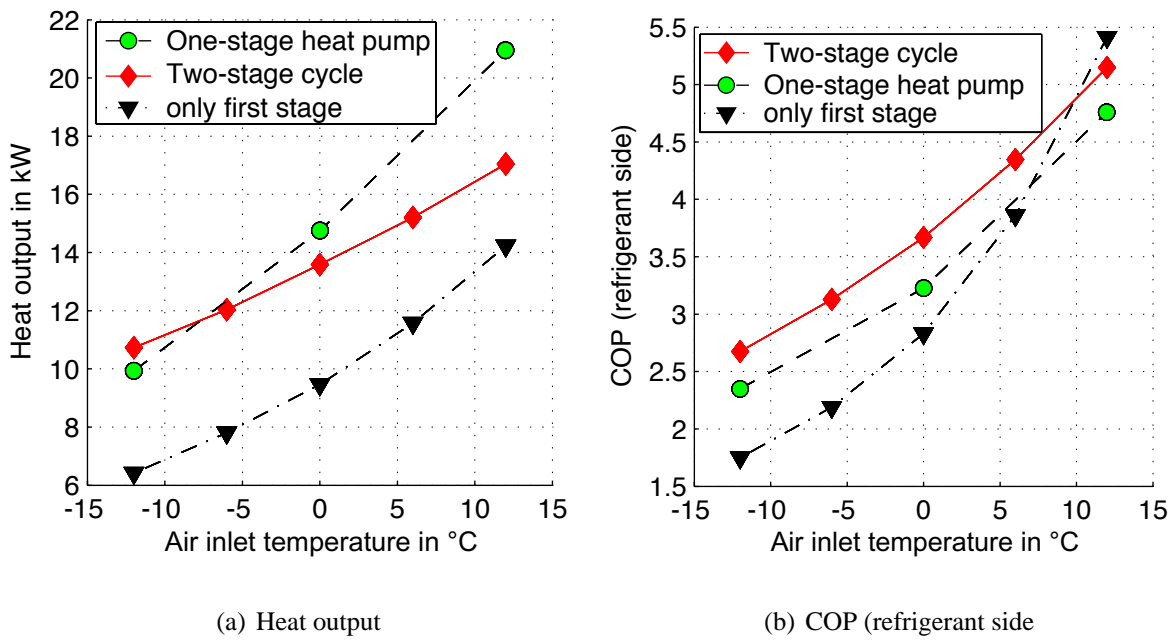


Figure 4.19: Performance comparison of a two-stage compression cycle, (operated either with both compressors or with only the base compressor) and one-stage compression cycle with same base heat output. Real mode calculations with R-407C and fixed external mass flow rates.

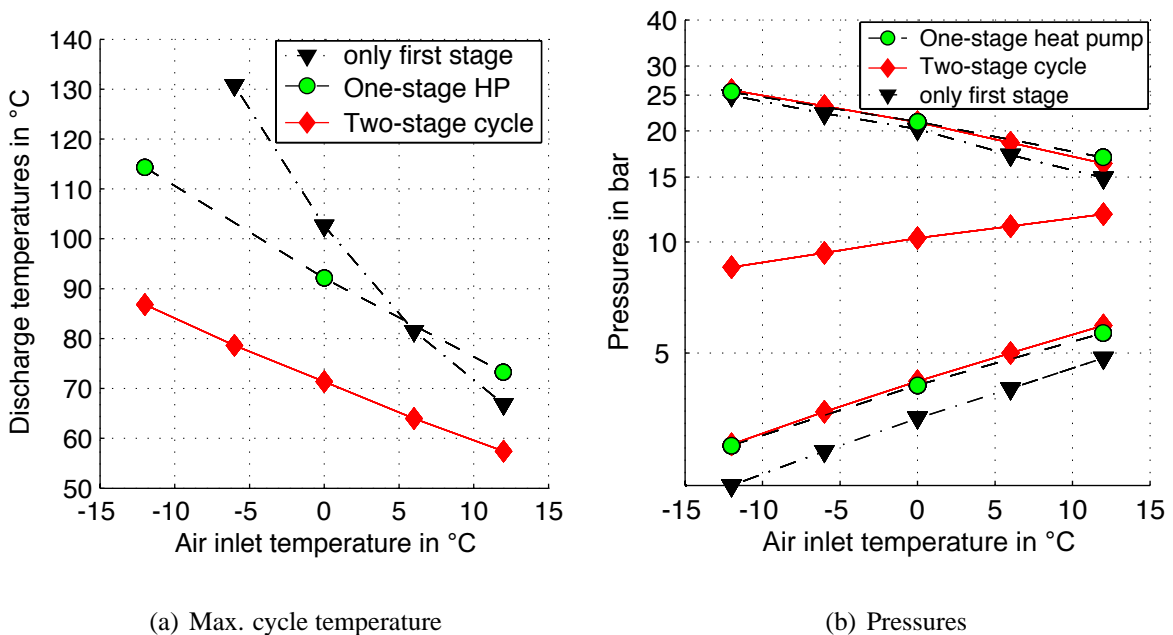


Figure 4.20: Comparison of discharge temperature and pressure levels in a two-stage compression cycle, (operated either with both compressors or with only the base compressor) and in a one-stage compression cycle with same mass flow rates. Real mode calculations with R-407C and fixed external mass flow rates.

Two-stage compression - booster configuration.

The booster configuration corresponds essentially to the two-stage compression cycle. The function of the two compressors is however inverse. In this setup, the second stage compressor is considered to be the main compressor and should be selected with a higher built-in volume ratio. The first stage compressor is only operated at high temperature lift, enabling an important increase of heat output, and allowing a reduction of the compression discharge temperatures by desuperheating the refrigerant at the compressor suction line.

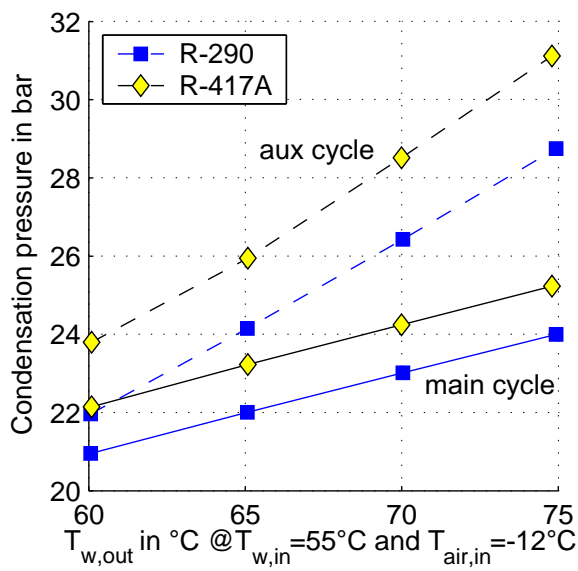
The booster concept, is based on a low cost compressor, which is intended to be used only for a restricted time period during a heating season. An extensive evaluation of this concept is presented in [Zehnder et al., 2002], including a thermo-economic optimization, to compare the two-stage booster concept with the one-stage compression heat pump with intermediate injection and with adding an electrical heat supply to satisfy the heat demand. Results from the mentioned work show, that even for reduced performances of the booster compressor (about 10% lower in overall compression efficiency compared to the main compression) the economic optimum is obtained with a respective compressor size of 133% to the main compressor (case without electric heat supply). This booster compressor should however be in operation for a considerable time during the heating season (up to the transition point of the COP curves in one-stage and two-stage compression).

4.2.1.3 Auxiliary cycle for liquid subcooling

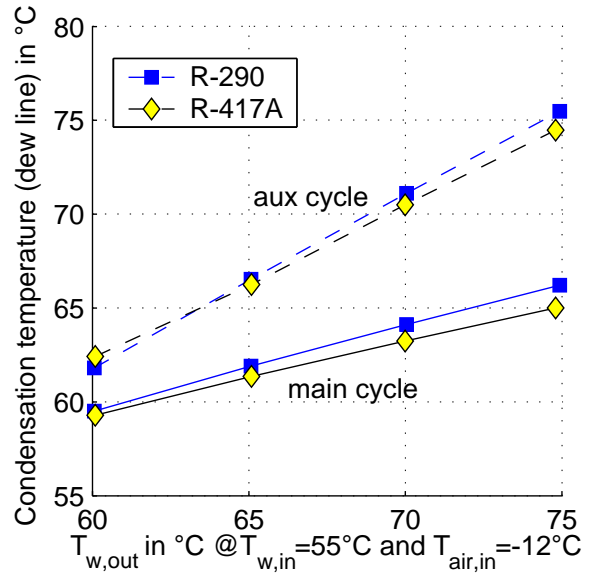
The main application domain, with respect of the high performance solutions presented in the preceding paragraphs, is the heating of two separate circuits, e.g. hot water preparation at higher temperature in parallel. To show the potential of this type of cycle, a 25 kW heating heat pump is calculated with standard hermetic scroll compressors. The heating side temperature glide is parametrized, ranging from 5 K to 20 K (with a fixed return line temperature of 55°C. From the refrigerant selection, only R-290 and R-417A, can be reasonably considered in the main compression cycle. For all the other refrigerants, the discharge temperatures are too high, except for R-134a, which although results in the highest pressure ratios (see Fig. 4.8 on page 153).

For both refrigerants, the ideal compressor pairs have been identified through a simulation process at the respective conditions A-12/W60 and A0/W52, using a pinch mode calculation for the heat exchangers. Knowing the compressor pairs, the heating water flow rates are calculated to match the specific temperature glides in the condenser, which are set to 5/10/15/20 K. Air inlet (-12°C) and water inlet (55°C) temperatures are held constant throughout the simulation.

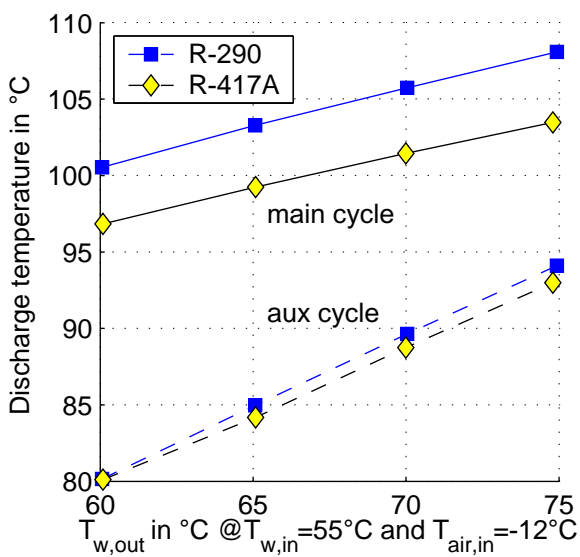
For this type of cycle, the behavior of the condenser stages of the main and the auxiliary subcooling cycle are of major interest, and the analysis will be concentrated on these characteristics. Figure 4.21 (a) shows the condensation pressure level of the main cycle and the auxiliary cycle.



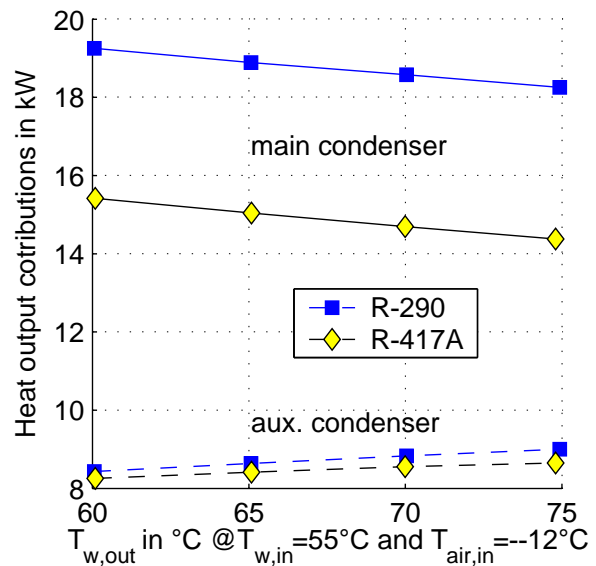
(a) Condensation pressure



(b) Dewline sat. temperature



(c) Cycle temperatures



(d) Heat output

Figure 4.21: Effects of variable temperature glide in the heating system on temperature, pressure and heat output, comparing main cycle to auxiliary cycle. Compressor selection $42.1 \text{ m}^3/\text{h}$ & $6.8 \text{ m}^3/\text{h}$. Operating conditions A-12/W60...75.

The shown difference corresponds to the gain, which is due to the auxiliary cycle, unloading the main compressor. With a higher temperature glide on the heating water, the pressure gain in the main cycle becomes quite important and corresponds, in terms of saturation temperature gain, to the half difference of the temperature glide in the heating system (see Fig. 4.21 (b)). For a heating case with water supply and return line temperatures of $75^{\circ}\text{C}/55^{\circ}\text{C}$, the saturation pressure of the main condenser is only at 65°C and that of the auxiliary cycle is at 75°C , which is about the level, which would be obtained by a conventional heat pump cycle. While the pressure level is more critical for the auxiliary cycle, the discharge temperatures are lower, compared to those of the main cycle. For the two refrigerants all the temperatures remain within the considered temperature limit of 120°C , Fig. 4.21 (c). The auxiliary cycle is more sensible to variations of the operating conditions. The proportion of provided heat rate of the auxiliary cycle is increased with a higher temperature glide in the heating system and corresponds to 33% and 37% of the total heat output. This proportion shows the interest of this concept. The main cycle can therefore be designed compact with smaller components. The auxiliary cycle can be used for two functionalities: As a heat supply during the coldest season and as a hot water utility during winter and by direct evaporation during summer.

4.2.2 Conclusions of the simulation results.

Improved thermodynamic concepts for high temperature lift heat pumps are presented within this work. These concepts unify the **classical one-stage compression cycle** (used as reference), the **one-stage compression cycle with economizer heat exchanger and intermediate injection flow**, the **two-stage compression cycle with economizer** and the **auxiliary cycle for liquid subcooling**. The simulation program includes a generalized model of a **scroll compressor with optional intermediate injection port**, a complete description of the **heat transfer including the up to date two-phase heat transfer flow map** developed by [Thome and El Hajal, 2002], and an integrated **fluid interface module**, named FLINT, allowing to use the calculated thermo-physical properties provided by Refprop, [Lemmon et al., 2002].

In a first step, a general approach in the search of adapted refrigerants has been adopted to a theoretical one-stage compression cycle and using a multi objective optimization tool, MOO, see [Leyland, 2002]. Optimization has been performed on two objectives, COP and specific heat output. Nine refrigerants were selected, among them, two new (flammable) blends, which have been found through the optimization process. These fluids are listed in Table 4.1 on page 150.

Simulations are performed on a characteristic heat curve, with a maximum heating temperature of 60°C. The theoretical evaluations, show that the two created blends high in the performance scale, while using real compressor characteristics, these low pressure fluids are partly penalized. The non flammable, commercial blends R-407C and R-407D are among the best performing refrigerants in real one-stage compression cycle. R-1270 results in high specific heat output and COP (like R-407C), while Mix_a1 is best in COP, but presents lower heat capacities and high discharge temperatures.

Using the same compressor technology (with high built-in volume ratio), the intermediate injection port and an economizer are added to the cycle. A sensibility analysis on the geometrical data of this injection has been performed, using R-407C. Simulation results show a potential increase of 40% in the heat output and an increased COP of 13% at the extreme operating conditions. In order to respect discharge temperature limitations, the optimal conditions cannot be chosen. This concept allows a sensible reduction of the maximum temperature, while still presenting a considerable improvement on the cycle performances (Fig. 4.12). In addition, the position of the injection has been virtually varied in order to see its effect on the characteristic performances of the cycle, for the extreme and the mean operating points. Increasing the angular position after sealing of the compression chambers has a reducing effect on the heat output, but clearly improves COP and further reduces cycle temperatures. Limit injection flow rates are calculated, in order to avoid the wet compression zone.

In two-stage compression cycles, the optimal size of the second stage compressor is within the range of 50%-60% for all fluids. With condensing temperatures approaching the critical point, the optimal size is decreased, shifting the intermediate pressure level closer to the condensation pressure. Available compressors have been selected and the cycle is evaluated with real components and fixed external flow rates, matching a water temperature glide of 5 K at the extreme operating conditions (Fig. 4.16-4.18). The range of pressure ratios on each compressor is highly reduced. Refrigerants R-407C, R-407D and R-1270, show the best COP in two-stage compression cycles, while the blend Mix_al is at a lower COP. Compared to the conventional one-stage heat pump cycle, improvements of 10%-15% over the entire application range are calculated. The comparison to the heating mode with the first stage compressor operated alone results in a difference of 30%, which is in agreement with the experimental observations. This operating mode, however, is performing better than the two-stage configuration at higher external air temperatures. The cross-over for a R-407C heat pump, is calculated at an air temperature of 10°C, which is close to the heating limit of 15°C. The heat output evolution is favorable in two-stage cycles and additionally allows a regulation step reducing the on/off switching frequency of the heat pump (Fig. 4.19).

The rather complicated approach of a heat pump with an auxiliary liquid subcooling cycle, shows a potential application at high temperature glide heating, or in double utility applications, for the medium capacity range (min. 20 kW heat rate). The main compressor can be considerably unloaded and the auxiliary subcooling cycle can be operated with an additional evaporator for hot water production during summer.

All these improved concepts enable an extended application range and are suited to the high temperature lift heating case. The most flexible and less restrictive approach is presented by the two-stage compression cycles, which however is limited by the unstable oil-migration leading to a failure of the lubrication of the upper stage compressor in long term operating conditions. This specific problem has been further analyzed experimentally.

Bibliography

- S. Bertsch and M. Ehrbar. **Verbesserung des Abtauens bei luftbeaufschlagten Verdampfern, Phase 2: Bewertung der Abtauprozesse.** Final report. Swiss Federal Office of Energy, 2002. ENET-Nr. 220187.
- G. Kulik, P. Hoffmann, and M. Zehnder. **Oberflächenbehandlung zur Vereisungsverringerung.** Final report. Swiss Federal Office of Energy, 2003. ENET-Nr. 230222.
- E. Lemmon, M. McLinden, and M. Huber. **NIST Reference Fluid Thermodynamic and Transport Properties - REFPROP, Version 7.0.** National Institute of Standards and Technology, 2002.
- G. Leyland. **Multi-Objective Optimisation Applied to Industrial Energy Problems, Thesis No. 2572.** PhD thesis, Swiss Federal Institute of Technology (EPFL), Lausanne, Switzerland, 2002.
- SIA. **Standard SIA 381/3, Society of Swiss Engineers and Architects,** 1982.
- SIA. **Standard SIA 384/2, Society of Swiss Engineers and Architects,** 1988.
- SNV. **EN 255-2: Air Conditioners, liquid chilling Packages and Heat Pumps with Electrically Driven Compressors - Heating Mode - Part 2: Testing and Requirements for Marking for Space and Heating Units.** Swiss Association for normization and Standards, 1997.
- J. Thome and J. El Hajal. **Two-Phase Flow Pattern Map for Evaporation in Horizontal Tubes: Latest Version.** In *1st Int. Conference on Heat Transfer, Fluid Mechanics and Thermodynamics*, page TJ2, 8-10 April, Kruger Park, South Africa 2002.
- U. University of Dayton. **Daily mean temperature, collected data since 1.1.1995,** 1995-2004. URL <http://www.engr.udayton.edu/weather/citylistWorld.htm>.
- M. Zehnder, F. Maréchal, S. Guex, J. Schiffmann, and D. Favrat. **Pompe à chaleur air-eau à haute température, Phase 2: Cycle à injection optimisé, essais journaliers et compresseur booster; Analyse thermo-économique.** Final report. Swiss Federal Office of Energy, 2002. ENET-Nr. 220219.

5. Oil migration in heat pumps

Lubricating oil is required to ensure the lubrication of the moving parts in a vapor compression refrigeration system. This oil is in contact with the refrigerant in hermetic compressor types and is partly entrained by the refrigerant vapor and migrates through the entire cycle. The initial charge of oil has consequently to consider the quantity of oil which is accumulated throughout the system. Oil is influencing the overall heat transfer coefficient in the heat exchangers, the frictional pressure drop in the conducts and is limiting the application range by its chemical and thermal stability. In system design the oil return to the compressor has to be considered, in order to ensure its lubrication in all regimes, during the lifetime of the heat pump.

Experiences with **two-stage compression heat pumps have clearly demonstrated one problem related to the oil migration**. An observation of the oil quantity in the two compressor shells, has shown a **departure of oil from the upper stage to the lower stage compressor**. In steady state heating, the upper stage compressor could run rapidly into failure, because of the lack of lubricant, if no equilibration is done. In order to reduce system related costs, oil separators and their related oil management system, can hardly be considered in small sized heat pump units.

A **reduction of the oil quantity¹**, is one of the issues in the actual research activities in the refrigeration sector. For addressing to this issue, a high precision on-line oil concentration measurement technique is required to enable a better understanding of the mechanisms governing the oil entrainment throughout the cycle. An improved method for oil concentration measurement applied to refrigerant mixtures, is presented in the next section.

5.1 Oil concentration measurement

5.1.1 Literature review of oil-concentration measurement techniques

Many different measurement techniques to evaluate the oil mass concentration in liquid refrigerant oil mixtures have been published in the open literature. The list below reviews these approaches and shows their application limits.

¹Oil free concepts have to be viewed as the final goal, but this technology is still very cost intensive and requires a new approach in the design of the compressor.

- **Mass sampling.**

This discontinuous method is based on the extraction of a mixture mass sample from the refrigeration system into a cylinder. By opening a needle valve on the vapor side of the cylinder, the refrigerant is slowly evaporating, and is separated from the liquid oil. The comparison of the measured weights of the cylinder in each step, allows to determine the oil mass concentration in the mixture. This approach is described in the ASHRAE/ANSI Standard 41.4 [ASHRAE, 1996]. The major advantages compared to other techniques are: high precision, low investment costs and the method can be applied without previous calibration to any refrigerant, including zeotropic mixtures. The main disadvantages of the mass sampling method is that it can not be applied for real time evaluations.

- **Techniques based on the physical properties of the fluids.**

Physical property based methods can reach a very high degree of precision (but require intensive calibration efforts). These precisions, however, are often limited to the calibrated fluids, and mostly are only reasonably applicable for binary mixtures. Several on-line methods are proposed in the literature.

- *Viscosity:*

The viscosity of liquid oil is in the order of 10^2 times higher than for the refrigerants and choosing a technique based on this property is a logical choice and has been applied in [Baustian et al., 1988a] with a bypass viscometer. The measured sensibility at low oil concentrations has been limited by a lower detection limit of ($\sim 2\%$), as has been confirmed later by [Cavestri and Schafer, 1999].

- *Density:*

[Bayini et al., 1995] presented a density based method with R-134a/POE oil mixtures at liquid temperatures between -10°C and 6°C , using a Coriolis effect density flow-meter. Average error of ($< 0.1\%$) are reported. If applied to heat pump cycles, the liquid temperatures are in a higher range (between 20°C and 50°C) and the density difference between the refrigerant (e.g. R-134a, R-407C) and the oil becomes very small, which reduces the resolution of this method, see also [Cavestri and Schafer, 1999].

- *Acoustic velocity:*

Several research groups have considered acoustic velocity measurements for an on-line detection of oil concentration in the refrigerant ([Baustian et al., 1988b; Meyer and Saiz Jabardo, 1994; Ahnefeld et al., 1996; Navarro de Andrade et al., 1999]) and reported good and reliable results ($< \pm 0.3\%$) based on calibration. The measurements showed temperature dependency but were considered to be poorly dependant with pressure.

- *Light refraction index:*

The in situ measurement of the light refraction angle of the refrigerant-oil mixtures

has been investigated by [Newell, 1996] and by [Zhou et al., 1997]. Test data with R-134a/PAG oil mixture, show a sensitivity of $< 0.1\%$ oil and a repeatability between data sets of $\pm 0.8\%$. This method is very interesting due to the low investment costs of the sensor, as is presented in the published article.

These property base approaches, however suffer from the uncertainty of the mixture composition, if applied to refrigerant mixtures. As this will be the case in the evaluated context, an alternative approach has to be considered.

- **High pressure liquid chromatography.**

[Cavestri and Schafer, 1999] investigated a high pressure liquid chromatography method using mass samples of $10\ \mu\ell$ volume. Lower detection limits have been found at oil concentrations, lower than 0.1% and when comparing the results with an adapted mass sampling technique, deviations of 1% between the two techniques are presented. Optimization of this method is still in progress. This approach is not recommended for detection of dynamic changes of the concentration, as one measurement takes several minutes.

- **Light absorption.**

The most promising approach to measure accurately mass concentrations of multi component mixtures are the methods detecting absorption of light. [Kutsuna et al., 1991; Suzuki et al., 1993] and [Biancardi et al., 1996] refer to UV-light absorption to measure oil concentration in binary mixtures, showing real time measurements with high sensitivity ($\sim \pm 0.1\%$) for refrigerant-oil mixtures at 1% or above. Temperature dependent calibration curves have to be set up for each analyzed mixing pairs.

This review shows, that many different approaches have been evaluated to measure oil mass concentration in refrigerants. Most of these techniques are reliably applicable to **binary mixtures**, but risk to produce high deviations if they are applied to refrigerant blends with oil. Measured concentration could be biased by a departure from the original composition of the refrigerant. Mass sampling or liquid chromatography are inconvenient, because of the mass extraction and time consuming measurement, preventing its use in real time measurement.

The measurement of light absorption is the most promising approach for high sensitivity analysis and for real time measurements. Measuring the absorption in a larger spectral range than showed by the articles of the above review, the composition control of the refrigerant mixture and the oil concentration measurement can be performed with the same results. **Fourier Transform Infrared Spectrometry** allows to combine these features and will be implemented in a calibration loop first and will then be applied to a two-stage heat pump cycle to measure the migrating oil.

5.1.2 Fourier Transform Infrared Spectrometry

Organic halogen molecules present strong characteristic vibrational absorptions in the mid region of infrared light. (The main absorptions are within the spectral range of 1500 -500 cm^{-1} .) By means of the **Fourier Transform Infrared Spectrometry (FT-IR)**, the qualitative and quantitative analysis of these compounds can be performed with very high sensitivity.

A *Nicolet - Magna IR 560* spectrometer, composed of an *Ever-Glo* light source, emitting light within the range of 4000 cm^{-1} to 650 cm^{-1} , a liquid nitrogen cooled *MCT-A detector* and a *KBr beam-splitter*, is used in this work. The ambiance of the optical components is purged with filtered and dried air with a constant air flow of 1200 l/h.

The measurement cell is an *attenuated total reflection* (Micro-ATR) cell. Using a single reflection on the surface of a diamond prism, the penetration depth of the immersing light into the refrigerant flow for the region of wavenumbers at 1000 cm^{-1} is at 4 μm ¹.

The number of reflections could be increased in order to improve the sensibility to low oil concentrations, but this has not been investigated in this project in order to keep the spectral output in the unsaturated range and therefore allow a control of the refrigerant composition.

The setup of the Micro-ATR /FT-IR measurement is represented in Figure 5.1.

FT-IR theoretical approach

The setup of the Figure 5.1 corresponds to a **Michelson interferometer** type of spectrometer. It is based on a separation and recombination by interference of the polychromatic electromagnetic waves.

According to the type of the laser source, the emitted light has a spectral intensity $B(\sigma)$. Assuming an ideal beam-splitter, 50% of the emitted light is deviated to the fixed mirror and the remaining light is transmitted to the moving mirror (which is translating at constant speed u). After reflection, the two contributions are recombined at the beam-splitter. The recombined signal contains the interference information corresponding to the relative distance of the two mirrors from the beam-splitter. Considering a single frequency σ , the recombined electromagnetic wave has a time dependent output of

$$I(t, \sigma) = B(\sigma) \cos(2\pi \sigma ut) \quad (5.1)$$

¹The penetration depth in ATR measurement is directly proportional of the wavelength and is function of the incident angle of the laser beam, of the refractive indexes of the prism and of the analyzed substance, see [Christy et al., 2001]. The output intensity is corrected by the software (OMNIC) provided with the spectrometer. This is mainly done to get a comparable output spectrum with commercial spectral libraries.

The integration of all the contributions over the entire spectral range results in the time dependent output signal.

$$I(t) = \int_0^{\infty} B(\sigma) \cos(2\pi\sigma ut) d\sigma \quad (5.2)$$

This interference $I(t)$ output, or **interferogram** is redirected by additional mirrors through the measurement unit (in the present case the Micro-ATR cell), where part of the energy is absorbed by the analyzed medium. The attenuated signal $I'(t)$ is arriving to the detector and the information is converted into a digital output.

The spectral intensity $B'(\sigma)$ of the transmitted signal is extracted by the algorithm of the *Fast Fourier Transformation*, using the output of an entire path length of the moving mirror (this is corresponding to one scan of the measurement).

The intensity of the laser source and the intensity losses along the traversed path of the laser beam are subjected to variations in time, conditioned by the purge state and by the presence of particles

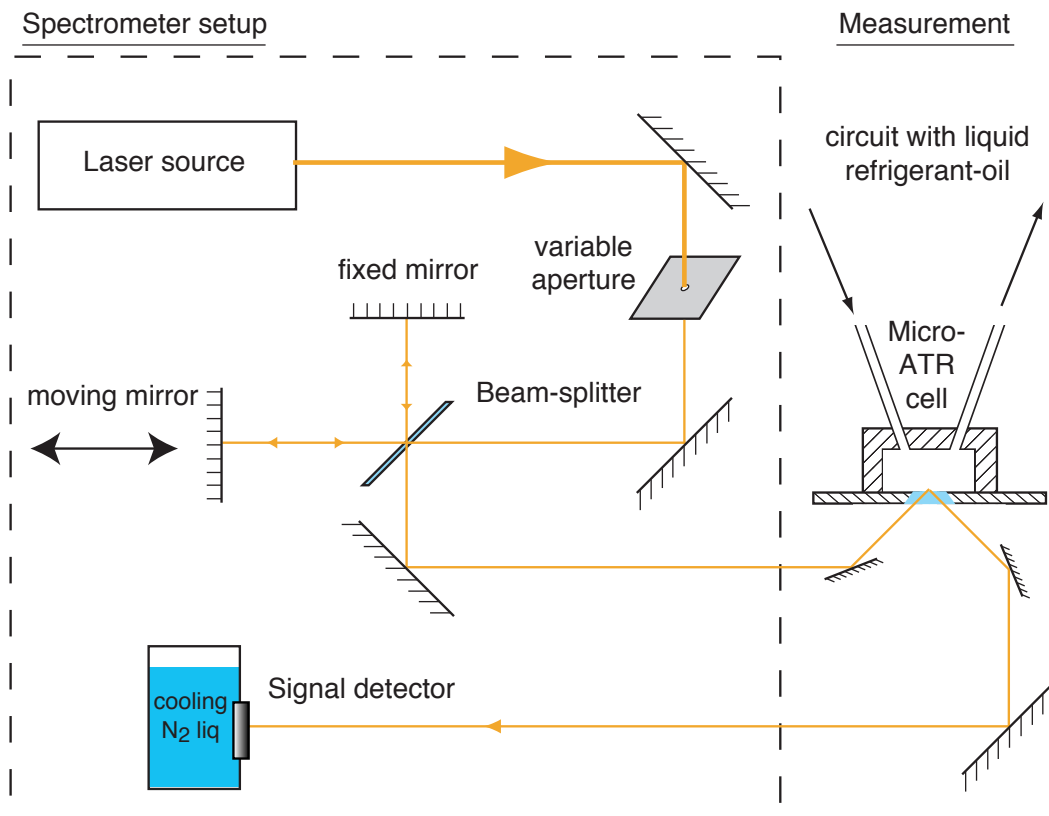


Figure 5.1: Schematic view of the measurement setup using a Fourier Transform Infrared Spectrometer with an ATR single reflection measurement cell, to measure weight concentration of refrigerant-oil mixtures.

in the environment. To get high quality spectral output, the collection of a reference spectrum with the **background** is required with an empty and clean measurement cell, following a standard procedure.

Quantitative Analysis

The infrared spectrometry allows high sensitive measurement of substances in the three phases solid, liquid or gas. Energy absorption in the infrared range is due to vibrational resonance of polar molecules. Mono-atomic substances or non polar compounds (e.g. the diatomic nitrogen and oxygen) are not influenced by the presence of an electromagnetic field and are thus not absorbing energy from electromagnetic waves. These gases are often used as diluent. Filtered and dehydrated air is also used as neutral gas, for example to permanently purge the spectrometer.

Quantitative analysis is based on the three following hypotheses:

1. The substance is absorbing energy in the spectral range, which is measurable with the spectrometer.
2. Each analyzed compound has its characteristic absorption spectrum.
3. For a fixed path length, the absorbed total energy is proportional to the molar concentration of each substance of the mixture.

The first two conditions can be verified experimentally and the third condition is known as **Lambert-Beer's Law**:

$$A = e \cdot b \cdot c \quad (5.3)$$

Where **A** is defined as the **absorbance** and is related to the **transmittance T** by the following expression.

$$A = \log \frac{1}{T} = \log \frac{B}{B'} \quad (5.4)$$

The coefficients composing the fundamental law (in eq. 5.3) are: e = molar extinction coefficient, b = sample path length and c = molar concentration. The molar extinction coefficient is characteristic for each substance and is linked to the frequency $e = e(\sigma)$. It defines the fingerprint of the compound and can be compared with spectral libraries.

Lambert-Beer's law is submitted to the following restrictions:

1. At high concentration or at non appropriate path length in the sample, the transmitted signal can saturate and the linearity of the law with concentration is not anymore valid.

2. The analysis has to be performed at equivalent thermodynamic conditions. As the substances can be influenced by the presence of other components, calibration has to be performed with the mixture to be considered.
3. The mixture has to be perfectly homogeneous, as the laser beam is only penetrating into a thin sublayer in proximity of the wall.
4. The mixture does not mutually react internally or with the materials of the cell.

Reference IR absorption spectra of the analyzed liquids are presented in section [5.2.2.1](#).

5.1.3 Coriolis densimeter (Bopp&Reuther DIMF 2.0 TRV)

A high precision Coriolis effect densimeter has been used to compare concentration measurements in the calibration loop and in the heat pump in the lower temperature range.

Indicated specifications are:

Repeatability of the measurement: $< \pm 0.02 \%$ ($\pm 0.2 \text{ kg/m}^3$ @ 1000 kg/m^3) with in the flow range of:

- Density range: $400 - 2000 \text{ kg/m}^3$
- Temperature limits: -40°C to 150°C
- Mass flow range: $0 - 50 \text{ l/min}$
- Limit pressure: 100 bar

Measured densities of pure fluids are very close to calculated values obtained by the program Refprop, comparisons are shown in section [5.2.2.2](#).

5.1.4 Mass sampling

The mass sampling method is described in [[ASHRAE, 1996](#)] as a standard method to measure oil concentration in liquid refrigerant. This method has been used to compare the obtained results from the other selected approaches.

The procedure is composed by:

1. Weighing of the cleaned and evacuated cylinder (300 ml).
2. Connection of the cylinder to the refrigeration circuit in the liquid line of interest and transfer of the mass sample during ~ 30 s.
3. Weighing of the total mass.
4. Controlled evaporation of the refrigerant through a liquid column (in order to control the evaporating flow.) The resulting evaporation flow has been measured at about 0.5 l/h (13 g/h).
5. When evaporation flow is terminated (no vapor bubbles are released anymore), the cylinder is again evacuated during a short time sequence (~ 30 s).
6. Weighing of the final mass of the cylinder including purified oil of the sample.

Sensibility of the balance is at ± 0.01 g.

5.2 Calibration tests

5.2.1 Calibration setup for oil-refrigerant concentration measurements

A separate test circuit has been built (Fig. 5.3), in order to compare measurements of the three presented methods (FT-IR, densimeter and mass sampling) and to calibrate the new approach of using the FT-IR spectrometer with a single reflection Micro-ATR cell.

The calibration test circuit is composed of:

- An oil free gear pump.
- A brine water cooled condenser heat exchanger to control temperature level of the liquid loop.
- A phase separation vessel to ensure a liquid phase only test section and to act as an expansion chamber when varying temperature/pressure conditions.
- A heat exchanger in the vapor phase, to control the pressure.
- An oil injection syringe, for injection of known oil quantity.



Figure 5.2: Oil concentration calibration test circuit with FT-IR Spectrometer on the left side, oil injection syringe in the center and the liquid refrigerant lines in the lower part of the picture.

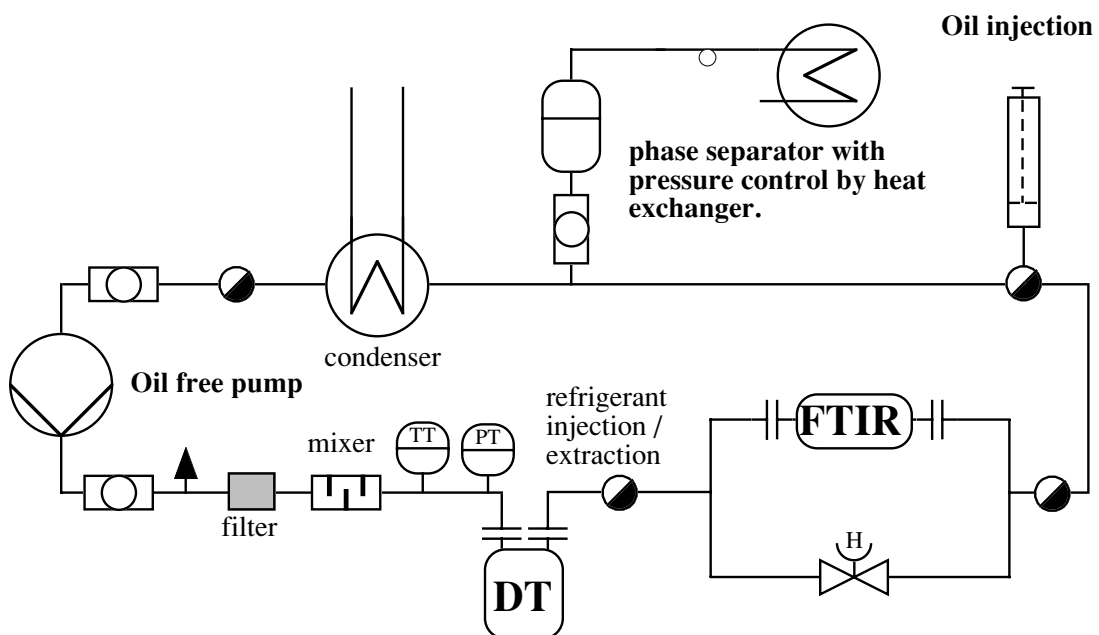


Figure 5.3: Schematic representation of the setup for calibration tests in a liquid circuit with controlled oil injection.

- A filter-dryer and a mixing tube, to ensure homogeneous conditions at the entry of the measurement devices.
- A pressure transducer and a thermocouple.
- A high pressure security valve.

The liquid volume of the circuit (until the level of the sight glass situated below the separator) is 3.77 ℓ , which corresponds to a refrigerant charge of 4.6 kg for R-134a and 4.4 kg for R-407C at saturated liquid at 20°C.

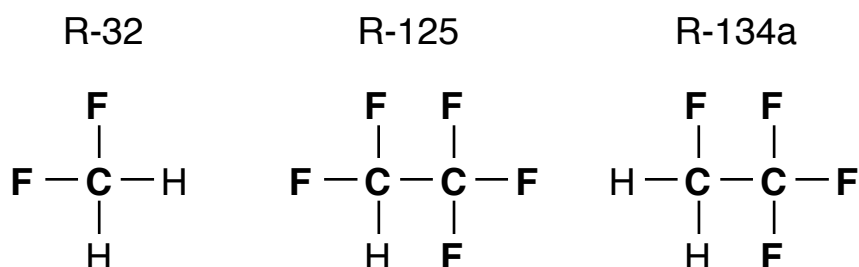
5.2.2 Pure fluid calibration

5.2.2.1 Vibrational-rotational infrared absorption spectra

Several test runs have been performed in order to optimize the test procedure for the FT-IR measurements with pure refrigerants. Spectral output of the refrigerants is first compared with pure oil, in order to ensure the applicability of this method with the chosen fluid combination.

The three pure refrigerants R-134a, R-125 and R-32 and the zeotropic mixture R-407C have been charged into the test loop and the resulting reference spectra at 21°C saturation temperature are presented in Fig. 5.4 and 5.5.

The absorption peak region of the three refrigerants is very similar, due to the similarity of their molecules, as shown below



Measured vibrational absorption spectra of the refrigerants are summarized in Table 5.1. Additional absorptions in the region of higher wavenumber ($\sim 3000 \text{ cm}^{-1}$), thus at lower wavelength, have not been considered, because of the low penetration depth of the light into the medium, when single total attenuated reflection cell is used. Common peaks of R-134a and R-407C, the two fluids on which the measurements will be focusing on, are located at $\sim 1167 \text{ cm}^{-1}$, 965 cm^{-1} and at

839 cm^{-1} . As will be shown later, the most important common peak at $\sim 1167 \text{ cm}^{-1}$ is also in the absorbance range of the analyzed POE oil.

Vibrational spectra of the corresponding fluids are found in [Nielsen and Halley, 1965; Mizuno and Saeki, 1976; Compton and Rayner, 1981]. The literature data is measured with refrigerants in the gas phase and peak locations are slightly shifted compared to the present results.

Table 5.1: Maximum absorbance of the strongest peaks for pure refrigerants R-134a, R-125 and R-32 including the zeotropic mixture R-407C at 21°C. Measured with Micro-ATR single reflection cell with liquid refrigerant.

Maximum Absorbance	Peak position [cm^{-1}]								
	719	839	862	965	1038	1055	1082	1126	~ 1167
R-134a	-	0.28	-	0.62	-	-	0.53	-	1.25
R-125	0.40	-	0.40	-	-	-	-	1.06	-
R-32	-	-	-	-	1.24	-	-	-	0.09
R-407C	0.13	0.16	0.16	0.38	-	0.66	-	0.40	0.77
	Peak position (cont.) [cm^{-1}]								
	1186	1281	1286	1296	~ 1431	1462			
R-134a	-	0.90	-	-	0.17	0.11			
R-125	1.10	-	-	0.40	-	-			
R-32	-	-	-	-	0.07	-			
R-407C	-	-	0.56	-	0.11	-			

The vibration-rotation spectrum of the POE type lubricating oil is summarized by the peak absorbance given in the list below (see also Fig. 5.5). The corresponding spectrum is compared to R-407C showing an important isolated vibrational absorption at 1740 cm^{-1} . This vibrational mode can be used for the quantitative analysis of refrigerant oil concentration measurement. A second strong absorption at 1150 cm^{-1} is situated very closely to the strongest absorption of the refrigerants R-407C and R-134a. In order to decouple mutual influence this absorption band has not been used for both, refrigerant and oil, in the concentration measurements.

Comment: Attention has to be paid to impurities of humidity in the housing of the spectrometer. One of the absorption regions of water is located between $1600\text{-}1800 \text{ cm}^{-1}$, which is in the corresponding range of the located free peak of the lubricating oil.

The strongest absorption modes for the lubricating oil are (strongest peaks are in bold):
EAL Arctic 22 CC: 1020, 1120, **1150**, 1220, 1370, 1470, **1740**, 2850, 2920, 2950 cm^{-1}

In order to verify the sensibility of the spectra with variable temperature and pressure, the refrigerants R-134a et R-407C have been tested at different conditions. Results are summarized in the Figures 5.6, presented with relative absorbance, referring to the most important absorbance of the

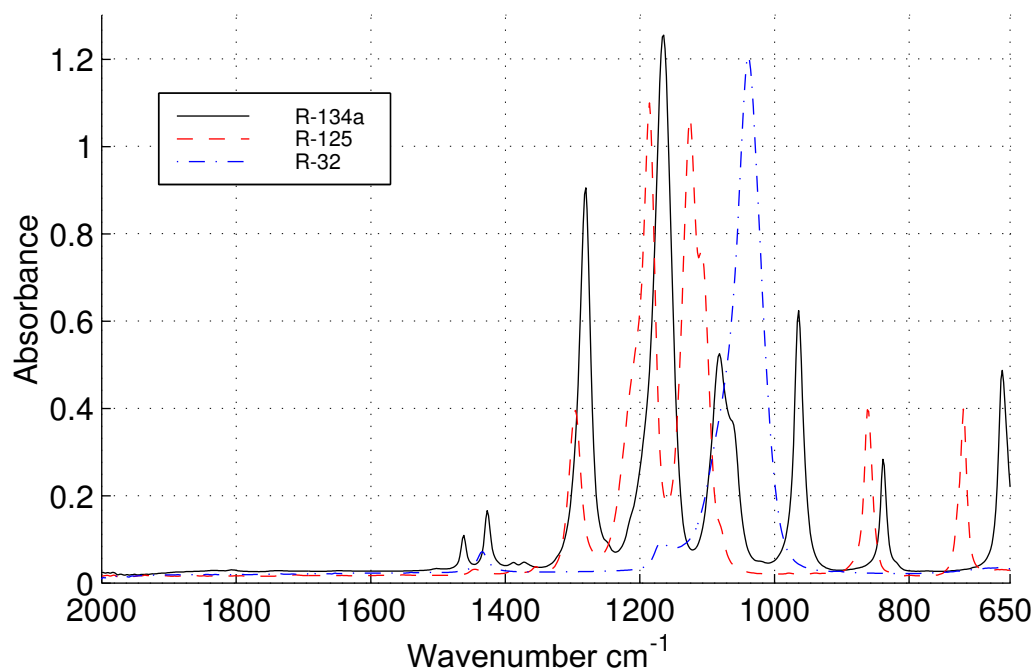


Figure 5.4: Liquid refrigerant infrared absorption spectra of R-134a, R-32 and R-125 at 21°C.

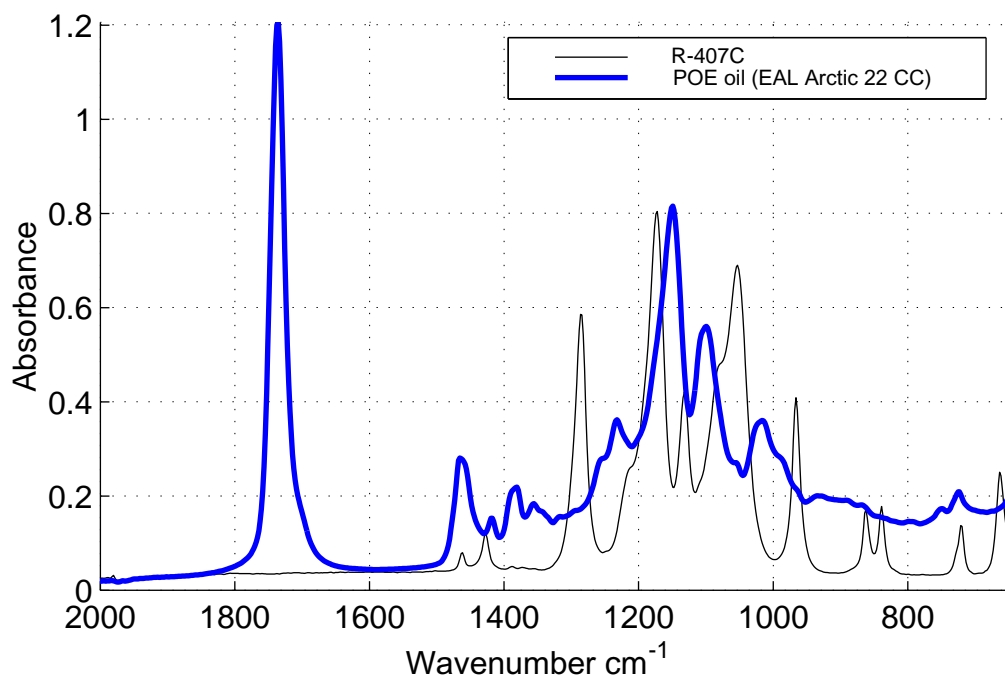


Figure 5.5: Liquid infrared absorption spectra of zeotropic refrigerant R-407C (R-134a, R-125, R-32 [0.52;0.25;0.23]) at 21°C and of POE lubricating oil EAL Arctic 22 CC.

respective fluid. Error bands show the minor change with variable pressure, while temperature influence is much more important. The graphs are useful for the verification of the composition of R-407C during heat pump tests.

5.2.2.2 Density measurements of pure refrigerants

Most of the collected refrigerant density data was obtained very close to liquid saturated conditions. Figure 5.7 shows the comparison of experimental and calculated data, using Refprop v.7, [Lemmon et al., 2002]. Relative errors of $\sim 0.05\%$ for R-134a and of $\sim 0.3\%$ for R-407C demonstrate the precision of the used densimeter¹. The density uncertainties of the mixture R-407C is sufficient high, that oil concentration measurement, based on the density measurement are subjected to errors of 2% in combination with the used oil.

5.2.3 Refrigerant-oil mixtures

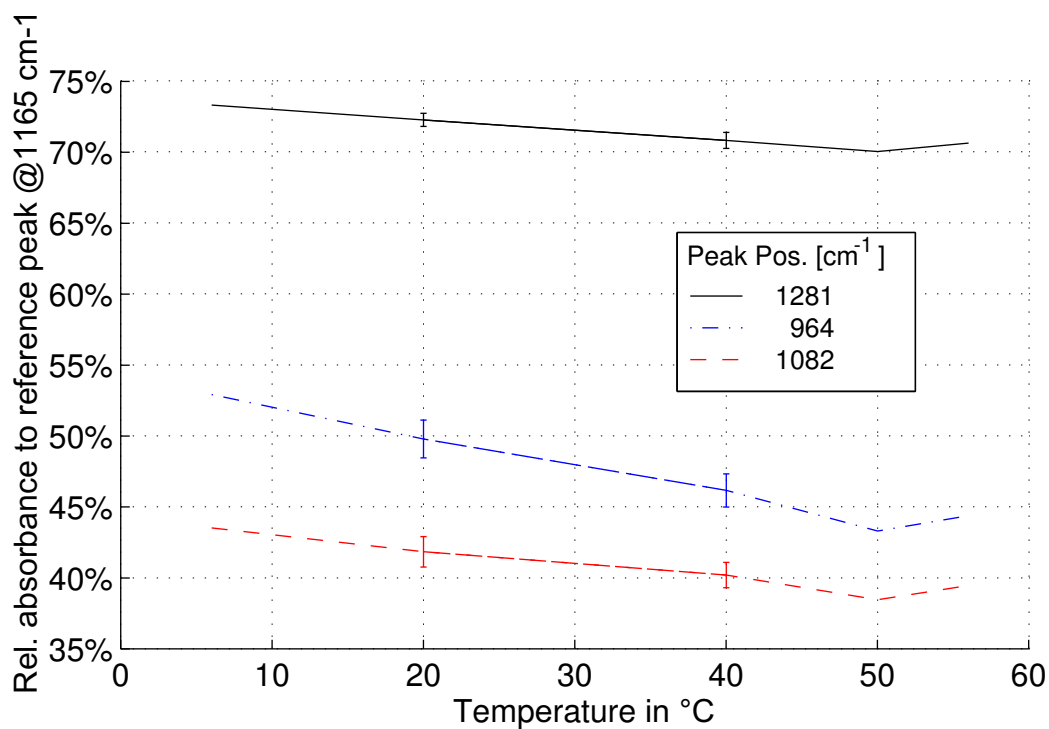
Calibration tests are performed with refrigerant-oil mixtures at known oil mass concentrations varying between 0.23% and 5%. Infrared vibrational measurements are then compared to the known nominal oil concentrations and to the density measurements over a range of pressure and temperature, showing the sensitivity of the applied new method.

The nominal oil concentration is calculated by mass balance of the circulating refrigerant (in a volume of 3.77 ℓ , resulting in a refrigerant charge of ~ 4.5 kg) and the injected oil through a syringe. This oil quantity is introduced by manually actuating the wheel of the syringe, which has a charging mass of 19.4 g oil per revolution of the wheel. This introduced mass corresponds to a oil concentration of $\sim 0.43\%$. The exact oil concentration is calculated, accounting for the effective circulating refrigerant mass, which is calculated with the corresponding density of the used refrigerant.

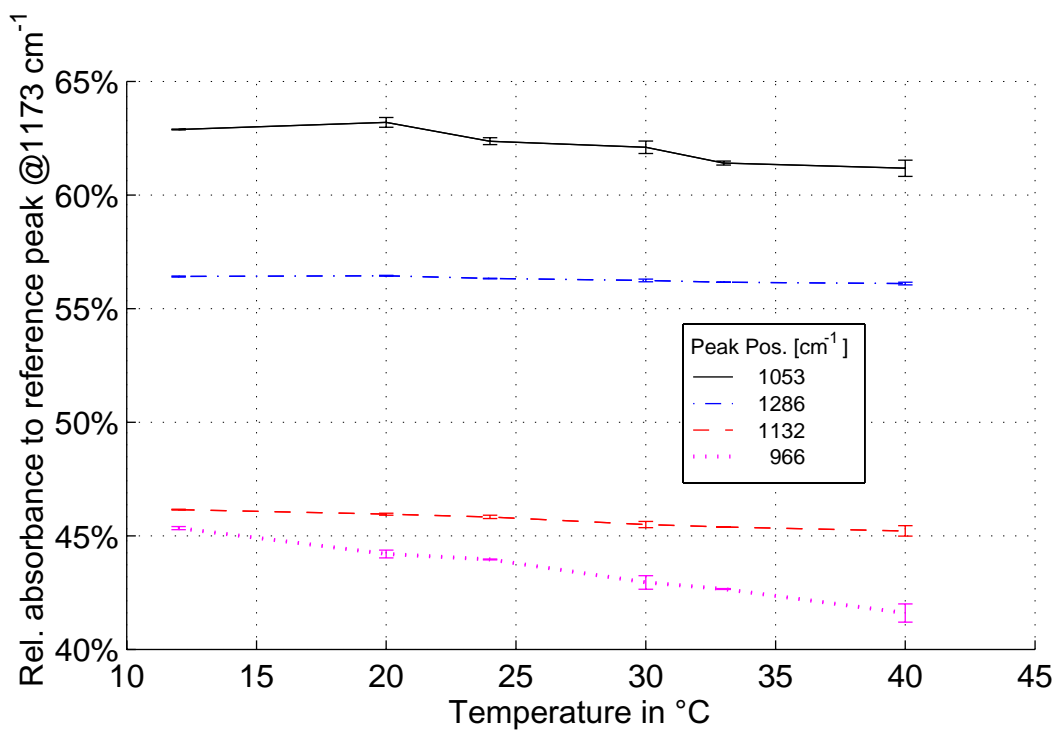
5.2.3.1 Oil concentration calibration tests with the FT-IR method

As the environmental measurement conditions (intensity of the laser source, temperature, purge state, alignment of the mirrors) are subjected to fluctuations, the best results for quantitative analysis are obtained by comparison of the peak intensities, selecting isolated absorption modes of

¹The equation of state used in the Refprop program for R-134a is known to be very accurate. It is based on the international standard formulation published by [Tillner-Roth and Baehr, 1994]. Industrial R-407C composition can deviate from the nominal concentration with maximal 2% on each component, which has an impact of up to 0.4% on the density error (saturated liquid at 20°C).



(a) R-134a



(b) R-407C

Figure 5.6: Relative absorbance in vibrational IR spectra of liquid R-134a and R-407C at variable temperature.

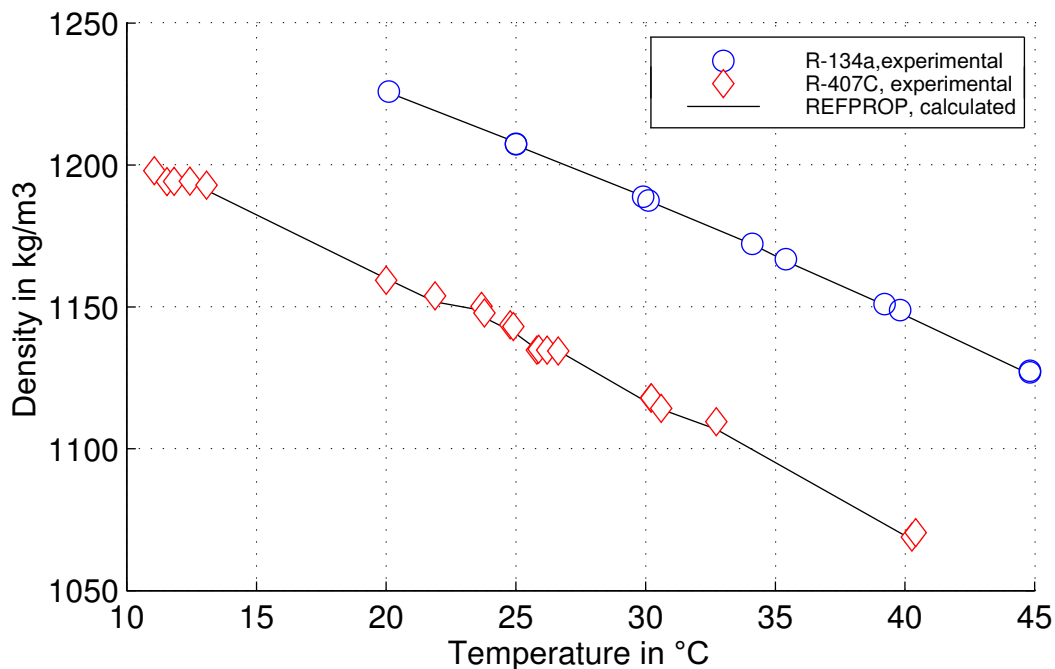


Figure 5.7: Comparison between experimental and calculated (with Refprop v.7) density of (oil free) R-134a and R-407C, using a Coriolis densimeter. (The departure from the continuous evolution, seen in the R-407C density points, is due to the subcooling compressibility.)

each constituent. Figure 5.8 shows the decoupled spectra of the three components of R-407C. Absorbance at 1038 cm^{-1} for R-32, 965 cm^{-1} for R-134a and 719 cm^{-1} for R-125 allows to define the contribution of these refrigerants in the R-407C spectrum. Deconvolution over the entire spectrum, in order to decompose the mixture into its pure contributions, is limited by the liquid interaction of the fluids. In Figure 5.9 measured and calculated infrared spectra of R-407C are compared and regions of fluid interactions (between $1300\text{--}1000\text{ cm}^{-1}$) are visible.

As R-134a is the most important contribution in R-407C, the associated absorbance at 965 cm^{-1} is selected and relative absorbance with the main oil peak at 1740 cm^{-1} (see Fig. 5.5) is computed for the oil mass concentration calibration. According to Lambert-Beer's law (eq. 5.3), linear evolutions are expected for increasing oil concentration. Data of the couples R-134a/POE oil and R-407C/POE oil are presented in Figures 5.10 (a+b).

The slope of the linear evolutions for the two refrigerants (R-134a and R-407C) is set by a 3rd degree correlation in temperature

$$f_{oil} = -6.77 \cdot 10^{-6} T^3 + 9.23 \cdot 10^{-4} T^2 - 4.28 \cdot 10^{-2} T + C_r \quad (5.5)$$

with the refrigerant dependent constant:

$$C_r = 1.21 \text{ for } R-134a \text{ and } C_r = 0.883 \text{ for } R-407C.$$

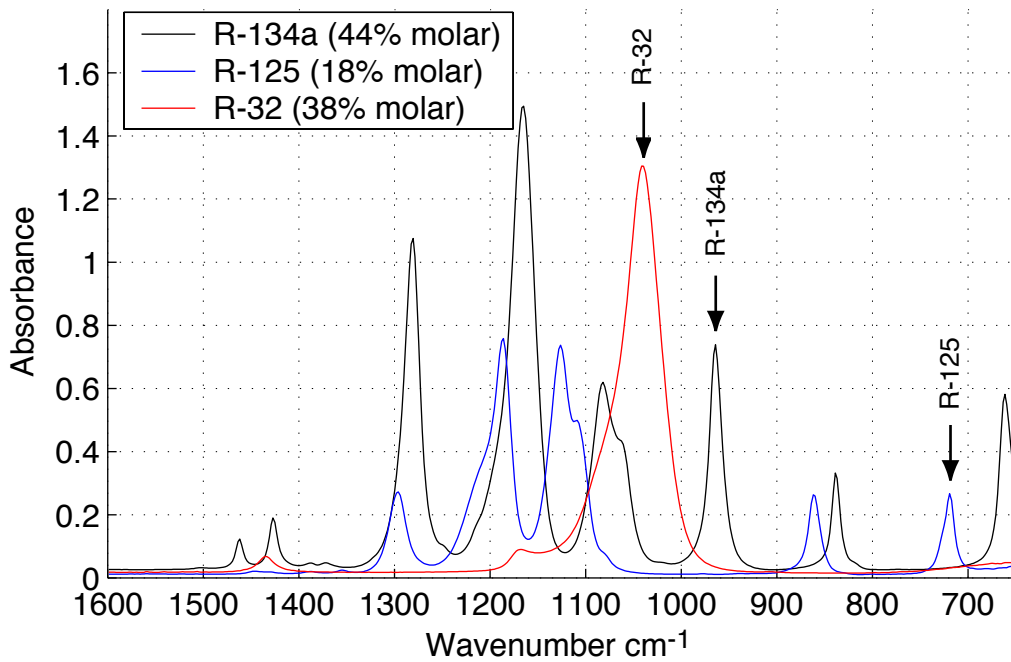


Figure 5.8: Infrared vibrational absorption spectra of liquid refrigerants R-125, R-32 and R-134a, measured at 20°C.

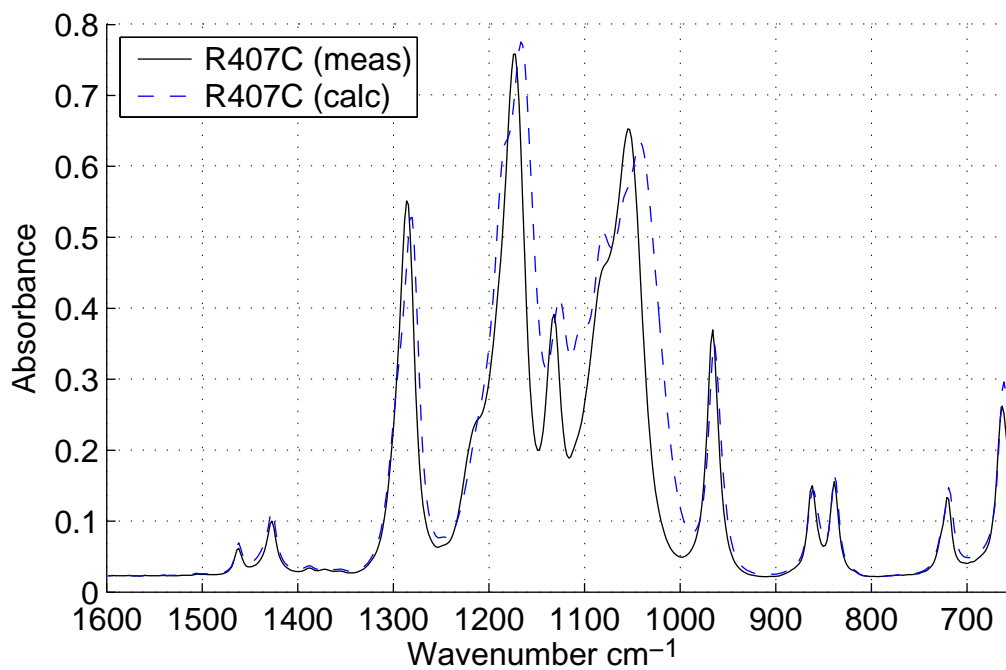
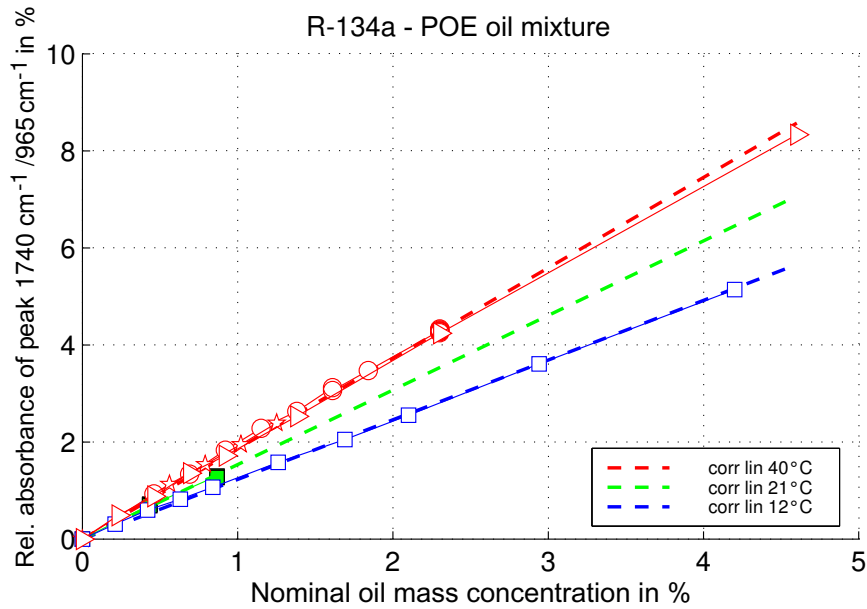
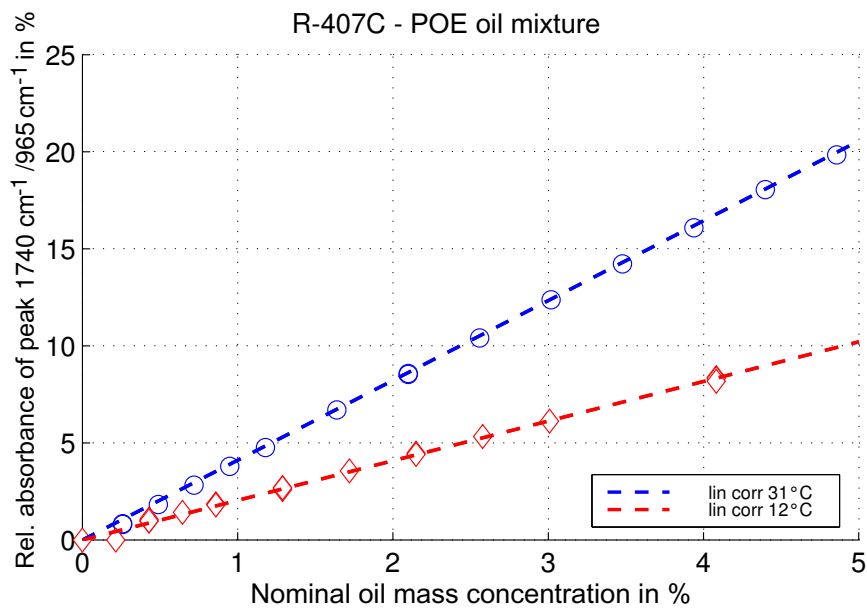


Figure 5.9: Comparison of calculated (ideal mixture) and experimental infrared vibrational absorption spectra of zeotropic R-407C at 20°C.



(a) R-134a



(b) R-407C

Figure 5.10: Relative absorbance of POE oil peak at 1740 cm^{-1} with refrigerant peak at 965 cm^{-1} of R-134a and R-407C refrigerants.

Using this empirical correlation, the oil concentration is calculated based on the relative peak absorbance of the oil to the refrigerant with

$$w_{oil} = f_{oil} \frac{A_{oil,1740}}{A_{refr,965}} \quad (5.6)$$

Collected data during heat pump tests, have shown the validity of the proposed correlation with mass samples taken in parallel and with dynamic oil injection tests. Comparison results are presented in section 5.3.

Detection limit of oil mass concentration with FT-IR measurement.

Oil mass concentration in refrigeration cycles are expected to be as low as 0.5% - 1.5%, see [Ahnefeld et al., 1996; Biancardi et al., 1996]. This requires for the measurement method to have with very low detection limits. In the spectrometric approach, the oil absorbance cannot be identified with confidence for oil concentrations below 0.3%. An evolution of the oil peak with increasing oil concentrations is shown in Figure 5.11. The oil absorbance at a nominal concentration of 0.43%, is clearly distinguishable from the noise. The noise level increases with time difference between the collected spectrum and the recording time of the last background spectrum. Variations of the ambient conditions (temperature and purging) influence the highly sensible spectral output and should be kept as constant as possible.

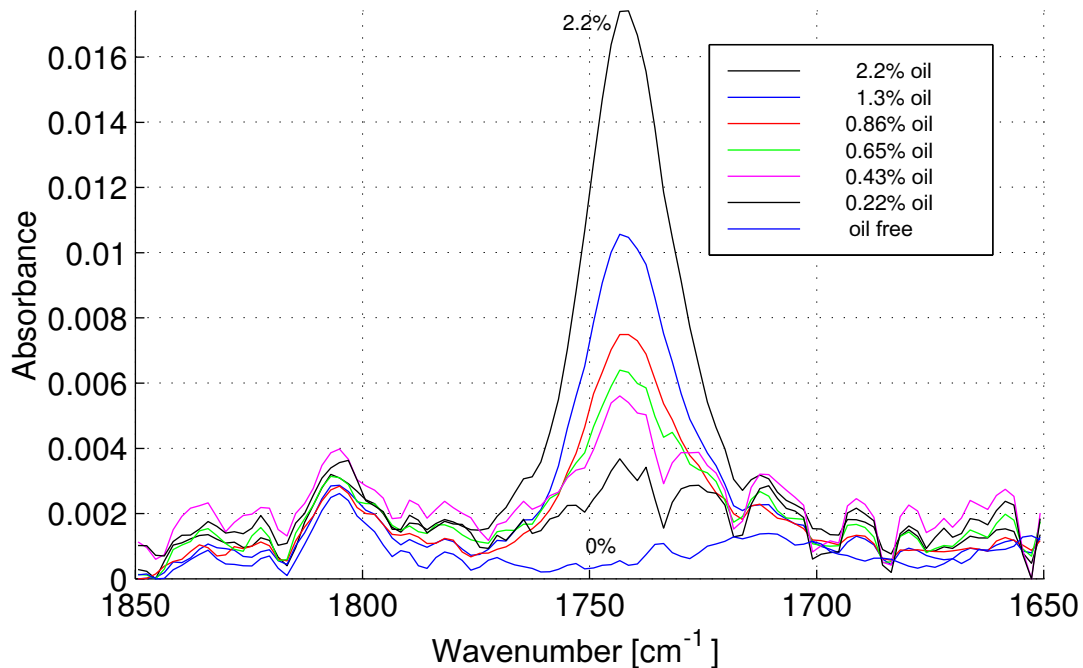
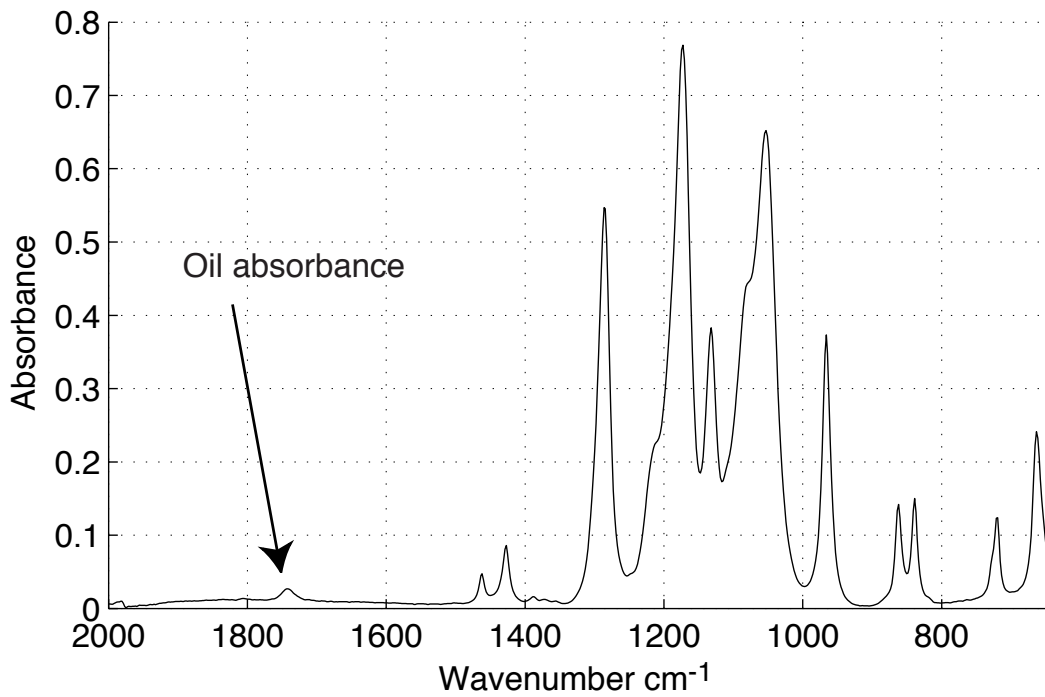
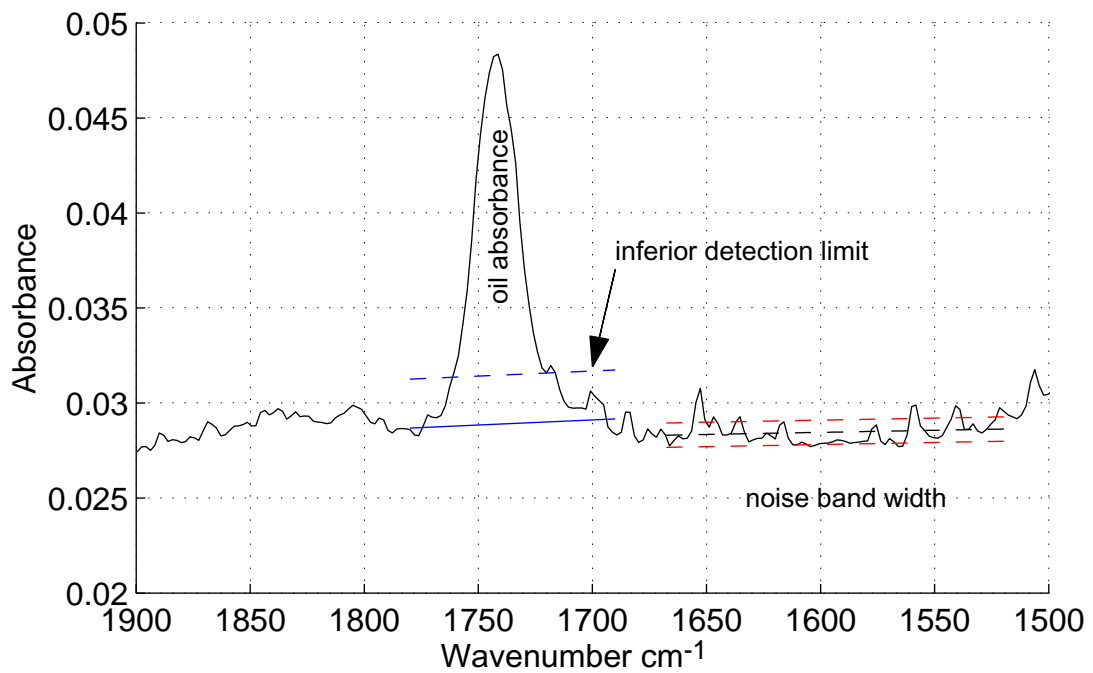


Figure 5.11: Evolution of POE oil absorbance at 1740 cm^{-1} from 0% oil to 2.2% oil mass fraction in R-407C.



(a) R-407C with 2% POE oil



(b) Noise level and oil peak absorbance

Figure 5.12: Example of measured refrigerant-oil spectrum and minimum peak level with indicated RMS-noise level bandwidth.

The noise of the measurement is defined by the absorbance fluctuations in non absorbing regions near to the oil peak. Minimum detectable absorbance peak height is set to a signal to noise ratio of 2. The noise level is defined by the RMS-fluctuations and is shown in Figure 5.12.

Signal to noise ratio can generally be increased by considering a longer path length traversing the sample. This also increases the sensitivity of the FT-IR method, but on the other hand saturation of the most important absorbances can occur¹ Detection limits in the range of 0.3% of oil and a sensitivity of <0.1% have been judged to be sufficient to continue with the selected setup.

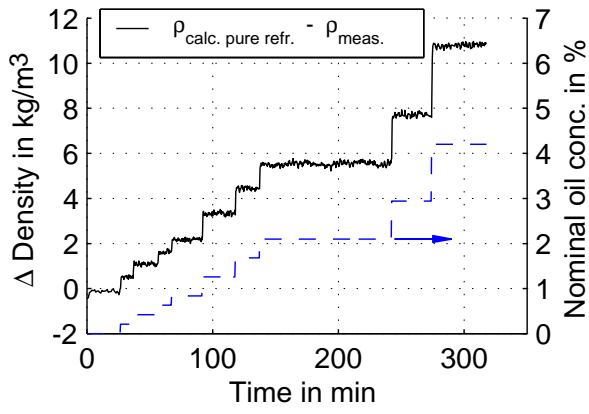
5.2.3.2 Oil concentration measurements using Coriolis type densimeter

Measured mixture density for oil injection series on the calibration loop are plotted in Figures 5.13 and 5.14 in differential form comparing calculated pure fluid density and measured mixture density.

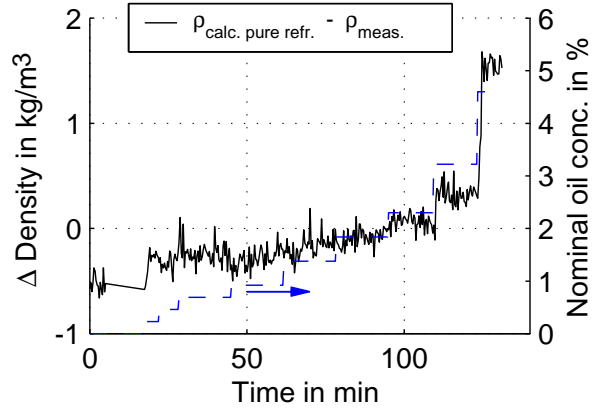
Measurements of R-134a/POE oil mixtures at 12°C show highly correlating results between nominal oil mass concentration and density evolution. Oil concentration could be predicted with the precision presented in [Bayini et al., 1995]. Measurements of the other mixture (R-407C/POE oil) have less density difference between each oil injection step but oil concentration can be predicted satisfactory at 12°C. In opposition to these results, measurements at 30°C and 40°C do not allow oil concentration predictions anymore. This is due to the small density difference of the pure oil and refrigerant and is also caused by liquid mixture effects (presence of an excess volume).

The indicated time scale also demonstrates the stability of the oil concentration during calibration tests and the frequency of the oil injection steps.

¹Absorbances near to the saturation (absorbing more than 95% of the light energy) are already occurring for the pure fluids, but not for the mixture R-407C. A compromise would consist of a setup with variable detection path length as is proposed by the FT-IR components supplier. But this option has been rejected due to the high additional costs.

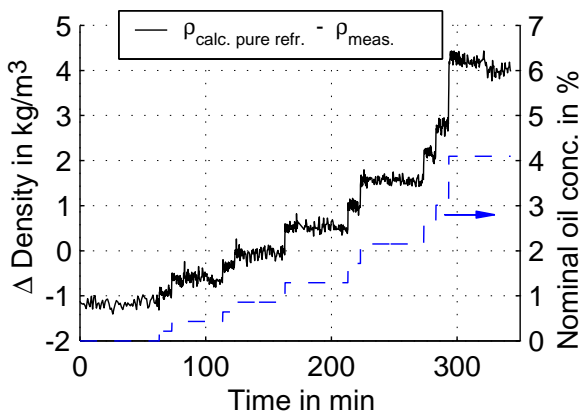


(a) R-134a, 12°C

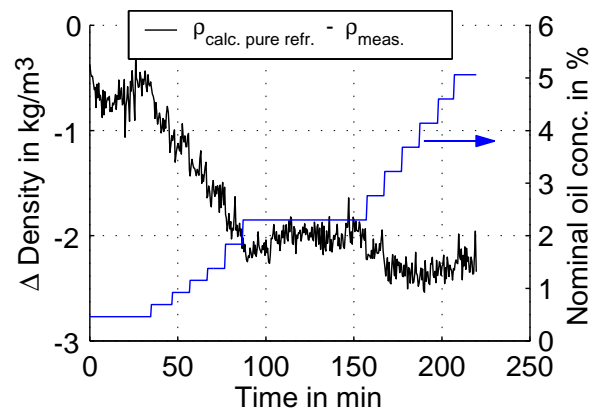


(b) R-134a, 40°C

Figure 5.13: Mixture density of R-134a and POE oil.



(a) R-407C, 12°C



(b) R-407C, 30°C

Figure 5.14: Mixture density of R-407C and POE oil.

5.3 Oil migration in heat pump cycle

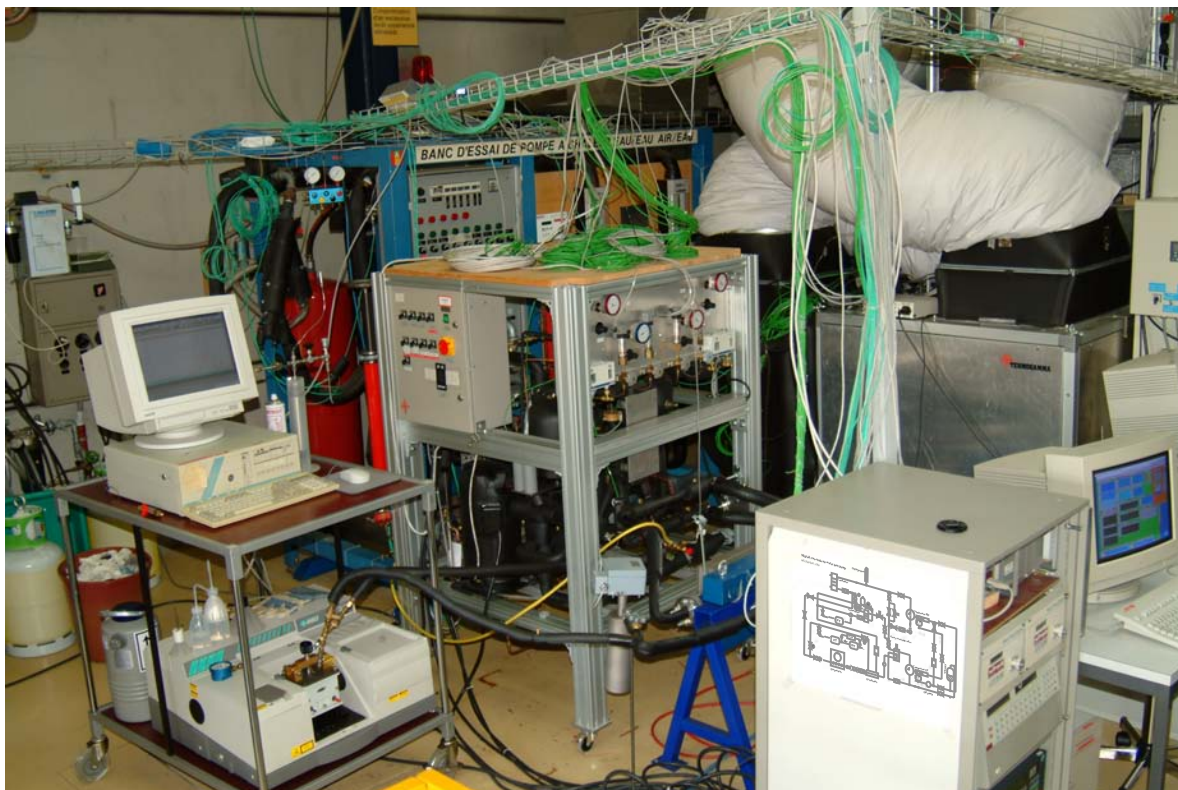


Figure 5.15: *Picture of the two-stage compression cycle, air-water heat pump. Base heat output 10 kW, refrigerant R-407C and POE oil EAL Arctic 22CC. Including oil migration measurements.*

Oil migration has been extensively measured on a 10 kW heating, air-water heat pump, including two-stage compression cycle with an economizer heat exchanger and a suction line overheater. Performance test results on this unit are presented in the third configuration of section 2.3.3. Test runs were performed with the zeotropic mixture R-407C. An annex oil circuit enables oil transfer, by means of a pump, from low to the high pressure level, to compensate for the important oil transfer during heating in steady stage operation.

The operating tests include one-stage and two-stage compression heating and defrosting modes.

5.3.1 Oil traps and size of the piping

According to the technical descriptions of the used POE oil, it is perfectly miscible with the employed refrigerants, within the temperature range of heat pump test conditions. It can therefore be assumed, that the liquid refrigerant-oil mixture is homogeneous and oil transport is guaranteed in the liquid parts of the heat pump cycle, regardless of the flow speed and flow direction. The ap-

appropriate design of the tube diameter in liquid flow is conditioned by pressure drop considerations. In horizontal and descending tubes no gravity force is opposing the flow, oil transport is done by fluid shear. In ascending vapor flow, with the presence of oil, an annular or mist flow is required in order to ensure the oil transport. This therefore depends on the flow speed, the flow orientation and the corresponding thermo-physical properties of the interacting fluids. The system has to be designed carefully in order to avoid possible oil traps on the circuit.

Critical locations for oil transport in the two-stage heat pump cycle are discussed below:

1. Collector tube at the exit of the evaporator and suction line to compressor.

Oil return to the compressor in refrigeration and air conditioning units is widely discussed in open literature, in order to minimize oil charge in the compressor and to ensure long time operating mode of the installation. The work of [Biancardi et al., 1996] has been depicted and equation 5.7 is used to calculate minimum mass velocity in all the vapor lines of the heat pumps.

$$G_{min} = 0.7225 \sqrt{\rho_{vap} g D (\rho_{vap} - \rho_{liq})} \tag{5.7}$$

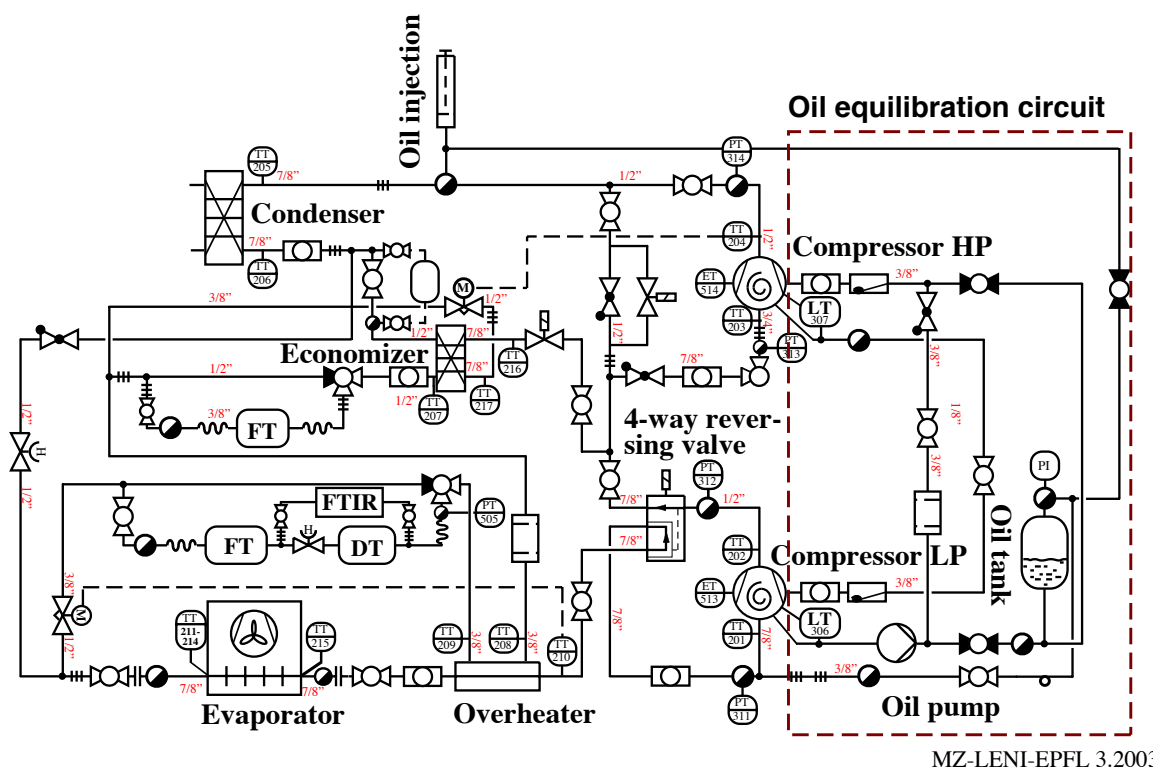


Figure 5.16: Flow chart of the experimental two-stage compression, air-water heat pump including annex oil equilibration system.

The minimal mass flow conditions for oil entrainment are represented in Table 5.2, using the corresponding layout of the prototype heat pump. Data are calculated with the thermodynamic conditions, issued from the cycle simulation program. In our test facility and in order to be conservative and to avoid oil accumulation, which would bias the analysis, real mass flow are at least three times higher than the calculated values for oil entrainment.

2. 4-way reversing valve.

A 4-way reversing valve is mounted on the suction and discharge lines of the lower stage compressor to initiate reversed cycle defrosting mode. An internal slide assembly, that moves to connect the appropriate ports in heating or in defrosting operating mode, generates additional pressure drop and leakage flow from the discharge to the suction flow. The leakage rate has been measured in [Bertsch and Ehrbar, 2002] for the same valve type and can be quantified in the order of 1 to 3 mg/(s bar) (leakage tests were performed with nitrogen and R-22). Assuming the maximum pressure difference of 20 bar, a leakage of 60 mg/s is resulting due to the presence of the reversing valve. This corresponds to 0.2% of the refrigerant mass flow in the lower stage compressor. In two-stage heat pump cycle the pressure difference is reduced and the leakage rate is much lower ($< 0.1\%$). Entrained oil is mainly transported with an annular film on the tube walls. Leakage flow in the reversing valve is assumed to be an oil rich flow, and it is possible, that at extreme operating conditions in single-stage configuration, the amount oil flow transiting into the remaining cycle is slightly reduced. In two-stage configuration, the pressure difference is reduced between the connected lines in the reversing valve and leakage can therefore be neglected.

3. By-pass line of the 2nd stage compressor.

The by-pass of the 2nd stage compressor is open in single-stage heating mode. This line is a vertical up-flow line with a T-separation in the discharge line of the first stage and the suction line of the second stage compressor. This flow bifurcation is the only critical point of the cycle, where the oil transport could be interrupted. Long time tests have however demonstrated a correct oil return during the single-stage heating runs. The liquid level in the operated compressor has remained at a stable level throughout the tests.

4. Refrigerant vessel.

The charged POE oil (EAL Arctic 22 CC) is a specific composition for the use with R-134a and R-407C and is miscible over the whole application range. For this reason, also in the refrigerant vessel after the condenser, no stratification is expected to be present and oil will entirely transit into the remaining circuit.

Table 5.2: Minimal mass flow rate [g/s] for oil entrainment in vertical upflow with refrigerant (R-407C) vapor.

Operating point	evaporator exit D=7/8"	suction HP compressor D=1/2"	inlet condenser D=1/2"	exit economizer D=1/2"
A-7/W60	11.1 [g/s]	17.7 [g/s]	6.6 [g/s]	4.3 [g/s]
A0/W50	12.6 [g/s]	18.5 [g/s]	6.0 [g/s]	4.7 [g/s]
A7/W40	14.2 [g/s]	19.5 [g/s]	5.3 [g/s]	5.7 [g/s]

5.3.2 Liquid level measurement in the compressors

In order to verify the real time measurements of oil mass concentration with the methods presented in the sections 5.1.2 and 5.1.3, the compressor vessels have been modified in order to add external sight glasses permitting a visual control of the liquid level in the compressor. This level indicators were filmed with a camera and allowed to guarantee a correct lubrication of the higher pressure compressor, which during all two-stage tests was continuously losing oil. Other types of level transducers have been evaluated, but had to be rejected due to lack of precision¹, especially during transitory operating modes, where foaming of the oil would have perturbed the oil level indicators.

Correspondence of liquid level and oil mass transfer

Based on the compressor technical drawings and on the estimated volumes of the annexe level indicator and the level regulator, a map linking the liquid level with the oil mass change (oil assumed at 20°C) has been established. This correspondence is represented by the Figure 5.17 for both compressors.

The total amount of oil added or removed from each compressor is calculated by integration of the mass function $m(h)$, defined for each compressor.

$$\Delta M_{oil} = \int_{h1}^{h2} m(h)dh \quad (5.8)$$

The observation of the liquid level change in both compressors enables to calculate variation of the total oil quantity accumulated in each compressor (eq. 5.8). This variation is the result of the flow balance between the suction and discharge port of the compressors.

In one-stage compression cycle, the liquid level is expected to be stable during steady-state operating conditions. A negative evolution would therefore indicate an oil loss and thus an oil accumulation in the heat pump cycle. During start-up conditions the liquid level decreases, due to the amount of absorbed refrigerant.

¹The high electric resistance and the low dielectric-constant are the main reasons, which do not allow a high precision level measurement by using an ultra-sound or radar type level transducer in this application.

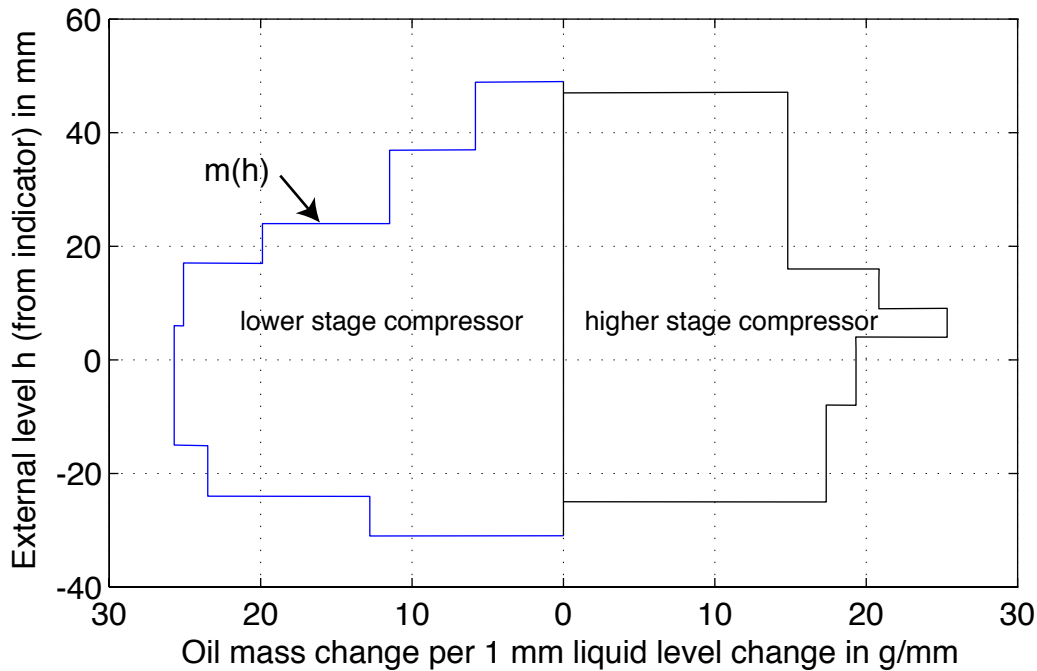


Figure 5.17: Corresponding oil mass in the compressors with the indicated external level height.

In two-stage steady-state operating mode, the measured level change indicated the amount of oil, which gradually migrates from one compressor to the other. In conditions of no oil accumulation in all the remaining circuit of the heat pump, the liquid level change in the compressors will be inverse, showing a gain in one compressor and a loss in the other. The gain and loss should be of equal absolute value, which is referred as the net oil transfer rate.

The effective oil concentration in the heat pump cycle is composed of the global oil flow and of the additional net oil transfer rate. Since the measurement of the liquid levels in the compressor does not provide any information of the global oil flow, this technique does not allow to conclude directly to the effective oil migration.

5.3.3 Oil mass concentration in single-stage and two-stage heat pump

5.3.3.1 Applied methods

All the localized measurements of oil mass concentration have to be applied in a liquid flow, in order to ensure a homogeneous fluid. This limits the possible locations for sample removal or the installation of the other measurement devices to the liquid line between the exit of the condenser and the inlet of the main expansion valve. Coriolis type densimeters are known to be very sensible of the presence of vapor bubbles. Sub-cooled liquid is found between the overheater/sub-cooler heat exchanger and the expansion valve. Fourier Transform infrared spectrometer (FT-IR) and the

densimeter (DT) are implemented in parallel and in line with the mass flow meter (DT, type K-20), as shown in Figure 5.18. Mass sample removal is done at the same level, through a schrader valve to transfer the refrigerant-oil sample into the test cylinder. The control of the presence of oil in the compressors has been made manually through the external level indicators mounted on both compressors. All the employed devices are shown by the pictures 5.19.

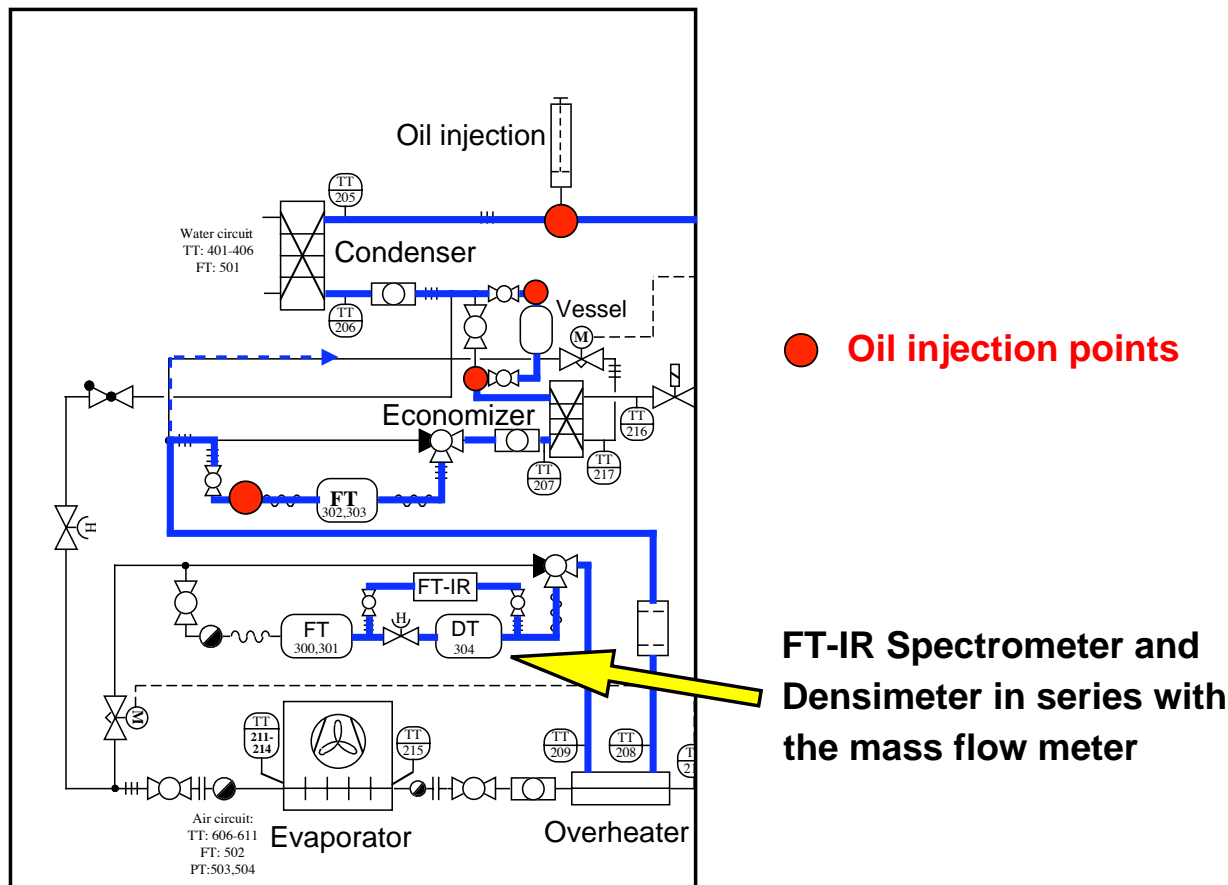
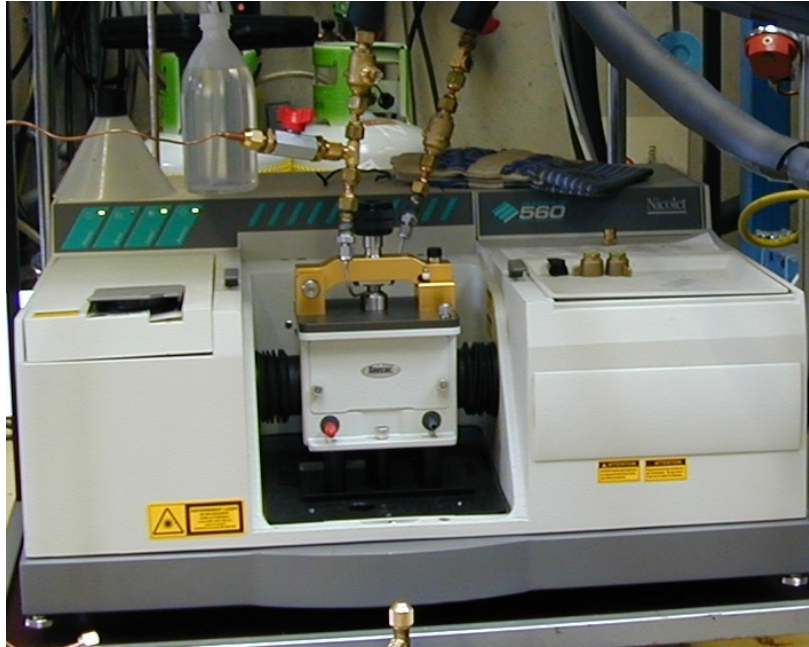


Figure 5.18: Schematic view of one part of the heat pump cycle with indication of the location for real time oil concentration measurements and of the oil injection points.

5.3.3.2 Injection of a known quantity of oil into the circuit

Injections of a known quantity of oil, as a package, into the heat pump cycle, allow to check if the applied methods, to determine the oil migration under real conditions, work appropriately. This approach shows also if any separation effects occur due to unexpected inhomogeneity of the liquid phase. The oil packages can be injected by means of an oil syringe at several locations in the heat pump cycle. The possible locations for direct injection are (see Figure 5.18):

- Condenser inlet, in the gas flow.
- Condenser exit / refrigerant vessel inlet.



(a) FT-IR spectrometer



(b) Densimeter



(c) oil level indicators



(d) Mass sampling

Figure 5.19: Pictures of measurement devices related to oil migration through the heat pump cycle.

- Refrigerant vessel exit.
- Exit of high stage mass flow meter (type K-100) located before mass bifurcation for the injection flow.

These multiple locations also enable the control whether an important quantity of the injected oil mass is retained by any of the elements, which are located between the injection point and the measurements. The elements, which can be verified by this method are: the condenser, the refrigerant vessel, the economizer, the high stage mass flow meter (type K-100), the filter dryer and the in-line overheat exchanger. The measured time delay between the injection start and the apparition of the oil peak in the vibrational spectra (FT-IR method), as well as the time dispersion of the peak compared to the duration of the injection are represented in the tabulated results (Tab. 5.3) of these injection series.

The amount of oil corresponds to a mass of 19.4 g (for one revolution of the actuated wheel of the oil syringe), which was introduced during an approximate time space of ~ 11 seconds. Some of the injections were realized with the double amount of oil. The manual action on the wheel did not allow a uniformly distributed injection flow introduced into the circuit. The maximum frequency for the collection of the infrared spectra is limited to one measurement each 3 seconds, density measurements were recorded with the time interval of 5 s. Transitory FT-IR responses are plotted in a 'waterfall' plot, using a selected reference spectrum, which was recorded during steady-state run before the injection. The differential data in the spectral region of the oil peak (1600 cm^{-1} to 1850 cm^{-1}) visualizes the appearance of the additional oil absorption (see Fig. 5.20), which passes through the spectrometer. The origin of the time scale is synchronized with the injection start.

Oil mass balance is calculated with the total mass flow measured with the high stage mass flow meter. As the measurement of the oil concentration is located after the mass flow separation point, the arriving oil quantity is reduced. The assumption of homogeneous flow mixture is also applied at this flow separation point and the concentration remains unchanged.

Table 5.3: Oil injection packages during steady stage two-stage heating.

	A-2/W50	A-2/W50	A-7/W50	A-7/W50	A-7/W50
Injection location	cond. inlet	cond. inlet	cond. inlet	after K-100	after K-100
Refrigerant vessel	open	closed	open	-	-
Oil conc. perm.	0.39%	0.36%	0.27%	0.25%	0.26%
Oil mass (nom) [g]	35.7 (38.8)	37.3 (38.8)	16.3 (19.4)	21.1 (19.4)	46.7 (38.8)
Duration transition	112 s	90 s	106 s	19 s	39 s
Duration injection	22 s	22 s	12 s	8s	18 s
Delay peak appear.	38 s	19 s	45 s	15 s	9 s

Table 5.3 shows the summary of the results obtained by oil injection. Operation mode and injection location are indicated. The nominal oil concentration corresponds to the concentration measured by FT-IR method before starting the injection. Summation of the additional oil concentration during the transition phase provided the cumulated oil mass, which is compared to the injected oil amount. These measurements have shown a good agreement between the nominal mass and the measured quantity. Oil mass loss has not been registered and precision is limited by the frequency of recorded spectral data. Time delay and signal disparity are both increasing significantly when the refrigerant vessel is connected and the refrigerant flow has to go through it. The data also provide an information about the filling of the vessel. The present data shows an additional delay of 20-30 s and an increased signal disparity of 20 s. These injection series show, that oil is not remaining for a long time in one of these elements and finally transits to the liquid lines of the cycle. Densimeter results are much less stable than the FT-IR spectral output, but the transition of the oil package is also visible.

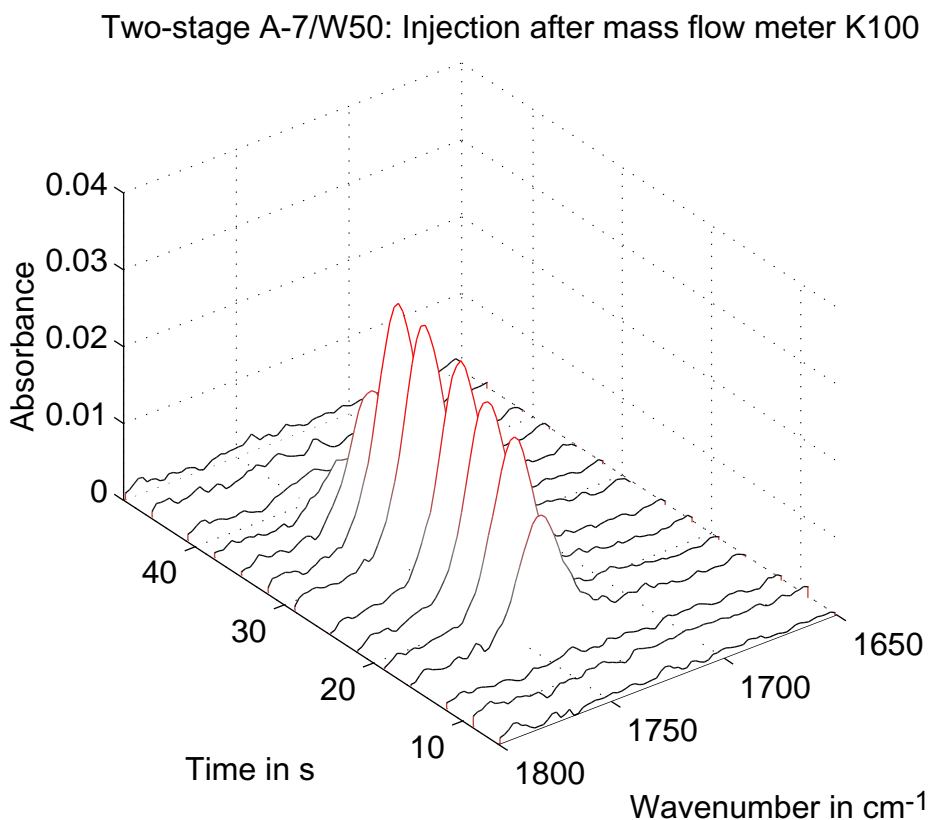


Figure 5.20: *Transiting oil package, which is injected after the high stage mass flow meter (K-100). Injected oil mass 39 g during 18 s.*

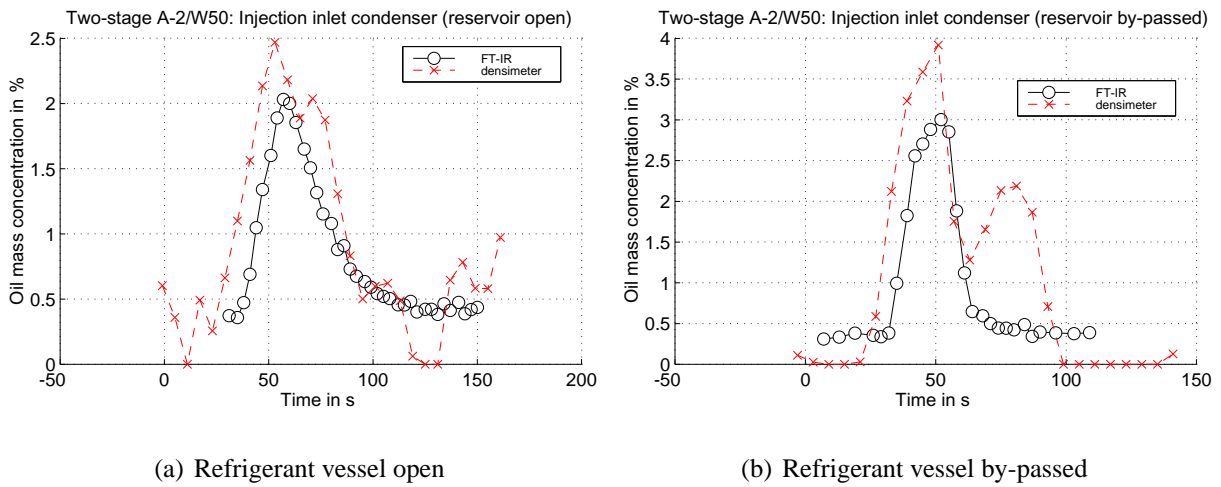


Figure 5.21: Oil mass concentration with oil injection in two-stage heating mode at A-2/W50. Evolutions measured with infrared vibrational absorbance and with density measurement. Injection at condenser inlet, refrigerant vessel open and closed.

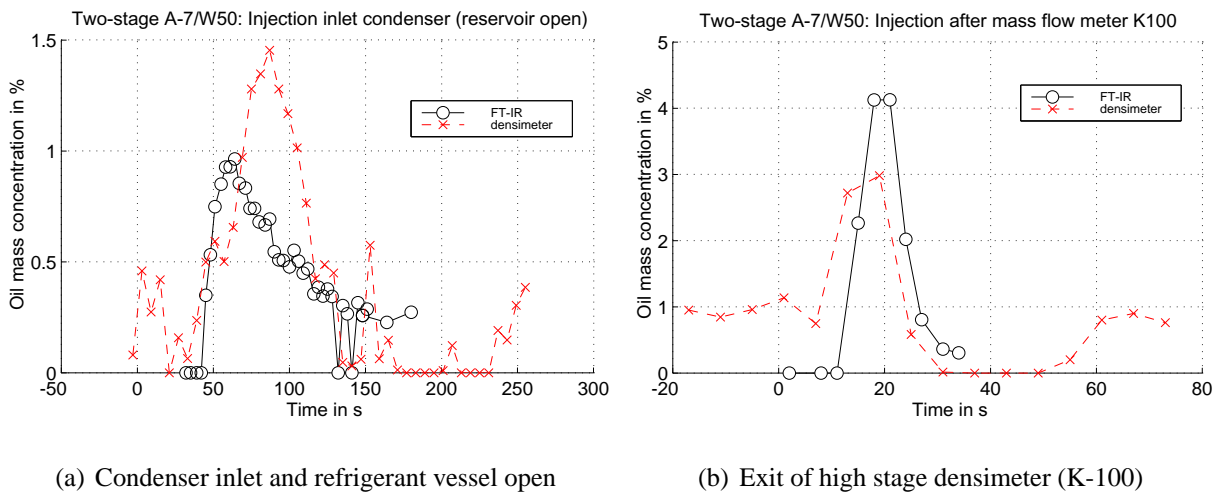


Figure 5.22: Oil mass concentration with oil injection in two-stage heating mode at A-7/W50. Evolutions measured with infrared vibrational absorbance and with density measurement. Injection at condenser inlet, refrigerant vessel open and at the exit of the high stage mass flow meter (K-100).

5.3.3.3 Oil migration in steady state operating conditions

The heat pump operating points are defined by the external temperature conditions (A=air inlet temperature in °C, W=water exit temperature in °C).

Heating, two-stage cycle: A-12/W50 A-7/W50 A-2/W50 A2/W50 A7/W50 A7/W60

Heating, one-stage cycle: A7/W50 A-2/W50 A-7/W50 A7/W35 A7/W60 A-7/W35

Measured oil mass concentration in steady state operating conditions, for the two-stage compression heating cycle, is rather low and corresponds to the lower values found in literature [Ahnefeld et al., 1996; Biancardi et al., 1996]). The thermodynamic conditions for the measurement with a densimeter are such, that a correct evaluation of the oil concentration should be possible, but as shown by the graphs of Figure 5.23, the fluctuations of the calculated oil mass concentration are still important and do not allow to define the mean concentration with high confidence (the flow conditions, although, could be kept very stable).

Figures 5.24 (a-f) show an overview of the measured oil concentration in the two-stage cycle and compare the results of the applied measurement methods. FT-IR spectra and oil mass sampling (if available) show corresponding results. The oil concentrations are found to be lower than expected and are in the range of the lower detection limit of the FT-IR method. By the variations of the liquid levels in the two compressors, the quantity of migrating oil is estimated, assuming 0% oil leaving the first stage compressor. This corresponds to a conservative estimation of the oil concentration and is in the same range as the other two methods (but is subjected to higher fluctuations).

Oil mass concentrations in two-stage cycle are measured in the range of 0.2% to 0.4% at A7 to A-2, and even below for evaporating conditions defined by air inlet temperatures of A-7 and A-12. The results are too close to the detection limit of the infrared absorption method to perform a correct sensitivity analysis (influence of the parameters, like flow speed, viscosity, density, temperature and pressure) with the obtained results.

Oil transfer from the higher stage compressor to the lower stage compressor is clearly detected and confirms the observations of a previous project including a two-stage compression cycle [Nidegger et al., 1997]¹. Oil mass transfer is in the range of 5 to 10 g/min, which requires regularly refilling by an auxiliary oil regulation system. Continuous heating is limited to 1-2 hours service, after this time period, the oil level in the upper compressor shell reaches the lower limit with a risk

¹In this former two-stage compression cycle, the lower stage compressor is a piston type compressor (Bristol-Inertia) and not a scroll type as is used in this second setup. The now implemented 4-way reversing cycle valve, situated between the two compressors, could be subjected to an increased internal leakage, acting as a bypass of the migrating oil. This type of valve is however not implemented in the first setup. In spite of these changes in the geometrical setup, the qualitative results of oil migration are however very similar.

of lubrication failure. Figure 5.25 shows an evolution of the liquid levels with intermediate oil refilling from an external oil tank.

No favorable operating conditions could be identified within the range of parameter regulation, to stabilize the oil distribution. Transitory effects are evaluated in the next section. An external oil equilibration mechanism is however required to ensure long term lubrication of the upper stage compressor in two-stage heating. Different solutions are discussed in section 5.4.

Oil migration in one-stage compression heating mode

When operating the lower stage compressor alone in a one-stage compression cycle, a very low amount of measured oil concentration results. The concentrations are lower than the detection limit of the on-line measurement devices (FT-IR spectra show an absorbance at the noise level, densimeter allow no conclusion). The very low oil mass concentration of 0.13% at A-7/W50 and

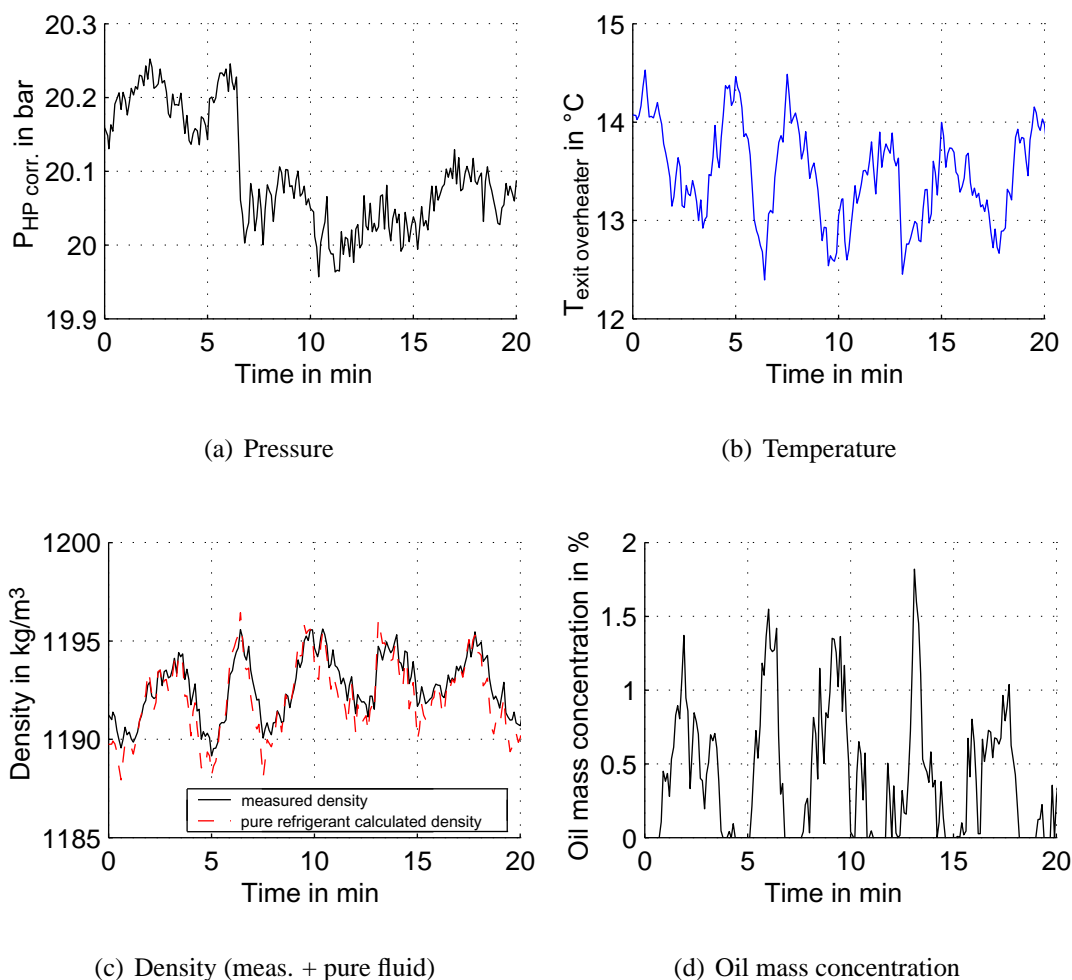


Figure 5.23: Influencing parameter for the determination of the oil mass concentration by the Coriolis type densimeter. Example of two-stage heat pump at A-2/W50.

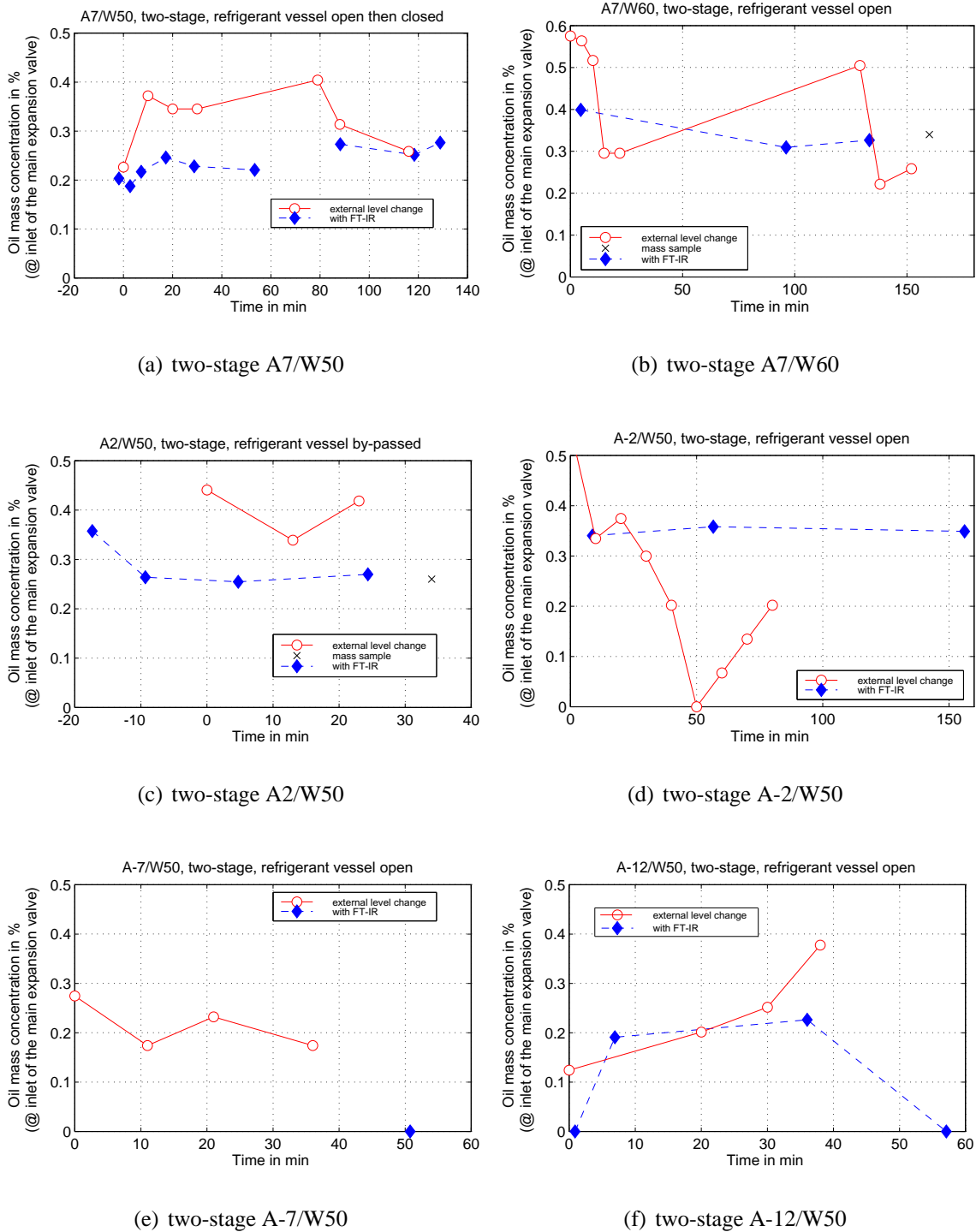


Figure 5.24: Oil mass concentration measurements in two-stage heating cycle. Comparison of infrared absorption method (FT-IR), mass sampling and corresponding concentration due to oil level change in the compressors (assuming no oil transfer from low stage to high stage compressor).

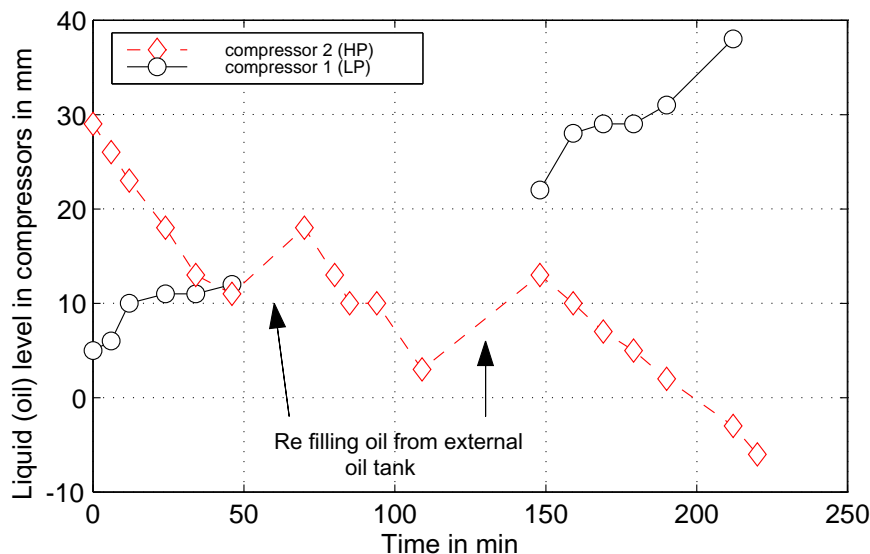


Figure 5.25: Evolution of the liquid levels in the compressors, in two-stage heating mode at A-7/W50.

~0% at A7/W50 have been measured by the mass samples and confirmed the observations.

The origins of this low oil concentration in the one-stage operating mode, as the amount of oil leaving the lower compressor in two-stage mode, cannot be entirely evaluated by the performed measurements and more fundamental work is required to check if this can be explained by some specificities in the geometrical setup or by the thermo-physical properties of the used fluids.

Accumulation of oil in the cycle (e.g. oil trapping) did not occur, as the liquid level in the operated compressor remained unchanged for long term steady state heating mode. Tests with a connected and by-passed refrigerant vessel have been performed in order to verify its influence. The measurement location can also not explain the low amount of oil, as the injected oil packages have been entirely measured (see results in section 5.3.3.2).

5.3.3.4 Transitory effects on oil migration during steady state heating

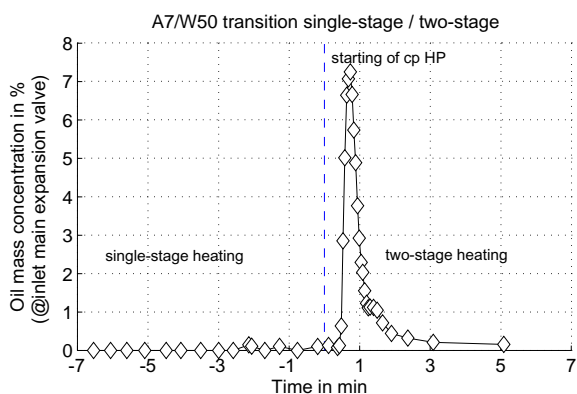
Several transitory effects in heating mode of the heat pump have been studied. Transitions have been generated by manual variation of the regulation parameter of the expansion valve, producing a variation of the superheat temperature at the compressor suction line and modifying the injection flow. Other transitions are related to the connection or the by-pass of the refrigerant vessel after the condenser or the change of one-stage to two-stage compression cycle.

Figure 5.26 (a) shows an important peak of increased oil concentration leaving the upper stage compressor, which has been started at the point 0 in the indicated time scale. This significantly higher migration of oil can be explained by the accumulation of refrigerant in the oil during the

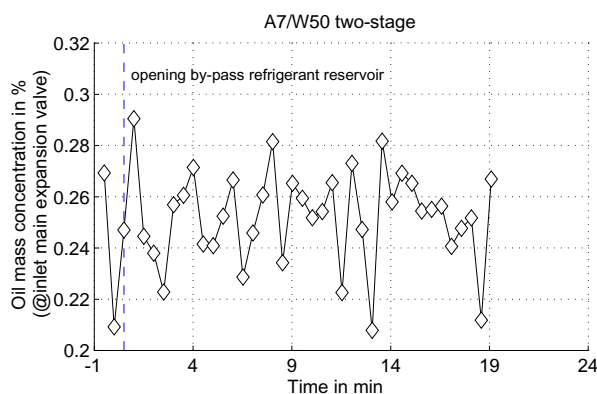
time, when the upper compressor is not operated. During startup the pressure level in the compressor shell decreases and the refrigerant evaporates forming an emulsion resulting in oil molecules to be entrained to the compression chamber from which they leave the compressor. The observed liquid level change in the compressor can therefore only partly be explained by the exhaust of solved refrigerant. According to measured oil concentration the additional amount of oil during compressor startup is in the order of 300 to 400 g !

By closing the connection to the refrigerant vessel placed after the condenser (Fig. 5.26 (b)) and by opening the bypass line, the oil concentration measured in the liquid line is practically unchanged and remains at a very low concentration level.

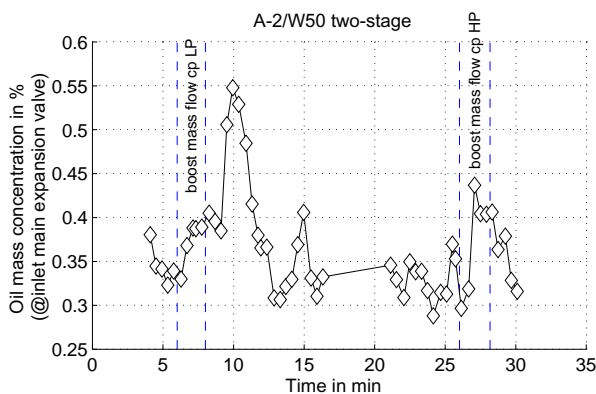
Interacting on the two electronic expansion valves, the mass flow conditions (Fig. 5.26 (c)) and the superheat (Fig. 5.26 (d)) at the entry of each compressor can be changed for a limited period. Marginal changes during a short time can be interpreted by the results shown in the graphs. Increased superheat results on a reduced oil mass concentration pulse.



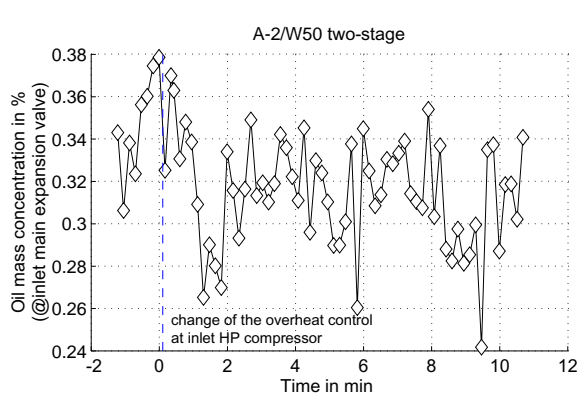
(a) Transition single-stage two-stage heating



(b) By-pass refrigerant vessel



(c) Boosting mass flow rates



(d) Increase of regulated overheat value.

Figure 5.26: Transitions applied in steady state heating mode. Impacts on measured oil mass concentration.

Defrosting of the evaporator coil by inversed cycle operation

Besides the heat pump startup, the defrosting in air-water heat pumps is one of the most frequent transitory operating modes during the heating season. An inversed cycle defrosting mode has been selected to the built two-stage heat pump. By shifting the register of the 4-way reversing cycle valve, the suction and the discharge line connection of the lower stage compressor are commuted. The compressed hot gas are directly flowing into the evaporator and release their heat to defrost the frosted finned-tube surface. By a by-pass line the condensed refrigerant is heated and re-evaporated in the hot condenser and return to the compressor. The oil migration during this defrosting sequence could not be measured by on-line measurements. A comparison of the liquid levels in the two compressors before and after the defrosting showed, however, a stable situation without significant losses in both compressor shells.

5.4 Propositions for balanced operating conditions in two-stage compression cycles

Oil migration in two-stage heat pump cycles is a major issue in order to ensure correct lubrication of both compressors. Experiences presented in this work, have demonstrated the unstable situation with a net oil migration flow from the higher stage compressor to the lower stage compressor. These observations correspond to those observed in a earlier project, see [Nidegger et al., 1997]. No self stabilizing configuration in two-stage compression could be identified within the recorded data set. All measurements show the deficit of oil in the high pressure stage, which requires an auxiliary mechanism to transport oil from the low pressure to the high pressure. The implementation of an oil separator in the discharge line of the upper stage compressor could improve the situation, allowing a longer operating period in steady state heating mode. These standard solutions, as they are applied in large size applications, represent important additional costs and can therefore not be considered in this application. Alternative, low cost solutions have to be considered to by-pass this technological bottleneck.

Stabilizing solutions applied to small and medium size two-stage heat pumps.

Two stage compression heat pumps have considerable advantages compared to single stage configurations. The main feature is the combination of heat output modulation, the restriction to a small range of pressure ratios applied to each compressor and the increase of performance during the heating season.

In order to enable two-stage configurations in small to medium sized heat pumps several adaptations from the original setup are proposed:

1. **Two-stage compressor within the same shell or lower stage compressor with shell at the discharge pressure**

Two-stage compressors are among the standard components for the refrigeration, using semi-hermetic screw or reciprocating type compressors¹. These are, however in a too high capacity range and cannot be easily adapted for small capacity residential heating. The only hermetic two-stage compressor at our knowledge is a high pressure, CO₂, rolling piston compressor, [Mukaiyama et al., 2002], although in a too small capacity range. Compressors with a shell at discharge pressure exist since the early 1990's, but compressor efficiency has been measured in a lower and tend to deteriorate all the performance gains in two-stage cycles. As the heat pump market still represents a minor part of the worldwide manufactured refrigerant cycles, chances to have in the near future an improved and adapted single-shell two-stage compressor are unfortunately weak.

2. **Oil minimum level detection and equalization line between the two compressors.**

The most simple solution, using available components, is the tandem approach. The two compressor shells are linked with an oil equalization line, which is equipped with a solenoid valve. The high stage compressor is additionally equipped by a minimum oil level switch, which stops the operating compressors and opens (after equilibration of the pressure in the shells) the equalization line. Oil is then transferred by gravity and the heat pump can again be restarted for the next time period.

A second approach, which has more impact on additional tubing, is to build the two-stage cycle with two-identical compressors, which are alternated when the high stage compressor reaches the minimum oil level. This solution however affects negatively the optimum ratio of pressures between the stages.

3. **Booster compressor without oil retaining shell.**

Using a high efficiency compressor and a single-stage heating configuration, is sufficient most of the time during a heating season. An additional booster compressor, which could be a low cost compressor allowing a two-stage cycle in the colder days of the year, has a high suction volume, a low built-in volume ratio and no shell space to accumulate oil. This configuration allows mainly to *boost* heat output at the coldest external conditions, and avoids the use of direct electric heating as supplying heat source. This solution has been evaluated and heat output could be double remaining at acceptable performance of the heat pump (see [Zehnder et al., 2002]).

4. **Oil free two-stage compression cycle.**

Oil free compression systems are very promising technical solutions, which for small sized systems are not ready for commercialization in the near future. An approach to develop an oil free two-stage air-water heat pump is part of an ongoing project [Schiffmann et al.,

¹<http://www.bitzer.de>, <http://www.ecopeland.com>

2002]. A higher capacity oil-free two-stage refrigeration system, using magnetic bearings, has already been developed and commercialized¹.

5.5 Conclusions

Oil migration is a major issue for two-stage compression cycles, and is also a key parameter in the system design of the compressor suction for all refrigeration systems. While in large scaled, industrial heat pumps, an oil management system can be integrated, in order to ensure correct lubrication of the compressors, in small capacity, residential heating heat pumps, these auxiliary modules represent additional investment cost, leading to uncompetitive products.

In order to evaluate the oil quantity which migrates through the heat pump cycle, a new measurement technique, based on infrared absorption and using a single total reflexion cell (Micro-ATR), has been adopted and calibrated on a separate circuit (sec. 5.2). Sensibility of oil mass concentrations $<0.1\%$ could be reached, but the lower detection limit ranges between 0.2% and 0.4% depending on the signal intensity. The latter vary with the type of fluids used and is dependent on the temperature of the liquid probe.

On-line measurements within the heat pump circuit have shown a very low oil quantity leaving the first stage compressor ($0.0\% - 0.2\%$), while the quantity of the second stage compressor is in the measurable range of $0.2\% - 0.4\%$ oil mass concentrations (Fig. 5.24). These low mass concentrations, disabled a detailed sensibility analysis of the operational conditions. Verifications of the measurements have been performed by injection of known amounts of oil into the circuit at several positions. With these injections, the absence of any oil retention in the elements between the compressor and the spectrometer, which is situated before the main expansion valve, has been verified.

In order to complete this investigation, transitional operating conditions have been tested. The most significant effect is shown by the commutation from one-stage compression, to two-stage compression mode. The second stage compressor, which is at the high pressure level during one-stage heating, initiates a flashing of the oil-refrigerant mixture and a high amount of oil transits the system. During 1-2 min, the amount of 300-400 g oil is transferred from the high stage compressor to the low stage. This is considerable and limits heat output modulation, using in/off mode of the second stage compressor. Other transitional operating modes do not show significant changes of the oil concentration (a minor increase is seen for decreased superheat of the compressor suction flow).

Approaches for continuous heating, are investigated for two-stage compression cycles. The ap-

¹See <http://www.turbocor.com>

proach using a booster compressor setup, which is a compressor with no oil accumulation capacities, has been verified experimentally. COP gains were partly removed by a lower compression efficiency. In the experimental setup a semi-hermetic scroll compressor has been adapted for the proper use (sec. 2.3.3). Other approaches for stabilized conditions are based on improved compressor technology (as the single shell two-stage compressor, or the high pressure compressor shell), but no such development in this capacity range is known to the authors. Finally different sequential operating modes are proposed, which however suggest a periodic stop of the heat pump to equalized or to transfer the oil to the designated place.

Bibliography

- G. Ahnefeld, R. Heide, and T. Näther. **Kontinuierliche Messung der Ölkonzentration in Kälteanlagen.** *Ki Luft- und Kältetechnik*, 12:545–548, 1996.
- ASHRAE. **ANSI/ASHRAE Standard 41.4-1996; Standard Method for Measurement of Proportion of Lubricant in Liquid Refrigerant**, 1996.
- J. Baustian, M. Pate, and A. Bergles. **Measuring the Concentration of a Flowing Oil-Refrigerant Mixture with a Bypass Viscometer.** *ASHRAE Transactions*, 94(2):588–601, 1988a.
- J. Baustian, M. Pate, and A. Bergles. **Measuring the Concentration of a Flowing Oil-Refrigerant Mixture with an Acoustic Velocity Sensor.** *ASHRAE Transactions*, 94(2):602–615, 1988b.
- A. Bayini, J. Thome, and D. Favrat. **Online Oil Measurement of Oil Concentrations of R-134a/Oil Mixtures with a Density Flowmeter.** *Int. J. HVAC&R Research*, 1(3):232–241, 1995.
- S. Bertsch and M. Ehrbar. **Verbesserung des Abtauens bei luftbeaufschlagten Verdampfern, Phase 2: Bewertung der Abtauprozesse.** Final report. Swiss Federal Office of Energy, 2002. ENET-Nr. 220187.
- F. Biancardi, H. Michels, T. Sienel, and D. Pandey. **Study of Lubricant Circulation in HVAC Systems, Volume 1: description of Technical Effort and Results.** Technical report, United Technologies Research Center, ARTI MCLR Project, DOE/CE/23810-71, 1996.
- R. Cavestri and W. Schafer. **Real Time Determination of Lubricant Concentrations Dissolved in Alternative Refrigerants.** *ASHRAE Transactions*, 105(2):386–399, 1999.
- A. Christy, Y. Ozaki, and V. Gregoriou. **Modern Fourier Transform Infrared Spectroscopy.** Elsevier, 2001, 2001. Chapter 7.
- D. Compton and D. Rayner. **An Analysis of the Vibrational Spectra of C_2F_5I , $n-C_3H_7I$, and the corresponding Perfluoroalkyl Radicals, $C_2F_5\cdot$ and $n-C_3F_7\cdot$.** *J. of Physical Chemistry*, 86(9): 1628–1636, 1981.
- K. Kutsuna, Y. Inoue, and T. Mizutani. **Real Time Oil Concentration Measurement in Automotive Air Conditioning by Ultraviolet Light Absorption.** In *International Congress and Exposition, Detroit, Michigan, Feb. 25 - March 1*, 1991.

- E. Lemmon, M. McLinden, and M. Huber. **NIST Reference Fluid Thermodynamic and Transport Properties - REFPROP, Version 7.0**. National Institute of Standards and Technology, 2002.
- J. J. Meyer and J. Saiz Jabardo. **An Ultrasonic Device for Measuring the Oil Concentration in Flowing Liquid Refrigerant**. *Revue Int. Froid*, 17(7):481–486, 1994.
- M. Mizuno and S. Saeki. **Infrared Absorption Intensities of Methylene Fluoride**. *Spectrochimica Acta*, 32A:1077–1082, 1976.
- H. Mukaiyama, T. Masuda, and K. e. a. Mizukami. **Development of CO₂ Compressor and its Application System**. In *7th Heat Pump Conference, Beijing*. Sanyo Electric Co., Ltd., Int. Energy Agency, 2002.
- E. Navarro de Andrade, E. Skowron, V. W. Goldschmidt, and E. A. Groll. **Oil Concentration in Liquid Refrigerants: in Situ Measurements**. *Int. J. of Refrigeration*, 22:499–508, 1999.
- T. A. Newell. **In Situ Refractometry for Concentration Measurements in Refrigeration Systems**. *Int. J. HVAC&R Research*, 2(3):247–255, 1996.
- E. Nidegger, D. Reymond, M. Zehnder, and D. Favrat. **Pompe à chaleur bi-étagée à haute performance**. Final report. Swiss Federal Office of Energy, 1997. ENET-Nr. 194463.
- J. Nielsen and C. Halley. **Infrared and Raman Spectra of Fluorinated Ethanes**. *J. of Molecular Spectroscopy*, 17:341–347, 1965.
- J. Schiffmann, A. Molyneaux, D. Favrat, F. Maréchal, M. Zehnder, and J. Godat. **Pompe à chaleur biétagée sans huile avec compresseur radial**. Final report. Swiss Federal Office of Energy, 2002. ENET-Nr. 220195.
- S. Suzuki, Y. Fujisawa, S. Nakazawa, and M. Matsuoka. **Measuring method of Oil Circulation Ratio using Light Absorption**. *ASHRAE Transactions*, 99(1):413–421, 1993.
- R. Tillner-Roth and H. Baehr. **An Int. Standard Formulation of the Thermodynamic Properties of 1,1,1,2-Tetrafluoroethane (R-134a) Covering Temperatures from 170 K to 455 K at Pressures up to 70 MPa**. *J. Phys. Chem. Ref. Data*, 23:657–729, 1994.
- M. Zehnder, F. Maréchal, S. Guex, J. Schiffmann, and D. Favrat. **Pompe à chaleur air-eau à haute température, Phase 2: Cycle à injection optimisé, essais journaliers et compresseur booster; Analyse thermo-économique**. Final report. Swiss Federal Office of Energy, 2002. ENET-Nr. 220219.
- B. Zhou, D. Nikanpour, and J. Venart. **Real-Time Determination of the Lubricant Oil Concentration in Refrigeration Systems using Fiber Optic Sensor Technology**. In *Thirteenth Symposium on Thermophysical Properties, June 22-27, Boulder, Colorado, USA*, 1997.

6. General Conclusions and Outlook

Heat pumps for residential heating allow a major reduction of the greenhouse gas emissions, if they can **replace existing fuel based heating systems**. For this application, however, the proposed heat pumps are inappropriate. The system temperatures of this heating application are generally in a higher range and atmospheric air is likely to be considered as heat source. This results in a **high temperature lift heating mode**, to which this work is addressed to.

The development of small capacity heat pumps (<20 kW heat rate) for the considered application is in a early stage and the improving potential of new concepts has been demonstrated by experimental testing, in order to proof the feasibility of these concepts and to show the availability of the needed components. The here presented experimental test runs have been assisted by the author and resulted from collaborations with several Swiss heat pump manufacturing companies, which demonstrates the great interest for this kind of developments.

The system approach applied in this work covers a large spectrum of research domains and provides several contributions, which lead to a better understanding of the key design aspects and which show the practical limits of the **proposed high efficiency approaches**.

In [chapter 1](#) the **evaluation of alternative refrigerant mixtures** is performed by a systematic approach, **using a multi objective optimization tool**. Environmentally benign, but highly flammable refrigerants are in general opposing non-flammable and non-toxic refrigerants, which allow to built heat pumps at reduced system cost. The optimization has been applied to the two complementary objectives: COP and specific heat capacity. The found refrigerant blends, are all mainly composed of flammable refrigerants. Repeating the optimization to limited flammability blends shows the potential of increasing the performance, while comparing to the actually widely used zeotropic refrigerant blend R-407C.

The main **design aspects, which enable improved performance** for the heat pump cycle, are analyzed in [chapter 2](#) and **assembled in the superstructure diagram**, presented in [Figure 2.4](#) on [page 33](#). Experimental results demonstrate the potential of the selected setups. The thermodynamic evaluation of the different cycles shows the most important gain, using two-stage compression concepts, including the economizer heat exchanger cycle. This type of cycle has been tested in the classical two-stage compression configuration and in a more compact setup, referring to a new prototype compressor, in a one-stage intermediate injection cycle. In addition to these two concepts,

the auxiliary cycle for liquid subcooling has been tested. Due to the relative small heat capacity of the auxiliary cycle, this solution shows potential advantages in medium size applications, which require a high heating temperature glide, or which need to provide heat to two distinguished temperature levels (e.g. to produce hot water in parallel).

A **generalized heat pump cycle model** is presented in [chapter 3](#), which includes the **new developed models of the compressor with intermediate injection port** and a generalized and **flow map based heat transfer model for the finned tube evaporators**. Including the generalized **models for the plate heat exchangers** and for the **capillary tube expansion**, the model components can be combined to any of the enhanced heat pump cycles, which are represented by the mentioned superstructure. An in house **built fluid interface module allows to calculate the fluid properties provided by the software Refprop**. A large number of predefined fluids new composed refrigerant blends can be used to calculate the performances of the selected concepts to a specific heating case. The simulation results and the comparison of the application ranges of the these cycles are performed in [chapter 4](#). For the compressor with intermediate injection port, a parametric analysis is evaluated, to show the impact on the system performances by variation of the injection flow geometry.

Experiences with **two-stage compression cycles showed** a major problem, which is generated by **the unbalanced oil migration through the heat pump cycle**. Lubrication failure would result in long term operating conditions at the higher stage compressor. In order to precisely measure the oil quantity, which is mixed to the refrigerant flow, a **new on-line oil concentration measurement method, using a Fourier Transform Infrared Spectrometer** with a single reflection cell has been applied in [chapter 5](#). Calibration tests and the comparison with other measurement approaches, as the mass sampling and the density based measurements show the interest and the precision of this approach.

On-line measurements on a prototype two-stage compression heat pump **showed oil mass concentration of 0.2% - 0.4%** in the liquid line at the exit of the economizer heat exchanger. These results **were confirmed with a complementary analysis**, by injection oil packages of known quantity, in order to verify the measured concentration and to check against oil accumulation in the elements located between the compressor discharge line and the location of the measurement. For the fluids used in this analysis (R-407C with POE oil), the use of a high precision densimeter has been highly restricted to the lower temperature range and could not be used in the present conditions. **Very low oil migration in steady state one-stage operating conditions has been found** and could only be detected by mass sampling. Transitional operating regimes were applied to detect the influence of changing the external control parameters. The variations of the oil concentration remained within the measured fluctuations, except for the compressor startup phase, when switching from one-stage to two-stage heating mode. An **important oil quantity (~300 g) is released during flashing of the oil rich mixture** in the compressor shell, an effect, which further limits the operation time of this concept.

Several recommendations have been evaluated **to avoid system failure in compact two-stage compression cycles**, the solution of a **booster type compressor has been successfully demonstrated**, without observing significant losses of oil in the main compressor. The used first stage compressor, an open scroll type compressor, however, still needs to be redesigned to the required specifications.

This work shows the important technological gaps for improved system design for small capacity, high temperature lift heat pumps. The main contributions are provided by a holistic approach, considering

- the **selection of alternative refrigerants, using an optimization tool.**
- the **design of improved configurations, by defining a superstructure and by experimental validation.**
- the **development of a generalized heat pump simulation model, including a new type of compressor with intermediate injection port.**
- the **development of a new oil concentration measurement method, using a Fourier Transform Infrared Spectrometer with a single reflection cell, allowing on-line oil concentration measurements with multi-component mixtures.**

Outlook for further developments

The proposed elements, which are extensively analyzed within this work conclude several activities within the framework of the 'High performance retrofit heat pump' for hydronic residential heating applications. Thank to several collaborations, the development of new components, as the here cited compressor, could be realized. This important contribution, which completes the now widely available high pressure heat exchangers, enables a reasonable (technically and economically) design of high temperature lift heat pumps, which present a highly extended application range compared to the available commercial products.

The **efforts for future concepts will have to be concentrated on two-stage compression cycle** representing the next generation of heat pumps (due to their modulation capacity and the potentially higher system performances). Further experimental work is needed to develop a concept, which inherently ensures a long term operational mode without system failure. **Developments on oil-free systems represent one complementary research theme** and adapted concepts for the refrigeration and heating systems will gradually be available in the future. These systems allow highly compact units with very low refrigerant charge, and allow to reconsider natural (and flammable) refrigerants, which potentially further increase the system COP.

Symbols

Latin symbols

A	m^2	Cross sectional area
A	–	Density correction
A	–	Spectral absorbance
B	W	laser beam intensity (emitted)
c_p	J/kgK	Heat capacity at constant pressure
D	m	Diameter
D_h	m	Hydraulic diameter
D^*	m	External diameter including coating fin
e	m	Surface rugosity
e	J/kg	Specific work
E	J, kWh	Energy
\dot{E}	W	Energy rate
e_{mf}	m	Microfin tube, fin height
E_{mf}	–	Microfin tube, heat transfer enhancement
\dot{E}_q	W	Exergy heat rate
E_{rb}	–	Microfin tube, boiling enhancement
\dot{E}_w	W	Exergy work rate
\dot{E}_y	W	Exergy transformation rate
F_c	–	Zeotropic refrigerant correction
f_{nom}	–	Nominal compression zone correction
f_{oil}	–	Oil absorbance correlation
f_{transm}	–	Empirical transmission losses coefficient
$f_{wet,is}$	–	Wet compression correction
$f_{wet,vol}$	–	Wet compression volumetric losses
f	–	Moody friction factor
f_i	–	Interfacial friction factor
f_h	m	fin height (element of repetition)
f_s	m	fin pitch
f_t	m	fin thickness
f_w	m	fin width (element of repetition)
g	m/s^2	Gravitational acceleration
G	$kg/s m^2$	Mass flux, mass velocity

h	J/kg	Enthalpy
h	m	Height
I	W	laser beam intensity (received)
k	J/kg	Co-enthalpy = $h - T_{atm} s$
k	W/m ² K	Overall heat transfer coefficient
L, ℓ	m	Characteristic length
\dot{L}	W	Irreversibility rate
\dot{L}	kg/s	Leakage rate
M	kg	Mass, charge
\dot{M}	kg/s	Massflow rate
\check{M}	g/mol	Molar mass
n	–	Number of specified unit
n	–	Polytropic transformation exponent
n	rev/s	Rotational speed (revolutions per seconds)
P	m	Perimeter
P	Pa, (bar)	Pressure
p_{mf}	m	Microfin tube, fin pitch
\dot{q}	W/m ²	Heat flux
\dot{Q}	W	Heat rate
\dot{q}_{ONB}	W/m ²	Critical heat flux for onset of nucleate boiling
r	J/kg	Specific dissipation
r	m	Radius
r_{crit}	m	Critical bubble size for departure of natural boiling
s	J/kg K	Entropy
S	m ²	Heat exchange surface
S	m ²	Surface
S	–	Specific gravity
t	s, (min)	Time
T	K, (°C)	Temperature
T	–	Transmittance
u	m/s	Velocity
v	m ³ /kg	Specific volume
V	m ³	Volume
\dot{V}	m ³ /s	Volumetric flow
VR	–	Volume ratio
VR_i	–	Built in volume ratio
w	–	Mass fraction
w_{oil}	–	Oil weight, oil mass fraction
\dot{Y}	W	Enthalpy rate

Greek letters

α	W/m ² K	Heat transfer coefficient
$\alpha_{recovery}$	—	Refrigerant recovery
β_{corr}	°	Corrugation pattern angle
β_{em}	CO _{2,eq.} /kWh	CO ₂ equivalent emission
β_L	m/s	Mass transfer coefficient
$\Gamma(n, \kappa)$	—	Isentropic or polytropic transformation factor
δ	m	Liquid Film thickness (in two-phase flow)
δ	m	Wall thickness
η	—	Efficiency
ε	—	Void fraction
ε_h	—	Homogeneous void fraction
ε_{ln}	—	Logarithmic void fraction
ε_{ra}	—	Void fraction, Rouhani-Axelsson definition
ε_{td}	—	Void fraction, Taitel-Dukler definition
ζ	°	Angular position
ζ_h	—	Liquid height factor
η_I	—	First Law efficiency
η_{II}	—	Second Law efficiency (exergetic)
η_{fin}	—	Fin efficiency
θ	rad	Dry surface angle
κ	—	Isentropic exponent
λ	W/mK	Conductivity
μ	kg/s m	Dynamic viscosity
ν	m ² /s	Kinematic viscosity
Π	—	Pressure ratio
ρ	kg/m ³	Density
σ	1/rad	Frequency
σ	N/m	Surface tension
φ	—	Molar fraction
φ_{mf}	°	Microfin tube, helix angle
χ	—	Vapor quality
χ_{I-A}	—	Quality at transition of intermittent to annular flow
ω	rad/s	Rotational speed

Subscript

0	Reference state	lam	Laminar
ad	Adapted	lat	Latent (heat)
adm	Admission	<i>liq</i>	Liquid
air	Air	max	Maximum
ann	Annual	meas	Measured
asp	Aspiration	mech	Mechanic
atm	Atmospheric	mf	Microfin tube
av	Average value	min	Minimum
cap	Capillary tube	mist	Mist flow
cd	Condensing	mix	Mixture
cold	Cold side flow	nb	normal boiling
conv	Convective	nb	Nucleate boiling
conv	Energy conversion	nom	Nominal
corr	Correction	out	Outlet
cp	Compressor	poly	Polytropic
crit	Critical value, @critical point	refr	Refrigerant
d	Diameter, reference length	red	Reduced (reference=critical point)
dis	Discharge	<i>sat</i>	Saturated
displ	Displacement	strat	Stratified
E	Excess value	th	Theoretical
el	Electric	tot	Total
eq	Equivalent	tp	Two-phase
ev	Evaporating	transm	Transmission
ext	External	turb	Turbulent
hot	Hot side flow	<i>vap</i>	Vapor
in	Inlet	vol	Volumetric
inj	Injection	w	Water
int	Intermediate	wavy	Wavy flow
int	Internal	<i>id</i>	ideal
is	Isentropic		
I-A	Intermittent to annular		

Abbreviations

ATR	Attenuated Total Reflection
COP	Coefficient of Performance
DD	Degree Days
FT-IR	Fourier Transform Infrared Spectrometry
GWP	Global Warming Potential
HP	Heat Pump
HOC	Heat of Combustion
LFL	Lower Flammability Limit
NBP	Normal Boiling Point
ODP	Ozone Depletion Potential
ONB	Onset of Nucleate Boiling
POE	Polyolester Oil
TEWI	Total Equipment Warming Impact
A _{xx} /W _{xx}	Running conditions (Air inlet temperature, water outlet temperature in °C.)
B _{xx} /W _{xx}	Running conditions (Brine inlet temperature, water outlet temperature in °C.)
W _{xx} /W _{xx}	Running conditions (Cold Water inlet and hot water outlet temperature in °C.)

Dimensionless Numbers

Froude number	$Fr = \frac{u^2}{gL}$	Ratio of inertial and gravitational forces.
Martinelli parameter	$X_{tt} = \left(\frac{1-\chi}{\chi}\right)^{0.875} \left(\frac{\mu_{liq}}{\mu_{vap}}\right)^{0.125} \left(\frac{\rho_{liq}}{\rho_{vap}}\right)^{0.5}$	Ratio of the theoretical pressure drops occurring if each phase would flow separately in the complete cross section (using expression of Steiner).
Nusselt number	$Nu = \frac{\alpha L}{\lambda}$	Dimensionless temperature gradient at the surface.
Prandtl number	$Pr = \frac{c_p \mu}{\lambda}$	Ratio of the momentum and thermal diffusivities.
Reynolds number	$Re = \frac{uL}{\nu}$	Ratio of inertia and viscous forces.
Weber number	$We = \frac{\rho u^2 L}{\sigma}$	Ratio of inertia to surface tension forces.

Appendix A

A.1 Exergy analysis applied to an air-water heat pump unit.

In order to quantify the exergetic flow of an entire heat pump system, a complete exergetic analysis has been performed, showing on one selected operating condition the repartition of the irreversibilities attribution to each transformation. This analysis includes on the **system level**, frictional losses in the external air and water flows, which are compensated by the auxiliary power input of the fan and the water pump. The transformation losses of the refrigerant flow through the main elements of the heat pump cycle are calculated, referring as the **cycle level** losses. Particular attention has been addressed to the conversion in the compressor(s), which considers separately the heat losses on the shell ($\dot{L}_{cp,heat\ loss}$) and the transformation irreversibilities ($\dot{L}_{cp,transf.}$) occurring between the inlet and the exit of the compressor.

An air-water heat pump at steady state heating conditions (no internal energy accumulation) is considered and a one-stage compression cycle is compared to an improved two-stage cycle at high temperature lift operating conditions.

Irreversibilities on the system level:

$$\dot{E}_{w,HP} - \dot{E}_{y,w} - \dot{E}_{y,air} = \dot{L}_{HP} \quad (A.1)$$

$$\text{with } \dot{E}_{w,HP} = \dot{E}_{w,cp} + \dot{E}_{w,pump} + \dot{E}_{w,fan} + \{\dot{E}_{w,others}\}$$

$$\text{and } \dot{E}_{y,w} = \dot{M}_w (k_{out} - k_{in}) = \dot{M}_w c_{p,w} \left[(T_{w,out} - T_{w,in}) - T_{atm} \ln \frac{T_{w,out}}{T_{w,in}} \right] \quad (A.2)$$

$$\text{and } \dot{E}_{y,air} = \dot{M}_{air} (k_{out} - k_{in}) = \dot{M}_{air} c_{p,air} \left[(T_{air,out} - T_{air,in}) - T_{atm} \ln \frac{T_{air,out}}{T_{air,in}} \right] \quad (A.3)$$

The co-enthalpy is given by: $k = h - T_{atm} s$

Assumptions: Unsaturated humid air and constant heat capacities, during the transformation.

Irreversibilities on the cycle level:

$$\dot{L}_{cycle} = \dot{E}_{w-mech.,cp} - \dot{E}_{q,cd} - \dot{E}_{q,ev} \quad (A.4)$$

Heat exergy is considered at the outer heat transfer surface of the condenser and the evaporator.

In order to simplify the calculation, the surface temperature is assimilated to that of the fluid. This results in equivalent exergy output and transformation exergy, which are calculated with the expressions A.2 and A.3.

The analytical expressions to calculate the irreversibilities on each component are provided here below:

for both cycles:

$$\begin{aligned} \text{compressor:} \quad \dot{L}_{cp,transf.} &= \dot{E}_{w,cp} - \dot{E}_{y,cp} \\ &\text{with } \dot{E}_{w,cp} = \dot{M}_{refr} (h_{cp,out} - h_{cp,in}) \quad (\text{energy balance}) \end{aligned}$$

$$\text{condenser:} \quad \dot{L}_{cd} = \dot{E}_{y,cd-refr} - \dot{E}_{y,cd-w}$$

$$\text{evaporator:} \quad \dot{L}_{ev} = \dot{E}_{y,ev-refr} - \dot{E}_{y,ev-air}$$

$$\text{expansion:} \quad \dot{L}_{exp} = \dot{E}_{y,exp}$$

$$\text{overheater:} \quad \dot{L}_{oh} = \dot{E}_{y,oh-hot} - \dot{E}_{y,oh-cold}$$

and for two-stage compression cycles only:

$$\text{economizer:} \quad \dot{L}_{eco} = \dot{E}_{y,eco-hot} - \dot{E}_{y,eco-cold}$$

$$\text{flow mixing:} \quad \dot{L}_{mix} = \dot{M}_{refr,inf} k_{cp1,out} + \dot{M}_{refr,int} k_{eco-int,out} - \dot{M}_{refr,sup} k_{cp2,in}$$

The total irreversibility of the cycle are:

$$\dot{L}_{cycle} = \dot{L}_{cp,transf.} + \dot{L}_{cd} + \dot{L}_{ev} + \dot{L}_{exp} + \dot{L}_{oh} + \dot{L}_{eco} + \dot{L}_{mix} \quad (\text{A.5})$$

Table A.1: Comparison of performances end exergetic efficiency of one-stage and two-stage compression heat pump cycle, external flow temperatures: air (in/out)=-12/-14.7°C and heating (in/out)=55/60°C. Refrigerant R-407C.

	one-stage	two-stage
Heat output	9.9 kW	10.7 kW
COP _{HP,ext}	1.86	2.38
$\eta_{II,refr-cycle}$	72.9%	79.4%
$\eta_{II,HP-ext}$	39.2%	50.1%
$\eta_{II,Lorenz}$	39.8%	51.2%
$\eta_{II,Carnot}$	40.2%	51.5%

Table A.2: Inventory of irreversibilities in one-stage and two-stage compression heat pump cycles, with external flow temperatures: air (in/out)=-12/-14.7°C and heating (in/out)=55/60°C. Refrigerant R-407C. Graphical representation, see fig. 2.1 on page 28.

Exergy loss rates	one-stage		two-stage	
	in kW	in %	in kW	in %
<u>System losses:</u>				
\dot{L}_{cycle}	2.11	65.6	1.72	77.8
$\dot{L}_{cp,heatloss}$	0.78	24.3	0.16	7.3
\dot{L}_{aux}	0.33	10.1	0.33	14.9
<u>Cycle losses:</u>				
\dot{L}_{cp}	1.07	50.5	0.51	29.5
$\dot{L}_{cp,aux}$	—	—	0.53	30.8
\dot{L}_{exp}	0.74	35.0	0.15	9.0
$\dot{L}_{exp,int}$	—	—	0.15	8.5
\dot{L}_{cd}	0.22	10.2	0.11	6.2
\dot{L}_{ev}	0.04	1.9	0.06	3.7
$\dot{L}_{overh.}$	0.05	2.3	0.02	0.9
\dot{L}_{eco}	—	—	0.14	8.1
\dot{L}_{mixing}	—	—	0.06	3.2

A.2 Precisions of measured data

This work represents a large number of measured data with provenience from several test rigs and specific configurations. An general estimation on the precision of these collected data is provided here. More specific error calculations are given within the respective project reports.

Table A.3: Precision of used data transmitters.

Data to be measured	Type of transmitter	Data range (calib.)	Precision (typical error)
Temperature	Thermocouple Type K	-20°C- +150°C	±0.1 K
Pressure	Piezo-resistive	1-30 bar	±0.05 bar (1%)
Diff. pressure	Piezo-resistive	0 - 200 Pa	±1 Pa (2%)
Relative humidity	Hygrometer	35% -100% r.h.	1%
Refrig. mass flow	Coriolis force	0 - 80 g/s	±0.5 g/s (1%)
Water flow rate	Coriolis force	0-250 l/min g/s	±0.2 l/min (0.5%)
Electric power - 3-ph	V-A measurement	0-5 kW	0.1%
Electric power - 1-ph	V-A measurement	0-2 kW	0.5%
Density	Coriolis force	400-2000 kg/m ³	±0.2%

Sensible data, as the water temperatures were collected with redundancy (3 thermocouples at the water inlet and exit point). Pressure and temperature sensor were manually calibrated in the laboratory. Other precision data are provided in the technical documentation of the used transmitters.

Error propagation:

With an error propagation evaluation , the resulting data, which is obtained by combination of collected measurements and error propagate. Error propagation is evaluated by the first order *Taylor series*, from the function $Z = f(Y_1, Y_2, \dots, Y_n)$:

$$\Delta Z = \sum_{i=1 \dots n} \left| \Delta Y_i \frac{\partial f}{\partial Y_i} \right| \quad (\text{A.6})$$

The errors on the calculated heat pump performances are estimated through the expressions:

$$\text{Heat output: } \dot{Q}_{hot} = \dot{V} \rho c_p \Delta T$$

$$\frac{\Delta \dot{Q}_{hot}}{\dot{Q}_{hot}} = \left| \frac{\Delta \dot{V}}{\dot{V}} \right| + \left| \frac{\Delta \rho}{\rho} \right| + \left| \frac{\Delta c_p}{c_p} \right| + \left| \frac{2}{3} \frac{\Delta(T_{out} - T_{in})^{**}}{(T_{out} - T_{in})} \right|$$

$$= 0.5\% + 0.2\% + - + 1.33\% = \pm 2.0\%.$$

$$\text{COP: } \text{COP} = \frac{\dot{Q}_{hot}}{\sum \dot{E}}$$

$$\frac{\Delta \text{COP}}{\text{COP}} = \left| \frac{\Delta \dot{Q}_{hot}}{\dot{Q}_{hot}} \right| + \left| \frac{\Delta \dot{E}}{\dot{E}} \right| = 2.0\% + 0.1\% = 2.1\%$$

*) Calculated value with error $< 0.1\%$ and its contribution can be neglected.

***) Error on the temperature difference (2x the single-sided error, using 3 thermocouples on each side.)

Data scanning:

The measured data is scanned, by means of a Hewlett-Packard HP 3852A data logging unit with specific acquisition card for the used thermocouples (Type K) and for tension measurements. Scanned data are passed as a vector to the computer, using a GPIB transmission protocol and are visualized on-line with LabView, a modular, programmable interface, specifically adapted for real-time input and output control and acquisition, see fig. A.1.

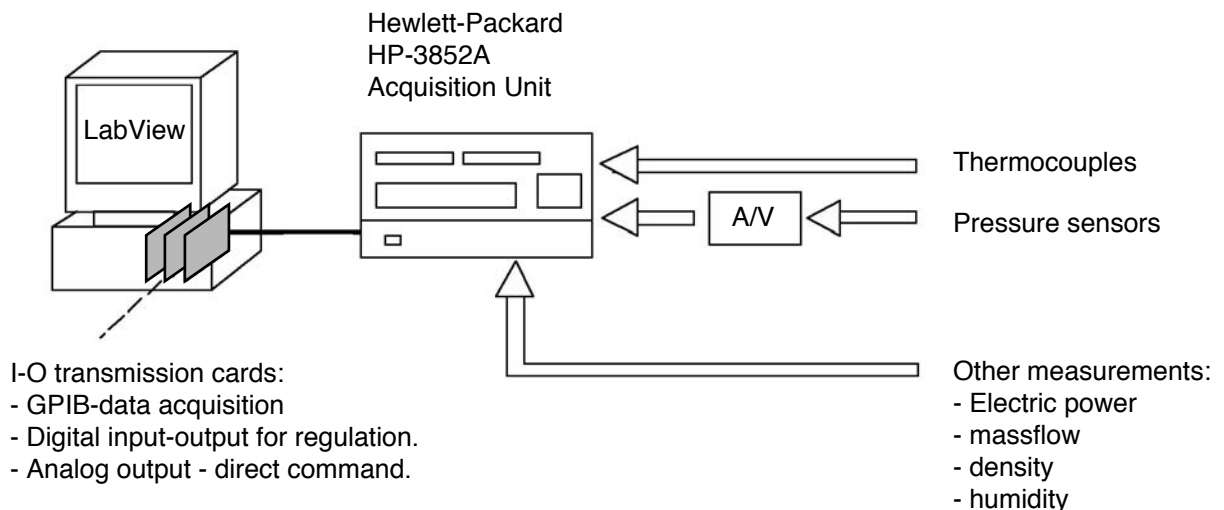


Figure A.1: Representation of data communication flow.

In order to maintain measurement precision at this nominal error level steady state running con-

ditions are scanned during 20 min after stabilization. In case of very important oscillating mode (generated by the thermostatic expansion valve), the number of data points data has been truncated in order to consider a number of completed oscillations. One measurement scan is during 5 s, and is continuously repeated.

An example of a real time observation of the operational conditions is represented with figure A.2.

A.3 The enhanced heat pump model - Toolbox

The heat pump cycle calculation module is built as a *Toolbox*, conforming to the structure of integrated Matlab-Toolboxes. The toolbox is composed of the heat pump cycle description, the component models, including the evaporation flow pattern map and the universal fluid interface, including the Refprop calculation core and different visualization tools. Table A.4 provides the listing of all included functions (excepting the fluid calculation interface, which is a separate Toolbox).

A.4 Simulation input data of available components

A.4.1 Compressors

The listing here below represents the selection of implemented compressor models.

Hermetic Scroll compressors (Copeland)

- Air-conditioning compressors (ZR): ZR18 - ZR81
Displacement in m³/h at 50 Hz: 4.4 / 5.3 / 6.8 / 8.0 / 9.4 / 11.5 / 11.7 / 14.4 / 17.0 / 19.2
Max. pressure: 29.5 bar, max. temperature: 120°C (measured in the refrigerant line). Built in volume ratio and global efficiency (by experimental data fitting) $VR_i = 1.8$, $\eta_{is,max} = 72\%$.
Released for R-134a, R-407C and R-22.
- Heat pump compressors (ZH): ZH15 - ZH38
Displacement in m³/h at 50 Hz: 6.0 / 7.4 / 8.1 / 9.9 / 11.7 / 14.4 / 17.1
Max. pressure: 26.4 bar, max. temperature: 120°C (measured in the refrigerant line). Supposed same geometrical setup as in the ZR Series (input parameters, see above).
Released for R-407C.
- Refrigeration compressors (ZF/ZB): ZB30 - ZB11M (ZB=medium/high temperature range)
Displacement in m³/h at 50 Hz: 11.8 / 14.5 / 16.2 / 17.2 / 20.9 / 28.8 / 35.6 / 42.1

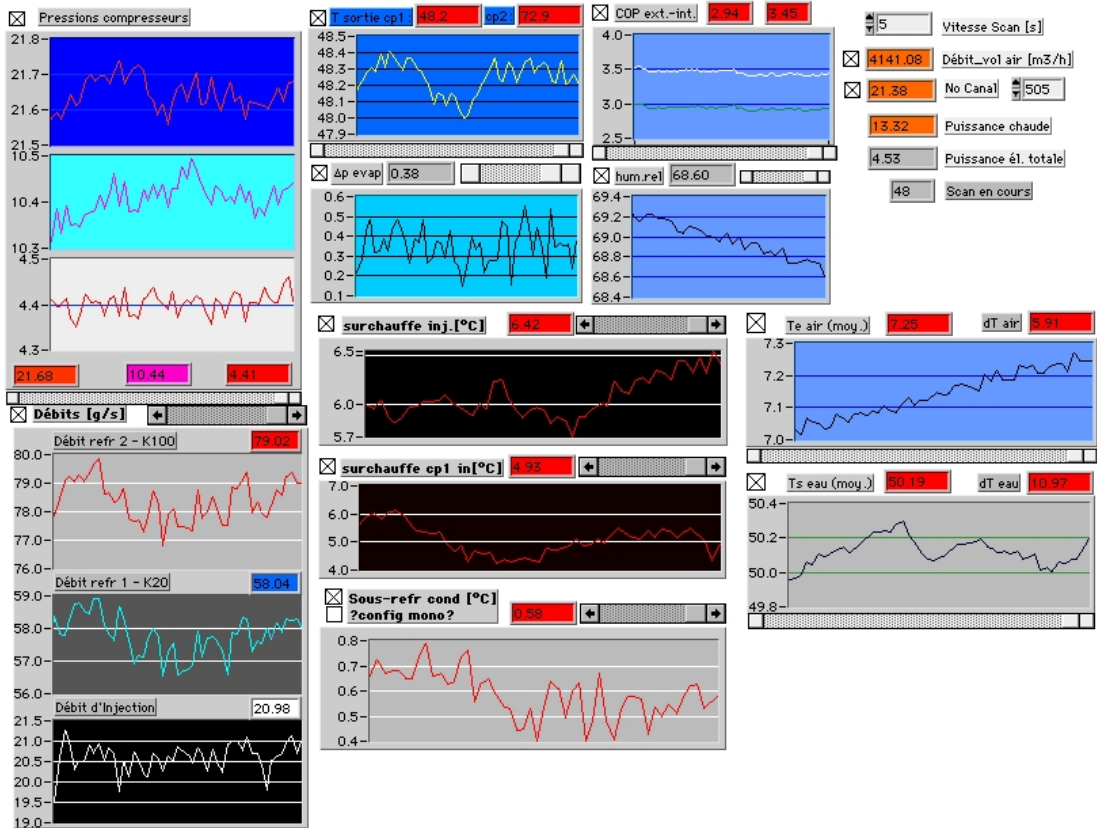
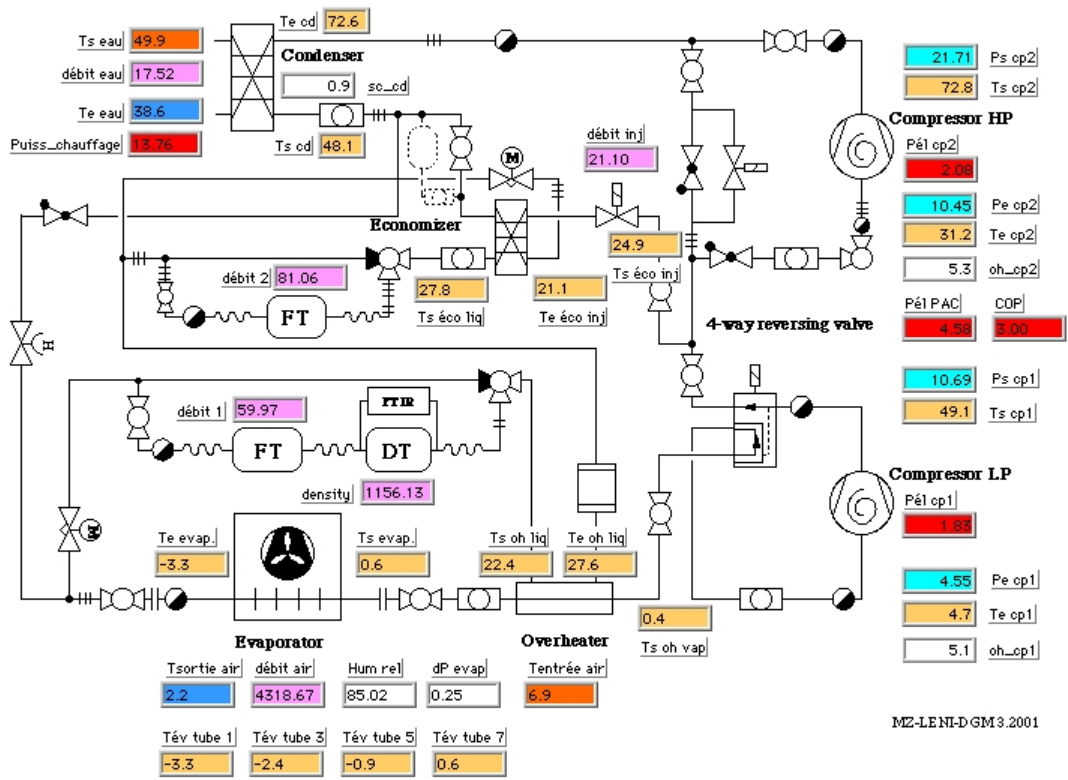


Figure A.2: Screen shots of the real-time measurement representation for the example of a running air-water heat pump in two-stage compression heating mode.

Table A.4: *Simulation toolbox for enhanced air-water heat pump cycles.*

MASTER Program	
enhanced_HP	master program for heat pump cycles.
enhanced_HP_cycle_calc	calculation core returning a vectorized convergence output
COMPONENTS	
plate_condenser	plate heat exchanger, condenser, to water (use init_plate)
plate_economizer	plate heat exchanger, economizer, refrigerant to refrigerant (use init_plate)
compressor	compressor in heat pumps (use init_comp before)
compressor_inj	scroll compressor with intermediate injection in heat pumps (use init_comp before)
finned_tube_evaporator	evaporator (including air side) for heat pumps (use init_evap)
capillary	capillary tube expansion, for use with subcooled liquid, two-phase and compressible vapor phase flow
SUBFUNCTIONS FOR COMPONENTS	
capillary_vap_calc	non-adiabatic and compressible vapor phase capillary tube
dehumid_air	condensate rate of water from subcooled saturated humid air
dT_humid_air	humid air properties with definition of saturated air
evap_heat_map	refrigerant evaporation flow map and heat transfer (including oil concentration)
init_comp	initialisation of the compressor and compressor_inj data
init_evap	initialisation of the finned_tube_evaporator data
init_plate	initialisation of the plate_condenser and plate_economizer data
iter_on_capillary	iterates to find solution using capillary
step_capillary	pressure drop in a capillary for a given partial length
step_Tcapillary	partial length in a capillary for a given temperature step
step_vap_capillary	pressure drop in vapor only flow
T_bub_refr_oil	local saturation temperature including mixed oil.
TOOLS	
adim_logP_h	logP-h diagram in non-dimensional axes
adim_T_s	T-s diagram in non-dimensional axes
diagr_logP_h	logP-h diagram
diagr_T_s	T-s diagram
dp_Friedel	pressure drop correlation, using Friedel correlation for mist flow
mach2phase	two phase Mach number
mollier	plotting Mollier diagram of humid air
plot_sat_lines_logP_h	saturation curve in logP-h diagram
plot_sat_lines_T_s	saturation curve in T-s diagram
speedofsound	speed of sound in liquid, vapor and two-phase region

Max. pressure: 28.8 bar, max. temperature: 140/110°C (at the discharge port / measured in the refrigerant line). Built in volume ratio and global efficiency (by experimental data fitting) $VR_i = 3.3$, $\eta_{is,max} = 68\%$.

Released for R-134a, R-404A R-407C and R-22.

- High pressure compressors (ZP): ZP23 - ZR120

Displacement in m^3/h at 50 Hz: 4.1 / 4.4 / 5.4 / 6.9 / 9.4 / 11.0 / 14.6 / 16.8 / 19.8

Max. pressure: 43 bar, max. temperature: 140/110°C (at the discharge port / measured in the refrigerant line). Evaluated from tabular output $VR_i = 1.9$, $\eta_{is,max} = 72\%$.

Released for R-410A.

- Compressors with intermediate injection.

1. Liquid injection port - ZF15KVE

Equivalent injection capillary analogy: $D=2.1$ mm, $L=0.6$ m

2. Vapor injection Prototype #1

ZR based compressor with capillary tube analogy: $D=3.6$ mm, $L=300$ mm

3. Vapor injection Prototype #2

ZH13VLE, ZF based compressor with capillary tube analogy: $D=3.5$ mm, $L=300$ mm

A.4.2 Finned tube evaporator

Table A.6: Geometrical input data for finned tube evaporator simulation. Geometries from the in the experimental part of this work.

	Evaporator #1	Evaporator #2
Total heat exchange surface (refrigerant side)	5.04 m ²	4.58 m ²
Fin surface increase factor	11.2	9.43
Apparent air flow surface	0.7 m ²	0.64 m ²
Refrigerant tube diameter	9.5 mm	9.5 mm
Tube wall thickness	0.3 mm	0.3 mm
Tube type	micro-finned	micro-finned
Number of circuits	11	24
Number of passes per circuit	24	8
Tube arrangement	staggered	staggered
Tube ranges	6 x 44	6 x 32
Fin pitch	3.2 mm	3.6 mm
Fin thickness	0.2 mm	0.2 mm
Number of fins	200	220

A.4.3 Plate heat exchangers

Table A.7: Geometrical input data for compact brazed plate heat exchanger simulation. Geometries from the in the experimental part of this work.

	Condenser #1	Condenser #2	Condenser from [Yan:1999]
Total heat exchange surface	1.51 m ²	4.68 m ²	0.11 m ²
Plate size	0.5 x 0.10 m ²	0.52 x 0.12 m ²	0.45 x 0.12 m ²
Channel height	2 mm	1.7 mm	3.3 mm
Plate thickness	0.4 mm	0.6 mm	0.4 mm
Number of plates	30	80	3
Corrug. pattern angle	19°	60°	60°
Plate surface enl.	1.17	1.22	1.22
Max. pressure	30 bar	40 bar	-
	Economizer #1	Economizer #2	
Total heat exchange surface	0.36 m ²	1.84 m ²	
Plate size	0.25 x 0.11 m ²	0.68 x 0.3 m ²	
Channel height	2 mm	1.7 mm	
Plate thickness	0.4 mm	0.6 mm	
Number of plates	14	10	
Corrug. pattern angle	27°	60°	
Plate surface enl.	1.22	1.22	
Max. pressure	30 bar	40 bar	

A.5 Experimental setup and listings of elements.

The presented experimental data in chapter 2, issue from different projects, in which the author has contributed. The listings in this section are intended to provide the complete list of all the collected measurements.

A.5.1 Brine-water heat pump, economizer cycle with intermediate liquid injection port compressor

List of transmitters and measurement data points

<i>Point No.</i>	<i>Measurement of</i>	<i>Unit</i>	<i>Transmitter</i>
<u>Annex circuits:</u>			
101	T_water_cd_in	°C	Temperature, PT100 (4-cond)
102	T_water_cd_out	°C	Temperature, PT100 (4-cond)
103	T_brine_ev_in	°C	Temperature, PT100 (4-cond)
104	T_brine_ev_out	°C	Temperature, PT100 (4-cond)
105	M_flow_brine	l/h	Endress&Hauser, Promag33AT
106	M_flow_water	l/h	Endress&Hauser, Promag33AT
<u>Heat Pump Circuit:</u>			
201	T_refr_cp_in	°C	Temperature, PT100 (4-cond)
202	T_refr_cp_out	°C	Temperature, PT100 (4-cond)
206	T_refr_cd_in	°C	Temperature, PT100 (4-cond)
207	T_refr_cd_out	°C	Temperature, PT100 (4-cond)
209	T_refr_eco_liq_in	°C	Temperature, PT100 (4-cond)
210	T_refr_eco_liq_out	°C	Temperature, PT100 (4-cond)
211	T_refr_eco_inj_in	°C	Temperature, PT100 (4-cond)
212	T_refr_eco_inj_out	°C	Temperature, PT100 (4-cond)
216	T_refr_ev_in	°C	Temperature, PT100 (4-cond)
204	P_cp_in	bar	Pressure, Haenni, ED510
205	P_cp_out	bar	Pressure, Haenni, ED510
208	P_cd_in	bar	Pressure, Haenni, ED510
213	P_int	bar	Pressure, Haenni, ED510
214	M_flow_refr_2	l/min	Turbine, Bachofen AG, Swissflow 800/6
215	M_flow_refr_1	l/min	Turbine, Bachofen AG, Swissflow 800/6
203	E_cp	kW	Power meter, Transmetra LVT 310

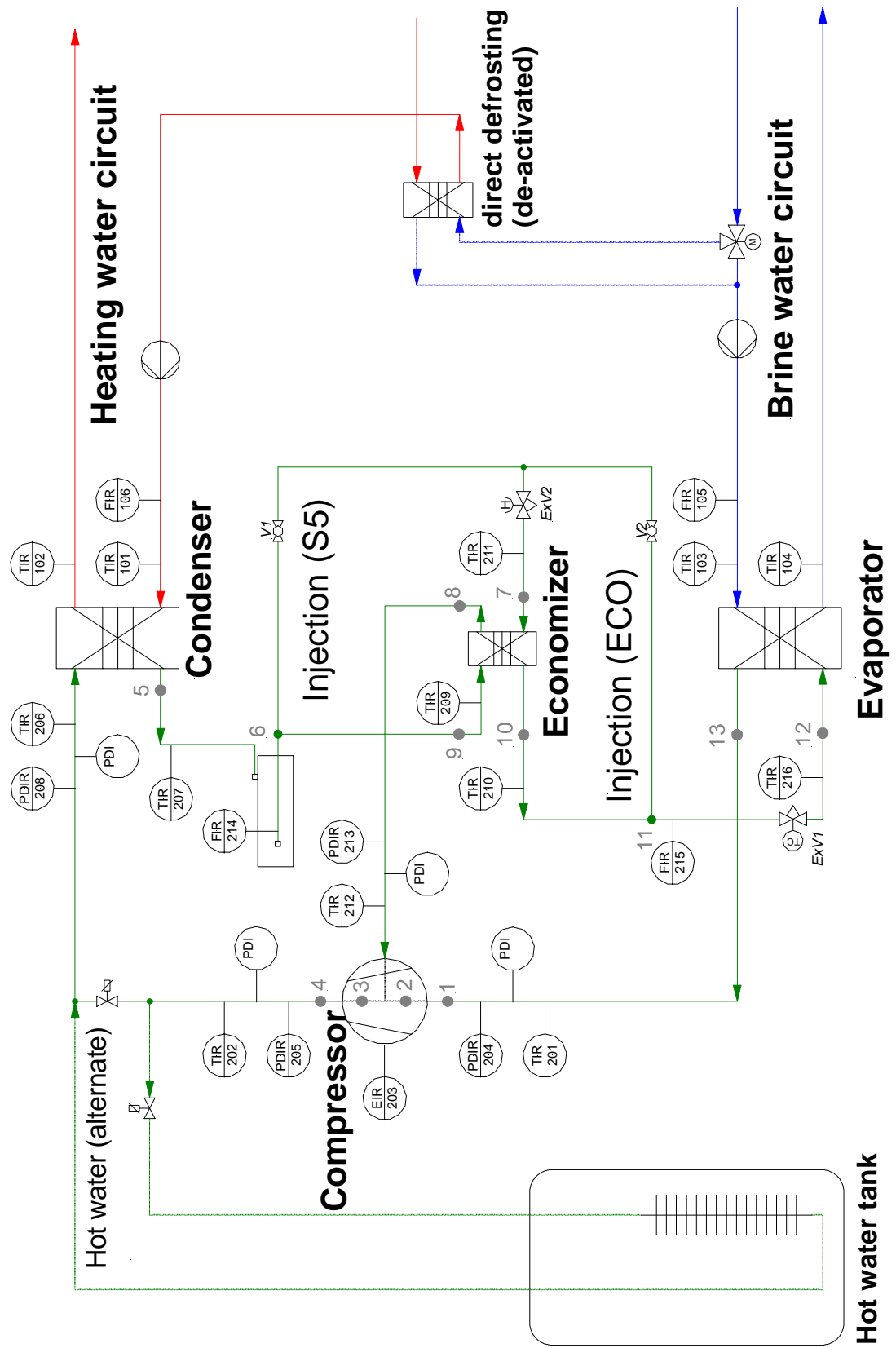


Figure A.3: KWT project, flow chart, measurement points

A.5.2 Air-water heat pump, economizer cycle with new intermediate vapor injection port compressor

List of transmitters and measurement data points

<i>Point No.</i>	<i>Cable No.</i>	<i>Measurement of</i>	<i>Unit</i>	<i>Transmitter</i>
Temperatures:				
401	B01	T_cp_out	°C	Thermocouple Type K
402	B02	T_cd_out	°C	Thermocouple Type K
403	B03	T_eco.inj_in	°C	Thermocouple Type K
404	B04	T_eco.inj_out	°C	Thermocouple Type K
405	B05	T_eco.liq_out	°C	Thermocouple Type K
406	B06	T_exp_in	°C	Thermocouple Type K
407	B07	T_ev_in	°C	Thermocouple Type K
408	B08	T_ev_out	°C	Thermocouple Type K
409	B09	T_cp_in	°C	Thermocouple Type K
410	B10	T_hp_amb	°C	Thermocouple Type K
414	B14	T_fin_surf1	°C	Thermocouple Type K
415	B15	T_fin_surf2	°C	Thermocouple Type K
Pressures:				
504	3	P_cp_in	bar	Kistler A20
505	4	P_cp_out	bar	Kistler A50
506	5	P_int	bar	Kistler A20
500	PDIF	ΔP_{evap_out}	mbar	Furness FCO40 25 mm H ₂
501	PDIF	ΔP_{air_nozzle}	mbar	Furness FCO40 10 mm H ₂
El. power:				
512	512	E_HP_tot	kW	Norma
513	513	E_cp	kW	Norma
Mass flow rates, Density:				
300	CORR1	M_flow_1	g/s	Witronic K-20
301	CORR1	Dens_1	kg/m ³	Witronic K-20
302	CORR2	M_flow_2	g/s	Witronic K-100
303	CORR2	Dens_2	kg/m ³	Witronic K-100
517	C1	Dens_water	kg/m ³	Witronic K-250
516	C1	M_flow_water	kg/m ³	Witronic K-250
Water temperatures:				
600	29	Tw_cd_out_1	°C	Thermocouple Type K
601	22	Tw_cd_out_2	°C	Thermocouple Type K
602	20	Tw_cd_out_3	°C	Thermocouple Type K
603	27	Tw_cd_in_1	°C	Thermocouple Type K
604	26	Tw_cd_in_2	°C	Thermocouple Type K
605	23	Tw_cd_in_3	°C	Thermocouple Type K
Air temperature:				
606	11	Tair_ev_out_1	°C	Thermocouple Type K
607	85	Tair_ev_out_2	°C	Thermocouple Type K
608	86	Tair_ev_out_3	°C	Thermocouple Type K
609	87	Tair_ev_in_1	°C	Thermocouple Type K
610	88	Tair_ev_in_2	°C	Thermocouple Type K
611	1	Tair_ev_in_3	°C	Thermocouple Type K
Other:				
507	HUM	hum_rel_air	-	Rotronic Hygromer
502	-	V_exp_el	-	HP 77405

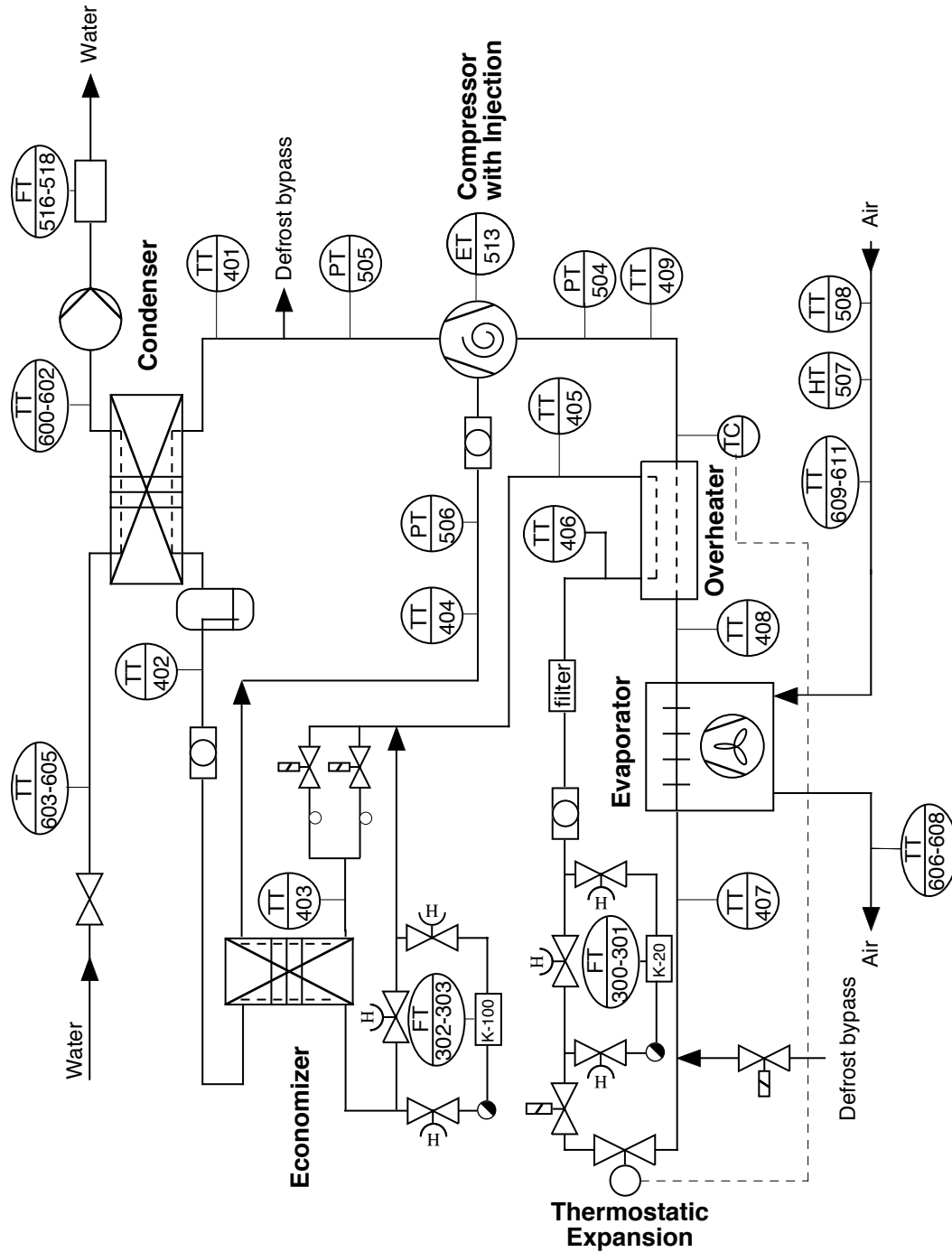


Figure A.4: Flow chart, high temperature heat pump with compressor with new injection port.

A.5.3 Brine-water heat pump with high pressure ratio main compressor and auxiliary subcooling cycle

List of transmitters and measurement data points

<i>Point No.</i>	<i>Measurement of</i>	<i>Unit</i>	<i>Transmitter</i>
Annex circuits:			
101	T_water_cd_in	°C	Temperature, PT100 (4-cond)
102	T_water_cd_out	°C	Temperature, PT100 (4-cond)
103	T_brine_ev_in	°C	Temperature, PT100 (4-cond)
104	T_brine_ev_out	°C	Temperature, PT100 (4-cond)
105	M_flow_brine	l/h	Endress&Hauser, Promag33AT
106	M_flow_water	l/h	Endress&Hauser, Promag33AT
107	T_water_desup_out	°C	Temperature, PT100 (4-cond)
108	T_water_cold_out	°C	Temperature, PT100 (4-cond)
109	T_water_cold_in	°C	Temperature, PT100 (4-cond)
Heat Pump Main Circuit:			
201	T_refr1_ev_out	°C	Temperature, PT100 (4-cond)
203	T_refr1_cp_in	°C	Temperature, PT100 (4-cond)
205	T_refr1_cp_out	°C	Temperature, PT100 (4-cond)
207	T_refr1_cd_in	°C	Temperature, PT100 (4-cond)
208	T_refr1_cd_out	°C	Temperature, PT100 (4-cond)
209	T_refr1_aux_ev_in	°C	Temperature, PT100 (4-cond)
210	T_refr1_aux_ev_out	°C	Temperature, PT100 (4-cond)
211	T_refr1_exp_in	°C	Temperature, PT100 (4-cond)
216	T_refr1_ev_in	°C	Temperature, PT100 (4-cond)
202	P_cp1_in	bar	Pressure, Haenni, ED513
206	P_cp1_out	bar	Pressure, Haenni, ED513
204	E_cp1	kW	Power meter, Transmetra LVT 310
Heat Pump Auxiliary Circuit:			
302	T_refr2_cp2_in	°C	Temperature, PT100 (4-cond)
304	T_refr2_cp2_out	°C	Temperature, PT100 (4-cond)
306	T_refr2_cd2_out	°C	Temperature, PT100 (4-cond)
307	T_refr2_ev2_out	°C	Temperature, PT100 (4-cond)
301	P_cp2_in	bar	Pressure, Haenni, ED513
305	P_cp2_out	bar	Pressure, Haenni, ED513
303	E_cp2	kW	Power meter, Transmetra LVT 310

List of main components:

Compressors:

Copeland Scroll ZF13K4E	67.8 cm ³
Danfoss Piston SC12DLX	12.9 cm ³

Heat Exchangers:

Main condenser	SWEP B25, Plate heat exchanger
Aux. condenser	SWEP B25, Plate heat exchanger
Main evaporator	SWEP B15, Plate heat exchanger
Aux. evaporator	SWEP B8, Plate heat exchanger
Suction line overheater	PACKLESS, HRX 150
Tap-Water, desuperheater	COAX, 2101 H
Tap-Water, subcooler	COAX, 2101 H

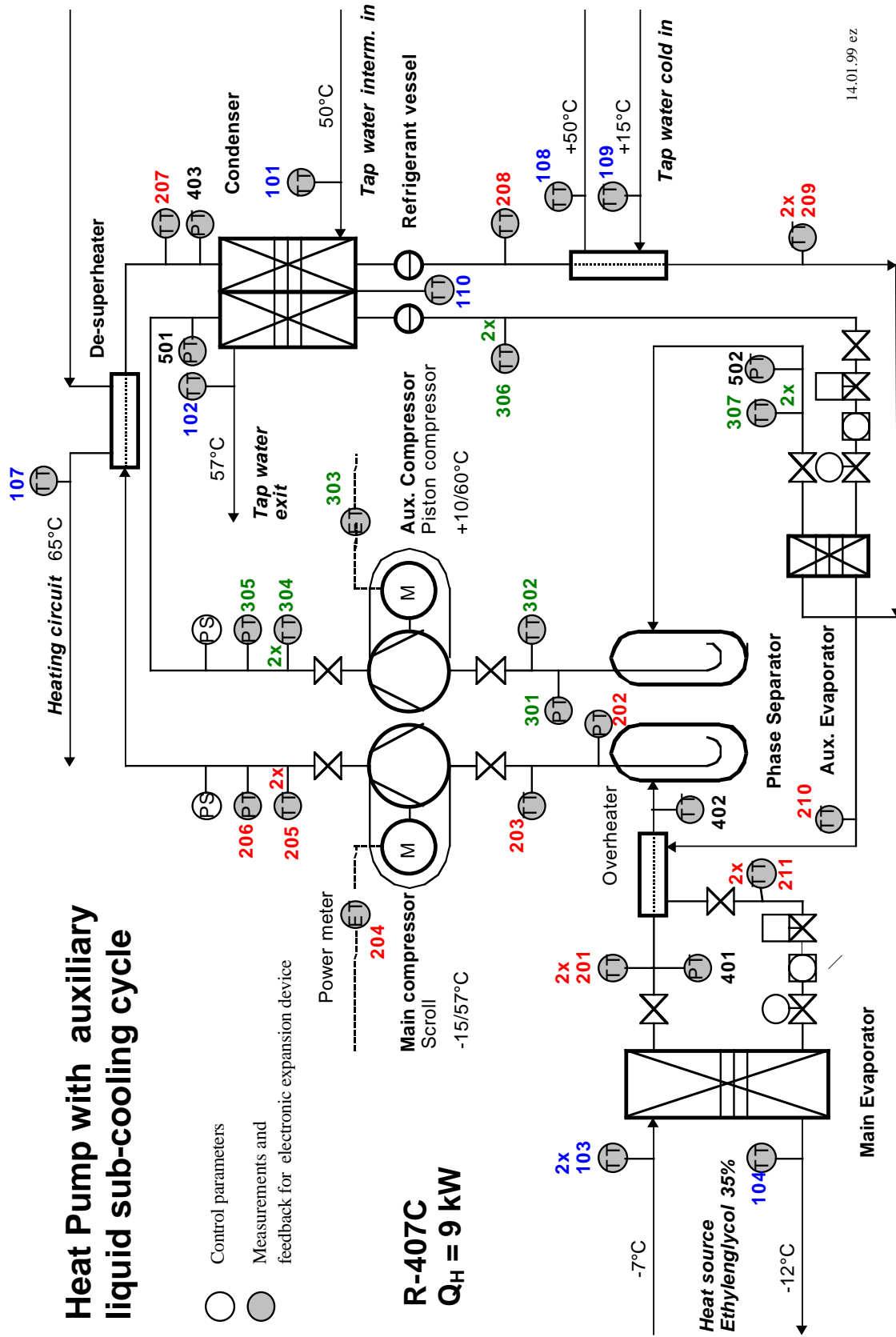


Figure A.5: Flow chart, brine-water heat pump with auxiliary cycle for subcooling

A.5.4 Two-stage compression air-water heat pump, including oil migration measurements

List of transmitters and measurement data points

<i>Channel</i>	<i>Point No.</i>	<i>Measurement of</i>	<i>Unit</i>	<i>Transmitter</i>
<u>Temperatures:</u>				
200	TR00	free	°C	Thermocouple Type K
201	TR01	T_cp1_in	°C	Thermocouple Type K
202	TR02	T_cp1_out	°C	Thermocouple Type K
203	TR03	T_cp2_in	°C	Thermocouple Type K
204	TR04	T_cp2_out	°C	Thermocouple Type K
205	TR05	T_cd_in	°C	Thermocouple Type K
206	TR06	T_cd_out	°C	Thermocouple Type K
207	TR07	T_eco_liq_out	°C	Thermocouple Type K
208	TR08	T_oh_liq_in	°C	Thermocouple Type K
209	TR09	T_oh_liq_out	°C	Thermocouple Type K
210	TR10	T_oh_vap_out	°C	Thermocouple Type K
211	TR11	T_ev_tube1	°C	Thermocouple Type K
212	TR12	T_ev_tube3	°C	Thermocouple Type K
213	TR13	T_ev_tube5	°C	Thermocouple Type K
214	TR14	T_ev_tube7	°C	Thermocouple Type K
215	TR15	T_ev_tube8	°C	Thermocouple Type K
216	TR16	T_eco_sat_out	°C	Thermocouple Type K
217	TR17	T_eco_sat_in	°C	Thermocouple Type K
<u>Pressures:</u>				
311	PR1	P_cp1_in	bar	Haenni
312	PR2	P_cp1_out	bar	Haenni
313	PR3	P_cp2_in	bar	Haenni
314	PR4	P_cp2_out	bar	Kistler
<u>El. power:</u>				
512	E_HP	E_HP_tot	kW	Norma
513	E_cp1	E_cp1	kW	Norma
514	E_cp2	E_cp2	kW	Sineax
<u>Mass flow rates, Density:</u>				
300	FR1	M_flow_1	g/s	Witronic K-20
301	DR1	Dens_1	kg/m ³	Witronic K-20
302	FR2	M_flow_2	g/s	Witronic K-100
303	DR2	Dens_2	kg/m ³	Witronic K-100
516	C1	M_flow_water	kg/min	Witronic K-250
517	C1	Dens_water	kg/m ³	Witronic K-250
305	DR3	Dens_high_prec	kg/m ³	Bopp&Reuther
306	LO1	Level_cp1	mm	visual
307	LO2	Level_cp2	mm	visual
<u>Water temperature:</u>				
600	29	Tw_cd_out_1	°C	Thermocouple Type K
601	22	Tw_cd_out_2	°C	Thermocouple Type K
602	20	Tw_cd_out_3	°C	Thermocouple Type K
603	27	Tw_cd_in_1	°C	Thermocouple Type K
604	26	Tw_cd_in_2	°C	Thermocouple Type K
605	23	Tw_cd_in_3	°C	Thermocouple Type K

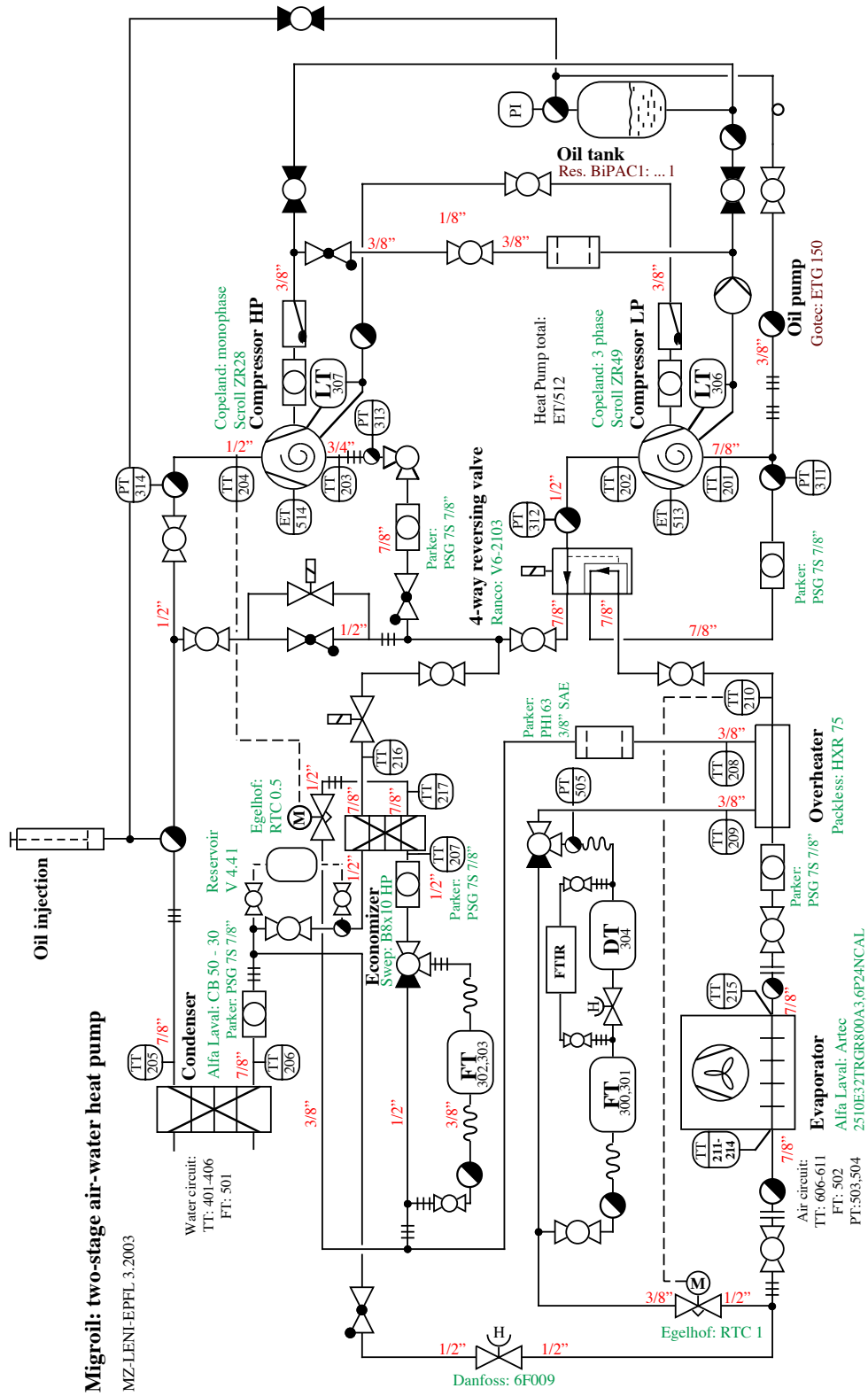


Figure A.6: Flow chart, including oil equilibration parts for two-stage heat pump.

Air temperature:

606	11	Tair_ev_out_1	°C	Thermocouple Type K
607	85	Tair_ev_out_2	°C	Thermocouple Type K
608	86	Tair_ev_out_3	°C	Thermocouple Type K
609	87	Tair_ev_in_1	°C	Thermocouple Type K
610	88	Tair_ev_in_2	°C	Thermocouple Type K
611	1	Tair_ev_in_3	°C	Thermocouple Type K

Differential pressure:

500	DP1	ΔP_{evap}	mbar	Furness
501	DP2	$\Delta P_{\text{air_flow}}$	mbar	Furness

Humidity:

507	HR	hum_rel_air	-	Rotronic Hygromer
-----	----	-------------	---	-------------------

Complete listing of components

Compressor HP	Copeland	Scroll ZR28, 6.75 m ³ /h, K1PFJ522
Compressor LP	Copeland	Scroll ZR49, 11.7 m ³ /h, K3TFD422
Oil pump	Gotec	ETG 150
Evaporator	Artec	Z510 E 32TR 6R 800A 3.6P 24NC AI
Condenser	Alfa Laval	CB50-30, 1.4 m ²
Overheater	Packless	HXR75
Economizer	SWEP	B8x10 HP, 0.184m ²
Oil tank	-	Volume 8 l
Refrigerant vessel	Charles Hasler	CHA 160 265 0, V 4.4 l
Fan+ motor	divers	Ventilator AT 18-18S+ El. motor
Manual exp. valve	Danfoss	6F009 Kv=0.07
Main el. exp. valve	Egelhof	RTC 1.0
Sec. el. exp. valve	Egelhof	RTC 0.5
Ac. el. exp. valve Egelhof	Portescap	Transmission card, Motor command.
Level regulator	AC&R	S-9030
Anti-return valve 3/8"	Castel	3130-3
Anti-return valve 1/2"	Castel	3130-4
Solenoid valve 7/8"		
Reversing cycle valve 4 way	Ranco	V6-2103
Ball valve 3 way 1/2"	Mueller	A-17540 1/2"- 3W
Ball valve 3 way 3/8"	Mueller	A-17539 3/8"- 3W
Ball valve angular 7/8"	Mueller	A-17555 7/8"-E
Ball valve 7/8"	Mueller	A-17264 7/8"
Ball valve 3/8"	Mueller	A-17260 3/8"
Tube reduction 7/8"- 3/4"	Mueller	W 01035
Tube reduction 7/8"- 1/2"	Mueller	W 01037
Tube reduction 1/2"- 3/8"	Mueller	W 01019
Sight glass 7/8"	kmp	KSG-R 7S 7/8"
Oil filter	AC&R	S-9105
Filter dryer	kmp	WAH 053 3/8"FLARE
Tube T 7/8"	Mueller	W 04031
Tube T 3/8"	Mueller	W 04000
Tube T 1/2"	Mueller	W 04001
Connections 7/8"	Fas	LP 25/22.4 7/8"
Siphon	Mueller	W 61000
Absorber	Packless	VAF 3
Isolation Aeroflex	Aeroflex	7/8", 10 mm
Refrigerant R-407C	ICI	Klea 407 C

Curriculum Vitae



Michele Zehnder

Born on the 2nd of June 1972 in Zürich (Switzerland)

Swiss citizen

Living with his partner and his 3 children, Laura-Maria (1995), Linus and Annika (2002) in Köniz near Berne.

Education:

1997: Diploma of Mechanical Engineering at the Swiss Federal Institute of Technology (EPFL) in Lausanne, with specializations on Energetics, Fluid Mechanics and Turbomachinery.

1991: High school diploma with scientific orientation, in Burgdorf, BE

Research activities:

1999-2003: Experimental analysis of oil migration in two-stage heat pump cycles.

1999-2002: Heat pump with intermediate liquid and vapor injection port.

1998-1999: Experimental and theoretic evaluation of the auxiliary cycle for liquid subcooling.

1997-1999: Measurements and simulation on two-stage heat pump.

Programming:

Development of a heat pump simulation toolbox, in Matlab programming language.

Co-development of a fluid interface, including Refprop calculation core, in C++ and Fortran.

Development of several data acquisition tools using LabView.

Teaching:

Supervision of student diploma and semester projects. Teaching in Thermodynamics and Energetics course for mechanical engineers, including exercise lessons.

Languages:

Very good in German, French, English.

Good in Italian.